



**HAL**  
open science

# Multimodal sensing polymer transistors for cell and micro-organ monitoring

Ariana A. Villarroel Marquez

► **To cite this version:**

Ariana A. Villarroel Marquez. Multimodal sensing polymer transistors for cell and micro-organ monitoring. Polymers. Université de Bordeaux, 2018. English. NNT : 2018BORD0449 . tel-03270771

**HAL Id: tel-03270771**

**<https://theses.hal.science/tel-03270771v1>**

Submitted on 25 Jun 2021

**HAL** is a multi-disciplinary open access archive for the deposit and dissemination of scientific research documents, whether they are published or not. The documents may come from teaching and research institutions in France or abroad, or from public or private research centers.

L'archive ouverte pluridisciplinaire **HAL**, est destinée au dépôt et à la diffusion de documents scientifiques de niveau recherche, publiés ou non, émanant des établissements d'enseignement et de recherche français ou étrangers, des laboratoires publics ou privés.

**Thèse**

Présentée à

***L'Université de Bordeaux***

*Ecole Doctorale des Sciences Chimiques*

Par

***Ariana A. Villarroel Marquez***

Pour obtenir le Grade de

DOCTEUR

Spécialité : Polymères

---

**MULTIMODAL SENSING POLYMER TRANSISTORS FOR CELL  
AND MICRO-ORGAN MONITORING**

---

Le 19/12/2018

Devant la Commission d'examen formée de :

|   |                    |
|---|--------------------|
| <b>Dr. Róisín M. Owens</b> , Professeur, Université de Cambridge          | Rapportrice        |
| <b>Dr. Pierre-Henri Aubert</b> , Professeur, Université Cergy Pontoise    | Rapporteur         |
| <b>Dr. Alexander Kuhn</b> , Professeur, Université de Bordeaux            | Examineur          |
| <b>Dr. Rodney O'Connor</b> , Professeur, Ecole de Mines de Saint-Etienne  | Examineur          |
| <b>Dr. Georges Hadziioannou</b> , Professeur, Université de Bordeaux      | Invité             |
| <b>Dr. Matthieu Raoux</b> , Maître de Conférences, Université de Bordeaux | Invité             |
| <b>Dr. Eric Cloutet</b> , Directeur de Recherche, Université de Bordeaux  | Directeur de thèse |
| <b>Dr. Jochen Lang</b> , Professeur, Université de Bordeaux               | Directeur de thèse |







# *ABSTRACT -RESUME*

*Le développement de nouveaux matériaux pour augmenter les performances des capteurs biologiques est très important lorsqu'on sait que les signaux électriques constituent la base des événements biologiques fondamentaux comme l'activité cérébrale, le battement du cœur ou la sécrétion hormonale. Ces signaux cellulaires sont souvent enregistrés avec des sondes qui nécessitent des modifications génétiques ou chimiques. Cependant, des signaux intrinsèques pourraient être exploités directement. Des matrices de microélectrodes extracellulaires (MEAs) et des transistors électrochimiques à base de polymères (OECTs) sont par exemple sensibles aux flux ioniques. Ils sont, de plus, non-invasifs et donnent des informations importantes sur l'activité cellulaire. Cependant, ils ne peuvent pas différencier les espèces ioniques impliquées dans les signaux pour l'obtention d'une image précise de l'activité électrique. Ce travail de thèse a ainsi consisté dans : le développement de polymères bivalents ion-sensibles et conducteurs électroniques, la démonstration de leur biocompatibilité avec des cellules bêta-pancréatiques, la fabrication de transistors OECTs intégrant ces matériaux et la preuve de concept de son applicabilité comme plateforme non-invasive pour la détection de flux ioniques.*

Au cours des dernières décennies, l'intérêt pour les matériaux issus de l'électronique organique pour les bio-applications s'est accru. L'un des sujets clés est le développement de dispositifs pour l'électrophysiologie, qui permet un contact direct avec les tissus vivants dans le but d'enregistrer ou de stimuler leur activité électrique. Les perspectives de l'état de l'art actuel nous permettent de constater que la bioélectronique a encore de nombreux défis à relever et qu'il y a encore du travail à faire du côté synthétique de la bioélectronique organique, surtout si l'on considère que le matériau le plus utilisé dans ce domaine, PEDOT:PSS, est le même depuis les vingt dernières années principalement en raison de sa disponibilité commerciale. L'objectif principal de cette thèse a donc été la synthèse de matériaux polymères ciblant leur interface avec des cellules  $\beta$  pancréatiques, et prenant en compte leur structure chimique pour obtenir les informations nécessaires. Comme il a été décrit, l'activité électrique des cellules pancréatiques met en jeu l'échange de cations par des canaux spécifiques. Par conséquent, il est important de les détecter. Certains de ces cations présentant un intérêt particulier sont les cations monovalents  $\text{Na}^+$  et  $\text{K}^+$  et, comme nous l'avons vu, ils présentent une grande affinité dans la complexation avec les éthers couronne. De plus, dans l'étude des cellules  $\beta$ , il est très intéressant de développer des monomères sensibles au  $\text{Zn}^{2+}$  en raison du rôle important de ce cation dans la co-sécrétion avec l'insuline dans ce type de cellules.

De nombreux groupes de recherche s'efforcent de mettre au point des méthodes permettant d'obtenir de nouveaux polymères à conduction mixte en remplacement du PEDOT : PSS.

Au cours de mes études doctorales, deux voies principales ont été suivies afin d'obtenir de nouveaux matériaux actifs pour constituer le canal des dispositifs OECT (Figure 0). D'une part, des dérivés du styrène ont été synthétisés et utilisés pour obtenir des polyélectrolytes de substitution au PSS (chapitre II). D'autre part, la fonctionnalisation a été réalisée directement dans le

monomère conjugué EDOT (chapitre III). Les cations impliqués dans les différents processus d'intérêt pour l'étude des cellules  $\beta$  pancréatiques (sodium, potassium et zinc) ont été le moteur du choix des chélates utilisés pour la modification des monomères au cours de cette étude. Ainsi, les structures de la plupart des produits synthétisés et analysés dans ce travail sont basées sur les éthers couronnes 15-couronne-5 et 18-couronne-6 ayant des tailles de cavité de 1,7-2,2 Å et 2,6-3,2 Å, respectivement, tandis que le groupe choisi pour piéger le cation divalent,  $Zn^{2+}$ , était la fraction dipicolyle (DPA).

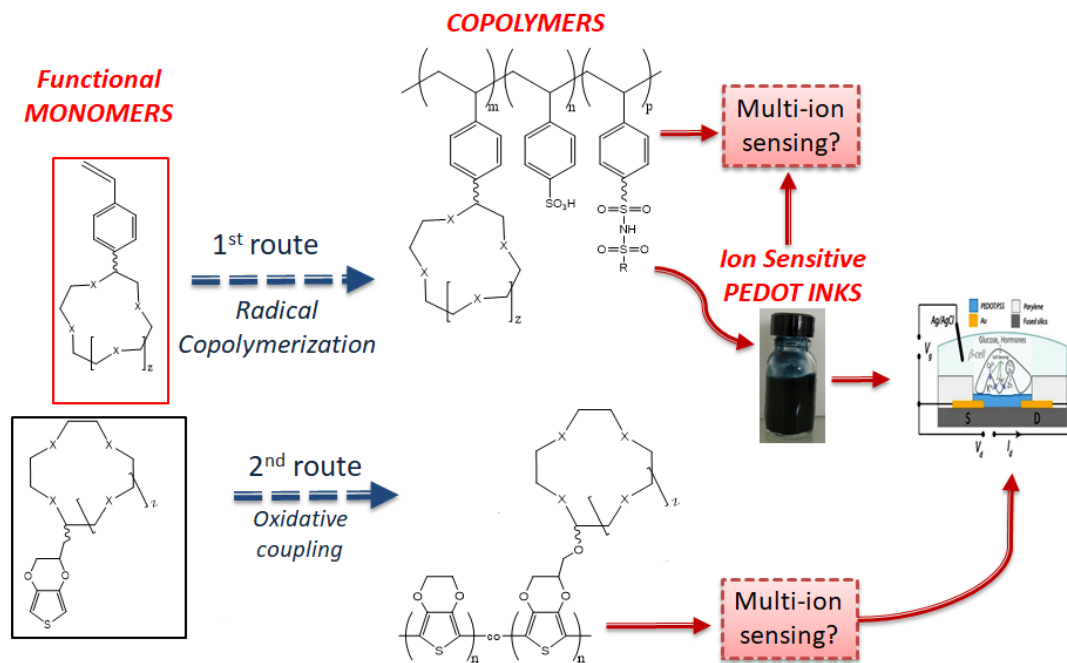


**Figure 0: Summary of the double route of functionalization developed during this PhD:** Top: Styrene derivatives with binding moieties (monomers), their copolymers to gain new ion-sensitive polyelectrolytes used to stabilize the water dispersed PEDOT based inks. Bottom: EDOT derivatives with the ion-sensitive fractions and their electropolymerization to obtain ion-sensitive films.

Dans ce travail, une approche à deux voies des matériaux fonctionnalisés avec des fractions chélates a été développée pour obtenir de nouveaux composants actifs pour constituer le canal des dispositifs OECT et l'interface avec les cellules  $\beta$  pancréatiques pour des enregistrements électrophysiologiques. La relation structure-propriétés de ces matériaux a été présentée et discutée tout au long de la thèse.

Au **chapitre I**, nous avons passé en revue certaines notions fondamentales de l'électrophysiologie et du rôle des cellules  $\beta$  du pancréas dans le diabète, ainsi qu'un bref résumé des méthodes actuelles utilisées pour surveiller et traiter cette maladie. De plus, la description des classes de

matériaux les plus importantes développées dans le domaine des polymères conducteurs ainsi que dans le domaine de la chimie supramoléculaire au cours des dernières décennies a été présentée, pour arriver à notre stratégie générale d'application de la combinaison de ces matériaux pour leur intégration dans les capteurs biologiques.

Le développement d'une première voie a été présenté au **Chapitre II**, en effectuant la synthèse de monomères de dérivés fonctionnalisés du styrène et de polyélectrolytes subséquents, utilisés comme stabilisants pour la polymérisation chimique oxydante de l'EDOT dans des dispersions aqueuses pour obtenir différentes encres contenant les groupes sensibles aux ions. La structure et la sensibilité ionique de ces matériaux ont été évaluées et les résultats préliminaires montrent que certains de ces matériaux conservent les avantages des encres de PEDOT : PSS traditionnel, présentant même une capacité volumétrique encore plus élevée, et possèdent une sensibilité ionique vers le cation ciblé due aux groupes chélateurs incorporés dans leurs structures.

Une deuxième voie de fonctionnalisation de l'EDOT a été explorée au **Chapitre III** où les groupes chélateurs étaient directement attachés au monomère "conducteur". L'étude de la relation structure-propriétés des différents monomères et polymères électropolymérisés obtenus à partir de ces dérivés EDOT a été réalisée. On a principalement évalué deux fractions de liaison entre l'EDOT et les fragments chélateurs d'ions, une liaison aniline et une liaison éther, montrant un profil charge-décharge inférieur pour les composés de l'aniline. Néanmoins, ils ont l'avantage de présenter un pic caractéristique qui pourrait être utilisé comme référence interne pour détecter l'affinité ionique des films polymères. Leur sensibilité aux ions a été évaluée et il a été constaté que ces films ont une affinité alcaline, mais des problèmes de reproductibilité ont été rencontrés avec des méthodes potentiodynamiques ou potentiométriques. La sélectivité du film par rapport au cation cible, conformément aux affinités des monomères de départ, a été mise en évidence par des mesures de conductivité *in situ* et la formation de courtes chaînes oligomères pendant la polymérisation des monomères contenant de l'aniline a été observée, suggérant l'influence de cette fraction dans le processus d'oxydation autocatalytique qui pourrait expliquer la variabilité observée avec les autres techniques.

Le **Chapitre IV** est le reflet des progrès interdisciplinaires réalisés au cours de cette thèse pour obtenir des enregistrements de cellules  $\beta$  plus adaptés avec la compilation de :

- L'amélioration du rapport signal/bruit pour la détection de signaux biologiques dans des enregistrements MEA grâce aux électrodes recouvertes d'un film PEDOT:PSS.
- La conception et le test d'une carte de traduction I/V (courant/tension) adaptée pour coupler des dispositifs OECT (sortie en courant) avec des enregistrements électrophysiologiques standard (entrée en tension) pour détecter, simultanément, des signaux de hauts et basse fréquence typiques des cellules  $\beta$  pancréatiques.
- L'intégration et le test des encres synthétisées lors de cette thèse dans des dispositifs OECT. Les résultats préliminaires ont démontré une transconductance relative accrue par

rapport au stimulus alcalin, ce qui pourrait être lié à la sensibilité ionique envisagé du dispositif.

Pour des travaux futurs, il pourrait être très intéressant d'effectuer une boucle de "contrôle de rétroaction" combinant le développement simultané du matériau et les essais de performance OECT pour déterminer le matériau et la méthode de synthèse et/ou de traitement les plus optimisés pour l'application de détection ciblée. De plus, des travaux plus exhaustifs sur l'étude structurelle des films polymères, ainsi que sur leur nanostructuration, pourraient permettre de clarifier l'effet des groupes chélateurs dans leur fonctionnalité et leur capacité de détection ionique. En conclusion, des échanges plus intensifs et interdisciplinaires sont nécessaires pour obtenir le système d'enregistrement final adapté aux cellules  $\beta$  pancréatiques, mais ce travail est déjà en cours dans le cadre du projet MULTISPOT financé par l'agence national de recherche (ANR).



## **ABSTRACT**

The generation of novel materials to harness the power of biological sensors is extremely attractive because precisely configured electrical activities form the base of key biological events such as brain activity, heart beat or vital hormone secretion. Cellular signals are often recorded using probes that require genetic or chemical manipulation. Intrinsic signals offer the huge advantage to harness these properties without further transformations. Extracellular microelectrode arrays (MEAs) and polymer-based organic electrochemical transistor arrays (OECTs) rely on the movement of ions, are non-invasive and provide some information on cell activity. However, they cannot resolve fluxes of specific species as targeted ions to obtain a precise picture of cell/organ activity. In this context, this work has consisted on the development of multimodal ion-sensing polymers, demonstration of their biocompatibility to beta-cells, the engineer of original OECTs incorporating these materials and demonstration of their viability as non-invasive platform of electrical cell activity and specific ion fluxes.

## **RESUME**

Le développement de nouveaux matériaux pour augmenter les performances des capteurs biologiques est très important lorsqu'on sait que les signaux électriques constituent la base des événements biologiques fondamentaux comme l'activité cérébrale, le battement du cœur ou la sécrétion hormonale. Ces signaux cellulaires sont souvent enregistrés avec des sondes qui nécessitent des modifications génétiques ou chimiques. Cependant, des signaux intrinsèques pourraient être exploités directement. Des matrices de microélectrodes extracellulaires (MEAs) et des transistors électrochimiques à base de polymères (OECTs) sont par exemple sensibles aux flux ioniques. Ils sont, de plus, non-invasifs et donnent des informations importantes sur l'activité cellulaire. Cependant, ils ne peuvent différencier les espèces ioniques impliquées dans les signaux pour l'obtention d'une image précise de l'activité électrique. Ce travail de thèse a ainsi consisté dans : le développement de polymères bivalents ion-sensibles et conducteurs électroniques, la démonstration de leur biocompatibilité avec des cellules bêta-pancréatiques, la fabrication de transistors OECTs intégrant ces matériaux et la preuve de concept de son applicabilité comme plateforme non-invasive pour la détection de flux ioniques.

**- Caminante no hay camino, se hace camino al andar -**

*Antonio Machado*

# *-Acknowledgments-*

I would like to express my most sincere gratitude to all the people who contributed to my PhD experience and without who this manuscript would not be possible. Foremost, I sincerely thank my academic supervisors, Dr. Eric Cloutet and Pr. Jochen Lang, for the confidence that you put in me to start this project, first collaboration between these two groups of LCPO and CBMN, that has born as a beautiful idea and became a very challenging and exciting topic. Eric, thank you for your continuous support and guidance over these three years, Jochen, thank you for your german perfectionism, your critical point of view and every question and suggestion done during our project meetings. You opened me a window through the “biology and medicine world”. It has been one of the most rewarding contributions to my development as a scientist. Moreover, I’m very grateful to both of you for your time during repetitions for any seminar or conference and your dedication to this manuscript during the last months.

This thesis could not see the light without the members of my PhD jury. Firstly, Pr. Roisin Owens and Pr. Pier-Henri Aubert, I thank you for accepting to evaluate this work and for your helpful comments, questions and suggestions. Furthermore, I would like to thank Pr. Alexander Kuhn, for his interest in this project and for providing insightful discussions and precious knowledge in electrochemistry, as well as Pr. O’Connor for welcoming me and allowing me to visit the laboratory BEL during the last months of my thesis to achieve the material integration into devices. Dr. Matthieu Raoux, thank you for transferring me your very precious knowledge on electrophysiology and thanks a lot for your kindness all along the thesis. Finally, Pr. Georges Hadziioannou, thank you for your attentional following of the project and for your support.

I’m thankful for the gratefully funding from the LabEx AMADEUS-0042 with the help of the French government “Initiative d’excellence” and from ANR MULTISPOT ANR-17-CE09-0015 and I’m thankful for help and scientific discussions with the staff of

ELORPrintTec (ANR-10-EQPX-28-01) and LCPO / Arkema / ANR Industrial Chair 'HOMERIC' (ANR-13-CHIN-0002-01), to my colleagues Dr. Tommaso Nicolini and Dr. Daniele Mantione from LCPO for precious scientific discussions, as well as Dr. Eva M. Muñoz from Affinimeter, thank you for so many hours of skype discussions and training.

I am very grateful to all the people that have collaborated in this interdisciplinary project. I cannot avoid to mention Dr. Dimitrios Katsigiannopoulos who introduced me to the chemical methods of polymerization used during this project in my first months as PhD student. Thanks for your kindness and interest in my project. A particular thank you for Dr. Gerardo Salinas, Jerry, from mentor in electrochemistry to friend. Thanks for so many hours dedicated to my project, to reply to my duds and questions, and to all the hours at work or outside of the lab dedicated and being more confident than me in my project in the strongest moments, eres mi *chilango* favorito. Dr. Mary J. Donahue, thank you so much for your help and to introduce me to the lithography world, to integrate my inks to OECT devices. It was wonderful to meet an amazing scientist and person as you in this project. I would like to not forget all the people working in the continuation of this project through the MULTISPOT network: Myriam, I'm confident that you will achieve the great  $\beta$ -recordings expected. Continue with your motivation and curiosity. Shekhar and Maël, good wind for the exploration in the material development and deeply structure-property understanding to advance in the device improvement.

In my every day-life as PhD I had the opportunity to be around a lot of amazing people, starting by LCPO members, especially the current members of team 4 and all the ex-B8ers that have followed their way around the world! You will always be the best memories of my thesis (and 1<sup>st</sup> Post-doctoral position).

Furthermore, this interdisciplinary work could not be possible without running to other labs, where I could cross (in more little experimental rooms) nice scientists and friends:

- In electrophysiology (CBMN), Julien and Romain, my mentors in MEAs,  $\beta$  cells (and picture with the phone on the microscope!), Manon, Antoine, Loïc, Eleonore, Alex and Pier...thanks for your help in biology -electronics and for your optimism!
- In electrochemistry (NsySa): Thanks to Alicia, Laura, Paul, Bhavana...and of course Top! Thank you for accepting me such a lot of time in your lab. Experiments with “strange” Thai music and crazy people run always much better. Good luck to all of you for your careers.

To finish, this is an important professional stage that arrived to its end, but it has been a most important personal growth step, that I could not easily pass if it was not for the support of important people. My Bordeaux family, *Nico* and *Alberto*, we started together and we finish together. I’m grateful I met you and start not only a professional experience, but a real friendship. To my “*french family*”, un grand merci à la famille De Pasquale et à Agnès Rudloff. Merci pour votre soutien pendant toutes ces années ! Of course, the huge motivation and strongness have come from the distance support of my *family*, gracias *Felipe Villarroel* y *Ana Rosa Márquez*. Este es el fruto de lo que ustedes sembraron. Muchísimas gracias por vuestro ejemplo, fuerza y amor. And to the one that spent his every-day life with my thesis and me...Gracias, *Clément*! Por tu paciencia, apoyo incondicional y optimismo. Sin ti, está claro que no hubiera sido posible.

*Table of Contents*  
&  
*Abbreviations*



# Table of Contents

|   |             |
|---|-------------|
| <b>ABSTRACT –RESUME.....</b>  | <b>ii</b>   |
| <b>Table of Contents&amp;Abbreviations .....</b>  | <b>xiii</b> |
| <b>-General Introduction- .....</b>   | <b>1</b>    |
| <br>  |             |
| <b>Chapter I.-Scientific Context.....</b>   | <b>5</b>    |
| 1 ORGANIC ELECTRONICS AND BIOELECTRONICS.....   | 7           |
| 2 IMPORTANCE OF ION SENSING AND DETECTION .....   | 9           |
| 2.1 ELECTRICAL SIGNALIZATION .....  | 9           |
| 2.2 METHODS .....   | 18          |
| 2.3 APPLICATIONS .....  | 30          |
| 3 DEVELOPPEMENT OF MATERIALS FOR ION-SENSING .....  | 35          |
| 3.1 CHELATORS .....   | 35          |
| 3.2 CONJUGATED POLYMERS: Thiophene derivatives & EDOT .....                                       | 40          |
| 4 SCOPE OF THE THESIS.....  | 46          |
| 5 BIBLIOGRAPHY .....  | 48          |
| <br>  |             |
| <b>Chapter II.-Ion-sensitive alternatives to PSS in PEDOT:PSS .....</b>                           | <b>55</b>   |
| 1 INTRODUCTION .....  | 56          |
| 2 SYNTHESIS OF STYRENE DERIVATIVES.....   | 57          |
| Cation affinity study .....   | 61          |
| 3 POLYELECTROLYTES: Copolymers between STFSI & the Ion scavengers modified styrene monomers ..... | 65          |
| 4 PEDOT based Ion-sensitive inks.....   | 70          |
| 5 CONCLUSION .....  | 80          |
| 6 EXPERIMENTAL PART.....  | 82          |
| 6.1 SYNTHESIS OF MATERIALS.....   | 82          |
| 6.2 CHARACTERISATION METHODS .....  | 86          |
| 6.3 NMR Spectrum .....  | 89          |
| 7 BIBLIOGRAPHY .....  | 94          |

|   |            |
|---|------------|
| <b>Chapter III.-Ion-sensitive EDOT and PEDOT derivatives .....</b>            | <b>93</b>  |
| 1 INTRODUCTION .....  | 95         |
| 2 MONOMERS .....  | 95         |
| Other synthetic routes .....  | 102        |
| 3 ELECTROCHEMICAL POLYMERS FORMATION .....                                    | 107        |
| Copolymerizations .....   | 113        |
| 4 ELECTROCHEMICAL CHARACTERIZATION.....                                       | 115        |
| 4.1 Potentiodynamic voltammetry .....   | 115        |
| 4.2 Potentiometric titrations.....  | 123        |
| 4.3 In-situ Conductivity Spectroscopy.....                                    | 125        |
| 5 CONCLUSION .....  | 129        |
| 6 EXPERIMENTAL PART.....  | 131        |
| 6.1 SYNTHESIS OF MATERIALS.....   | 131        |
| 6.2 Characterization methods .....  | 134        |
| 6.3 NMR Characterization .....  | 137        |
| 7 BIBLIOGRAPHY.....   | 142        |
| <br>  |            |
| <b>Chapter IV.-APPLICATIONS.....</b>  | <b>143</b> |
| 1 IMPROVING DETECTION OF $\beta$ -CELLS RECORDINGS WITH MEA .....             | 144        |
| 1.1 INTRODUCTION .....  | 145        |
| 2 STUDY OF THE CYTOTOXICITY OF GENERATED ION-SENSITIVE INKS .....             | 153        |
| 2.1 INTRODUCTION .....  | 153        |
| 2.2 CELL CULTURE & MORPHOLOGICAL STUDY .....                                  | 153        |
| 2.3 APOPTOSIS STUDY: Live/Dead Cell Imaging and Thapsigargin effect .....     | 154        |
| 3 I/V CONVERSION CARD: an OECT recording system adapted to $\beta$ -cell..... | 157        |
| 3.1 INTRODUCTION .....  | 157        |
| 3.2 I/V CONVERSION CARD: Installation and Testing.....                        | 157        |
| 4 ION-SENSITIVE OECT.....   | 160        |
| 4.1 INTRODUCTION .....  | 160        |
| 4.2 INTEGRATION OF THE ION-SENSITIVE INKS ON OECT .....                       | 160        |
| 4.3 ELECTRICAL CHARACTERIZATION AND ION SENSITIVITY STUDY .....               | 162        |
| 5 CONCLUSION .....  | 169        |
| 6 EXPERIMENTAL PART.....  | 171        |

|  |  |            |
|--|--|------------|
| 6.1  | Impedance and Capacitance characterization of MEA .....          | 171        |
| 6.2  | Cytotoxicity Evaluation: Apoptosis test-Thapsigargin effect..... | 171        |
| 6.3  | OECT CHARACTERIZATION AND TRANSLATION .....                      | 172        |
| 6.4  | OECT DEVICES FABRICATION .....                                   | 173        |
| 7  | BIBLIOGRAPHY .....   | 176        |
| <b>-General Conclusion &amp; Perspectives- .....</b> |  | <b>177</b> |
| <b>Chapter V.-APPENDICES.....</b>                    |  | <b>xvi</b> |
| 1  | MATERIALS AND INSTRUMENTATION.....                               | xviii      |
| 1.1  | CHEMICALS: .....   | xviii      |
| 1.2  | TECHNIQUES AND INSTRUMENTATION: .....                            | xviii      |
| 2  | TABLES .....   | xx         |
| 3  | Supplementary Information .....                                  | xxi        |
| 4  | Table of Figures .....   | xxxviii    |
| 5  | Bibliography.....  | xxxix      |



## ***LIST OF ABBREVIATIONS AND NOMENCLATURE***

|                     |   |
|---------------------|---|
| %vol                | Volume percentage   |
| %wt.                | Weight percentage   |
| Z*                  | Impedance (magnitude)                                     |
| °C                  | Celsius degree  |
| $\delta$            | Chemical shift  |
| $\mu\text{m}$       | micrometre  |
| <sup>13</sup> C-NMR | Carbon Nuclear magnetic resonance                         |
| <sup>1</sup> H-NMR  | Proton Nuclear magnetic resonance                         |
| ACN                 | Acetonitrile  |
| AcOH                | Acetic acid   |
| ADP                 | Adenosine Diphosphate                                     |
| Ag                  | Silver  |
| AIBN                | azobisisobutyronitrile                                    |
| aq.                 | aqueous   |
| ATP                 | Adenosine Triphosphate                                    |
| Au                  | Gold  |
| cAMP                | Cyclic adenosine monophosphate                            |
| CDCl <sub>3</sub>   | Deuterated Chloroform                                     |
| CE                  | Counter electrode   |
| CHCl <sub>3</sub>   | Chloroform  |
| CP                  | Conductive polymer  |
| CTA                 | Chain transfer agent                                      |
| DBSA                | dodecyl benzene sulfonic acid                             |
| DMF                 | N,N-Dimethylformamide                                     |
| DMSO                | Dimethylsulfoxide   |
| DNA                 | Deoxyribonucleic acid                                     |
| DPA                 | dipicolyl   |
| EDOT                | ethylenedioxythiophene                                    |
| E <sub>λ</sub>      | Half-cell potential                                       |
| E <sub>ox</sub>     | Oxidation potential                                       |
| EP                  | Peak potential  |
| E <sub>red</sub>    | Reduction potential                                       |
| ESI-HRMS            | Electrospray ionization-High Resolution Mass spectroscopy |
| f                   | Frequency   |
| F                   | Faraday   |
| f <sub>c</sub>      | Cut-off frequency   |
| FYTC                | Fluorescein isothiocyanate                                |

|             |  |
|-------------|--|
| G           | Conductance  |
| $g_m$       | Transconductance                                     |
| GOPS        | (3-glycidyloxypropyl)- trimethoxysilane              |
| HP-F        | Highpass filter                                      |
| $i$         | Current  |
| $I_D$       | Drain current  |
| ITO         | Indium tin oxide                                     |
| K           | kelvin   |
| $K^+$       | Potassium cation                                     |
| KATP        | ATP-sensitive $K^+$ channel                          |
| KCl         | Potassium chloride                                   |
| KDa         | Kilo Dalton  |
| $Kir_{6.2}$ | Inward-rectifier potassium ion channel 6.2           |
| LiBr        | Lithium bromide                                      |
| $LiClO_4$   | Lithium perchlorate                                  |
| LP-F        | Lowpass filter                                       |
| M           | Molar concentration (mol·L <sup>-1</sup> )           |
| MEA         | Microelectrode array                                 |
| MHz         | Megahertz  |
| Mw          | Molecular weight                                     |
| $N_2$       | Nitrogen   |
| $Na^+$      | Sodium cation  |
| NaCl        | Sodium chloride                                      |
| NAD         | Nicotinamide adenine dinucleotide                    |
| NADP        | Nicotinamide adenine dinucleotide phosphate          |
| nm          | nanometre  |
| NMR         | Nuclear magnetic resonance                           |
| OAP         | Operational amplifier                                |
| OCV         | Open circuit voltage                                 |
| OECT        | Organic electrochemical transistor                   |
| PaC         | Parylene - C   |
| ppm         | Parts per million                                    |
| PSS         | poly(styrene sulfonate)                              |
| PSTFSI      | poly(styrene sulfonyl(trifluoromethylsulfonyl)imide) |
| Pt          | Platinum   |
| RE          | Reference electrode                                  |
| rpm         | revolutions per minute                               |
| S           | Siemens  |
| s           | Seconds  |

|            |   |
|------------|---|
| SEC        | Size exclusion chromatography                   |
| SEM        | Scanning electron microscopy                    |
| $S_N^2$    | Bimolecular nucleophile substitution            |
| STFSI      | styrene sulfonyl(trifluoromethylsulfonyl)imide) |
| SUR        | Sulfonylurea receptor                           |
| SW-CNT     | Single wall- carbon nanotube                    |
| UV -Vis    | Ultraviolet-visible                             |
| V          | volume  |
| v          | Speed   |
| v/v        | Volume/ volume fraction                         |
| $V_{DS}$   | Bias source-drain                               |
| $V_{G(S)}$ | Bias gate-source                                |
| WE         | Working electrode                               |
| YFP        | Yellow Fluorescent Protein                      |
| $Zn^{2+}$  | Zinc cation                                     |
| $ZnCl_2$   | Zinc chloride                                   |



# *General Introduction*

*Biosensing* is a very large research field that involves the use of the basics of biology, chemistry and mathematics that we study from the high-school to try to understand mechanisms or interactions happening between different species, using devices that include at least one element of biological nature (life-science). Some examples of biosensors used in our daily life goes from food analysis, waste water treatment, glucose monitoring, blood tests, DNA analysis or cancer diagnosis.

One ramification of this field is known as *bioelectronics*, where the biological material interacts with an electronic system. First steps on this field have started with the stimulation of muscles and after years of development arrived the origin of Pacemaker devices. Nowadays, multiple recent efforts and important projects, mainly in neuroscience, have focused in exciting topics such as the *deep brain stimulation* that could improve treatments of Parkinson or epilepsy diseases, for example<sup>1</sup>.

Last examples find their origin in neuron cells mechanisms, but it exists other biological cells electrically active. One example are the pancreatic  $\beta$  cells. The failure in their normal-working mechanism is at the base of Diabetes disease. This is the reason why the understanding of the mechanisms that produce the sensing ability of this kind of cells has attracted the attention of an important electrophysiology community. Further this fundamental understanding, the information obtained from this biological material could be used in the future for the development of multiparametric artificial pancreas or for the quality control on clinical applications.

---

<sup>1</sup> See [1] Ashkan, K.; Rogers, P.; Bergman, H.; Ughratdar, I. Insights into the mechanisms of deep brain stimulation. *Nat. Rev. Neurol.* **2017**, *13*, 548–554, doi:10.1038/nrneurol.2017.105.

The main methods used today to record the electrical activity of pancreatic cells, present some drawbacks, the low amplitude with which is detected the electrical signals emitted by these cells being the most important, as well as the few specific information that they bring with them.

To overcome these issues, we looked into *organic electronics*, a field based on organic semiconductor materials (OSC) presenting advantages as a low-cost fabrication, lightweight or mechanical flexibility and that we can find today in our daily lives in smartphones and colourful screens (OLEDs), in flexible and portable solar cells (OPVs) or in transistors (“switches”) used in biosensors. One important advantage of these organic materials is that their molecular properties can be perfectly modified by chemical design.

In this thesis, this property was exploited to gain new active materials to integrate in a class of transistors, the organic-electrochemical transistors (OECTs), well known by their amplification power. We expect that the use of this approach could help to develop better systems more adapted to record the pancreatic cells activity. This manuscript is divided in four chapters.

In **Chapter I** are reviewed some fundamental notions of electrophysiology and the role of pancreatic  $\beta$ -cells in diabetes, as well as a brief description of the most important classes of materials developed in one hand on conducting polymers, and in the other, in supramolecular chemistry field, during last decades to introduce the general strategy applied during my thesis.

**Chapters II and III** describe the two routes used in this thesis to obtain chelates functionalized materials dedicated to metal cations  $K^+$ ,  $Na^+$  &  $Zn^{2+}$  (involved in the  $\beta$  cells activity), with the aim to use them as active components constituting the OECT devices to interface with pancreatic  $\beta$  cells for electrophysiological recordings. The synthesis and

structure-properties relationship of these materials is presented and discussed in each chapter.

A summary of the advances obtained during this thesis on different lines of this interdisciplinary research toward the gain of a more adapted  $\beta$ -cells recordings set-up is presented on **Chapter IV**. This includes the improvement of MEA recordings, the advanced work in a translation card development needed for OECT recordings, as well as the biocompatibility study and OECT integration of the synthesized materials.

Finally, the main findings of this thesis and an outlook are given in the **Conclusion & Perspectives** followed by the **Appendices chapter IV**.



*Chapter I.-  
Scientific Context*



## 1 ORGANIC ELECTRONICS AND BIOELECTRONICS

Organic semiconductor materials (OSM) is a type of carbon-based materials that exhibit optical and electronic properties. Research on these materials has known an important rise during the last two decades, mainly due to the industrial interest on applications such as the development of solar cells. This interest has allowed to develop other technologies such as the fabrication of smartphones screens, diodes or flexible displays [2].

The first organic conductive material, polyaniline, was described in 1862 by Henry Letheby [3]. Almost a century passed by until this research field gained the general interest of the scientific community [4] and only from 1970 onwards organic electronics start to be developed thanks to novel polymers similar to the polyaniline [5].

The OSM structure is based on the  $sp^2$  configuration of *carbon* atoms instead of *silicium* atoms traditionally used in electronics. And this family of materials are classified into two groups based on the weight, namely  $\pi$ -conjugated polymers and small molecules. In the small molecules semiconductors charge transport between molecules requires adequate overlap of the p orbitals on adjacent molecules. Such overlap generally occurs for conjugated molecules because the chemical bonding forces the structure to be planar. In the case of polymers, the  $\pi$ -electron system is delocalized along the backbone (the transfer integral between the p valence and  $\pi^*$  conduction bands can reach 1–3 eV). Thus, this delocalization promotes much easier intrachain charge transport, although interchain transport is still required for the usual size range of devices made using polymer semiconductors. To sum up, the common property is that they are  $\pi$ -conjugated systems. This means that they are characterized by the presence of double bonds forming a delocalized  $\pi$ - electron cloud. This conjugation is at the origin of their most characteristic properties, their electrical conductivity which falls between that of a conductor (such as metals) and an insulator (such as glass).

## *Ch. I.-Scientific Context*

In most of the cases, these materials have a low electrical conductivity. But their conducting properties can be modified by the controlled introduction of impurities (additives) into the crystal structure, a process known as “doping”, bringing them to a «doped» state allowing a better transport of electrical charges. In many examples, this transition between the two states (undoped and doped) is reversible because it occurs through a redox mechanism. Note that doping can be negative or positive depending on the nature (charge) of the dopant used. Moreover, the transition between these two states can be induced by ion exchanges between the semiconductor material and an electrolyte which is in contact with it [2].

As stated before, generally, organic conductive polymers present much lower conductivity than their inorganic alternatives. However, they present many other advantages. Their processability (possibility to deposit them on surfaces such as screens by printing) as well as their specific mechanical properties (i.e. flexibility) have allowed the continuous development and applications of new materials. It is important to note that one of these materials, poly (3,4-ethylenedioxythiophene), abbreviated as PEDOT, has gained a major attention due to its numerous advantages for the organic electronics [2,6]. All these properties and especially their “soft” nature makes these materials good candidates to interface with biological tissues, giving rise to a new impulses to the field known as *bioelectronics* [7].

Origin of bioelectronics can be found at the beginning of the 18<sup>th</sup> century when Luigi Galvani discovered that the muscles of dead frogs' legs twitched when struck by an electrical spark [8]. Nowadays, the field of bioelectronics includes a broad range of applications that goes from the medical devices to the detection of molecules in the context of environment protection. Relevant examples are the numerous patients that have seen an improvement of their quality of life thanks to devices such as cardiac pacemakers, cochlear and retinal implants or glucose sensors. Bioelectronics is now part

## *Ch. I.-Scientific Context*

of our daily life and has received a notable relevance in the media, either by science fiction or real scientific research advances [7,9].

The development of bioelectronics has seen exponentially increased mainly due to the advancement of material sciences. Indeed, as we can note from the few examples of applications previously introduced, several life-science studies used bioelectronics to measure or record electrical signals coming from the biological activity. This is the reason why electronic components interfacing biological systems have to allow the transmission of these signals in an efficient manner [7]. Moreover, challenges of today are notably related to the small amplitude of these signals, increasing the need of new materials to overcome this issue.

As it was already pointed, research using organic semiconductors materials, most particularly polymers, has increased exponentially during last years. The advantages of these materials, combined to their ability to reduce impedance or increase the life-time of many implants, make of them ideal candidates for use in the life-sciences, and especially in *Organic Bioelectronics* [7].

In this chapter, basic notions of electrophysiology and the role of pancreatic islet  $\beta$ -cells in diabetes will be introduced, as well as a brief summary of current methods used to monitor and treat this disease in order to understand the context and the methodology used in my project.

## **2 IMPORTANCE OF ION SENSING AND DETECTION**

### **2.1 ELECTRICAL SIGNALIZATION**

#### **2.1.1 Why are electrical signals important?**

Many major capacities of the human body are controlled by responses to different stimuli, being at the origin of several effects from movements to thoughts or dreams.

## *Ch. I.-Scientific Context*

This is possible via many biological events based on signal transmission between the different organs (i.e. senses, brain, heart... and the “actuation” members, such as muscles or endocrine organs). An important way of signal transmission is represented by the electrical signalization. This mode of signalization takes place in the biological medium through the exchange of ions through the cell membrane. The cell membrane forms the interface of the cell with extracellular medium and the other cells and organs. Moreover, the plasma membrane structures and protects cells as well as being the cell’s gate to exchange with its external medium.

Physiological behaviour of cells or organs as well as the whole body homeostasis requires a fast adaptation to the environment. Electrical signalling is rapid and can be fine-tuned. This requires ion fluxes across membranes. For that reason, cells and tissues have chosen (through millions of years of evolution) the ionic transport as one of the main mechanisms of adaptation and communication. This electrical communication forms the basis of such elementary functions as neuronal brain activity, heart-beat, muscle contraction or release of vital hormones such as insulin. In the next section, I will introduce a short explanation of the mechanism of these ion signalization and transport required to understand the context, the objectives and the work done in my PhD.

### 2.1.2 General description

The electrical properties of electrogenic cells come from the electrical properties of the plasma membrane. The plasma membrane is mainly composed of lipids and proteins. Thus, these membranes are insulators, via their lipid bilayers, meaning they have control over what molecules and electrical charges pass through or not. The movement of molecules across the membrane occurs by mechanisms that differ mainly in the need of energy requirements for this process: passive (no energy needed, as diffusion, relying on gradients such as ion channels) or active (requires energy, such as many ion transporters).

## Ch. I.-Scientific Context

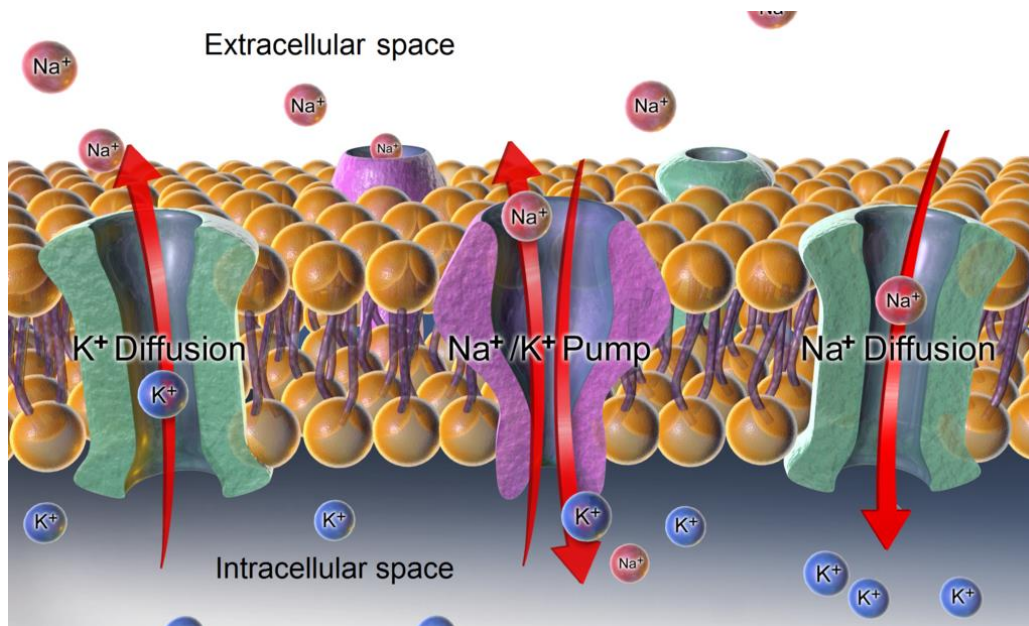


**Figure 1: Scheme of ion channels of the cell membrane: K<sup>+</sup>/ Na<sup>+</sup> Pump and Na<sup>+</sup> and K<sup>+</sup> ion channels** (taken from <https://blausen.com>)

A difference of potential exists between the interior and exterior of cells due to the existence of different ionic concentrations (electrochemical gradient) and the insulating capacity of the cell membrane. In other words, there is a disequilibrium between mediums separated by this membrane mainly due to the activity of the pumps (i.e. extracellular concentration of cation K<sup>+</sup> in mammals cells is <5 mM and of 70-150 mM in the intracellular medium). This difference of charges gives origin to a difference in potential across the cellular membrane (“transmembrane potential”). For a better understanding, we can first consider the movement “up” or “down” of an object with mass between two points of different gravitational potential. Because the lipid membrane is a good insulator, the transmembrane potential remains constant as long as ion-conducting pores or channels remain closed. However, when one (or several) of these pores or channels opens, the ensuing flow produces a deviation from this disequilibrium and the difference of potentials between extracellular and intracellular potentials tends to be reduced i.e. to get closer to 0 mV, because a charged object (ion) gains or loses energy as it moves between places of different electrical potential.

## *Ch. I.-Scientific Context*

Cells trends to recover their “steady-state” (which is in fact based on a disequilibrium in regard to intra- versus extracellular space), that means they tend to recover the initial gradient concentration. In electrogenic cells this recovering of membrane resting potential occurs by the passing of ions by “pumps and transporters”, proteins present in membranes (plasma membrane as well as intracellular membranes of organelles), which harness a chemical energy (such as ATP hydrolysis) to move ions across membranes and against a gradient. As example, we can consider one of the most important pumps, the Na<sup>+</sup>/ K<sup>+</sup> -ATPase. Indeed, two cations of the same charge (Na<sup>+</sup> and K<sup>+</sup>) flow through this “tunnel” structure against their gradient concentration (three cations of Na<sup>+</sup> leaves and two cations of K<sup>+</sup> enters the cell) to re-establish the basal level. As it can be noted, moving these cations against their concentration gradient requires energy which is provided by hydrolysis of ATP. This ATP, a molecule rich in energy, is generated via the catabolic metabolism of lipids or sugars.

In addition, it is important to take into account that each type of ion has a different equilibrium potential, as each type of ion is distributed at different concentrations across the membrane. This fact is at the origin of the depolarizing or hyperpolarizing effects of the different voltage-dependent channels. These channels, also known *as voltage-gated*, are activated when a defined change in membrane voltage happens in excitable cells. Their opening leads to a flow of ions towards the inside or the outside of the cell (according to their concentration gradient) which consequently hyperpolarizes or depolarizes the plasma membrane.

## Ch. I.-Scientific Context

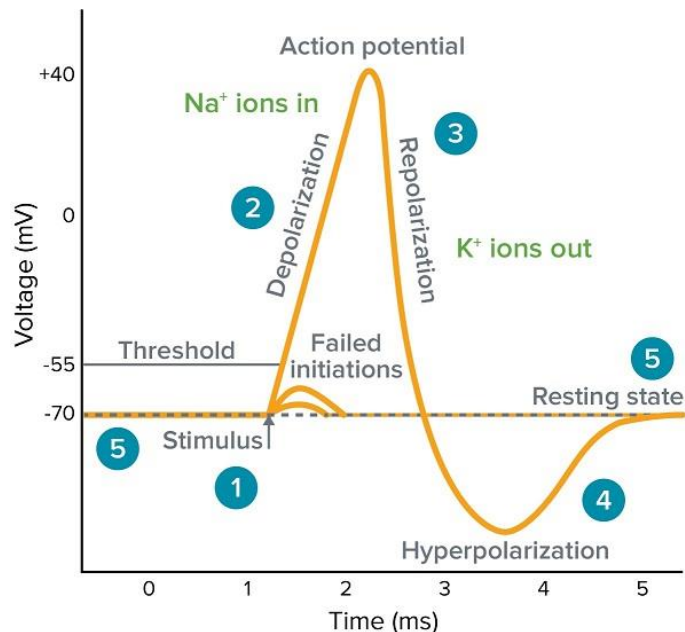


**Figure 2: Scheme of AP formation:** **1)** A Stimulus arrives at the cell, for example a change in voltage. If it has the intensity needed to overcome the threshold voltage of depolarizing voltage-gated channels (Na<sup>+</sup> in this case), the latter open; **2)** This induces a depolarization of the plasma membrane; **3)** The inactivation of depolarizing channels and the opening of repolarizing ion channels permeable to K<sup>+</sup> repolarizes the plasma membrane **4)** In some cells the membrane potential goes beyond the desired potential producing a hyperpolarization. **5)** The membrane recovers its resting state until the arrival of a new stimulus. (Reproduced from <https://www.moleculardevices.com>)

Cycles of depolarizations and repolarizations/hyperpolarizations happen in electrically excitable cells (or electrogenic cells) due to activation and inactivation sequences of different voltage-gated ion channel families as illustrated in Figure 2. This gives as a result characteristically shaped electrical signals (periodic potential changes) known as *Action Potentials* (APs) that can propagate along the cell membrane. Sequences of APs in bursts encode cellular information by patterned ion fluxes implying on downstream effects that differ depending on the cell type. As example, neurons communicate by propagation of these signals through their axons and the effect is the transmission of information from one cell to another via synapses. Most synapses release chemical compounds that activate or inactivate the next (postsynaptic) cell (chemical synapses). In some organs in

## *Ch. I.-Scientific Context*

the immature fetal nervous system and in invertebrates, the transmission of the electrical activity occurs by diffusion through gap junctions. An example is the electrical synapses, which let pass small molecules (ions, ATP, etc.). Such gap junctions also play a major role in cardiomyocytes, where the synchronisation of APs via gap causes the heart to beat in a synchronized fashion. A similar mechanism in pancreatic islet beta-cells synchronizes insulin secretion.

Electrically encoded processes are vital processes requiring a rapid reactivity of the organism to adapt to the different stimuli from the environment. For example, in case of hypoxemia, propagation of electrical signals from a special sensor at the carotids and subsequently through corresponding neurons happens instantaneously to send the “order” to the respiratory system to increase the ventilation and heart frequency.

Other electrogenic cell, such as the  $\beta$ -cells, are found in the endocrine cells responsible of insulin secretion. To understand the major role of this hormone, it is important to notice that it is the only hormone of the body able to decrease the blood sugar level. The regulation of the physiological role of these cells is achieved by coupling metabolism mechanisms to insulin secretion. Arrival of nutrients and their metabolism in  $\beta$  cells generates coupling factors, mainly a change in the ATP/ADP ratio, that governs certain ion channels, the nucleotide sensitive  $K_{ATP}$  channel, which allows to translate changes in metabolism in an electrical signal (via the regulation of ion channels). This electrical signal provokes the opening of voltage-dependent calcium channels, influx of calcium which finally triggers insulin secretion. The basic mechanisms is thus similar to the one at the synapses, only that in the case of  $\beta$ -cells nutrients are the stimulus and not neurotransmitters but insulin is released. Failure or lack in adaptation of  $\beta$ -cells to the demands of the body is at the origin of diabetes, and provokes severe health problems in other organs (heart, kidney, eyes) and increases morbidity.

### 2.1.3 $\beta$ - Cell

$\beta$ -cells are the main component of the pancreatic islets in most species including mammals. The latter are endocrine micro-organs that are embedded in the pancreas. The mature *Islets of Langerhans* are formed of several types of endocrine cells (secreting hormones in the blood circulation). The insulin-secreting  $\beta$ -cells represent 50% - 60% of islet cells in human and up to 90% in rodents (Figure 3) and having an average diameter of 13-18  $\mu\text{m}$  [10]. Insulin is stored in crystalline form in the secretory vesicles as  $\text{Zn}_2\text{-Insulin}_6$  complex and it represents 5%-10% of the total protein content in the  $\beta$ -cells. These vesicles fuse with the membrane upon an increase in nutrient metabolism (that is when more nutrients are available, such as after a meal) via metabolism-secretion coupling (see above). The vesicle content, insulin, is released in the blood stream by exocytosis.

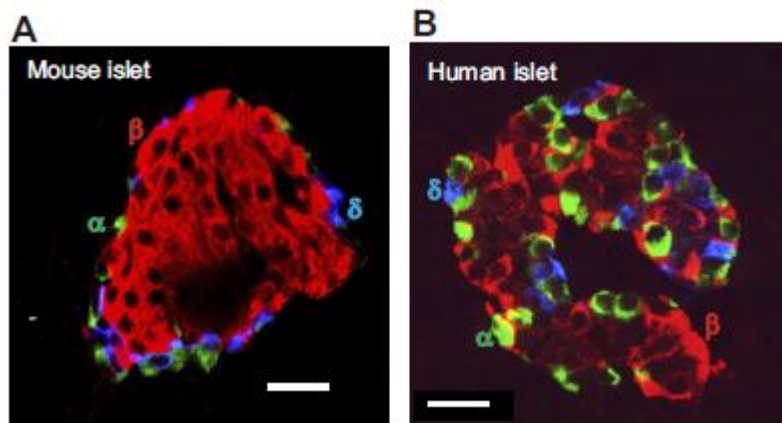


**Figure 3: Histological comparison of Human and Mouse Pancreas:**  $\beta$ -cells (in red), secreting insulin;  $\alpha$ -cells (in green), secreting glucagon, a hormone that increases blood glucose such as in between meals;  $\delta$  (in blue), secreting somatostatin (adapted from [11]).

Physiologically, insulin is released following food ingestion. However, only a few nutrients are able to produce the insulin secretion per se. This is why they are known as “initiators” of insulin secretion, they are sugars, lipids and some amino-acids. Secretion can also be stimulated pharmacologically by drugs (i.e. the antidiabetic sulfonylureas acting on components of the  $\text{K}_{\text{ATP}}$  channel). Other factors enhance the release of insulin, but only

## Ch. I.-Scientific Context

in presence of the “initiators”, so they are called “amplifiers” of insulin secretion (i.e. gut hormones and neurotransmitters)[12,13]. Other neuro-hormonal signals such as adrenaline and noradrenaline inhibit insulin secretion in order to preserve elevated glucose during stress or physical activity. This permits to take into account not only the arrival of food but also the physiological situation of the entire body and a corresponding adaptation to the specific demands of the situation.

Glucose induced-insulin secretion (GIIS) follows a biphasic profile, with a first transient phase (1st phase) followed by a slower, long-lasting phase of lesser amplitude (2nd phase) [14] (Figure 4). These two phases are necessary as insulin will first go to the liver, where a large amount is retained and insulin will only subsequently reach other peripheral organs. In pharmacological terms, the first phase represents a loading dose (saturating the insulin receptors in the liver) and the second phase is a maintenance dose (for the periphery and keeping levels up). It is well known that this GIIS needs the metabolic degradation of the sugar and an increase in intracellular ATP. But *how is Glucose coupled to insulin secretion?*

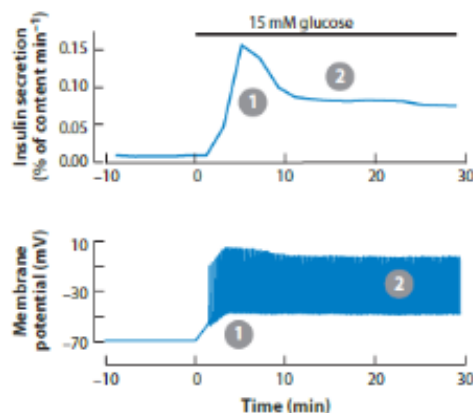


**Figure 4: *Insulin secretion triggered by the glucose-induced electrical activity:*** Biphasic profile of the AP bursts and the insulin secretion (adapted from [11]).

Glucose, a polar molecule, enters the  $\beta$ -cell via the Glut2 transporter, and the ensuing metabolic breakdown of the sugar leads to extraction of energy through the generation of ATP at the expense of ADP. This results in the plasma membrane in the closure of the

## Ch. I.-Scientific Context

$K_{ATP}$  channels (see Figure 5), a specific  $K^+$  channel that can sense the changes in ATP and ADP. This closure leads to membrane depolarization and initiation of the electrical activity (Figure 2 and bottom of the Figure 4). Action potential firing is dependent on the opening of voltage-gated calcium channels, and the resulting increase of calcium concentration inside the cells triggers exocytosis of insulin granules, as it is illustrated in Figure 5. Insulin travels via the blood stream to its target organs. As a result, glucose levels in the blood decreases as insulin controls several mechanisms in the target cells. It increases glucose transport into the muscle and adipose tissues[15] thus reducing glucose in the blood stream. In the liver, it reduces regeneration of glucose (neoglucogenesis) and promotes storage of sugars newly arrived from a meal. To achieve this, insulin controls a signalling pathway: it activates a protein called AKT (also known as Protein kinase B, PKB) which inhibits the rate-controlling enzymes of gluconeogenesis resulting in the promotion of glycogen synthesis[16,17]. Glycogen is the main repository for glucose uptake in the liver. When glucose concentration returns to lower (“normal”) levels, glucose metabolism in  $\beta$ -cells is decreased, which decreases ATP levels in the cell and  $K_{ATP}$  channels are reactivated (reopened) and thus switching off insulin secretion. This mechanism provides a feedback regulation of insulin secretion.

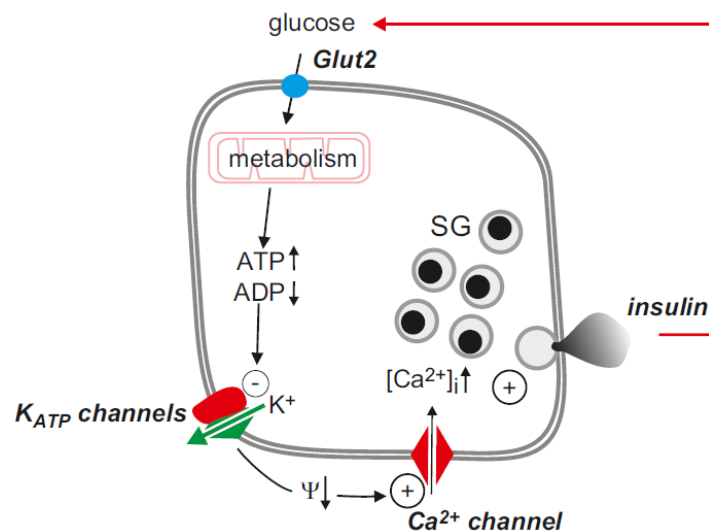


**Figure 5: Scheme of the model of GIIS:** The signs (+) indicate a stimulation and (-) an inhibition. And the arrows ( $\uparrow$ / $\downarrow$ ) indicate an increase or a decrease of the indicated parameter (reproduced from [11]).

## *Ch. I.-Scientific Context*

$\beta$ -cell dysfunction can be due to ion channels mutations. For example, mutations in the  $K_{ATP}$  channels (in subunits  $K_{ir}6.2$  or SUR1) produces hyperinsulinism, due to a permanent membrane depolarization and persistent insulin release. Thus, discrete changes in protein structure can produce important changes in the activity of the channel, and lead to disease.

The description above of the ion channels involved simplifies the biological situation. The properties of activation or inactivation of every voltage-dependent channel are intrinsic to the channel and depend on the molecular characteristics of the channel, which is dictated by the existence of different proteins isoforms. For example, 10 different types of voltage-gated calcium channels (VGCC) exist in mammals, and they have different functions in cellular signalization. Activation of these VGCCs allows entry of calcium to the cell and results in different effects depending of the type of cell, some examples are the opening of potassium or sodium channels, muscle contraction or gene expression [18].

Although we have mainly focussed our discussion here on potassium channels, sodium channels and corresponding fluxes are also involved in the depolarisation of electrogenic cells in general and islet  $\beta$ -cells in particular. Thus to fully monitor and evaluate the electrical signalling in these excitable cells, a more precise view of several different ion movements through channels is of great help. Therefore, it will be important not to observe only the overall changes in total ion concentration, but to have a precise view on the changes in the different ion species, for example  $K^+$  and  $Na^+$ .

## **2.2 METHODS**

In this section, I will describe several methods used to the study the physiology of pancreatic  $\beta$ -cell and diabetes.

## *Ch. I.-Scientific Context*

The possibility to study pancreatic islets in a non-invasive and fast way could represent noteworthy advantages in many aspects. Some examples are the quality control of the function of an organ previous to transplantation as well as the pharmaceutical studies that could be run on real-time on the organs to develop effective medical treatments. A last example, but not least, could be found on the monitoring of the differentiation process of the stem cells[19] which implies a maturation also of the signal transduction machinery and consequently of the glucose-induced ion fluxes. This approach appears as a promising option to advance the use of stem cells derived  $\beta$ -cells in diabetes therapy, especially in type 1 diabetes where most of endogenous cells are lost. Islet cell transplantation is an established therapy in very severe cases of type 1 diabetes, but precise quality controls of the transplanted material is lacking[20]. Transplantation always depends on the (scarce) availability of organs. In the future, it may be also possible to replace organ function by newly generated organs. The procedure may begin with any cell or cell population and convert it directly into enough beta cells to treat a patient, starting with easily obtained blood cells or skin cells and manipulate their gene expression with sufficient specificity to convert them to functional  $\beta$  cells [21]. Here again, it would be of great help if the development of specific ion currents, as encountered during the differentiation of these cells to  $\beta$ -cells, could be monitored directly.

In conclusion, many applications depend on the better understanding of the complex regulation systems and the possibility to record them in real-time.

We can differentiate intracellular approaches, being invasive, and extracellular or non-invasive methods. I will focus on the techniques used for the study of Islets cells.

### 2.2.1 “Probes” methods: Fluorescent and genetic techniques

Optical methods have allowed the study of metabolic oscillations and important secondary messengers such as the calcium or cAMP. These techniques are based on the use of fluorescent protein probes which are load inside the cells to interact with an

## *Ch. I.-Scientific Context*

analyte. First probes conceived were organic calcium fluorescent indicators[22] and their development together with that of fluorescent probes motivated the attribution of the Nobel Prize of Chemistry in 2008 to several researchers and notably Roger Tsien. Since then, continuous improvements were obtained, allowing to detect activity in the cellular and subcellular compartments using derived organic or specialized fluorescent proteins directed only to specific parts of a cell. In the  $\beta$  cell study, these probes have helped in the elucidation of multiple oscillatory signals, such as the changes on intracellular calcium concentration or the metabolic activity (i.e. NADH / NAD(P)H, mitochondrial respiration, etc.).

### *2.2.1.1 Organic fluorescents Probes*

Regulated secretion is an essential biological process that operates in numerous secretory cells. Understanding secretory cells including neurons, endocrine cells, and exocrine cells governing regulated mechanisms is not only an important topic in basic biological and biomedical research, but may also offer insights to facilitate development of effective treatments for human diseases by defective secretory activity[23,24]. Due to the high sensitivity of fluorescent sensors, they have been the target of many synthetic groups developing new probe engineering to apply in bio-imagery. One example is the fluorescent zinc indicator, ZIMIR, used for monitoring  $Zn^{2+}$ /insulin release[25]. A drawback of these techniques is, on the one hand, the need of highly accurate instruments, including a light source to produce the probe excitation, which will also heat the samples and, thus, damage them in the long runs. On the other hand, as in every fluorescent method, recording time is limited by the photobleaching of the probe and generation of toxic radicals. This limits exposure time and inherent difficulties in equipment and data transfer (for camera to chip, i.e.) also restrict the frequency of images taken. This temporal resolution currently less than 100 Hz, severely limits monitoring of fast events. Another important drawback is that this technique remains difficult to miniaturize and, therefore, not easily complies with being this important requirement in biosensors development.

## *Ch. I.-Scientific Context*

### *2.2.1.2 Genetic Probes*

Genetic probes are based on incorporation of a transgene to the studied animal or cell as a reporter and monitoring the gene expression profiles of pancreatic  $\beta$ -cells under several genetic or chemical perturbations. This technique has shed light on genes and pathways involved in disease. Some research projects where have developed functional beta cells, or even islets, that could be used for drug screening[26–29]. These screens would likely include a search for compounds that increase the survival of beta cells, improve their insulin secretion and could therefore be used in patients where there is no immune component (i.e. Type 2 diabetes). However, an important challenge remains to overcome immune attack of transplanted tissues (especially in a patient where the immunity system attacks its own  $\beta$  cells, such as in type 1 diabetes).

One approach to overcome such immune attacks is to genetically modify stem- $\beta$  cells, making them unrecognizable by the immune system[30]. In the longer term, it should be possible to determine the source and classes of immune cells that are responsible for the autoimmunity, elucidating ways to eliminate them or block their activity by combining genetic modifications with cell transplantation.

Even though these genetic probes are powerful methods in the  $\beta$  cell study, they have some drawbacks. Indeed, introducing novel genes in transplantable cells may rise ethical considerations and safety issues. It remains extremely difficult to exclude unwanted insertions or other side effects as a result genetic modifications. Moreover, even if genetic manipulation is advancing at an impressive pace (reviewed by La Russa and Qi, 2015), it is not presently possible to accurately rewire thousands of genes [31].

## 2.2.2 Electrophysiology

Many of the electrophysiological techniques have been developed initially in the study of neurons and muscles. Here I will introduce techniques used to study specifically the electrical activity of Islet cells and their main advantages and drawbacks.

We can distinguish between intracellular (invasive) techniques, the sharp or patch-clamp, and extracellular (non-invasive) methods, the use of MEA (*Microelectrodes Array*) or more recently the OECT (*Organic Electrochemical transistor*) devices. Note that the use of the latter is still very novel and only few successful approaches at the cellular level have been published.

### 2.2.2.1 Recordings with intracellular electrodes

- **Sharp microelectrodes**

Membrane potential recordings were the first method classically used to study pancreatic islets by the use of sharp intracellular microelectrodes.[11,32] They recorded changes in membrane potential and electrical activity. Main drawbacks of this technique are the great risk of current leaking when the electrode is impaled into the cell and the high resistance of the electrode (because of its sharp shape). Thus, the difference in potential observed is due to the global activity in the neighbourhood of the electrode, which does not allow the analysis of single or just a few channels.

- **Patch-clamp**

This is another method of measurements of membrane currents or voltages with a glass micropipette (larger than sharp) which is filled with an ionic solution of well-known concentrations. A seal with a resistance  $>1 \text{ G}\Omega$  is obtained between the electrode and the plasma membrane, thus limiting the leak of currents. Several configurations are possible permitting whole-cell measurements in voltage-clamp and current-clamp as well as investigations at the single channel level. This technique

## Ch. I.-Scientific Context

constituted an unprecedented improvement and opened the molecular functional analysis of ion channels, reason why the Nobel prize in Medicine and Physiology in 1991 was given to Erwin Neher and Bert Sakmann, who pioneered this approach[33]. The invasive nature of this technique excludes its exploitation in long-term recordings and the different configurations could influence the ion channel under study. In addition, it doesn't allow to have a complete picture of what happens in the whole Islet (i.e. couplings between the different kind of cells, obtained by extracellular recordings, are illustrated in Figure 6) because data are obtained in single cells.

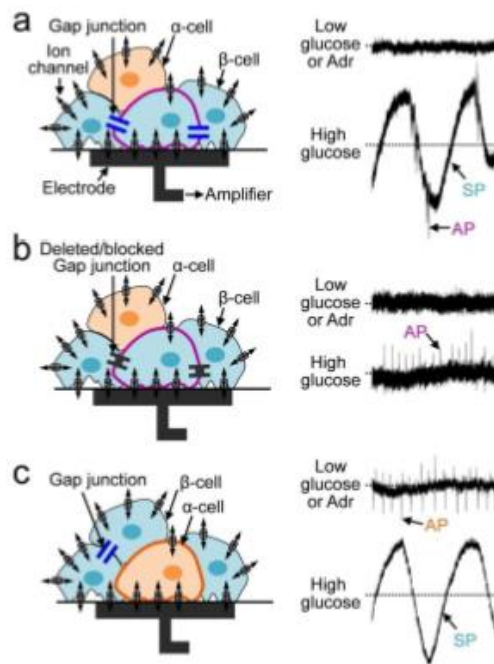


**Figure 6: Electrical signals due to individual cell activity or to different types of coupling between cells. Left:** Scheme of an electrode covered with pancreatic islet ( $\beta$ -cell in blue,  $\alpha$ -cell in orange). **Right: a)**  $\beta$ -cell signalling, presenting high frequency signals, the characteristic *action potentials* (AP) overlapping with the *slow potentials* (SP), lower frequency wavy multicellular signals due to coupling with other  $\beta$ -cells under high glucose concentration (stimulus); **b)** Suppression of junctions on  $\beta$ -cells doesn't allow the couplings, recording only individual cell signals, the AP; **c)**  $\alpha$ -cell signalling, presenting characteristic AP only under low concentration of glucose or adrenaline stimulation, not appearing overlap with the SP at high glucose concentration (taken from [34]).

### 2.2.2.2 Extracellular recordings

Major examples of extracellular monitoring are the electrocardiogram (ECG) or the electroencephalogram (EEG). These techniques allow to record the electrical activity without any previous modification of the cells and allow long-term recordings as a non-invasive technique, meaning that cells are not affected[19]. Another general property of electronic components is their capability to be miniaturized, an important aspect in the development of future devices and specifically in implants.

- **MEA**

A device invented by Thomas et co. [35], the *Microelectrode Array* (MEA) has been often used for extracellular recordings, mainly in the neurosciences. Even if it appeared for the first time 30 years ago, it found finally its important role during last decade on the bioelectronics field. This device is constituted by a large number of electrodes integrated on a flat substrate, normally glass. It is compatible with cell culture and allows the recording of field potentials, which reflect the differences in potentials close to the electrode. This gives access to electrical signals of weak amplitude produced by the ionic fluxes corresponding to biological activity (i.e. Figure 6). This method enables doing long-term recordings (hours-days) in a non-invasive way[36].

Even though the several advantages of this technique, one major issue is the low signal-to-noise (S/N), mainly due to the small size of the electrodes which results in recordings with a large noise. Moreover, amplification of the recorded signal is performed at distance from the electrode and the wiring necessary will forcibly increase the noise. Consequently, detection of biological events becomes complex due to their weak amplitude and the presence of high noise levels. This problem was addressed recently by the use of an intermediate layer of a semi-conducting polymer on the surface of the electrodes, allowing a considerable improvement of the S/N ratio [37]. Nevertheless, signals were still amplified at distance from the electrode.

## Ch. I.-Scientific Context

Moreover, the recordings obtained give only a global image of the electrical activity, without allowing to know the precise contribution of distinct ions (and their channels) involved in the biological events.

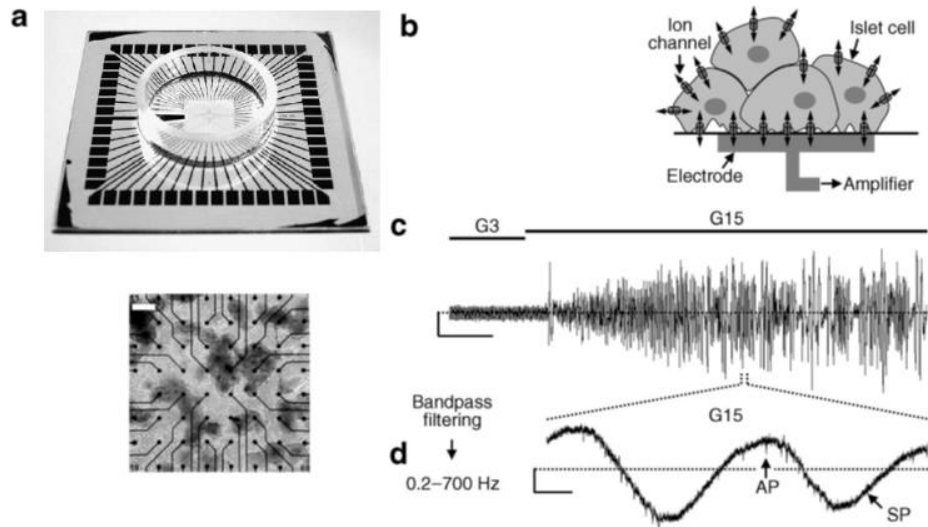


**Figure 7: Microelectrode Array (MEA): a)** MEA device (32 electrodes, MCS) (top) and the same device with cultured of pancreatic islets on it (bottom); **b)** Scheme of the  $\beta$ -cells cultured on one electrode of the MEA; **c)** Electrophysiological recording of the electrical activity with MEA: no activity at low concentration of Glucose (G3, [Glucose]=3 mM) and high intensity of activity under glucose stimulation (G15, [Glucose]=15 mM); **d)** Characteristics signal of the electrical activity of  $\beta$ -cells: Actions Potentials (AP) corresponding to individual cells activity and Slow Potentials (SP) giving information of global response of the islet.

- **OECT**

The first **O**rganic **e**lectrochemical **t**ransistor (OECT) was described by White and co-workers[38]. This device was constituted by gold electrodes and a poly(pyrrole) channel. OECTs take benefit of the mixed character of organic semiconductor materials conducting electrons as well as ions. This kind of devices has attracted great interest in biosensing for several reasons. Transistors amplify signals close to the

## Ch. I.-Scientific Context

source and thus reduce noise levels as compared to metal electrodes and their amplifiers. Moreover, these OECTs can work in aqueous media, a prerequisite for any application to a biological sample.

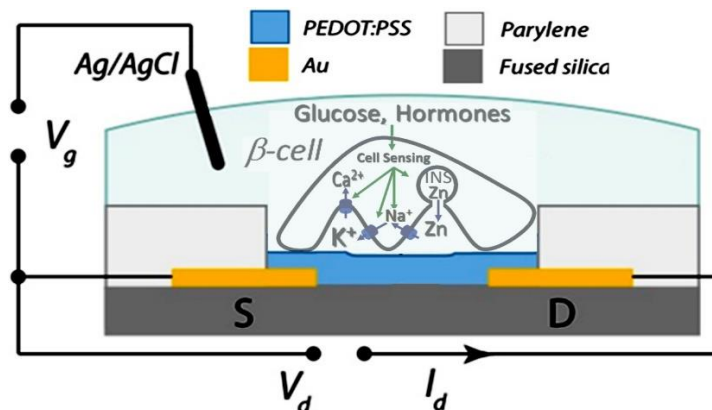


**Figure 8: Scheme of an organic electrochemical transistor (OECT):** A bias is applied between two electrodes, source and drain, which are connected by a channel, constituted of an organic semi-conductor, usually PEDOT:PSS. This channel is in direct contact with an electrolyte where is immersed a third electrode, the gate electrode, i.e. Ag/AgCl electrode. [Adapted from G.G. Malliaras group]

As shown in the Figure 8, this kind of transistor is constituted by two electrodes, called source and drain. Between them a channel is placed which is made of semiconductor material. The semiconductor is traditionally based on a p-type material, even if more recently McCulloch and co-workers have shown the use of a n-type polymer also provides OECT behaviour[39]. Except for recent developments, the most used material during last decade has been PEDOT:PSS. This is a complex between the semi-conductive polymer poly(3,4-ethylenedioxythiophene) doped with poly(styrene sulfonate), a polyelectrolyte with sulfonic groups that plays the role of stabilize the quinoid conformation of PEDOT (for more details see PEDOT:PSS structure, section 3.2.1 of this chapter, Figure 16). In its oxidized state, PEDOT:PSS is conductive due to the presence of “holes” allowing the movement of electrons along the conjugated backbone[40].

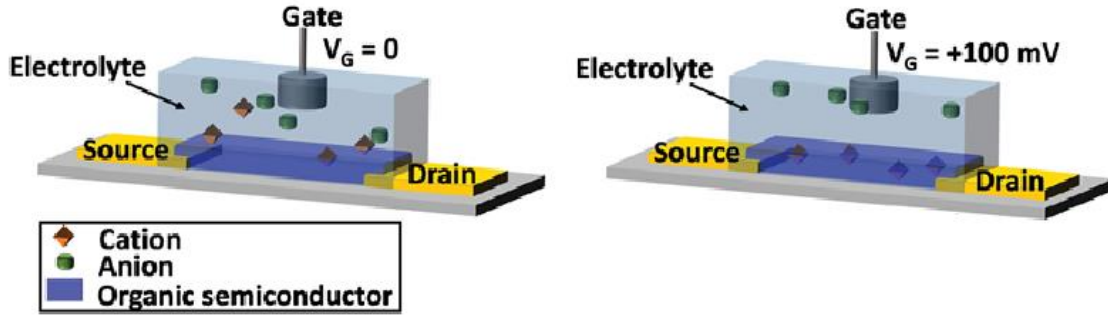


**Figure 9: Scheme of the working mechanism of an OECT: Left:** No application of a gate voltage. **Right:** Application of positive gate voltage [40]

In an OECT, drain current is modulated by the presence of cations in the electrolyte solution where is immersed the gate. When a positive voltage is applied to the gate electrode (Figure 9-right), cations from the electrolyte due to an electrostatic repulsion diffuse through the electrolyte and penetrate into the polymer matrix. Consequently, a balance of charges with the polyelectrolyte  $PSS^-$  takes place, producing the reduction of PEDOT as it is shown in *Equation 1*:



( $M^+$  represents the cations from the electrolyte).

Consequently, drain current is decreased due to the non-conductive character of this reduced state ( $PEDOT^0$ ). This working mode is known as “depletion mode”[41].

Two important characteristics to define an OECT are the transconductance ( $g_m$ ) and the response time ( $\tau$ ). The transconductance is the modulation of the current in the semiconductor material (channel) as a function of the variation on the applied gate potential. As it is expressed on *Equation 2*, it reflects at which gate voltage ( $\delta V_G$ ) we obtain the bigger change in current ( $\delta I_D$ ), so, it relies with the amplification power of the OECT.

$$g_m = \frac{\partial I_D}{\partial V_G} \quad \text{Equation 2}$$

## Ch. I.-Scientific Context

The response time ( $\tau$ ) measure the change speed of the current in the semi-conductor[40]. The time required for the movement of ions impose a maximal speed of working to the transistor in analogy to the speed limit for a resistance-capacitor circuit (RC). Response time is limited so by the movement of ionic species, considered traditionally as a long process ( $t = 1 - 100$  ms). Nevertheless, recent studies have shown that it is possible to measure with a short delay of only  $20 \mu\text{s}$  between the input voltage at the gate and the measurement of current at the drain. This response time is sufficient to do biological recordings, because it is obtained a signal that retains until a 90% of its final value at the semi-conductor[40].

It is of interest to note that also ionic liquids or gels have been used as electrolytes to develop OECT devices, exploring new pathways through enzymatic electrochemical sensors[42].

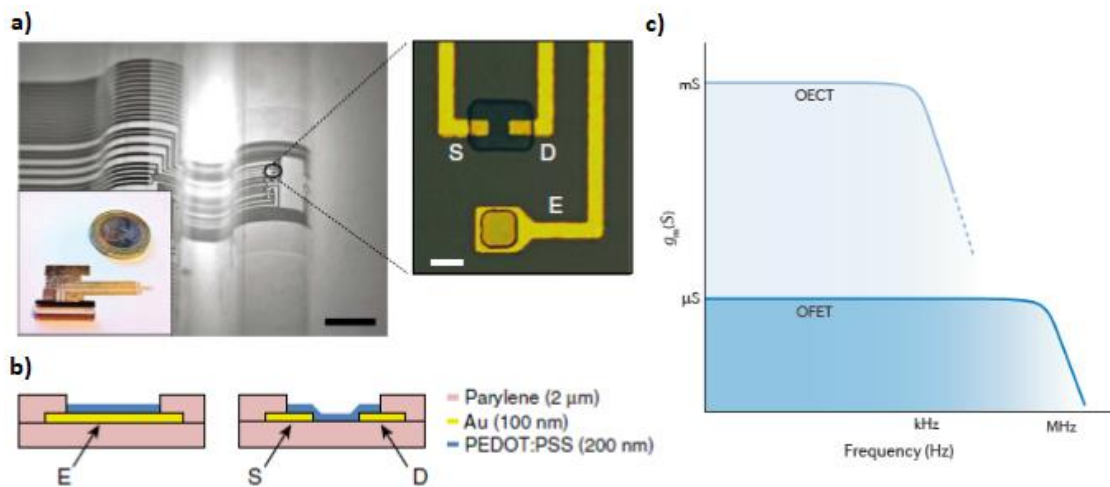


**Figure 10: Summary of structure and characteristics of OECT vs other devices: a)** Image of a “multidevice” platform. The image reflects the conformability and mechanical resistance of the devices. *Inset:* Zoom to one OECT (S: source electrode; D: drain electrode, E: Electrode); **b)** Scheme of the electrode (left) and the transistor (right) showed in a). Both devices have similar dimensions[43]; **c)** Comparison of the amplification power of an OECT (light blue) against an OFET (dark blue) (adapted from [44]).

The use of OECT devices could be extended to many applications due to their large range of advantages: low-cost fabrication (printability), flexibility and their interesting

## *Ch. I.-Scientific Context*

and unrivalled properties (large input impedance, low working voltage)[45]. Moreover, it has been demonstrated that OECT go further than the traditional field-effect transistors (FETs or OFETs). In the latter the superficial active area is confronted with the bulky effect on the former (along all the volume of the semi conductive active material). This results in a much higher amplification power in the case of the OECT (higher transconductance,  $g_m$ ) in all the range of frequencies interesting for biological recordings (Figure 10-c).

Moreover, these devices appear to be an interesting alternative to MEAs mainly due to their amplification abilities and the potential to chemically alter the polymers. In fact, Hsing and co-workers have recently demonstrated their efficacy in the study of cardiomyocytes, monitoring cardiac spikes with an average signal-to-noise (S/N) ratio record of 4-10 [46].

Nevertheless, it is important to note, that in contrast with MEA, this kind of devices stays still a very recent technology, with all the issues that go along with it: they are not commercially available, require a high technicity (preparation, recordings, electrical analysis), numerous aspects are still not thoroughly characterized in biological, chemical and physical terms, and only systems with high-amplitude signals (heart, neurons) have been studied.

## 2.3 APPLICATIONS

Tall these efforts open new applications in a number of fields. Indeed, there is a general demand for highly sensitive chemical and biological sensors such as environmental monitoring, medical analysis, healthcare products, food safety tests, agriculture industry, and security. A chemical sensor can be used to obtain an analytically useful signal of a system by measuring its chemical information (from the concentration of a specific component to total composition analysis) and values may relate to the chemical reaction of an analyte or a physical property of the system investigated. A biological sensor is an analytical device for the detection of biological analytes, such as proteins, DNA, antibodies, enzymes, tissues, micro-organisms, etc. based on physicochemical measurements. Here will be present few examples of increasing relevance for our research.

### 2.3.1 Basic Research

Biomedical research aims to provide novel therapies and a major goal is the generation of a large amount of high-quality analytical data in non-transformed primary (“physiological”) cells or micro-organs. This market for research and for industrial pharmacological/toxicological/environmental screening is considerable as ion channels constitute major drug targets due to their central role and easy accessibility to molecules from outside the cell[47,48]. The global ion channel modulator market amounts to about 10 billion US \$ and expansion is limited due to poor understanding of targets and complex assays required[49].

### 2.3.2 Environmental analysis

It is notable that OECT-based sensors have shown excellent performances in aqueous environments and are thus suitable for *in situ* measurements. In fact, there are recent examples of their use in humidity, pH or H<sub>2</sub>O<sub>2</sub> detection. Therefore, sensitivity, stability, selectivity, and architecture (e.g. miniaturization) of the devices can be

## *Ch. I.-Scientific Context*

optimized by choosing more suitable fabrication techniques and materials for both the active layers and the electrodes of the devices.

### 2.3.3 Phenotyping, disease, iPSC

Important progress has been obtained in the development of microfluidic devices and cell printing to provide microphysiological “Organ-on-Chip” configurations for evaluations closer to physiology[50,51] of complex organ-level functions, clinically relevant disease phenotypes and pharmacological/toxicological responses[52]. This also permits to overcome restrictive animal welfare regulations or poor correlations between rodent and human physiology.

Many organs, such as brain or islets, are not amenable to tissue biopsies in patients (except in the case of cancer). Patient derived stem cells (iPSCs) and their differentiation to surrogate organs with a genetic profile identical to the patient’s ones, are already used in a few instances as a very powerful tool to understand the role of patient’s genetic alterations on organ function. Monitoring approaches such as OECT in combination with patient derived stem cells (iPSCs) may provide unique opportunities for diagnostics and even personalized therapies.

The global Organ-On-Chip market is predicted to grow annually by around 70% to approximately \$6.13 billion by 2025[53]. However, capturing “native” signals without chemical or genetic modifications remains a major impediment especially in view of the small sample and analyte volume. Moreover, assays must be reliable and robust, and not require specialized personnel with unique technical expertise, which currently excludes most electrophysiological work. Clearly OECTs may provide very interesting solutions here in terms of monitoring.

### 2.3.4 Biosensors / Type 1 Diabetes

Biomedical monitoring devices have already improved patients' health and represent a considerable growing market. Moreover, existing devices provide an important gain in autonomy for the patient and avoid life-threatening complications. Automatic sensing of blood sugar has recently been introduced. This avoids painful "finger pricking" and allows even commanding an insulin pump. However, only glucose is measured, and thus a number of parameters remain unknown which are normally seen by islet cells in a healthy person. Thus current approaches receive only part of the information required for precise regulation and they still need considerable user intervention, for example to adapt to meal size, physical activity, etc. It is tempting to hypothesize that using islet beta-cells as primary sensor would be far more adapted. The signals generated in  $\beta$  cells, such as the electrical ones, may then be recorded by micro-electrodes or even OECTs and subsequently analysed to drive an insulin pump.

In the same vein the generation of huge amounts of stem-cell derived surrogate cells or micro-organs requires strict quality controls[54]. As example, curing type 1 diabetes by surrogate islets just in the US would require the yearly generation and quality testing of  $10^{15}$  cells or  $10^{12}$  islet micro-organs in a non-invasive manner. Current biotechnical approaches relying on genetic modifications are not suitable in technical or regulatory terms. Again, testing for electrical responses may be feasible on a large scale and is moreover non-destructive in the case of MEAs or OECTs.

#### 2.3.4.1 DT1

Diabetes is among the five main culprits of mortality worldwide and the number of people affected has reached epidemic proportions, getting up to 5% of the world population[55]. Generally, diabetes is classified into two different subtypes, type 1 and type 2. Whereas type 2 occurs more often in elder persons, type 1 diabetes starts generally in childhood or in adults (although it may start in the fifties, such as for Theresa May) and accounts for 5 to 10% of all cases of diabetes. Type 1 diabetes (DT1)

## *Ch. I.-Scientific Context*

is an autoimmune metabolic condition in which the body kills the pancreatic beta cells that produce the insulin needed for glucose regulation in the body. In the absence of insulin, an increase on the glucose concentration on the bloodstream leads to a disease of large and small blood vessels. Thereby it increases the risk of cardiovascular diseases, nerve or kidney damage, retina blood vessel damage, poor blood flow producing secondary effects as bone and joint problems, teeth infections and in the most dramatic cases, death. [56,57]. Diabetes is actually the major reason in developed countries for renal failure, vision loss and non-traumatic amputations. Patients with type 1 diabetes and some patients with type 2 diabetes<sup>2</sup> inject insulin, and occasionally glucagon, to regulate their blood glucose, which is critical to lower the risk of having the long-term complications mentioned before.

When managing diabetes, many patients must vigilantly test blood glucose as insulin is a very potent hormone and overdose may easily kill the patient. To measure glucose concentrations, often a glucometer is used and analytes are obtained either by finger pricking or via a subcutaneous glucose sensor. Subsequently, insulin doses have to be calculated, and necessary insulin doses are administered with a needle or insulin infusion pump to lower blood glucose. Glucagon may be injected in an emergency to treat severe low blood glucose.

On the other hand, some patients benefit from additional monitoring with a so-called "artificial pancreas", a system of devices that is meant to mimic the glucose regulating function of a healthy pancreas. Most Artificial Pancreas<sup>3</sup> consists of three types of devices: a continuous glucose monitoring system (CGM), an insulin infusion pump and a blood glucose device (such as a glucometer) used to calibrate the CGM. A computer-controlled algorithm connects the CGM and insulin infusion pump to allow

---

<sup>2</sup> The pancreas does not produce enough insulin or the body becomes resistant to the insulin that is present.

<sup>3</sup> Sometimes an artificial pancreas device system is referred to as a "closed-loop" system, an "automated insulin delivery" system, or an "autonomous system for glycaemic control."

## *Ch. I.-Scientific Context*

continuous communication between the two devices. Indeed, these systems not only monitor glucose levels in the body, but also adjust the delivery of insulin to reduce high blood glucose levels (hyperglycaemia) and avoid the incidence of low blood glucose (hypoglycaemia). As only glucose is measured but not the other parameters of nutrient homeostasis (lipids, gastrointestinal hormones, stress hormones, etc.), patient input is still required despite the presence of highly developed algorithms.

### *2.3.4.2 Monitoring (glucose)*

As it was described before, it is important to get a better understanding on the cellular mechanisms in the endocrine pancreas. Not only because of the potential healthcare benefit, but also in an economical point of view, considering the high price of the diabetes treatments nowadays[58]. It is for this reason that it is not surprising to realize that most of the work done on development of *in vivo* sensors focus on the reduction of problems related to the regulation of glucose in the blood (i.e. organs breakdown, amputation, blindness, etc.)[59]. As stated above, today, most of the sensors rest exclusively upon the detection of glucose concentration, but insulin regulation depends on multiple factors. In fact,  $\beta$ -cells are sensitive to other hormones, as well as other proteins having an effect on their electrical activity and the variation of the membrane potential. Thus, transmembrane ion flux is the first integrative signal in  $\beta$ -cell activation on the way to insulin secretion. Hence, it could be really convenient to measure this membrane potential and ion fluxes in a direct way[34].

In this context, it is clear that development of better sensing devices that incorporate all these other parameters, in addition to glucose concentration, is needed to have more realistic algorithms. These could be incorporated to control the CGM in future more performant artificial pancreas.

### *2.3.4.3 Islet Basal Sensor (Zn<sup>2+</sup>)*

Detection of Zn<sup>2+</sup> may be an important asset in  $\beta$ -cell biology and also represents an important challenge in the understanding of mechanisms related to the diabetes. Indeed, this cation is co-secreted with the insulin [60]. Its detection could allow studying the exocytosis on the final stage, the release of the final product. Thus, coupled to the detection of other cations of interest, it could increase our understanding on mechanisms related with the secretion and origin of the signalization related to the diabetes. Moreover, as this signal is due to a released product, a large change in the analyte concentration with respect to the basal level is expected, which could give a big S/N ratio without impacting the normal cell function, as it is the case for fluorescent methods often used nowadays. Finally, in the context of the biosensor described above using islet cells, detection of Zn<sup>2+</sup>-release may be an excellent signal, as it is specific proxy for insulin release.

## **3 DEVELOPEMENT OF MATERIALS FOR ION-SENSING**

Sensors are becoming more dependent on novel material development. After reviewing the importance and mechanisms of the ion sensing in the cellular signalization, I'll give a brief overview of the most important classes of materials developed in the supramolecular chemistry field as well as in conducting polymers during last decades. These materials are endowed with superior performance in terms of several properties of other devices in applications ranging going from optics to sensing [61].

### **3.1 CHELATORS**

Crown ethers are macrocycles containing a symmetric distribution of ether groups and they were discovered by Pedersen in 1967 as a sub-product of the bisphenol. Their particular shape of "crown" is at the origin of their name[62]. Concerning their

## Ch. I.-Scientific Context

nomenclature, the use of the IUPAC system become easily complicated, so it is usually used the followed nomenclature:

(Function) - total number of atoms forming the “cavity” - crown- number of heteroatoms

Some examples are shown in Figure 11. For example, the fourth example illustrated in the latter is named as dibenzo-18-crown-6.

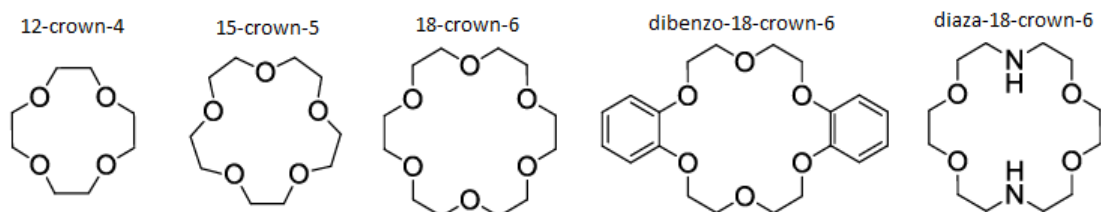


**Figure 11: Chemical structures of some crown ethers often used in the literature**

These compounds have seen exponentially increased use after the discovery because of their cation complexing capacity. This complexation is mainly selective in function of the size of their cavity and the nature of the heteroatoms forming the macrocycles. Complexation occurs by the interaction between a ligand (donor) and a receptor (acceptor) and could be facilitated by a particular configuration that allows the hosting of the ion species (inclusion complexation).

Crown ethers have been an important focus of research for years and some of this work has allowed to increase the knowledge of the properties of a broad series of macrocycles as the size or the complexation ability through different cations [62].

Complexes formed with the crown ethers may have different morphologies such as nest, perched or sandwich as it is illustrated in Figure 12. Formation of the complexes depends thus on different parameters such as the size of both species, the cation and the hosting cavity, as well as the conformation of the macromolecule. For example, the sandwich morphology is more often found in the polymers with pending crown

## Ch. I.-Scientific Context

ethers because of the closer disposition between both species one respect to each other[62]



**Figure 12: Scheme of the different complexation hosting modes of a crown-ether with a ligand: nest (left), perched (centre) or sandwich (right) [63].**

It is important to take into account the water solubility of the complexes formed, because this could be a drawback in some applications, requiring to adopt extraction processes. Alternatively, a solution to this drawback could be their grafting as pending groups on the monomers to build lower toxic polymer chains, more easily to purify and to decomplex [63]

As described before, polymers containing crown ethers used to form “sandwich” complexes, but it is not only a conformational change. Indeed, the mobility of the macromolecular chain, as well as the increase on the charge concentration along the backbone, are two important parameters that determine the macrocycles properties. In the case of a network polymer the crosslinking degree as well as the polymer swelling are also to take into account[63]

In some positively doped polymers, it has been observed that the complexation capacity of the crown ethers is strongly diminished[63] and the improvement in performances was obtained by two dedoping methods proposed by Simonet and coworkers: making an indirect reduction during the polymerization step; or, as alternative, the direct reduction of the polymer with an amine[64].

## Binding Quantification

As discussed before, supramolecular chemistry got a rise after the Nobel prize in 1967 and it continuously develops until our days in unimaginable applications by Pedersen and co-workers at that time[65,66]. These fields of supramolecular interactions are based on the molecular recognition, relying on the interactions between the electrostatic fields of each species involved. The interaction is produced if these species are energetically compatible taking place their association.

The main issue in supramolecular chemistry is the quantitative analysis of these intermolecular interactions. The most used method is supramolecular titration. For this, a component (host) is usually kept in constant concentration, and a second component (guest) is gradually added to this system. At the same time a physical property such as a specific chemical resonance (NMR) or absorption band (UV) that is sensitive to the supramolecular interaction (signal). The resulting information can be compared and fitted with different binding models.

The choice of the binding model is strongly dependent on the stoichiometry of the interaction. This term refers to the number of ligands (the guest component) that can bind to a single receptor (host component). For their choice, it is necessary a little review of few thermodynamics notions of bimolecular recognition.

The general case of a supramolecular association is defined by the followed equilibrium:



where H=host, G= Guest and  $\beta_{mn}$ =overall association constant for an  $m:n$  host-guest complex formation. The 1:1 binding equilibrium is the simplest case of formation of supramolecular association when only one guest is bound per molecule of host, being  $m=n=1$ , and defined as:

## Ch. I.-Scientific Context



$$K_a = \frac{[HG]}{[H][G]} \quad \text{Equation 5}$$

where  $K_a$ = association constant,  $[H]$ = host concentration,  $[G]$ =guest concentration,  $[HG]$ = Complex formed concentration. We could also note that the thermodynamic association constant,  $K_x$ , is related to the kinetics of the system, being the ratio between the forward (on),  $K_1$ , and backward (off),  $K_{-1}$ , rate constants for the equilibria of interest, being  $K_a = K_1 / K_{-1}$ .

Unfortunately, it is usually not possible to measure  $[HG]$  in supramolecular experiments, but this knowledge is required to determine the  $K_a$ . To overcome this problem, the classical methods have been transformed a series of derivatives expressions of *Equation 5* to linear equations that could be plotted. From these regressions could be obtained the  $K_a$  and other parameters of interest by inspection of the slope and the intercepts. Some examples are the Benesi-Hildebrand plot [67], the related Scott or Hanse-Woolf transformations or the Scatchard plot[68,69]. However, these linear transformations methods present some associated drawbacks: they distort the experimental errors[70,71] or even the results due to the assumptions taken (i.e. the presence of a guest large excess, or the fully formation of complex at the end of the titration).

Nowadays, with the power of modern computers and the associated softwares, non-linear regression approach with exact solutions of quadratic equations (Annex 2 in the Appendices chapter) based on *Equation 6* and *Equation 7* produces the most accurate results.

$$\Delta Y = Y_{\Delta HG} \left( \frac{[HG]}{[H]_0} \right) \quad \text{Equation 6}$$

$$\Delta Y = Y_{\Delta HG} ([HG]) \quad \text{Equation 7}$$

## Ch. I.-Scientific Context

These equations indicate the change in mole fraction (*Equation 6*) and absolute concentration (*Equation 7*) dependent physical property  $Y$  up on a titration. During the titration, the physical changes in the system are monitored, usually spectroscopically, and this change is plotted as a function of guest added to host. The resulting titration curve known as a *binding isotherm* is the mathematical model that is derived from the assumed equilibria to obtain the association constant ( $K_a$ ) and/or the other physical constants of interest.

### 3.2 CONJUGATED POLYMERS: Thiophene derivatives & EDOT

Conducting polymers have been studied and used worldwide for around 40 years and they are the base of numerous recent advances in many applications due to their excellent electrical and optical properties, including sensory signal amplification[61]. The most commonly studies and fundamental theories and applications are focused on PANis, PPys, PThs and their composites due to their outstanding properties and stability.

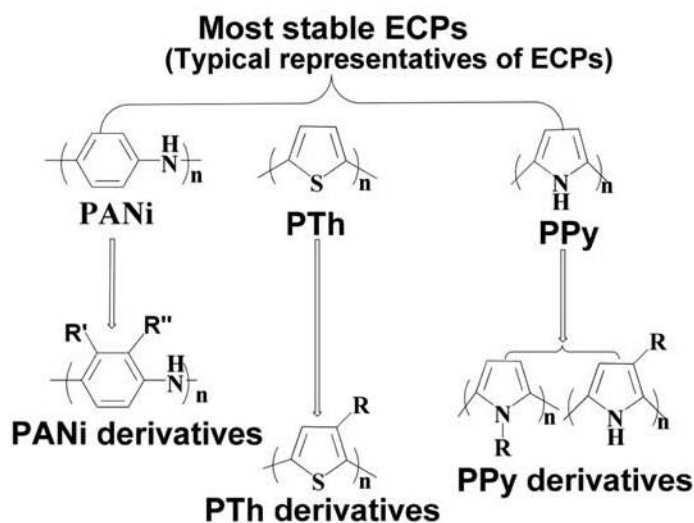


**Figure 13: Scheme summarizing the families of most used electronically conducting polymers (ECP): Polyanilines (PANis), polythiophenes (PThs) and polypyrroles(PPys) (adapted from [72]).**

## Ch. I.-Scientific Context

As shown in Figure 14, PEDOT is a polymer constituted by ethylenedioxythiophene (EDOT) units, a derivative monomer of a thiophene cycle. Even if the PTh is an important polymer family often used in the organic electronics and relatively stable in comparison with other conjugated polymers, a decrease in their conductivity is observed over time which limit its use in many applications[72].

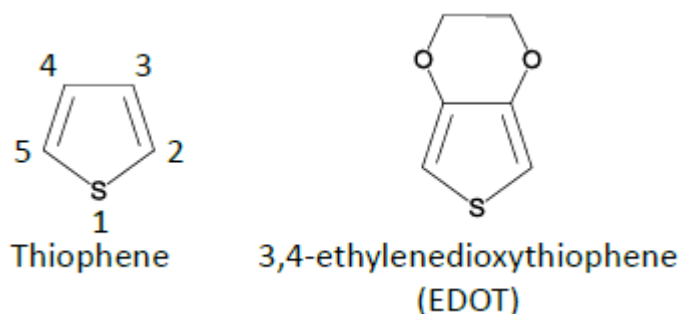


**Figure 14: Scheme of the chemical structures** of thiophene (left) compare to its derivative EDOT (right).

Introduction of an alkoxy group, electron donor, in the structure of the thiophene results in a reduction of the oxidation potential of the monomer and an increase on the stability. Moreover, this change reduces the numbers of polymerization sites (because positions 3 and 4 are “blocked” with the alkoxy group) obtaining a better regularity in the polymer structure (see Figure 14)[73].

Although longer chains were tested for the ether bridge on the monomer, it was shown that the obtained polymer chains are deformed and presented a lower conductivity[2]. Moreover, other alternatives are the EDOT derivatives obtained from its functionalization with alkyl chains, but their lower conductivities in comparison with EDOT were also demonstrated as it is reviewed by Groenendaal et al.[74]

PEDOT has many interesting properties which could explain the huge and increasing number of research groups working with this material. In opposite to many other polymers, it is possible to dope and dedope repeatedly, fact that comes with a

## Ch. I.-Scientific Context

characteristic colour change, electrochromic property really exploited in optical applications[73]. It is important to notice, that some of the derivatives mentioned before, such as ProDOT, have a higher Band Gap and a better electrochromism than PEDOT; however, their conductivity is lower, being PEDOT the better compromise.[75]

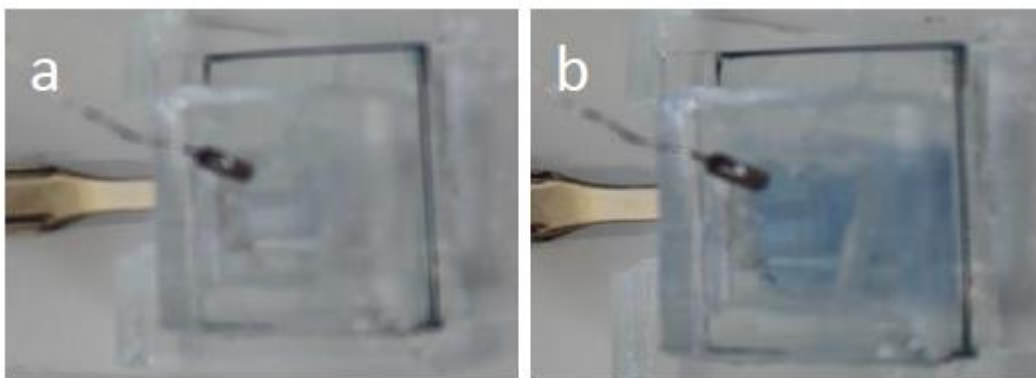


**Figure 15: Electrochromic property of PEDOT based inks: a) Oxidized state; b) Reduced state**

As it was pointed before, because of the presence of the alkoxy groups, EDOT has a very good environmental and long-term stability making this material a good candidate for ion-sensors[73]. In the conductive point of view, PEDOT has a low bandgap of 1.5 eV that could be decreased until 1 eV after doping. It is not extremely sensitive to temperature changes and has a great electrical conductivity after formulation and stabilisation with PSS polyelectrolyte (550 S/cm).

The increasing efforts and interest of the organic chemists towards the materials improvement for bioelectronics applications can be represented by the interesting work of Martin et al., who have recently synthesized polyhedral oligomeric silsesquioxane (POSS-ProDOT) crosslinker via hydrosilylation and thiol-ene “click” chemistry to improve the stability of PEDOT coatings in metallic electrodes which could improve their exploitation in biocompatible neural probes.

### 3.2.1 STABILISATION WITH POLYELECTROLYTES: PSS & Other alternatives

One of the most popular material used in organic electronics, either for the OLED, OPV or electrochromic electrodes fabrication, is the mixed of two polymers, the poly(ethylenedioxythiophene) doped with a poly(styrene sulfonate) polyelectrolyte better known as PEDOT:PSS (structural details illustrated in Figure 16)[76].

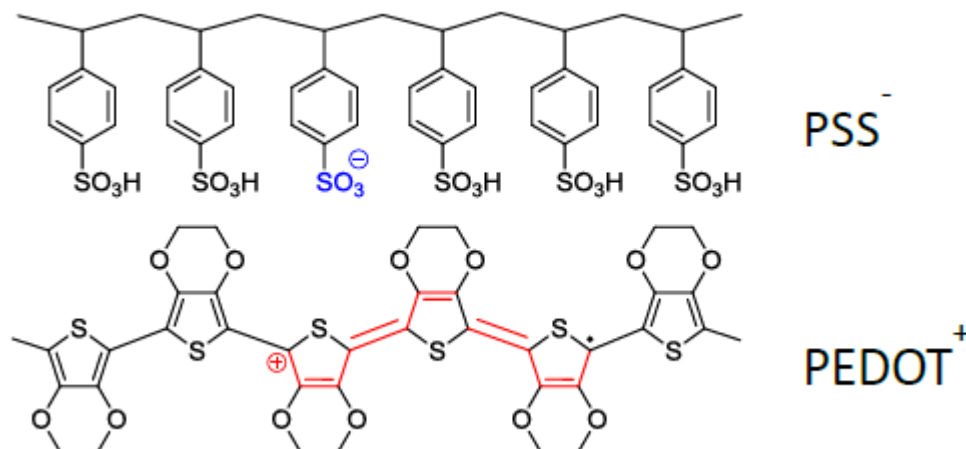


**Figure 16: Chemical structure of polymer complex PEDOT:PSS.** In red, a polaron is represented in the conjugated chain of PEDOT. In blue a counterbalance charge of the sulfonate group is represented as a pending group in the PSS backbone.

PSS has a double role doping the PEDOT and stabilizing the complex in aqueous media. These dispersions can be used to form thin films exploited in different applications to develop interesting devices such solar cells or flexible screen as mentioned before[77]. Moreover, transistors have been also fabricated by photolithography with these polymer dispersions forming a thin film on a specific area forming the channel between two electrodes, source and drain, made generally of a metal such as gold[78]. All the advantages of PEDOT: PSS have been widely reviewed[79], however, some of the drawbacks of this material are related with its integration into devices, especially in the interfacing with other layers such as ITO in organic solar cells due to the hygroscopic nature of PSS producing the etching of the ITO layer[80].

## *Ch. I.-Scientific Context*

Recent works have been done to look for alternative to this commercial material, substituting the PSS dopant by alternatives polyelectrolytes, such as poly(styrene sulfonyl(trifluoromethylsulfonyl)imide) (PSTFSI) and obtaining similar PEDOT based aqueous dispersions[81]. It was demonstrated that these alternative materials can be used to extend printability of big surface substrates and they have found place in applications requiring flexible transparent electrodes[77].

### 3.2.2 SENSING: Some examples

These conductive polymers have been also used for sensing applications. Some examples of chemical sensing include the use of these materials without any modification, i.e. the photodiode vapour sensors developed by Pomije and co-workers[82], based on two-layer devices where one layer was composed of a linear array of mixed-stack platinum complexes previously synthesized in the Miller group [83,84], which are responsive to organic vapours. These devices were constructed by electropolymerization of the conjugated monomer onto ITO electrode, followed by spin coating the stack complexes onto the polymer film, and final deposition of an aluminium layer. After exposure to acetone vapour, LED devices showed a shift in his maximum emission peak of c.a. 40 nm.

More sophisticated examples can be found with functionalized polymers. For example, the entrapment of macrocycles such as 18-dibenzo-crown-6[85] into CPs has been used for sensing potassium ions by observing redox changes in the polymer film as a function of potassium concentration. In this example, a polyindole coated platinum electrode was covered with a layer with a PVC/18-crown-6 membrane. The film showed a positive potentiometric shift, which was linear with  $K^+$  concentrations. Other example, is the use of differential-pulse voltammetry by Lyons et al., demonstrating that the polypyrrole-DBS film could distinguish between ascorbic acid oxidation and dopamine[86].

## *Ch. I.-Scientific Context*

In 2003, the pH and ion dependence of calixarene-based conducting polymers was demonstrated by Swager and co-workers[87], who subsequently, exploit the charge sensitivity property designing a crown ether structure that displayed similar binding constants to potassium and divalent cations, having different conductivity responses to these ions[88].

Moreover, we can find several examples using CPs for transduction of an analyte-enzyme binding. An example is the work of Contractor et al. who used an electropolymerized polyaniline film between two platinum electrodes and the over coated layer was entrapped with glucose oxidase. Upon reaction with glucose, this enzyme produces gluconolactone and hydrogen peroxide, which alters the pH of the local environment. The authors correlated polymer oxidation with the change observed in conductivity when monitored the OPV of the bilayer film while increasing glucose concentration, measured also by conducting potentiodynamic voltammetry with and without glucose[89].

Finally, many work is being developed in materials development to applications going from drug delivery[90] where electroactive polymers are used to obtain a target response to an electrical stimuli or as scaffold for composites used in tissue engineering[91].

## **4 SCOPE OF THE THESIS**

During last decades, there is an increasing interest on the materials from the organic electronics field for bio-applications. One of the key topics is the development of devices for the electrophysiology, which allowed a direct contact with live tissues with the purpose to record or stimulate its electrical activity.

The outlook of the current state-of art allows us to note that bioelectronics have still many challenges to master, and there is still work to do on the synthetic side of organic bioelectronics, especially when considering that the material most used in this field, PEDOT:PSS, has been the same for the last twenty years mainly because it is commercially available. Therefore, the main objective of this thesis has been the synthesis of polymer materials targeting the  $\beta$ -cell interfacing, and taking into account their chemical structure to get the information required.

As it was described before, electrical activity of pancreatic cells brings into play cations exchange through specific channels. Consequently, it is important to detect them. Some of these cations with particular interest are the monovalent cations  $\text{Na}^+$  and  $\text{K}^+$  and as it was discussed, they present a high affinity in the complexation with crown ethers. Moreover, in the study of  $\beta$ -cells it is really interesting the development of  $\text{Zn}^{2+}$  sensitive monomers because of the important role of this cation in the co-secretion with insulin in this kind of cells.

Great efforts in many research groups are done on the development of methods to obtain new mixed-conductor polymers alternatives to PEDOT: PSS.

During my PhD studies two main routes have been followed in order to obtain new active materials to constitute the channel of OECT devices (Figure 17). On the one hand, styrene derivatives were synthesized and used to obtain polyelectrolytes alternatives to PSS (Chapter II). On the other hand, functionalization was done

## Ch. I.-Scientific Context

directly in the conjugated monomer, EDOT (Chapter III). The cations involved in the different processes of interest for the study of pancreatic  $\beta$ -cells (sodium, potassium and zinc) have been the driving force to choose the chelates used for the monomers modification during this study. Thereby, the structures of most of the products synthesized and analysed in this work are based on the crown ethers 15-crown-5 and 18-crown-6 having cavity sizes of 1,7-2,2 Å and 2,6-3,2 Å respectively[63] while the group chosen to trap the divalent cation,  $Zn^{2+}$ , was the dipicolyl fraction (DPA).

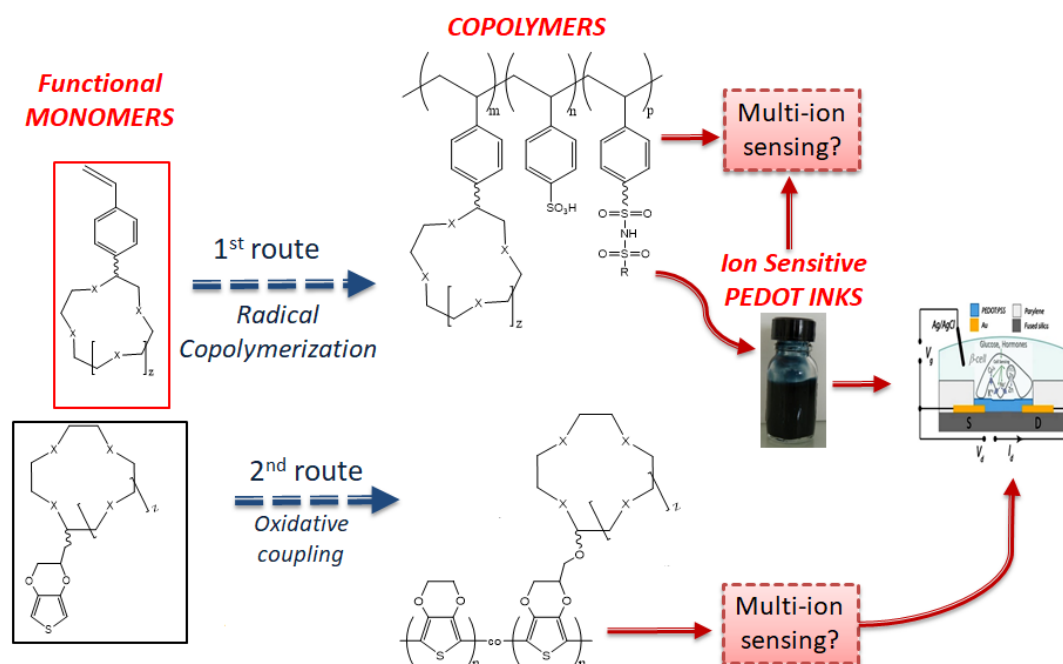


**Figure 17: Summary of the double route of functionalization developed during this PhD:** Top: Styrene derivatives with binding moieties (monomers), their copolymers to gain new ion-sensitive polyelectrolytes used to stabilize the water dispersed PEDOT based inks. Bottom: EDOT derivatives with the ion-sensitive fractions and their electropolymerization to obtain ion-sensitive films.

## 5 BIBLIOGRAPHY

1. Ashkan, K.; Rogers, P.; Bergman, H.; Ughratdar, I. Insights into the mechanisms of deep brain stimulation. *Nat. Rev. Neurol.* **2017**, *13*, 548–554.
2. PEDOT: Principles and Applications of an Intrinsically Conductive Polymer Available online: <https://www.crcpress.com/PEDOT-Principles-and-Applications-of-an-Intrinsically-Conductive-Polymer/Elschner-Kirchmeyer-Lovenich-Merker-Reuter/p/book/9781420069112> (accessed on Aug 13, 2018).
3. Rasmussen, S.C. The Early History of Polyaniline: Discovery and Origins. *Subst. Vol 1 No 2 2017* **2017**.
4. McNeill, R.; Siudak, R.; Wardlaw, J.H.; Weiss, D.E. Electronic Conduction in Polymers. I. The Chemical Structure of Polypyrrole. *Aust. J. Chem.* **1963**, *16*, 1056–1075.
5. Contat-Rodrigo, L.; Pérez-Fuster, C.; Lidón-Roger, J.V.; Bonfiglio, A.; García-Breijo, E. Characterization of Screen-Printed Organic Electrochemical Transistors to Detect Cations of Different Sizes. *Sensors* **2016**, *16*, 1599.
6. Malliaras, G.; Friend, R. An Organic Electronics Primer. *Phys. Today* **2005**, *58*, 53–58.
7. Rivnay, J.; Owens, R.M.; Malliaras, G.G. The Rise of Organic Bioelectronics. *Chem. Mater.* **2014**, *26*, 679–685.
8. Bresadola, M. Medicine and science in the life of Luigi Galvani (1737–1798). *Brain Res. Bull.* **1998**, *46*, 367–380.
9. Bouton, C.E.; Shaikhouni, A.; Annetta, N.V.; Bockbrader, M.A.; Friedenber, D.A.; Nielson, D.M.; Sharma, G.; Sederberg, P.B.; Glenn, B.C.; Mysiw, W.J.; et al. Restoring cortical control of functional movement in a human with quadriplegia. *Nature* **2016**, *533*, 247–250.
10. Gribble, F.M.; Loussouarn, G.; Tucker, S.J.; Zhao, C.; Nichols, C.G.; Ashcroft, F.M. A Novel Method for Measurement of Submembrane ATP Concentration. *J. Biol. Chem.* **2000**, *275*, 30046–30049.
11. Rorsman, P.; Ashcroft, F.M. Pancreatic  $\beta$ -Cell Electrical Activity and Insulin Secretion: Of Mice and Men. *Physiol. Rev.* **2018**, *98*, 117–214.
12. Ashcroft, F.M.; Rorsman, P. KATP channels and islet hormone secretion: new insights and controversies. *Nat. Rev. Endocrinol.* **2013**, *9*, 660–669.
13. Henquin, J.C.; Ravier, M.A.; Nenquin, M.; Jonas, J.C.; Gilon, P. Hierarchy of the  $\beta$ -cell signals controlling insulin secretion. *Eur. J. Clin. Invest.* **2003**, *33*, 742–750.
14. Neshler, R.; Cerasi, E. Modeling Phasic Insulin Release: Immediate and Time-Dependent Effects of Glucose. *Diabetes* **2002**, *51*, S53–S59.
15. Molina, S.A.; Moriarty, H.K.; Infield, D.T.; Imhoff, B.R.; Vance, R.J.; Kim, A.H.; Hansen, J.M.; Hunt, W.R.; Koval, M.; McCarty, N.A. Insulin signaling via the PI3-kinase/Akt pathway regulates airway glucose uptake and barrier function in a CFTR-dependent manner. *Am. J. Physiol.-Lung Cell. Mol. Physiol.* **2017**, *312*, L688–L702.
16. Wan, M.; Leavens, K.F.; Hunter, R.W.; Koren, S.; von Wilamowitz-Moellendorff, A.; Lu, M.; Satapati, S.; Chu, Q.; Sakamoto, K.; Burgess, S.C.; et al. A Noncanonical, GSK3-Independent Pathway Controls Postprandial Hepatic Glycogen Deposition. *Cell Metab.* **2013**, *18*, 99–105.
17. Li, X.; Monks, B.; Ge, Q.; Birnbaum, M.J. Akt/PKB regulates hepatic metabolism by directly inhibiting PGC-1 $\alpha$  transcription coactivator. *Nature* **2007**, *447*, 1012–1016.
18. Wilson, D.P.; Susnjar, M.; Kiss, E.; Sutherland, C.; Walsh, M.P. Thromboxane A<sub>2</sub>-induced contraction of rat caudal arterial smooth muscle involves activation of Ca<sup>2+</sup> entry and Ca<sup>2+</sup> sensitization: Rho-associated kinase-mediated phosphorylation of MYPT1 at Thr-855, but not Thr-697. *Biochem. J.* **2005**, *389*, 763–774.

## Ch. I.-Scientific Context

19. Raoux, M.; Bornat, Y.; Quotb, A.; Catargi, B.; Renaud, S.; Lang, J. Non-invasive long-term and real-time analysis of endocrine cells on micro-electrode arrays: Long-term and real-time analysis of endocrine cells. *J. Physiol.* **2012**, *590*, 1085–1091.
20. Vantghem, M.-C.; Defrance, F.; Quintin, D.; Leroy, C.; Raverdi, V.; Prévost, G.; Caiazzo, R.; Kerr-Conte, J.; Glowacki, F.; Hazzan, M.; et al. Treating diabetes with islet transplantation: Lessons from the past decade in Lille. *Diabetes Metab.* **2014**, *40*, 108–119.
21. Melton, D.A. Chapter Four - Applied Developmental Biology: Making Human Pancreatic Beta Cells for Diabetics. In *Current Topics in Developmental Biology*; Wassarman, P.M., Ed.; Essays on Developmental Biology, Part B; Academic Press, 2016; Vol. 117, pp. 65–73.
22. Grynkiwicz, G.; Poenie, M.; Tsien, R.Y. A New Generation of Ca<sup>2+</sup> Indicators with Greatly Improved Fluorescence Properties. *11*.
23. Rutter, G.A.; Varadi, A.; Tsuboi, T.; Parton, L.; Ravier, M. Insulin secretion in health and disease: genomics, proteomics and single vesicle dynamics. *Biochem. Soc. Trans.* **2006**, *34*, 4.
24. Lin, W.-J.; Salton, S.R. The Regulated Secretory Pathway and Human Disease: Insights from Gene Variants and Single Nucleotide Polymorphisms. *Front. Endocrinol.* **2013**, *4*.
25. Li, D.; Chen, S.; Bellomo, E.A.; Tarasov, A.I.; Kaut, C.; Rutter, G.A.; Li, W. Imaging dynamic insulin release using a fluorescent zinc indicator for monitoring induced exocytotic release (ZIMIR). *Proc. Natl. Acad. Sci. U. S. A.* **2011**, *108*, 21063–21068.
26. Jørgensen, M.C.; Ahnfelt-Rønne, J.; Hald, J.; Madsen, O.D.; Serup, P.; Hecksher-Sørensen, J. An Illustrated Review of Early Pancreas Development in the Mouse. *Endocr. Rev.* **2007**, *28*, 685–705.
27. Xie, R.; Carrano, A.C.; Sander, M. A systems view of epigenetic networks regulating pancreas development and  $\beta$ -cell function. *Wiley Interdiscip. Rev. Syst. Biol. Med.* **2015**, *7*, 1–11.
28. Wang, A.; Yue, F.; Li, Y.; Xie, R.; Harper, T.; Patel, N.A.; Muth, K.; Palmer, J.; Qiu, Y.; Wang, J.; et al. Epigenetic priming of enhancers predicts developmental competence of hESC-derived endodermal lineage intermediates. *Cell Stem Cell* **2015**, *16*, 386–399.
29. Dhawan, S.; Tschen, S.-I.; Zeng, C.; Guo, T.; Hebrok, M.; Matveyenko, A.; Bhushan, A. DNA methylation directs functional maturation of pancreatic  $\beta$  cells. *J. Clin. Invest.* **2015**, *125*, 2851–2860.
30. Rong, Z.; Wang, M.; Hu, Z.; Stradner, M.; Zhu, S.; Kong, H.; Yi, H.; Goldrath, A.; Yang, Y.-G.; Xu, Y.; et al. An effective approach to prevent immune rejection of human ESC-derived allografts. *Cell Stem Cell* **2014**, *14*, 121–130.
31. Russa, M.F.L.; Qi, L.S. The New State of the Art: Cas9 for Gene Activation and Repression. *Mol. Cell. Biol.* **2015**, *35*, 3800–3809.
32. Atwater, I.; Ribalet, B.; Rojas, E. Cyclic changes in potential and resistance of the beta-cell membrane induced by glucose in islets of Langerhans from mouse. *J. Physiol.* **1978**, *278*, 117–139.
33. Hamill, O.P.; Marty, A.; Neher, E.; Sakmann, B.; Sigworth, F.J. Improved patch-clamp techniques for high-resolution current recording from cells and cell-free membrane patches. *Pflüg. Arch. - Eur. J. Physiol.* **1981**, *391*, 85–100.
34. Lebreton, F.; Pirog, A.; Belouah, I.; Bosco, D.; Berney, T.; Meda, P.; Bornat, Y.; Catargi, B.; Renaud, S.; Raoux, M.; et al. Slow potentials encode intercellular coupling and insulin demand in pancreatic beta cells. *Diabetologia* **2015**, *58*, 1291–1299.
35. Thomasjr, C.; Springer, P.; Loeb, G.; Berwaldnetter, Y.; Okun, L. A miniature microelectrode array to monitor the bioelectric activity of cultured cells. *Exp. Cell Res.* **1972**, *74*, 61–66.
36. Hofmann, F.; Bading, H. Long term recordings with microelectrode arrays: Studies of transcription-dependent neuronal plasticity and axonal regeneration. *J. Physiol.-Paris* **2006**, *99*, 125–132.
37. Koutsouras, D.A.; Perrier, R.; Villarroel Marquez, A.; Pirog, A.; Pedraza, E.; Cloutet, E.; Renaud, S.; Raoux, M.; Malliaras, G.G.; Lang, J. Simultaneous monitoring of single cell and of micro-organ activity by PEDOT:PSS covered multi-electrode arrays. *Mater. Sci. Eng. C* **2017**, *81*, 84–89.

## Ch. I.-Scientific Context

38. White, H.S.; Kittlesen, G.P.; Wrighton, M.S. Chemical derivatization of an array of three gold microelectrodes with polypyrrole: fabrication of a molecule-based transistor. *J. Am. Chem. Soc.* **1984**, *106*, 5375–5377.
39. Giovannitti, A.; Nielsen, C.B.; Sbircea, D.-T.; Inal, S.; Donahue, M.; Niazi, M.R.; Hanifi, D.A.; Amassian, A.; Malliaras, G.G.; Rivnay, J.; et al. N-type organic electrochemical transistors with stability in water. *Nat. Commun.* **2016**, *7*, 13066.
40. Friedlein, J.T.; Donahue, M.J.; Shaheen, S.E.; Malliaras, G.G.; McLeod, R.R. Microsecond Response in Organic Electrochemical Transistors: Exceeding the Ionic Speed Limit. *Adv. Mater.* **2016**, *28*, 8398–8404.
41. Bernards, D.A.; Malliaras, G.G. Steady-State and Transient Behavior of Organic Electrochemical Transistors. *Adv. Funct. Mater.* **2007**, *17*, 3538–3544.
42. Yi, Z.; Natale, G.; Kumar, P.; Mauro, E.D.; Heuzey, M.-C.; Soavi, F.; Perepichka, I.I.; Varshney, S.K.; Santato, C.; Cicoira, F. Ionic liquid–water mixtures and ion gels as electrolytes for organic electrochemical transistors. *J. Mater. Chem. C* **2015**, *3*, 6549–6553.
43. Khodagholy, D.; Doublet, T.; Quilichini, P.; Gurfinkel, M.; Leleux, P.; Ghestem, A.; Ismailova, E.; Hervé, T.; Sanaur, S.; Bernard, C.; et al. In vivo recordings of brain activity using organic transistors. *Nat. Commun.* **2013**, *4*.
44. Rivnay, J.; Inal, S.; Salleo, A.; Owens, R.M.; Berggren, M.; Malliaras, G.G. Organic electrochemical transistors. *Nat. Rev. Mater.* **2018**, *3*, 17086.
45. Basiricò, L.; Cosseddu, P.; Scidà, A.; Fraboni, B.; Malliaras, G.G.; Bonfiglio, A. Electrical characteristics of ink-jet printed, all-polymer electrochemical transistors. *Org. Electron.* **2012**, *13*, 244–248.
46. Gu, X.; Yao, C.; Liu, Y.; Hsing, I.-M. 16-Channel Organic Electrochemical Transistor Array for In Vitro Conduction Mapping of Cardiac Action Potential. *Adv. Healthc. Mater.* **2016**, *5*, 2345–2351.
47. Lanzani, G. Organic electronics meets biology: Materials for bioelectronics. *Nat. Mater.* **2014**, *13*, 775–776.
48. Conte Camerino, D. Grand challenge for ion channels: an underexploited resource for therapeutics. *Front. Pharmacol.* **2010**.
49. Markets, R. and Ion Channel Modulators Market 2015-2022: Global Strategic Business Report 2018 - Industry & Product Overview, Recent Industry Activity & Focus on Key Players Available online: <http://globenewswire.com/news-release/2018/02/14/1347899/0/en/Ion-Channel-Modulators-Market-2015-2022-Global-Strategic-Business-Report-2018-Industry-Product-Overview-Recent-Industry-Activity-Focus-on-Key-Players.html> (accessed on Sep 27, 2018).
50. Lind, J.U.; Busbee, T.A.; Valentine, A.D.; Pasqualini, F.S.; Yuan, H.; Yadid, M.; Park, S.-J.; Kotikian, A.; Nesmith, A.P.; Campbell, P.H.; et al. Instrumented cardiac microphysiological devices via multimaterial three-dimensional printing. *Nat. Mater.* **2017**, *16*, 303–308.
51. Loskill, P.; Marcus, S.G.; Mathur, A.; Reese, W.M.; Healy, K.E.  $\mu$ Organo: A Lego®-Like Plug & Play System for Modular Multi-Organ-Chips. *PLOS ONE* **2015**, *10*, e0139587.
52. Esch, E.W.; Bahinski, A.; Huh, D. Organs-on-chips at the frontiers of drug discovery. *Nat. Rev. Drug Discov.* **2015**, *14*, 248–260.
53. Organ-On-Chip Market Analysis & Trends - Organ (Heart-on-chip, Human-on-chip, Intestine-on-chip, Kidney-on-chip, Liver-on-chip, Lung-on-chip), Application - Forecast to 2025 Available online: <https://www.prnewswire.com/news-releases/organ-on-chip-market-analysis--trends---organ-heart-on-chip-human-on-chip-intestine-on-chip-kidney-on-chip-liver-on-chip-lung-on-chip-application---forecast-to-2025-300393217.html> (accessed on Sep 27, 2018).
54. Harding, J.; Mirochnitchenko, O. Preclinical Studies for Induced Pluripotent Stem Cell-based Therapeutics. *J. Biol. Chem.* **2014**, *289*, 4585–4593.
55. Rorsman, P.; Braun, M. Regulation of Insulin Secretion in Human Pancreatic Islets. *Annu. Rev. Physiol.* **2013**, *75*, 155–179.

## Ch. I.-Scientific Context

56. Atkinson, M.A.; Eisenbarth, G.S.; Michels, A.W. Type 1 diabetes. *The Lancet* **2014**, *383*, 69–82.
57. La Torre, D.; Lernmark, Å. Immunology of  $\beta$ -Cell Destruction. In *The Islets of Langerhans*; Islam, Md.S., Ed.; Advances in Experimental Medicine and Biology; Springer Netherlands: Dordrecht, 2010; pp. 537–583 ISBN 978-90-481-3271-3.
58. Roze, S.; Saunders, R.; Brandt, A.-S.; de Portu, S.; Papo, N.L.; Jendle, J. Health-economic analysis of real-time continuous glucose monitoring in people with Type 1 diabetes. *Diabet. Med.* **2015**, *32*, 618–626.
59. Ashcroft, F.M.; Rorsman, P. Diabetes Mellitus and the  $\beta$  Cell: The Last Ten Years. *Cell* **2012**, *148*, 1160–1171.
60. Qian, W.-J.; Gee, K.R.; Kennedy, R.T. Imaging of  $Zn^{2+}$  Release from Pancreatic  $\beta$ -Cells at the Level of Single Exocytotic Events. *Anal. Chem.* **2003**, *75*, 3468–3475.
61. McQuade, D.T.; Pullen, A.E.; Swager, T.M. Conjugated Polymer-Based Chemical Sensors. *Chem. Rev.* **2000**, *100*, 2537–2574.
62. Lehn, J.M. CRYPTATES: INCLUSION COMPLEXES OF MACROPOLYCYCLIC RECEPTOR MOLECULES. 22.
63. Lehn, J.M.; Sauvage, J.P. Cation and cavity selectivities of alkali and alkaline-earth “cryptates.” *J Chem Soc D* **1971**, *0*, 440–441.
64. Simonet, J.; Rault-Berthelot, J. Electrochemistry: A technique to form, to modify and to characterize organic conducting polymers. *Prog. Solid State Chem.* **1991**, *21*, 1–48.
65. Sauvage, J.-P. From Chemical Topology to Molecular Machines (Nobel Lecture). *Angew. Chem. Int. Ed.* **2017**, *56*, 11080–11093.
66. Swager, T.M. 50th Anniversary Perspective : Conducting/Semiconducting Conjugated Polymers. A Personal Perspective on the Past and the Future. *Macromolecules* **2017**, *50*, 4867–4886.
67. Benesi, H.A.; Hildebrand, J.H. A Spectrophotometric Investigation of the Interaction of Iodine with Aromatic Hydrocarbons. *J. Am. Chem. Soc.* **1949**, *71*, 2703–2707.
68. Scott, R.L. Some comments on the Benesi-Hildebrand equation. *Recl. Trav. Chim. Pays-Bas* **2010**, *75*, 787–789.
69. Hanes, C.S. CLXVII. STUDIES ON PLANT AMYLASES. 16.
70. Motulsky, H.; Christopoulos, A. Fitting Models to Biological Data using Linear and Nonlinear Regression. 351.
71. Motulsky, H.J.; Ransnas, L.A. Fitting curves to data using nonlinear regression: a practical and nonmathematical review. *FASEB J.* **1987**, *1*, 365–374.
72. Wen, Y.; Xu, J. Scientific Importance of Water-Processable PEDOT-PSS and Preparation, Challenge and New Application in Sensors of Its Film Electrode: A Review. *J. Polym. Sci. Part Polym. Chem.* **2017**, *55*, 1121–1150.
73. Wang, Y. Research progress on a novel conductive polymer–poly(3,4-ethylenedioxythiophene) (PEDOT). *J. Phys. Conf. Ser.* **2009**, *152*, 012023.
74. Groenendaal, L.; Zotti, G.; Aubert, P.-H.; Waybright, S.M.; Reynolds, J.R. Electrochemistry of Poly(3,4-alkylenedioxythiophene) Derivatives. *Adv. Mater.* **2003**, *15*, 855–879.
75. Ponder, J.F.; Österholm, A.M.; Reynolds, J.R. Designing a Soluble PEDOT Analogue without Surfactants or Dispersants. *Macromolecules* **2016**, *49*, 2106–2111.
76. Wen, Y.; Xu, J. Scientific Importance of Water-Processable PEDOT–PSS and Preparation, Challenge and New Application in Sensors of Its Film Electrode: A Review. *J. Polym. Sci. Part Polym. Chem.* **2017**, *55*, 1121–1150.
77. Hofmann, A.I.; Cloutet, E.; Hadziioannou, G. Materials for Transparent Electrodes: From Metal Oxides to Organic Alternatives. *Adv. Electron. Mater.* **2018**, 1700412.
78. Svensson, P.-O.; Nilsson, D.; Forchheimer, R.; Berggren, M. A sensor circuit using reference-based conductance switching in organic electrochemical transistors. *Appl. Phys. Lett.* **2008**, *93*, 203301.

## Ch. I.-Scientific Context

79. Groenendaal, L.; Jonas, F.; Freitag, D.; Pielartzik, H.; Reynolds, J.R. Poly(3,4-ethylenedioxythiophene) and Its Derivatives: Past, Present, and Future. *Adv. Mater.* **2000**, *12*, 481–494.
80. de Jong, M.P.; van IJzendoorn, L.J.; de Voigt, M.J.A. Stability of the interface between indium-tin-oxide and poly(3,4-ethylenedioxythiophene)/poly(styrenesulfonate) in polymer light-emitting diodes. *Appl. Phys. Lett.* **2000**, *77*, 2255–2257.
81. Hofmann, A.I.; Smaal, W.T.T.; Mumtaz, M.; Katsigiannopoulos, D.; Brochon, C.; Schütze, F.; Hild, O.R.; Cloutet, E.; Hadziioannou, G. An Alternative Anionic Polyelectrolyte for Aqueous PEDOT Dispersions: Toward Printable Transparent Electrodes. *Angew. Chem. Int. Ed.* **2015**, *54*, 8506–8510.
82. Grove, L.J.; Rennekamp, J.M.; Jude, H.; Connick, W.B. A New Class of Platinum(II) Vapochromic Salts. *J. Am. Chem. Soc.* **2004**, *126*, 1594–1595.
83. Zhou, Q.; Swager, T.M. Method for enhancing the sensitivity of fluorescent chemosensors: energy migration in conjugated polymers. *J. Am. Chem. Soc.* **1995**, *117*, 7017–7018.
84. McCullough, R.D.; Ewbank, P.C.; Loewe, R.S. Self-Assembly and Disassembly of Regioregular, Water Soluble Polythiophenes: Chemoselective Ionchromatic Sensing in Water. *J. Am. Chem. Soc.* **1997**, *119*, 633–634.
85. Pandey, P.C.; Prakash, R. Polyindole modified potassium ion-sensor using dibenzo-18-crown-6 mediated PVC matrix membrane. *Sens. Actuators B Chem.* **1998**, *46*, 61–65.
86. Lyons, M.E.G.; Breen, W.; Cassidy, J. Ascorbic acid oxidation at polypyrrole-coated electrodes. *J. Chem. Soc. Faraday Trans.* **1991**, *87*, 115.
87. Yu, H.; Xu, B.; Swager, T.M. A Proton-Doped Calix[4]arene-Based Conducting Polymer. *J. Am. Chem. Soc.* **2003**, *125*, 1142–1143.
88. Yu, H.; Pullen, A.E.; Büschel, M.G.; Swager, T.M. Charge-Specific Interactions in Segmented Conducting Polymers: An Approach to Selective Ionoresistive Responses. *Angew. Chem. Int. Ed.* **2004**, *43*, 3700–3703.
89. Hoa, D.T.; Kumar, T.N.Suresh.; Puneekar, N.S.; Srinivasa, R.S.; Lal, R.; Contractor, A.Q. A biosensor based on conducting polymers. *Anal. Chem.* **1992**, *64*, 2645–2646.
90. Hardy, J.G.; Mouser, D.J.; Arroyo-Currás, N.; Geissler, S.; Chow, J.K.; Nguy, L.; Kim, J.M.; Schmidt, C.E. Biodegradable electroactive polymers for electrochemically-triggered drug delivery. *J Mater Chem B* **2014**, *2*, 6809–6822.
91. Broda, C.R.; Lee, J.Y.; Sirivisoot, S.; Schmidt, C.E.; Harrison, B.S. A chemically polymerized electrically conducting composite of polypyrrole nanoparticles and polyurethane for tissue engineering. *J. Biomed. Mater. Res. A* **2011**, *98A*, 509–516.
92. Shi, H.; Wang, R.; Yang, J.; Ren, H.; Liu, S.; Guo, T. Novel imprinted nanocapsule with highly enhanced hydrolytic activity for organophosphorus pesticide degradation and elimination. *Eur. Polym. J.* **2015**, *72*, 190–201.
93. Llanes, P.; Sayalero, S.; Rodríguez-Eschrich, C.; Pericàs, M.A. Asymmetric cross- and self-aldol reactions of aldehydes in water with a polystyrene-supported triazolylproline organocatalyst. *Green Chem.* **2016**, *18*, 3507–3512.
94. Moad, G.; Rizzardo, E.; Thang, S.H. Living Radical Polymerization by the RAFT Process – A Second Update. *Aust. J. Chem.* **2009**, *62*, 1402.
95. Meziane, R.; Bonnet, J.-P.; Courty, M.; Djellab, K.; Armand, M. Single-ion polymer electrolytes based on a delocalized polyanion for lithium batteries. *Electrochimica Acta* **2011**, *57*, 14–19.
96. Proctor, C.M.; Rivnay, J.; Malliaras, G.G. Understanding volumetric capacitance in conducting polymers. *J. Polym. Sci. Part B Polym. Phys.* **2016**, *54*, 1433–1436.
97. Inal, S.; Malliaras, G.G.; Rivnay, J. Benchmarking organic mixed conductors for transistors. *Nat. Commun.* **2017**, *8*.

## Ch. I.-Scientific Context

98. Koutsouras, D.A.; Gkoupidenis, P.; Stolz, C.; Subramanian, V.; Malliaras, G.G.; Martin, D.C. Impedance Spectroscopy of Spin-Cast and Electrochemically Deposited PEDOT:PSS Films on Microfabricated Electrodes with Various Areas. *ChemElectroChem* **2017**, *4*, 2321–2327.
99. Stavrinidou, E.; Leleux, P.; Rajaona, H.; Khodagholy, D.; Rivnay, J.; Lindau, M.; Sanaur, S.; Malliaras, G.G. Direct Measurement of Ion Mobility in a Conducting Polymer. *Adv. Mater.* **2013**, *25*, 4488–4493.
100. Degirmenci, A.; Iskenderkaptanoglu, D.; Algi, F. A novel turn-off fluorescent Pb(II) probe based on 2,5-di(thien-2-yl)pyrrole with a pendant crown ether. *Tetrahedron Lett.* **2015**, *56*, 602–607.
101. Heinze, J.; Frontana-Uribe, B.A.; Ludwigs, S. Electrochemistry of Conducting Polymers—Persistent Models and New Concepts †. *Chem. Rev.* **2010**, *110*, 4724–4771.
102. Merz, A.; Kronberger, J.; Dunsch, L.; Neudeck, A.; Petr, A.; Parkanyi, L. Radical Dimerization of 5,5'-Diphenyl-3,3',4,4'-tetramethoxy-2,2'-bipyrrole:  $\pi$  Dimer in the Crystal,  $\sigma$  Dimer in Solution. *Angew. Chem. Int. Ed.* **1999**, *38*, 1442–1446.
103. Valencia, D.P.; González, F.J. Estimation of diffusion coefficients by using a linear correlation between the diffusion coefficient and molecular weight. *J. Electroanal. Chem.* **2012**, *681*, 121–126.
104. Ćirić-Marjanović, G. Recent advances in polyaniline research: Polymerization mechanisms, structural aspects, properties and applications. *Synth. Met.* **2013**, *177*, 1–47.
105. Shimidzu, T.; Ohtani, A.; Iyoda, T.; Honda, K. Charge-controllable polypyrrole/polyelectrolyte composite membranes: Part II. Effect of incorporated anion size on the electrochemical oxidation-reduction process. *J. Electroanal. Chem. Interfacial Electrochem.* **1987**, *224*, 123–135.
106. Aubert, P.-H.; Groenendaal, L.; Louwet, F.; Lutsen, L.; Vanderzande, D.; Zotti, G. In situ conductivity measurements on polyethylenedioxythiophene derivatives with different counter ions. *Synth. Met.* **2002**, *126*, 193–198.
107. Smie, A.; Synowczyk, A.; Heinze, J.; Alle, R.; Tschuncky, P. *i,i*-Disubstituted oligothiophenes, a new oligomeric approach towards the synthesis of conducting polymers. *J. Electroanal. Chem.* **1998**, *9*.
108. Salinas, G.; Del-Oso, J.-A.; Espinoza-Montero, P.-J.; Heinze, J.; Frontana-Uribe, B.A. Electrochemical polymerization, characterization and in-situ conductivity studies of poly-3,4-orthoxylendioxythiophene (PXDOT). *Synth. Met.* **2018**, *245*, 135–143.
109. Voortman, T.P.; Bartesaghi, D.; Koster, L.J.A.; Chiechi, R.C. Cross-Conjugated n-Dopable Aromatic Polyketone. *Macromolecules* **2015**, *48*, 7007–7014.
110. Pedraza, E.; Karajić, A.; Raoux, M.; Perrier, R.; Pirog, A.; Lebreton, F.; Arbault, S.; Gaitan, J.; Renaud, S.; Kuhn, A.; et al. Guiding pancreatic beta cells to target electrodes in a whole-cell biosensor for diabetes. *Lab. Chip* **2015**, *15*, 3880–3890.
111. Perrier, R.; Pirog, A.; Jaffredo, M.; Gaitan, J.; Catargi, B.; Renaud, S.; Raoux, M.; Lang, J. Bioelectronic organ-based sensor for microfluidic real-time analysis of the demand in insulin. *Biosens. Bioelectron.* **2018**, *117*, 253–259.
112. Donahue, M.J.; Williamson, A.; Strakosas, X.; Friedlein, J.T.; McLeod, R.R.; Gleskova, H.; Malliaras, G.G. High-Performance Vertical Organic Electrochemical Transistors. *Adv. Mater.* **2018**, *30*, 1705031.
113. Rivnay, J.; Leleux, P.; Sessolo, M.; Khodagholy, D.; Hervé, T.; Fiocchi, M.; Malliaras, G.G. Organic Electrochemical Transistors with Maximum Transconductance at Zero Gate Bias. *Adv. Mater.* **2013**, *25*, 7010–7014.

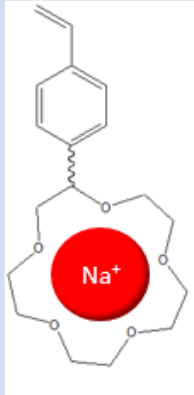
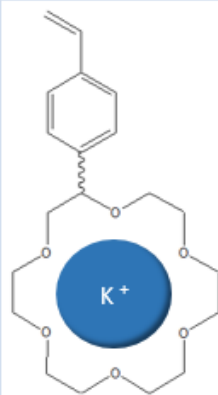
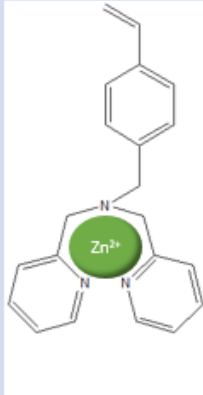


*Chapter II.-  
Ion-sensitive alternatives  
to PSS in PEDOT:PSS*



## 1 INTRODUCTION

Considering that the referent material in Organic Bioelectronics has been for many years the PEDOT: PSS, the main objective in this approach was the development of styrene derivatives integrating functional moieties, ion-sensitive groups as illustrated below:

| Targeted Cations | Sodium ( 102 pm)  | Potassium ( 138 pm)  | Zinc ( 74 pm)   |
|------------------|---|--|---|
| Monomers         |  |  |  |
| Function         | 15-crown-5<br>(15)  | 18-crown-6<br>(18)   | Dipicolylamine<br>(DPA)   |

**Figure 18: Scheme of targeted monomers designed to recognize the cations of biological interest: 18-crown-6 moiety for  $K^+$  (blue), 15-crown-5 moiety for  $Na^+$  (red), dipicolyl (DPA) for  $Zn^{+2}$  (green).**

These original monomers were employed for the synthesis of alternative polyelectrolytes to PSS and they were used as stabilisers in the synthesis of water dispersions of ion-sensitive PEDOT based inks.

## 2 SYNTHESIS OF STYRENE DERIVATIVES

As it is illustrated in **Error! Reference source not found.**, the first step in this approach has been the development of a library of styrene derivatives monomers with selected ion-

sensitive scavengers, as it can be seen in Figure 19. All the experimental details can be found at the end of the chapter.

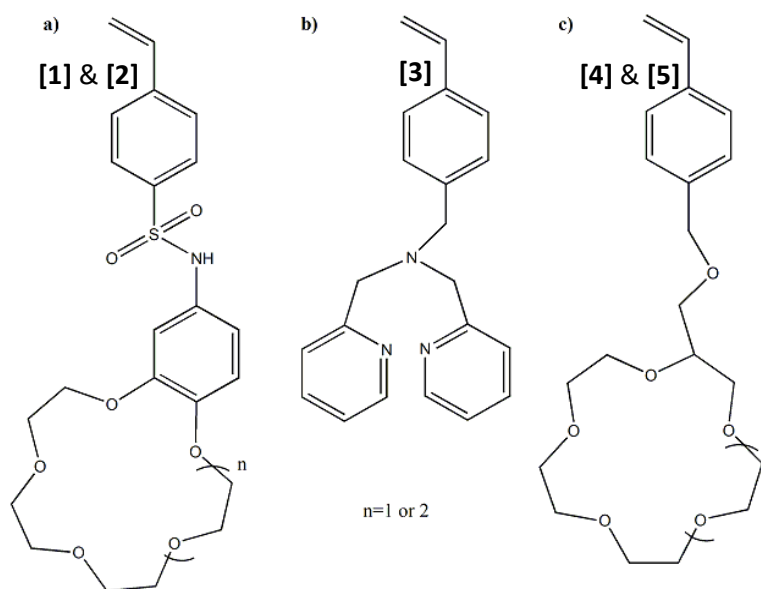


**Figure 19: Summary of the chemical structures of the monomers synthesized: a) 4-styrenesulfonyl(phenyl-15-crown-5) imide [1] when  $n=1$  and 4-styrenesulfonyl(phenyl-18-crown-6) imide [2] when  $n=2$ ; b) *N*-(4-vinylbenzyl)-di-(2-picoly) amine [3]; c) 15-crown-5-methyl-(4-vinylbenzyl)-methyl ether [4] when  $n=1$  and 18-crown-6-methyl-(4-vinylbenzyl)-methyl ether [5] when  $n=2$ .**

In the case of monomers [1] and [2] (see a) at Figure 19) the synthesis has been done by a two-steps reaction. The formation of the styrenesulfonyl chloride was followed by the reaction with the functionalized amino-crown to obtain the desired sulfamide as schematized in Figure 20. The product was obtained with a 64 % yield as a brown solid powder.

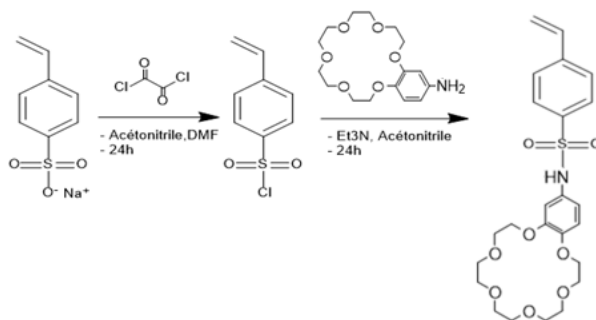


**Figure 20: Reactional Scheme of the synthesis of monomer [2]: Step 1: Vilsmeier-Haack to formed the styrenesulfonyl chloride. Step 2: Amination and formation of 4-styrenesulfonyl(phenyl-18-crown-6) imide [2].**

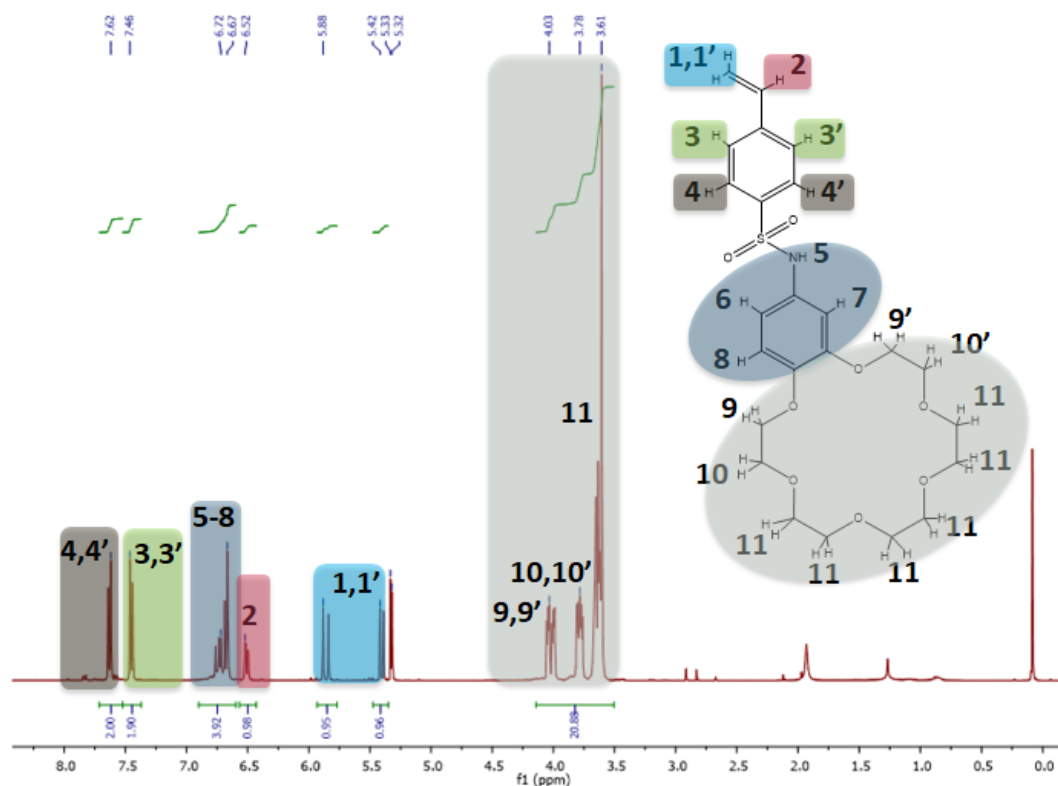


**Figure 21: Structural characterization of 4-styrenesulfonyl(phenyl-15-crown-5) imide (1):**  $^1\text{H-NMR}$  ( $\text{CDCl}_3$ , 400 MHz, 128 scans).

$^1\text{H-NMR}$  spectrum of [2], given in Figure 21, clearly shows the peaks corresponding to the styrene at 7.46 (3,3' in green) and 7.62 ppm (4,4' brown square). Vinyl protons are evidenced by the presence of the signal at 5.88 ppm and 5.42 ppm (1,1' in light blue). Ether function from the crown moiety is confirmed by the presence of the signals at 3.6-3.4 ppm (violet square). Last, the multiplet signal at 6.67 ppm (dark blue) overlaps the vinyl signal with the coupling between the phenyl aromatic protons and the amine proton.

Synthesis of the monomer [3] has been performed by an amination reaction as previously described in the literature[92]. In the reactional scheme (Figure 22) are described the basic conditions used during this thesis to produce the linking between the styrene chloride and the dipicolyl (DPA) moiety by an amination reaction to obtain monomer [3]. We were interested in this functionalization because of its simplicity, the low cost of

the precursors and the gain of the binding functionalization with nitrogen atoms as heteroatoms acting as a clamps well-known in the fluorophore probes market for its affinity towards divalent cations such as  $Zn^{2+}$ [25].

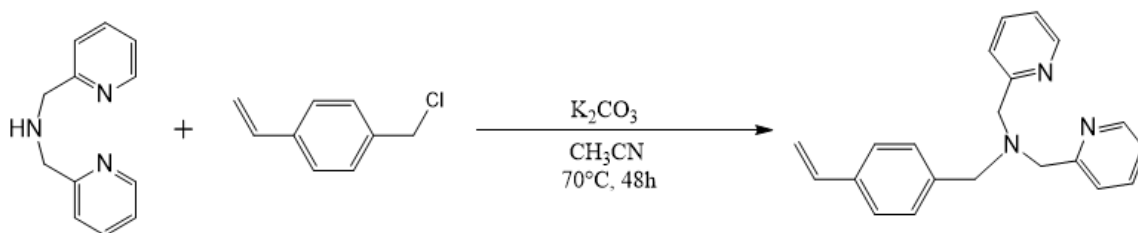


**Figure 22: Reactional Scheme of the synthesis of monomer [3]:** Amination reaction between the 4-vinylbenzylchloride and the di-(2-picolyl)amine to obtain the 4-vinylbenzyl-di-(2-picolyl)-amine or Styrene-DPA [3]

Moreover, monomers [4] and [5] have been synthesized by an etherification one-step reaction at low temperature under the presence of sodium hydride[93] (Figure 23). Structural characterization details are available in the experimental part (section 6.3).

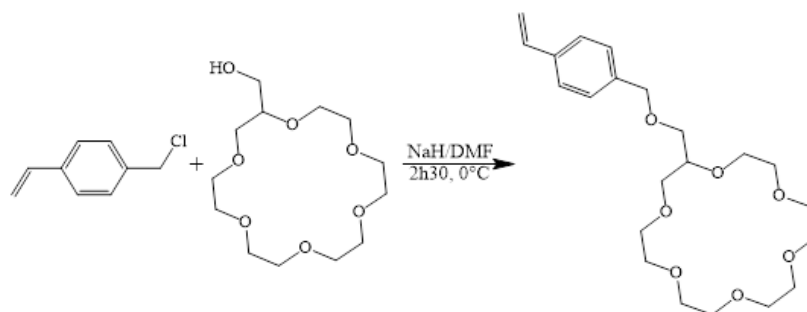


**Figure 23: Reactional Scheme of the synthesis of monomer (4):** Etherification reaction between 2-hydroxymethyl-15-crown-5 and 4-vinylbenzylchloride to obtain the 15-crown-5-methyl-(4-vinylbenzyl)-methyl ether [4]

## Cation affinity study

The binding ability of the functionalized monomers used for the subsequent synthesis of polyelectrolytes (see section 3 of this chapter), monomers [1] to [3], have been evaluated by  $^1\text{H}$ -NMR titration to study their ion sensitivity. Titrations of monomer [4] and [5] will be performed in the future to compare the linking binding effect. As example, it is described in detail (Figure 24) the titration of monomer [3] with zinc chloride (II).

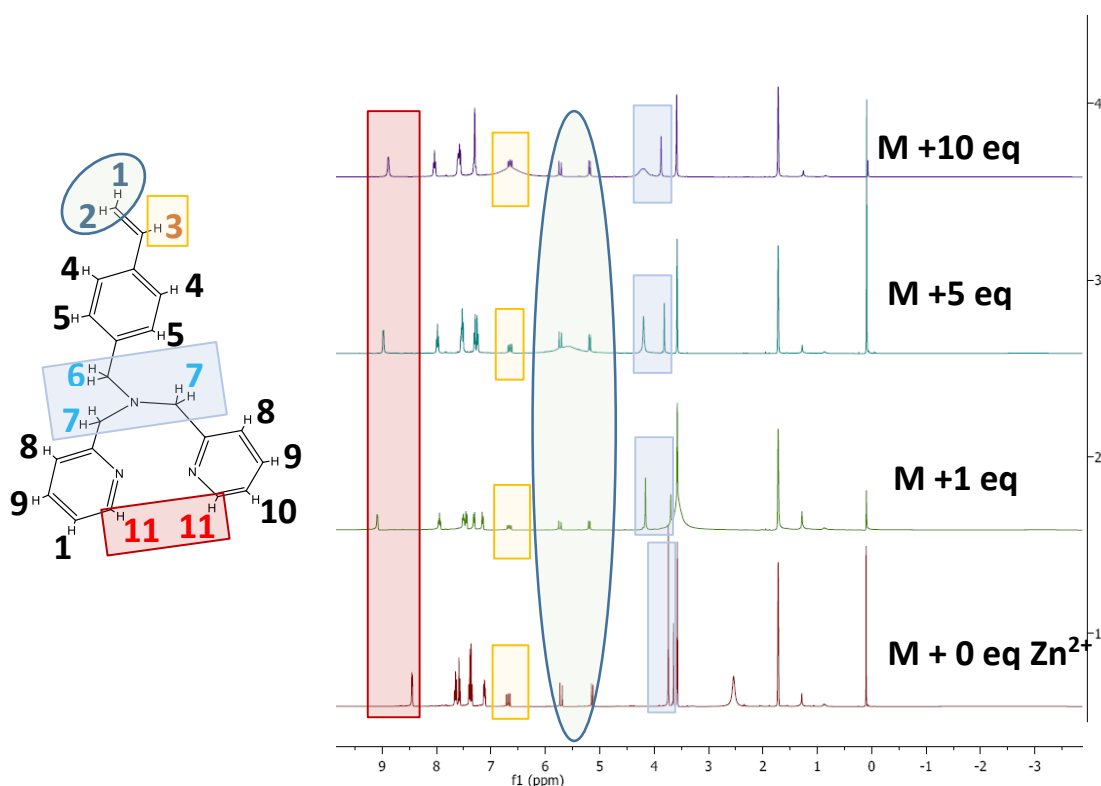


**Figure 24: Binding ability evaluation by  $^1\text{H}$ -NMR titration of monomer [3]:**  $^1\text{H}$ -RMN Spectrum (TDF, 400 MHz) obtained for the titration of the monomer [3] under variable concentrations (from 0 to 10 molar equivalents) of zinc chloride (II).

In the latter, we observed the  $^1\text{H}$ -NMR spectrum of the monomer [3] (bottom of Figure 24, red curve) without complexation. Afterwards, a great chemical shift is observed in the peaks related to the pyridine units (peak 11) when an equivalent of zinc (II) is added (Figure 24, green curve), while the chemical shifts related to the vinyl protons seems to

be not affected by the presence of the cation (peaks 1-3). This fact confirms that the binding interaction with the divalent cation occurs through the free electron pairs of the nitrogen atoms. In the same way, a little shift is observed in the alkyl protons forming the bridge of the picolyl fraction (peaks 6-7) what could confirm that this structure has the expected binding site ability. It is noteworthy that after the extra addition of equivalents of zinc, up to 10 (blue curves, spectrum 3 and 4 of Figure 24), the variation of the chemical shift observed is globally the same. This could be expected by the fact that the [picolyl: cation] interaction follows a 1:1 binding model.

From the quantification of these changes observed in the chemical shift in function of the salt concentration, we could obtain binding curves (**Error! Reference source not found.**) from which were extracted the association constants of the three styrene derivatives used for subsequent polymerization<sup>4</sup>, as it is summarized in Table 1.

**Table 1: Summary of the binding constants obtain for ion-sensitive monomers [1], [2] and [3] by <sup>1</sup>H-RMN titrations.** Monomers and the binding constants obtained for the different titrations with the target cations (Na<sup>+</sup>, K<sup>+</sup>, Zn<sup>2+</sup>). Mix solvent: DMSO (20%)/ H<sub>2</sub>O (80%). Std (K<sub>A</sub>): Standard error of the binding constant (K<sub>A</sub>). GoF (Goodness of Fit) ≥80%.

| Monomer | Binding Site | K <sub>A</sub> (M <sup>-1</sup> ) |                      |                   |                      |                   |                      |
|---------|--------------|-----------------------------------|----------------------|-------------------|----------------------|-------------------|----------------------|
|         |              | NaClO <sub>4</sub>                | Std(K <sub>A</sub> ) | KClO <sub>4</sub> | Std(K <sub>A</sub> ) | ZnCl <sub>2</sub> | Std(K <sub>A</sub> ) |
| [1]     | 15-crown-5   | 3.50E+00                          | 8.80E-01             | 5.49E+01          | 2.74E+00             |                   |                      |
| [2]     | 18-crown-6   | 1.22E+02                          | 6.89E+00             | 1.03E+03          | 1.18E+02             |                   |                      |
|         |              |                                   |                      | 1.22E+02          |                      |                   |                      |
| [3]     | DPA          | 2.46E+01                          | 4.63E+00             |                   |                      | 2.54E+03          | 1.83E+01             |

From the association constants obtained from the global fitting to a 1:1 binding model of the crown-ether functionalized styrene monomers, appears a larger affinity of the 18-crown-6 containing monomer [2] for the target cation, K<sup>+</sup>, as expected. Thus, it presents a larger constant with one order of magnitude of difference with respect to the binding constant obtained with sodium cation (1,030 vs 122 M<sup>-1</sup>). It is important to note that this

<sup>4</sup> All the <sup>1</sup>H-RMN titrations curves where fitted with Affinimeter software. See experimental part.

binding affinity is significantly lessened when the titration is done in a mix solvent of DMSO / H<sub>2</sub>O probably due to the much higher solvation of the salt and the hydrophobicity of the monomer making more difficult the interaction. Nevertheless, the affinity<sup>5</sup> of monomer [1] with the smaller 15-crown-5 moiety presents an unexpected higher affinity towards potassium cation instead of sodium. This may indicate a higher reversibility in the *complexation-decomplexation* process of this monomer with sodium cation. In any case, the binding ability of this monomer is much lower than its equivalent [2]. In the case of monomer [3], it appears a much larger affinity of the cation for the divalent zinc cation than for the monovalent sodium cation, obtaining a binding constant two orders of magnitude higher from zinc cation compared to the other. All the binding constants were extracted from fitting with at least 80% of good of fitness (GoF) representing a very small difference between the experimental values and the fitting curve.

To validate this results with a second technique, the binding ability and sensitivity of monomer [2] toward the different monovalent cations was evaluated by a second method using UV-Vis spectroscopy. As illustrated in Figure 25, the 18-crown-6 functionalized monomer was specifically sensitive to potassium cation in preference to the sodium as we could expect due to presence of the 18-crown-6 sensing moiety.

---

<sup>5</sup> This term refers to how strong the binding is and it is defined by the binding of association constant ( $K_A$ ).

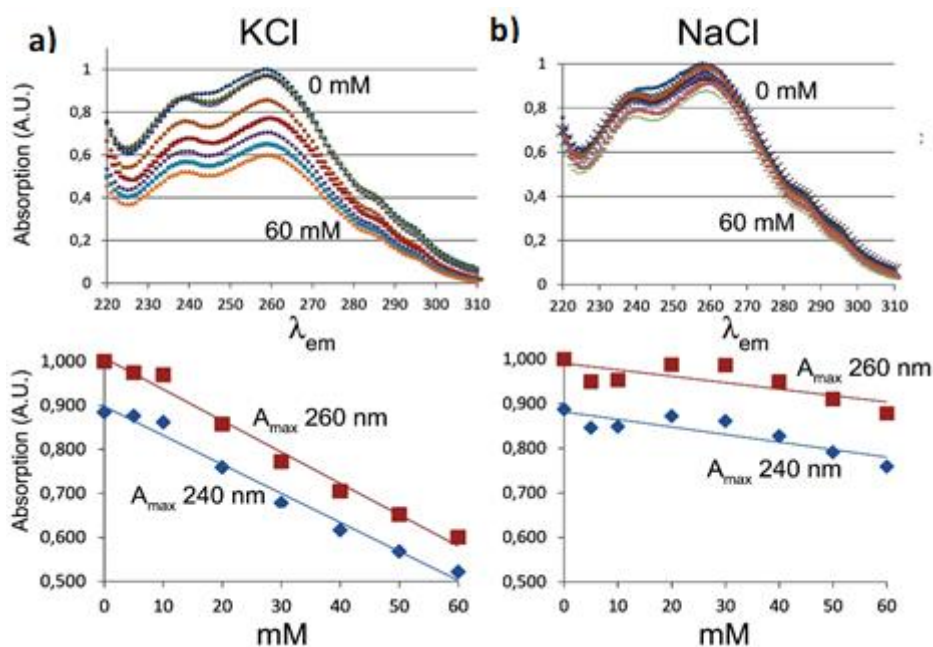


**Figure 25: Ion-specific changes in Absorption of 4-styrenesulfonyl(phenyl-18-crown-6)imide (SP18Cr6)[2].** Absorbance spectra were measured for SP18Cr6 (50  $\mu\text{M}$ ) at different KCl or NaCl concentrations (10 mM steps from 0 to 60). Upper panel: spectra; Lower panel, Absorption maxima at 240 or 260 nm.

As comparative and more visual presentation of data, a linear regression fit was applied to the difference of absorbance shift observed in the titration of the monomer with the alkaline cations ( $\text{K}^+$  and  $\text{Na}^+$ ) in the two absorption bands of the monomer (240 and 260 nm). At both wavelengths we observed the same tendency: the shift is larger as the concentration of potassium cation is higher (Figure 25-a bottom), whilst the change is negligible when the titration is done in presence of sodium cation (Figure 25-b bottom).

This result is in total agreement with the higher association constant found for monomer [2] to potassium by  $^1\text{H-NMR}$  titration (Table 1), showing a higher affinity for potassium as we could expect due to presence of the 18-crown-6 sensing moiety. As future work, titrations of monomer [4] and [5] will be performed to compare the linking binding effect in the monomers, polyelectrolytes and ink properties.

### 3 POLYELECTROLYTES: Copolymers between STFSI & the Ion chelating agents modified styrene monomers

The new styrene derivatives described on section 2 were used for the generation of original polyelectrolytes through radical polymerization methods well-known in the literature. Reversible Addition-Fragmentation Chain Transfer (RAFT) polymerization has been employed as controlled radical polymerization to take benefit of the main advantages of this method such as: many types of polymerizable monomers (including styrene derivatives of our interest in this work), conditions (solvent, temperature...), variety of chain transfer agent (CTA), etc. [94] In addition, polyelectrolytes based on the well-known STFSI monomer and the new styrene derivatives synthesized were imagined for sensing applications, so statistical copolymers of high molecular weights were obtained by long-term RAFT polymerizations (until 120 hours). Moreover, I could benefit of the know-how achieved in the LCPO laboratory acquiring the transfer knowledge of the method that I could adapt to the desired copolymerizations.

Different families of copolymers between the most common monomer 4-styrenesulfonyl(trifluoromethylsulfonyl)imide (STFSI), used in our group for transparent electrodes[77,81] or well known for their application in lithium batteries[95], and different functionalized monomers with ion-sensitive chelating moieties (section 2) were synthesized.

The STFSI fraction gives solubility in water, whilst the functionalized monomer brings the ion-recognition ability. The latter was added in increasing molar ratio with respect to the STFSI constituting a series of families of copolymers (Table 2): *P1* for 15-crown-5 containing polyelectrolytes derivatives of monomer [1], *P2* for polyelectrolytes with 18-crown-6 moieties from monomer [2] and *P3* for DPA containing polyelectrolytes from [3]. Monomers [4] and [5] will be exploit in this stage and for the inks formation (Section 3) in future work.

As illustrative example, a scheme of the general polymerization method for the *P3* family is presented in Figure 26:

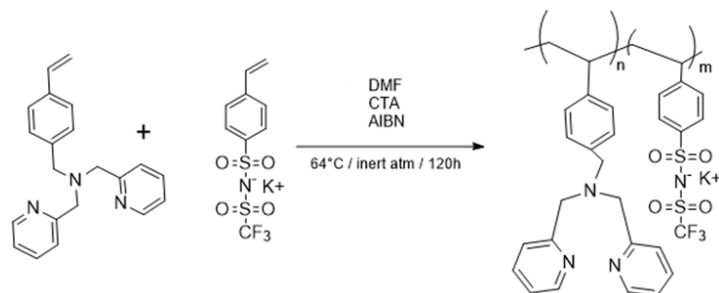


**Figure 26: Scheme of the RAFT polymerisation of *P3* Copolymers family between STFSI and [3]:** CTA: Control transfer reagent; AIBN: Initiator 2,2'-Azobis(2-methylpropionitrile);  $m$ : fraction of STFSI;  $n$ : fraction of DPA functionalized monomer [3].

A summary of the different families of polymers synthesized is shown in Table 2.<sup>6</sup> They are classified by colours related to the ion-sensitive moiety present in their structure: 15-crown-5 (orange) for  $\text{Na}^+$ , 18-crown-6 (blue) for  $\text{K}^+$  and DPA (green) for  $\text{Zn}^{2+}$ . It is important to notice that long times of polymerization were necessary to achieved high molecular weights polyelectrolytes, higher than 100 KDa.

<sup>6</sup> (\*) Mw (KDa) and  $\bar{M}_w$  were obtained from calibration with polystyrene standards. All details are in experimental part and Appendices chapter. <sup>a</sup> nd: Not determined. n.s.: not stable. Y: "Yes": Synthesized.

**Table 2: Summary of CP synthesized and *posteriori* used for the stabilization of Ion-sensitive PEDOT dispersions.** M: Monomer; CP: Copolymer; M<sup>0</sup>: STFSI monomer; M: functionalized monomer ([1] to [3]); n<sub>m0</sub> / n<sub>M</sub>: molar ratio between both monomers; M<sub>w</sub>: Molecular weight of the obtained copolymers\*; Đ: Dispersity obtained from SEC\*; Ink: PEDOT derivative ink synthesized with this copolymer (see section 4 of this chapter).

| M   | Serie - CP | Composition electrolyte (M <sup>0</sup> <sub>WT%</sub> - M <sub>WT%</sub> ) | n <sub>m0</sub> / n <sub>M</sub> | M <sub>w</sub> / KDa* | Đ*              | Ink  |
|-----|------------|---|----------------------------------|-----------------------|-----------------|------|
| [1] | P1-A       | PSTFSI <sub>50</sub> -PS15cr5 <sub>50</sub>                                 | 0.8                              | nd <sup>a</sup>       | nd <sup>a</sup> | -    |
|     | P1-B       | PSTFSI <sub>60</sub> -PS15cr5 <sub>40</sub>                                 | 1.2                              | 154                   | 2.6             | -    |
|     | P1-C       | PSTFSI <sub>65</sub> -PS15cr5 <sub>35</sub>                                 | 1.5                              | 128                   | 2.2             | -    |
|     | P1-D       | PSTFSI <sub>70</sub> -PS15cr5 <sub>30</sub>                                 | 1.8                              | 115                   | 2.2             | -    |
|     | P1-E       | PSTFSI <sub>80</sub> -PS15cr5 <sub>20</sub>                                 | 3.2                              | 130                   | 2.3             | ①    |
|     | P1-F       | PSTFSI <sub>85</sub> -PS15cr5 <sub>15</sub>                                 | 4.5                              | 29                    | 1.6             | ②    |
|     | P1-G       | PSTFSI <sub>90</sub> -PS15cr5 <sub>10</sub>                                 | 7.1                              | 108                   | 1.8             | -    |
|     | P1-I       | PSTFSI <sub>95</sub> -PS15cr5 <sub>5</sub>                                  | 15.0                             | 152                   | 2.4             | -    |
|     | P1-H       | PSTFSI <sub>0</sub> -PS15cr5 <sub>100</sub>                                 | -                                | nd <sup>a</sup>       | nd <sup>a</sup> | -    |
| [2] | P2-A       | PSS <sub>95</sub> -PS18cr6 <sub>5</sub>                                     | 13.6                             | 112                   | 1.3             | ③, ⑥ |
|     | P2-B       | PSTFSI <sub>90</sub> -PS18cr6 <sub>10</sub>                                 | 6.5                              | 127                   | 2.3             | -    |
|     | P2-C       | PSTFSI <sub>85</sub> -PS18cr6 <sub>15</sub>                                 | 4.1                              | 135                   | 2.6             | ④    |
|     | P2-D       | PSTFSI <sub>85</sub> -PS18cr6 <sub>15</sub> (250KDa)                        | 4.1                              | 208                   | 2.8             | ⑤    |
|     | P2-E       | PSTFSI <sub>70</sub> -PS18cr6 <sub>30</sub>                                 | 1.7                              | 144                   | 2.3             | Y    |
|     | P2-F       | PSTFSI <sub>60</sub> -PS18cr6 <sub>40</sub>                                 | 1.1                              | 44                    | 1.4             | Y    |
|     | P2-G       | PSTFSI <sub>50</sub> -PS18cr6 <sub>50</sub>                                 | 0.7                              | 96                    | 2.3             | n.s. |
| [3] | P3-A       | PSTFSI <sub>50</sub> -PSDPA <sub>50</sub>                                   | 1.1                              | nd <sup>a</sup>       | nd <sup>a</sup> | -    |
|     | P3-F       | PSTFSI <sub>60</sub> -PSDPA <sub>40</sub>                                   | 1.7                              | nd <sup>a</sup>       | nd <sup>a</sup> | -    |
|     | P3-C       | PSTFSI <sub>70</sub> -PSDPA <sub>30</sub>                                   | 2.6                              | nd <sup>a</sup>       | nd <sup>a</sup> | -    |
|     | P3-E       | PSTFSI <sub>80</sub> -PSDPA <sub>20</sub>                                   | 4.5                              | nd <sup>a</sup>       | nd <sup>a</sup> | -    |
|     | P3-G       | PSTFSI <sub>85</sub> -PSDPA <sub>15</sub>                                   | 6.4                              | nd <sup>a</sup>       | nd <sup>a</sup> | ⑦    |
|     | P3-B       | PSTFSI <sub>90</sub> -PSDPA <sub>10</sub>                                   | 10.1                             | nd <sup>a</sup>       | nd <sup>a</sup> | -    |
|     | P3-D       | PSS <sub>95</sub> -PSDPA <sub>5</sub>                                       | 21.3                             | nd <sup>a</sup>       | nd <sup>a</sup> | -    |

(\*) Mw (KDa) and Đ were obtained from calibration with polystyrene standards. All details are in experimental part and Appendices chapter. <sup>a</sup>nd: Not determined. n.s.: not stable. Y: "Yes": Synthesized.

$^1\text{H-NMR}$  of *P1-C* (with moieties of 15-crown-5 ether, Table 2) is presented in detail to illustrate the structural characterisation of the copolymers (Figure 27). It could be distinguished the broad band ( $\delta=3.72$  ppm, green square) corresponding to the different units of crown ether successfully incorporated to the copolymer structure, as well as the band related to the alkyl backbone after the polymerization ( $\delta=1.57$  ppm, orange) and the band corresponding to the aromatic rings ( $\delta=6.78$  and  $\delta=7.73$ , violet and brown).

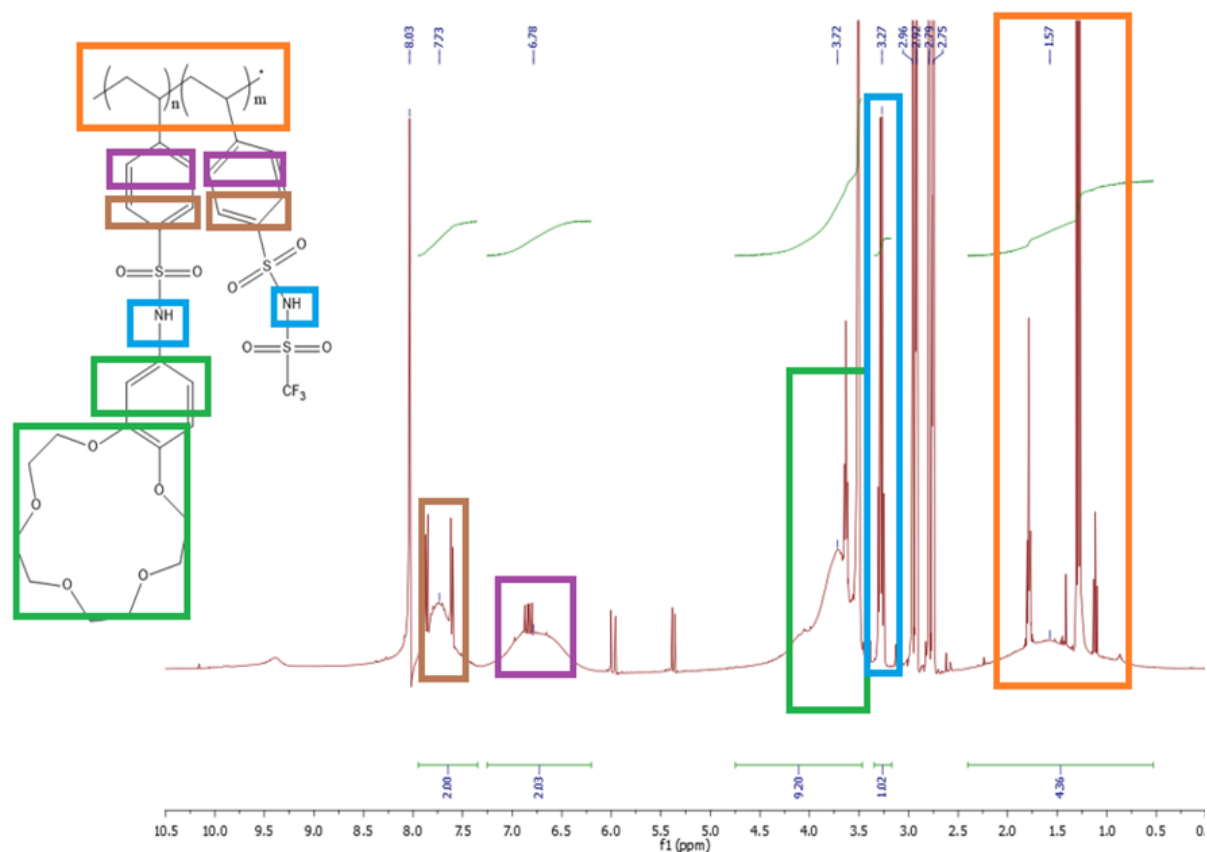


**Figure 27: Structural characterization of copolymer *P1-C* (see Table 2):  $^1\text{H-NMR}$  Spectrum (d-DMF, 400 MHz) of a copolymer *P1-C* synthesized from STFSIK (65% wt.) and 15-crown-funtionalized monomer [1] (35 %wt.).**

Moreover, it is shown in Figure 28 a SEC chromatogram of a *P2-G* (18-crown-6 family) copolymer where it is observed a Gaussian size distribution.

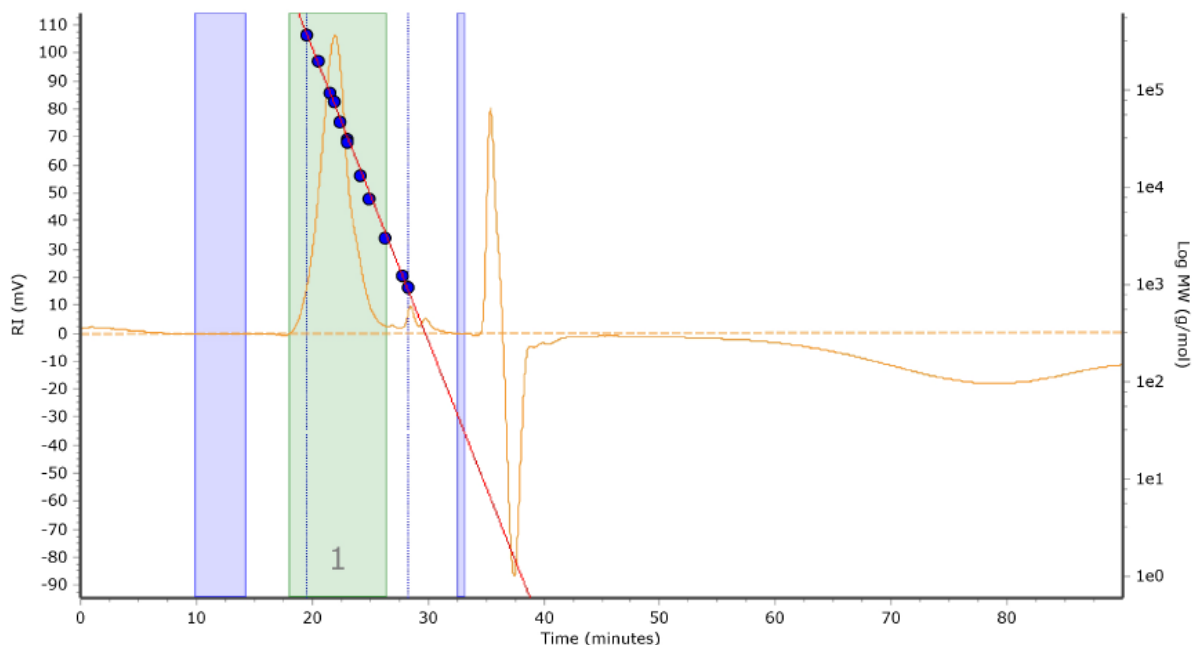


**Figure 28:** Size exclusion chromatogram of a *P2-G* (18-crown-6 family) showing a monomodal distribution (Mw: 96 KDa. Obtained from SEC calibrated with polystyrene standards. DMF, LiBr, 70°C).

The size of the family of copolymers formed between STFSI and monomer [3], *P*(3), could have not been fully characterized by size exclusion chromatography, due to their extremely viscous nature, preventing the filtration of the samples and consequently not allowing to determine the size of the main polymer chains present in the random copolymers. Nevertheless, we observed the progressive incorporation of the ion-sensitive moiety (DPA) when the molar ratio of [3] is increased with respect to STFSI to take place the synthesis of these copolymers (Figure 29). Analysis of the  $^1\text{H-NMR}$  spectra evidenced a linear increase of the integration area under the peaks related to DPA fraction when the more weight fraction of [3] is used for the copolymerization.

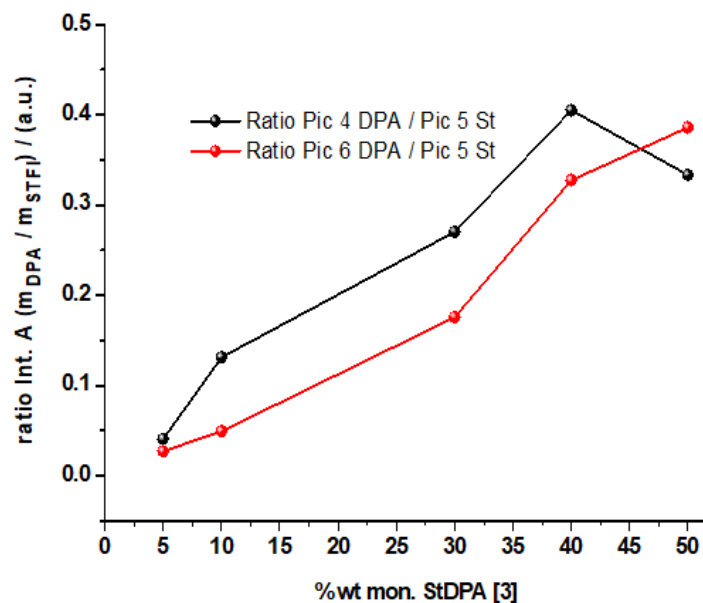


**Figure 29: Integration of DPA in copolymers of the serie P3 (see Table 2-serie P3):** Ratio between the integration area under the NMR peaks (**Int A**) related to monomer [3] ( $m_{DPA}$ ) vs STFSI ( $m_{STFSI}$ ) with respect to the weight percentage added of [3] (%wt. mon StDPA [3]).

It is important to note that complexation and cation sensitivity of some copolymers synthesized was evaluated also by UV-Vis titration showing that the sensing ability is well preserved in the copolymers (as shown in the Annex 4 in the *Appendices* Chapter).

## 4 PEDOT based Ion-sensitive inks

The ion-sensitive functionalized polyelectrolytes synthesized (section 3) were used as stabilisers of PEDOT water dispersions as substitutes of PSS. The reactional scheme of the oxidative polymerization of EDOT shows the radical formation and sequential interaction to give dimers, tetramers, etc. until achievement of the final PEDOT chains (Figure 30).

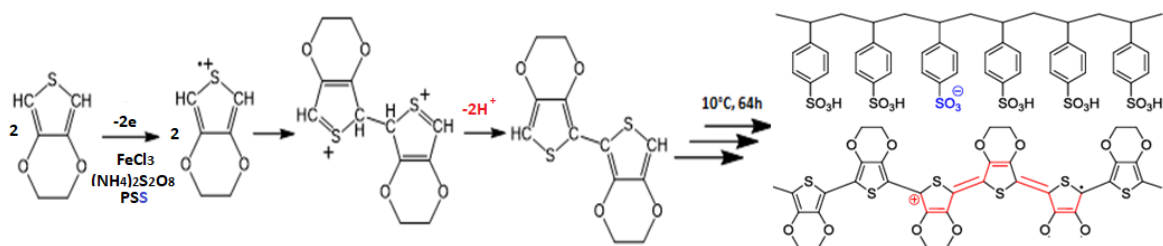


**Figure 30: Oxidative polymerization of EDOT in the presence of oxidants (iron chloride (III) and ammonium persulfate) and stabiliser in water (example of PSS).**

The same process happens in water with the functionalized polyelectrolytes. As illustrative example, it is presented an initial polyelectrolyte solution of one of the copolymer, P2-C from Table 2 (Figure 31-a) acting as stabiliser of PEDOT favouring the complex formation and stability of the PEDOT dispersion in its reduced form in water due to the presence of the counter anions of the STFSI moieties (Figure 31-b).

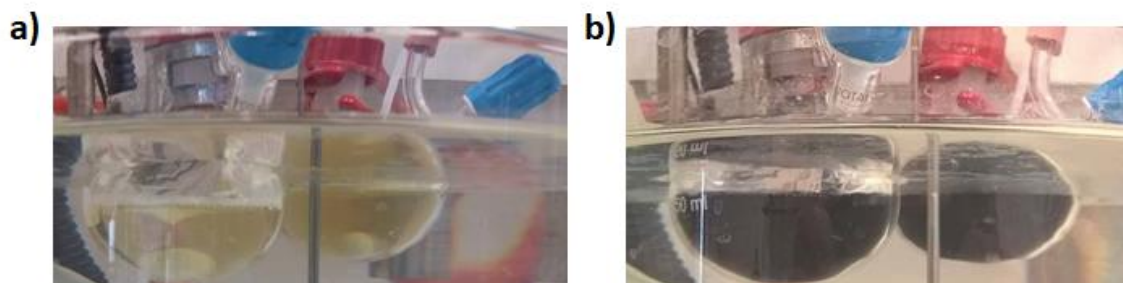


**Figure 31: Aqueous dispersion formation of the ion-sensitive PEDOT based inks:** Reactors of water dispersions of the polyelectrolyte: **a)** Before the addition of the oxidants, brownish colour polyelectrolyte solution; **b)** After addition of the oxidants, formation of the PEDOT based ink.

Polyelectrolytes obtained from monomers [1] to [3] were used as stabilisers for the formation of different PEDOT based inks. Polyelectrolytes from [4] and [5] will be explored in the future work to study the linking binding effect. The molar concentration of EDOT and the concentration of polyelectrolyte used to stabilize the PEDOT dispersion in water were kept constant. The changes were done in the composition (ratio between STFSI and functionalized monomer) and molecular weight of the copolymers (the polyelectrolytes). Thus, the counter anion was the sulfonamide present in STFSI or the

sulfonic group present in PSS. The iron chloride and ammonium persulfate were used as oxidants.

It was possible to obtain processable inks with the different polyelectrolytes families. It was noticed that stable dispersions of PEDOT were achieved only when they were stabilized by polyelectrolytes that contain the ion-sensitive functionalized monomer fraction (wt% crown- ether) lower than a 50 wt %.

A summary of the different processable inks synthesized is shown in Table 3:

**Table 3: Summary of the aqueous dispersion inks synthesized and characterized with the ion-sensitive polyelectrolytes.** Sheet resistance ( $R_s$ ), thickness ( $t$ ) and conductivity ( $\sigma$ ) of thin films. **M**: Monomer: 1-3 refers to the respective functionalized monomers; 0 refers to the STFSI monomer without any ion-sensitive moiety; Ctrl: Control (PSS polyelectrolyte). **CP**: Copolymer. **CNT**: Carbon nanotube.

| M    | Serie - CP | INK   | Polyelectrolyte Composition   | t/ nm | $R_s/K\Omega\cdot sq$ | $\sigma/ mS\cdot cm^{-1}$ |
|------|------------|-------|---|-------|-----------------------|---------------------------|
| 1    | P1-E       | 1     | PSTFSI <sub>80</sub> -PS15cr5 <sub>20</sub>                         | 250   | 44.8                  | 893                       |
|      | P1-F       | 2     | PSTFSI <sub>85</sub> -PS15cr5 <sub>15</sub>                         | 150   | 62.8                  | 1062                      |
| 2    | P2-A       | 3     | PSS <sub>95</sub> -PS15cr5 <sub>5</sub>                             | 380   | 0.22                  | $120\cdot 10^3$           |
|      | P2-C       | 4     | PSTFSI <sub>85</sub> -PS15cr5 <sub>15</sub>                         | 250   | 29.4                  | 1366                      |
|      | P2-C       | 4-CNT | PSTFSI <sub>85</sub> -PS15cr5 <sub>15</sub>                         | 270   | 3600                  | 11                        |
|      | P2-D       | 5     | PSTFSI <sub>85</sub> -PS15cr5 <sub>15</sub> (250KDa)                | 180   | 36.8                  | 1598                      |
|      | P2-A3      | 6     | PSS <sub>95</sub> -PS15cr5 <sub>5</sub> (3)                         | 290   | 0.35                  | $98.5\cdot 10^3$          |
| 3    | P3-A       | 7     | PSTFSI <sub>85</sub> -PS15cr5 <sub>15</sub>                         | 250   | 3360                  | 12                        |
|      | P3-B       | 8     | (EDOT <sub>50</sub> -PEDOTDPA <sub>50</sub> ):PSTFSI <sub>100</sub> | 200   | 0                     | 0                         |
| 0    | P0-L       | 9     | PSTFSI (100 KDa)  | 250   | 0.084                 | $110\cdot 10^3$           |
|      | P0-H       | 10    | PSTFSI -HMW (250 KDa)   | 250   | 0.125                 | $164\cdot 10^3$           |
| Ctrl | PSS        | 11    | PSS (Heraus PH1000)   | 250   | 0.145                 | $190\cdot 10^3$           |

Thin films of the different ion sensitive inks were fabricated by spin-coating, tuning the thickness of the films by varying the rpm. The different inks (1-11) are classified by colours related to the ion-sensitive moiety present in their structure: 15-crown-5 (orange) sensitive to Na<sup>+</sup>, 18-crown-6 (blue) sensitive to K<sup>+</sup> and DPA (green) for Zn<sup>2+</sup>. They were

also used referent material inks, based on PSTFSI (*Ink 9 and 10*) or PSS (*Ink 11*) polyelectrolytes, to compare to the ion-sensitive inks.

With the aim to improve the electrical conductivity of the inks, few composite tests were done with the addition of SW-CNT in one of 18-crown-6 containing ink (*Ink 4-CNT*). Nevertheless, the composite obtained presented an absence of conductivity, fact that may be ascribed to the low dispersability of the carbon nanotubes and the presence of aggregates in the dispersion.

To sum up, it was possible to obtain processable inks with the different polyelectrolytes families and, even if their conductivities were found lower than PEDOT:PSS, they present conductivities going from mS to S range, highly enough to take benefit of the sensitivity of these materials in transistors devices.

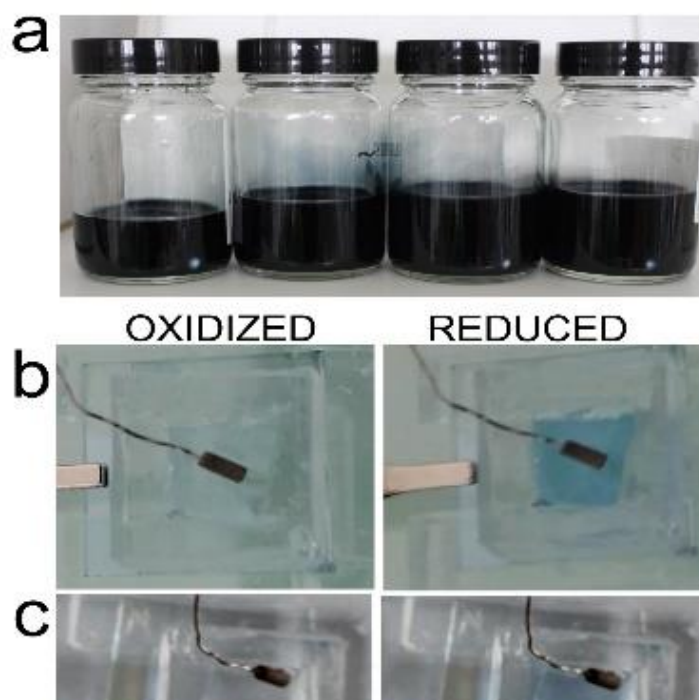


**Figure 32: PEDOT based inks.** a) Some examples of the stable aqueous dispersions synthesized containing crown-ether moieties; b - c) Electrochromic behaviour of these inks showing their doped (transparent) and dedoped state (light blue),  $V=-0.75\text{mV}$ : b) PEDOT: PSS (commercial); c) PEDOT ink with 18-crown-6 moieties (*Ink 4*, Table 3). Conditions: electrolyte 0.1 M NaCl (aq.)

The electrochemical activity was monitored by electrochemically dedoping the films and more precise quantification was done by electrochromic spectroscopy experiments.

## 4.1 Electrochromic Spectroscopy

The electrochemical doping rates were extracted by measuring the absorbance over time upon applying a positive bias (see Annex 5). The changes in the initial peak absorbance intensity were measured and the logarithm of normalized relative values of the absorbance were plotted to allow a comparison of different films. At least two linear functions could be fitted to extract the electrochemical response rates from the slopes (green and blue linear fittings in Figure 33).

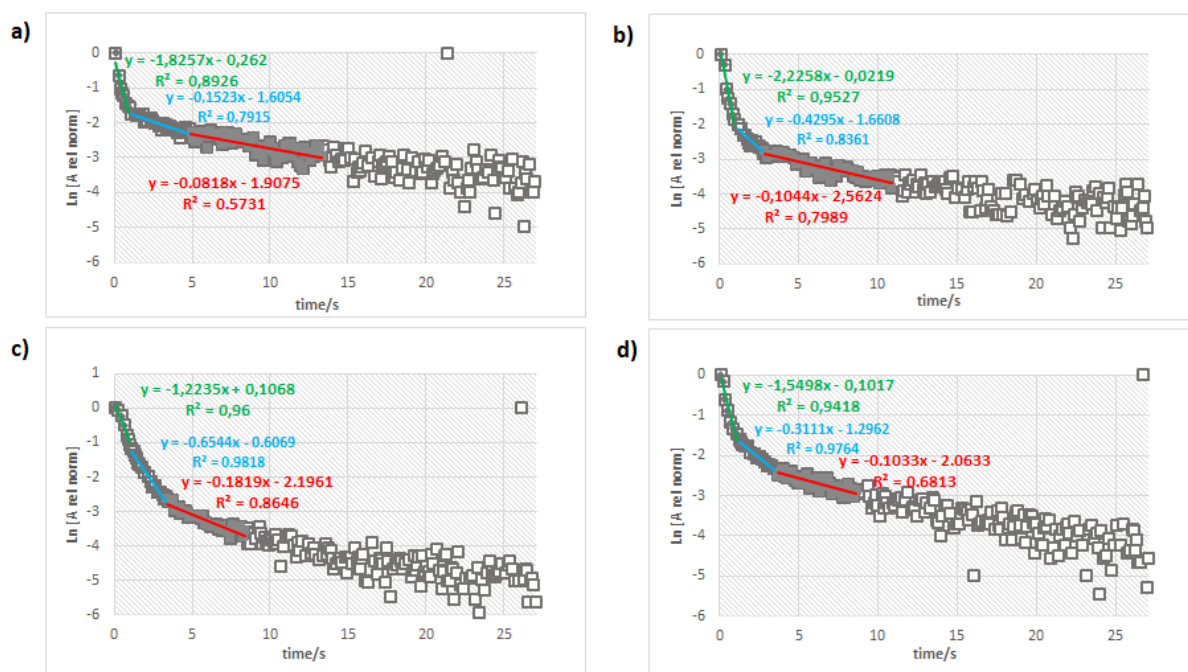


**Figure 33: Electrochromic response of thin films (150 nm) of referent vs 18-crown-6-functionalized ink:** Electrochemical rates of PEDOT based inks in different aqueous electrolytes: Ink containing 15 wt% of 18-crown-6 (*Ink 4* of P2-C) in 0.1M NaCl (aq.) **(a)** and 0.1M KCl (aq.)**(b)**; PEDOT:PSS in 0.1M NaCl (aq.) **(c)** and 0.1M KCl (aq.)**(d)**.

The first regime is likely related to the actual dedoping of the film reflecting the larger percentage of the electrochemical response of the film, whilst in the other two regimes are involved other phenomena as cation diffusion and swelling of the polymer. In order to gain a better insight of the doping/depoing process and the mass transport inside the polymer matrix, in-situ electrochemical-conductivity and EQCM experiments should be performed.

Comparison of the first regime (green line) obtained when the electrochromic profile of polymer films of PEDOT:PSS and a 18-crown-6 containing ink, Ink 4, was evaluated in aqueous electrolytes containing different alkaline cations, Na<sup>+</sup> or K<sup>+</sup> (Table 4).

**Table 4: Influence of alkaline effect on the electrochromic rates:** Constants rates of the first linear regime fitted to the electrochromic responses of films of *Ink 4* and PEDOT:PSS in different aqueous electrolytes: 0.1 M of NaCl (red) and 0.1 M of KCl (light blue). Their ratio ( $K_{K^+}/K_{Na^+}$ ) is also shown (green). PE: Polyelectrolyte. Conditions: Substrate: ITO film, RE: Ag/AgCl.

|       |        | Cation |                 |                | $K_{K^+}/K_{Na^+}$ |
|-------|--------|--------|-----------------|----------------|--------------------|
|       |        | PE     | Na <sup>+</sup> | K <sup>+</sup> |                    |
| PEDOT | PSS    |        | -1.2235         | -1.5498        | <b>1.27</b>        |
|       | PCr15% |        | -1.8257         | -2.2258        | <b>1.22</b>        |

We observed a response in the same order of magnitude as for the PEDOT:PSS film which is a good indication of preservation of electrochromic properties and good swelling of the functionalized films, demonstrated by the fact that the change from oxidized to reduced state is produced by the good penetration of ions into the film when applied a positive voltage in the referent electrode ( $E = + 0.75$  V). Moreover, we found a slightly larger ratio for the ink containing 18-crown-6 moieties than for the classical PSS electrolyte. This could be a preliminary demonstration of the higher affinity for the target cation in the case of functionalized ink.

To confirm that this response is mainly due to a good dedoping in the volume of the film and that this ink act as mixed conductor (ion and electronic conductivity). These preliminary tests, lead us to measure the electroactivity of different films by impedance spectroscopy to evaluate in a more quantitative manner this property.

## 4.2 Electrochemical Impedance Spectroscopy (EIS)

Considering the importance of the volumetric capacitance to account for the volume-dependence of OECT performance[96] and in the figure of merit for mixed conductors materials used in this kind of devices[97], the impedance of some of the ion-sensitive inks synthesized was measured by EIS to elucidate their capacitive behaviour as a function of composition, doping extent and film thickness.

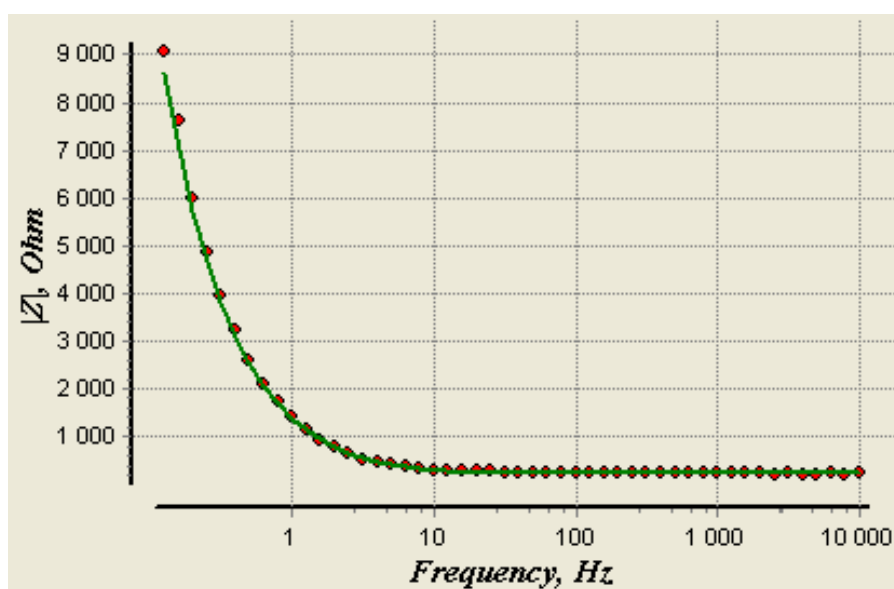


**Figure 34: Electrochemical impedance fitting and capacitance extraction:** Bode plot ( $|Z^*|$  vs.  $f$ ) of a film of *Ink 4*, based on a polyelectrolyte PSTFSI\_85%-PS18cr6\_15% (P2-C), (red scatter) and its fitting (green line).

The capacitances of the films were extracted by EIS modelling and the fitting was done using the previously reported model by our co-workers[98]. This model is based in a simple circuit consisting of a resistor and a capacitor in series representing the polymer electrode/electrolyte interface (see Annex 6). The resistive element corresponds to the

resistance of the solution to ion diffusion and the contact resistances are also incorporated into this term. The capacitive element corresponds to the polymer capacitance.

In the thin films evaluated, we found a profile similar to the model with this two clear components: at high frequencies being predominant the resistive component (plateau at Figure 34); and, at low frequencies, it is the capacitance of the polymer film (linear regime at Figure 34). Thus, it was possible to do the fitting of these experimental curves and extract their capacitance values (Table 5,  $V_{\text{thin films}}$  and  $C^*$ ).

**Table 5: Summary of volumetric capacitance ( $C^*$ ) extracted from EIS data:** Thickness: 120-150 nm (thin films) and 250 nm (thick films). Colours: Indication of the ion-sensitive moiety present in the structure: orange for 15-crown-5 and blue for 18-crown-6 (see **Error! Reference source not found.**). M: Monomer. CP: Copolymer. V: volume.  $C^*$ : Volumetric capacitance. Avg ( $C^*$ ): Average volumetric capacitance.

| M | Serie - CP | # sample EIS | INK   | Polyelectrolyte Composition                             | $V_{\text{thin film}}/\text{cm}^3$ | $C^*/\text{F}\cdot\text{cm}^{-3}$ | $V_{\text{thick film}}/\text{cm}^3$ | $C^*/\text{F}\cdot\text{cm}^{-3}$ | Avg ( $C^*$ )/ $\text{F}\cdot\text{cm}^{-3}$ |
|---|------------|--------------|-------|---|------------------------------------|-----------------------------------|-------------------------------------|-----------------------------------|--|
| 1 | P1-E       | 5            | 1     | PSTFSI <sub>80</sub> -PS15cr5 <sub>20</sub>             | 1.99E-06                           | 49.9                              | -                                   | -                                 | 49.9   |
| 2 | P2-C       | 2            | 4     | PSTFSI <sub>85</sub> -PS18cr6 <sub>15</sub>             | 2.05E-06                           | 50.1                              | 3,98E-06                            | 36                                | 43.05  |
|   | P2-C       | 4            | 4-CNT | PSTFSI <sub>85</sub> -PS15cr5 <sub>15</sub>             | 2.00E-06                           | 44.6                              | -                                   | -                                 | 44.6   |
|   | P2-D       | 3            | 5     | PSTFSI <sub>85</sub> -PS15cr5 <sub>15</sub><br>(250KDa) | 3.43E-06                           | 3.3                               | 3,98E-06                            | 5.7                               | 4.5  |

Higher volumetric capacitances as compared to the referent material, PEDOT:PSS ( $C^*=39 \text{ F}\cdot\text{cm}^{-3}$ )[97] were evidenced for all the inks evaluated except for the *Ink 5*, constituted by a higher molecular weight polyelectrolyte. Nevertheless, it is important to note that the fit of this model was poor for this film and for most of the other thick films (250 nm), as it is illustrated in Annex 7. This fact could be an indication that the increasing percentage of crown-ether moieties present in the polyelectrolyte chains have an important impact on the physical properties of the film and the higher this percentage is, the higher is the capacitive component. In the model employed is not taking into account the film resistance. To validate these approximations, SEM and AFM experiments should

be performed. Thus, as perspective work, it may be necessary in the future to explore this relation to have a better understanding of these materials. Indeed, it is likely that swelling is facilitated in the case of higher crown-ether content. The development of an appropriate model that could integrate all these variations should allow a better fitting of these experimental curves to extract the capacitance values and other physical parameters of interest.

In addition, we compared the effect of polyelectrolyte molecular weight used here for the synthesis of the dispersible inks with the volumetric capacitance. We observed a considerable decrease on the electrode impedance when the electrode was covered by a low-molecular weight polyelectrolyte based ink (film 1 vs film 2 in Figure 35) over the complete frequency range of biological interest. We expect that the use of this type of polyelectrolyte may favour biological recordings with lower noise level[98].

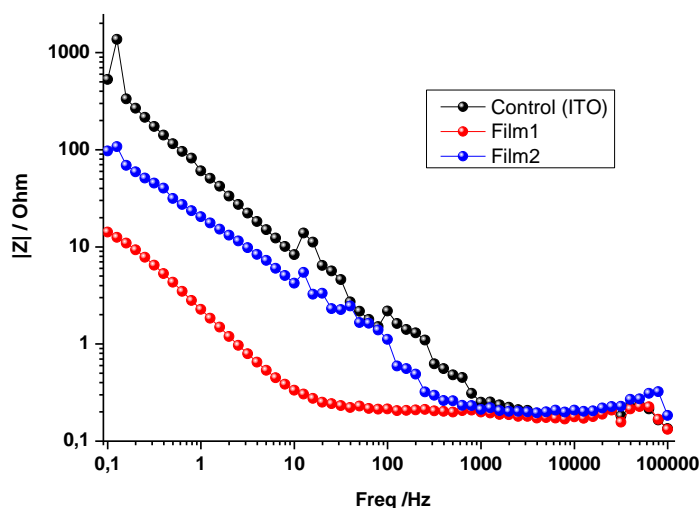


**Figure 35: Molecular weight effect on the electrochemical impedance profile:** Bode plots of inks films constituted by the same polyelectrolyte composition as Figure 34 (PSTFSI<sub>85%</sub>-PS18cr<sub>615%</sub>) with different Molecular weights: 100 KDa (Film1) and 250 KDa (Film 2). Control: ITO substrate (Black curve).

To sum up, variable capacitance was demonstrated by applying different levels of voltage offset. The volumetric capacitance of different films was calculated and compared to that

## Chapter II- Ion sensitive alternatives to PSS in PEDOT:PSS

of PEDOT: PSS. The results of these experiments indicate that these ion-sensitive inks act as mixed conductor with similar swelling properties as the referent.

## 5 CONCLUSION

Synthesis and characterization of a series of functionalized styrene derivatives with ion-sensitive moieties [1] to [5] were performed. These monomers were used to the synthesis of polyelectrolytes, afterwards they were used for the synthesis of aqueous dispersion inks alternatives to PEDOT:PSS. The study of the structure and properties of these three group of species (monomers- polyelectrolytes- inks) were characterized by different techniques to elucidate their structure, ion affinities, processability and mix-conduction ability.

In the family of monomers, it was found the expected affinity for the targeted cation in the case of monomers [2] for  $K^+$  and [3] for  $Zn^{2+}$ . The monomer [1] shows unexpectedly a bigger binding association with potassium cation than sodium. Likely the interaction with sodium could be more reversible explaining this result. Nevertheless, alternatives kinetics study could help to validate this hypothesis.

Different series of polyelectrolytes have been successfully synthesized by copolymerization the classical STFSI with these functionalized monomers in different weight percentage. The preservation of the sensitivity for the targeted cations was also observed by UV-Vis spectroscopy. These polyelectrolytes were used as stabilisers for the chemical oxidative polymerization of EDOT in water dispersions to obtain different inks containing the ion-sensitive groups. These inks appear very stable and easily processable, obtaining thin films with traditional deposition techniques as spin-coating. Their electrochromic properties were studied and compared with the referent material. In addition, volumetric capacitance and electrochemical impedance properties were evaluated and show their potential to act as mixed-conductors, property that would be exploited in sensing devices.

## Chapter II- Ion sensitive alternatives to PSS in PEDOT:PSS

To conclude, these inks preserve the advantages of traditional PEDOT:PSS inks, presenting even higher volumetric capacitance, and possess an ion-sensitivity towards the targeted cation due to the chelating groups incorporated in their structures. The cytotoxicity and application of these materials is described on the Chapter 4 of Applications.

## 6 EXPERIMENTAL PARTSYNTHESIS OF MATERIALS

### 6.1.1 MONOMERS

- **Potassium 4-styrenesulfonyl(trifluoromethylsulfonyl)imide**

Step 1- Formation of 4-styrenesulfonyl chloride (GENERAL PROCEDURE):

A round bottom flask, previously flame-dried, was charged with dry and degassed acetonitrile (V=60 mL). Oxalyl chloride (5.91 g, 46.6 mmol, 1.2 eq.) and DMF were added. This solution was kept under stirring at room temperature to solubilize the reagents and promote the Vilsmeier-Haack complex formation for 4 or 5 hours. Once the characteristic yellow colour of the solution became stable, 4-styrenesulfonic acid sodium salt (8.0 g, 38.8 mmol, 1.0 eq.) was added slowly to the solution under nitrogen atmosphere and at room temperature. After 24h of reaction, the salt precipitated was separated by filtration and the reaction mixture was used in the second step.

Step 2- Synthesis of Potassium 4-styrenesulfonyl(trifluoromethylsulfonyl)imide (STFSIK) (GENERAL PROCEDURE):

In a second flame-dried round bottom flask containing dry and degassed acetonitrile (V=50 mL), triethylamine (16.55 g, 116 mmol, 3 eq.) and trifluoromethylsulfonamide (5.78 g, 38.8 mmol, 1 eq.) were added and stirred for one hour. During this time, the 4-styrenesulfonyl chloride/acetonitrile solution (formed during Step 1) was cooled at 0 °C. Then, the trifluorosulfonamide solution is added in vacuum atmosphere to the former. Afterwards, the mixture was allowed to warm up to room temperature and reaction was kept running under stirring for 16h. Purification has been done firstly removing under low pressure the mixture solvent and solubilizing the monomer into dichloromethane. The product was obtained by extraction with potassium carbonate and subsequently a last washing with chlorhydrique acid 1M solution. Solvent was removed under low pressure and after drying overnight at 45°C under vacuum, the product is recovered as a viscous brown product. Ion exchange has been done putting in an excess potassium carbonate solution followed by recrystallization to obtain the potassium salt STFSIK (yield=54%).<sup>1</sup>H-

NMR (300 MHz; DMSO-d<sub>6</sub>; 298K):  $\delta$ (ppm)= 7.73 (d, 2H); 7.57 (d, 2H); 6.79 (q, 1H); 5.95 (d, 1H); 5.38 (d, 1H). <sup>13</sup>C-NMR (75 MHz; DMSO-d<sub>6</sub>; 298K):  $\delta$ (ppm)= 144.21; 139.55; 135.57; 126.43; 125.87; 126.36–122.06–117.77–113.47 (q CF<sub>3</sub>); 116.55; <sup>19</sup>F-NMR (282 MHz; DMSO-d<sub>6</sub>; 298K):  $\delta$ (ppm)= 21.715. FTIR (ATR cm<sup>-1</sup>): = 1400, 1329, 1281, 1195, 1172, 1159, 1140, 1090, 1058, 844, 776, 735, 655. m/z (ESI-HRMS) 313.9779 ([M<sup>-</sup>] C<sub>9</sub>H<sub>7</sub>F<sub>3</sub>NO<sub>4</sub>S<sub>2</sub> requires 313.9769).

- **4-styrenesulfonyl(phenyl-18-crown-6) imide [2]**

Step 1- Formation of 4-styrenesulfonyl chloride:

Same method describes before (see Step1 for Potassium 4- styrenesulfonyl (trifluoromethylsulfonyl)imide).

Step 2- Synthesis of 4-styrenesulfonyl(phenyl-18-crown-6) imide (Sph18cr6SI):

In a second flame-dried round bottom flask containing dry and degassed acetonitrile (V=50 mL), triethylamine (4.29 g, 30.2 mmol, 3 eq.) and 4'-aminobenzo-18-crown-6 (3.00 g, 10.1 mmol, 1 eq.) were added and stirred for one hour. During this time, the 4-styrenesulfonyl chloride/acetonitrile solution (formed during Step 1) was cooled at 0 °C. Then, the trifluorosulfonamide solution is added in vacuum atmosphere to the former. Afterwards, the mixture was allowing to warp up to room temperature and reaction was kept running under stirring for 16h. Purification has been done firstly removing under low pressure the mixture solvent and solubilizing the monomer into dichloromethane. The product was obtained by extraction with potassium carbonate and subsequently a last washing with chlorhydrique acid 1M solution. Solvent was removed under low pressure and after drying overnight at 45°C under vacuum, the product is recovered as a porous-viscous brown solid product. (yield=54%). <sup>1</sup>H-NMR (400 MHz; d-DMSO; 298K):  $\delta$ (ppm)= 7.79 (d, 2H); 7.61 (d, 2H); 6.80 -6.52(q, s, dd, 4H); 5.99-5.94 (d, 1H); 5.48-5.36 (d, 1H); 3.98 – 3.50 (m, 20H). <sup>13</sup>C-NMR (75 MHz; d-DMSO; 298K):  $\delta$ (ppm)= 147.9; 145.46; 141.1; 138.4; 135.2; 130.54; 127.9; 127.15; 126.84; 126.63; 117.76; 113.93; 113.14; 107.7; 68.82; 69.74-67.97. m/z (ESI-HRMS) (516.17 ([MNa<sup>+</sup>] C<sub>24</sub>H<sub>31</sub>NO<sub>8</sub>SNa requires 516.57).

- **4-styrenesulfonyl(phenyl-15-crown-5) imide [1]**

Step 1- Formation of 4-styrenesulfonyl chloride:

Same method describes before (see Step1 for Potassium 4- styrenesulfonyl (trifluoromethylsulfonyl)imide).

Step 2- Synthesis of 4-styrenesulfonyl(phenyl-15-crown-5) imide (Sph15cr5SI):

Same method describes before (see Step2 for 4-styrenesulfonyl(phenyl-18-crown-6) imide).

<sup>1</sup>H-NMR (400 MHz; CHCl<sub>3</sub>; 298K): δ(ppm)= 7.63 (d, 2H); 7.41 (d, 2H); 6.69-6.51 (m, d, 4H); 5.84 (d, 1H); 5.40 (d, 1H); 4.02-3.72 (m, 17H). <sup>13</sup>C-NMR (150 MHz; CHCl<sub>3</sub>; 298K): δ(ppm)= 149.5; 147.5; 142.1; 137.8; 135.5; 129.8; 127.8; 126.7. 117.6; 116.3; 114.1; 110.2; 71.1 – 68.9. m/z (ESI-HRMS) 472.14 ([MNa<sup>+</sup>] C<sub>22</sub>H<sub>27</sub>NO<sub>7</sub>SNa requires 472.52).

- **N-(4-vinylbenzyl)-di-(2-picolyl) amine [3]**

Synthesis was done as described in the literature (ref1). Under an inert gas atmosphere, Di-(2-picolyl) amine (2 mmol), p-(chloromethyl)-styrene (2 mmol) and anhydrous sodium carbonate (10 mmol) was dissolved in 50 ml dichloromethane and stirred for 24 h at room temperature. Then 50 mL deionized water was added to the solution. The organic phase was washed once with 50 mL water, dried over anhydrous sodium sulfate and concentrated under vacuum. Silica gel column purification with dichloromethane/diethyl ether (10:1, v/v) gave 0.5 g of yellowish oil (91%). <sup>1</sup>H NMR (400 MHz, CDCl<sub>3</sub>): δ (ppm)= 8.52 (s, 2H); 7.66 (d, 2H); 7.54 (d, 2H); 7.36 (s, 4H); 7.13 (t, 2H); 6.88 (m, 1H); 5.73 (d, 1H); 5.22 (t, 1H); 3.81 (s, 4H); 3.68 (s, 2H). <sup>13</sup>C-NMR (150 MHz, CDCl<sub>3</sub>, 298K): δ(ppm)= 159.8; 149.2; 138.7; 136.6; 129.2; 126.4; 123.0; 122.2; 113.7; 60.1; 58.4.

- **15-crown-5-methyl-(4-vinylbenzyl)-methyl ether [4]**

A solution of 2-Hydroxymethyl-15-crown-5 (1.55 g, 5.9 mmol) in 15 ml of DMF, was added dropwise to a solution of sodium hydride (0.307 g, 7.67 mmol) in 15 ml of DMF under inert atmosphere at 0°C. After 30 min at this temperature, 4-vinylbenzyl chloride (1.109 ml, 7.08 mmol) was added. The reaction mixture was stirred at 0°C for 2 h and after being

warmed at room temperature it was quenched with water (70 mL). The organic phase was extracted with ethyl acetate and the combined organic layers were dried over anhydrous  $\text{Na}_2\text{SO}_4$  and concentrated under vacuum. Flash chromatography using silica gel chromatography with DCM/ $\text{Et}_2\text{O}$  (10:1) as eluent provided a colourless oil (2.4 g, 93% yield).  $^1\text{H-NMR}$  ( $\text{CDCl}_3$ , 400 MHz):  $\delta(\text{ppm})= 7.30$  (dd, 2H), 7.21 (dd, 2H), 6.63 (q, 1H), 5.68 & 5.54 (d, 2H), 4.46 (s, 2H), 3.59 (m, 4H), 3.59 (m, 19 H).  $^{13}\text{C-NMR}$  (150 MHz,  $\text{CDCl}_3$ , 298K):  $\delta(\text{ppm})= 136.9$ ; 135.8; 126.7; 125.1; 112.7; 77.7; 69.5; 69.4.

- ***18-crown-6-methyl-(4-vinylbenzyl)-methyl ether* [5]**

Same method describes before for 15-crown-5-methyl-(4-vinylbenzyl)-methyl ether using a solution of 2-Hydroxymethyl-18-crown-6 (1.83 g, 5.9 mmol). (2.2 g, 91% yield).  $^1\text{H NMR}$  ( $\text{CDCl}_3$ , 400 MHz):  $\delta(\text{ppm})= 7.31$  (dd, 2H), 7.21 (dd, 2H), 6.63 (q, 1H), 5.67 & 5.16 (d, 2H), 4.46 (s, 2H), 3.59 (m, 2H), 3.59 (m, 23 H).  $^{13}\text{C-NMR}$  (150 MHz,  $\text{CDCl}_3$ , 298K):  $\delta(\text{ppm})= 136.9$ ; 135.8; 126.7; 125.1; 112.7; 77.7; 69.5; 69.4

## 6.1.2 POLYMERS

- **Radical Polymerizations and copolymerizations**

The different series of copolymers between the polyelectrolyte PSTFSI and the different ion-sensitive Styrene derivatives were synthesized by reversible addition-fragmentation chain-transfer (RAFT) polymerization by mixing, according to the target molar mass, the proper quantity of the STFSIK monomer, the 2-(Dodecylthiocarbonothioylthio)-2-methylpropionic acid as CTA and azobisisobutyronitrile (AIBN) in DMF[81,95]. After several freeze-thaw cycles, the mixture was left to polymerize at 65°C from several hours to few weeks, depending on the molar mass that should be obtained. The polymer was ready after precipitation in tetrahydrofuran (THF) or the adequate solvent mixture, filtration, washing with THF and drying in vacuum oven at 65°C for at least one day.

### 6.1.3 AQUEOUS DISPERSIONS INKS

Three solutions of iron chloride (III) (0.036 g, 0.22 mmol), ammonium persulfate (0.161 g, 0.71 mmol) and the styrene-based copolymer (see section 4) chosen (0.210 g-0.420g) were prepared in individual aqueous solutions and stirring during 5h previous to use. Afterwards, the polyelectrolyte solution is transferred to the reactor and EDOT monomer is added (0.038 mL, 0.36 mmol) keeping under nitrogen flow at 10°C for 30 min. Addition of the half of the oxidants solutions prepared of iron chloride and ammonium persulfate starts the polymerization. Reaction is kept running under static inert atmosphere during 64h. Purification has been done by ultrafiltration, washing firstly with a hydrochloric acid 1M solution (150mL). Concentration of the aqueous dispersion ink has been done and diluted with the previous used acid solution. After stirring for 2 more hours, a last water washing was done. Filtration and analysis in UV have been done to find a 1% of dry content. Subsequent concentrations were done until the obtention of a c.a 1% weight content. Inks were storage protected from light at constant temperature and under stirring.

## 6.2 CHARACTERISATION METHODS

### 6.2.1 NMR and UV-Vis Titrations

Supramolecular titration experiments have been done at constant concentration of the monomer under study (host) and at zero / increasing concentration of the salt (ligand) between the different samples. Spectra were run of every sample observing the change in the maximum of absorbance in the case of UV-Vis Spectroscopy or the change in the chemical shift in the case of  $^1\text{H-NMR}$  spectroscopy. Fitting was done following linear regression in the case of UV analysis and compare the slopes obtained in function of the different salts (cation influence) evaluated. Variation in the chemical shift observed

in  $^1\text{H-NMR}$  spectroscopy was fitted to 1:1 binding model using Affinimeter software<sup>7</sup> and extracting from data treatment the global association constants.

## 6.2.2 Electrochemical Impedance Spectroscopy of thin films

A three electrode configuration cell has been used for all the experiments, with a AgAg/Cl reference electrode, a Pt electrode as counterelectrode and a ITO/ glass substrate covered with the PEDOT based film to characterize on the top (deposition was done by spin coating). When assembling the film on the cell, only a surface of 78.54 mm<sup>2</sup> of the film is in direct contact with the electrolyte. It was measured the Impedance curve in function of frequency between 0.1 and 10<sup>5</sup> Hz. Data was fitting using EISA-1 software and fitting to a model of an equivalent circuit based on a resistor-capacitor structure.

## 6.2.3 Ion Mobility in thin films - 1D Dedoping Front

Planar junctions were fabricated using standard microfabrication techniques[99]. The fabrication started with the deposition of a 2  $\mu\text{m}$  thick PaC film (SCS Labcoater2, SCS, USA) on a glass substrate (26 mm  $\times$  76 mm). Following this, a 100 nm gold electrode was deposited at one side of the glass/PaC substrate using photolithography techniques. Subsequently, spin-coating of PEDOT:PSS as well as the ion-sensitive inks was carried out. The PaC film and Au electrode were mildly etched with oxygen plasma (100 W for 1 min, Reactive Ion Etcher, Oxford) just before the deposition of the polymer films, in order to enhance adhesion of the polymers with the substrate and ensure good electrical contact to the electrode. The ion-sensitive inks used in this study were formulated analogous to the often-used formulation of PEDOT:PSS (5 vol% EG, 0.1 vol% DBSA, and 1 wt% of GOPS). Subsequently the ink formulations were spin-cast (speed rates:  $v_1= 500$  rpm,  $v_2=1200$  rpm) in two steps with a soft bake at 50°C for 1 min between each deposition. The films were then cured at 50°C for 30 min and at 140°C for 30 min to crosslink the film. In first trials, a 10  $\mu\text{m}$ -thick SU-8 film was spin-coated on top of the conductive polymer films to

---

<sup>7</sup> Data fitting was performed with the AFFINImeter server (<http://www.affinimeter.com>). Unless stated otherwise the experimental data was fit using a simple 1 : 1 binding model.

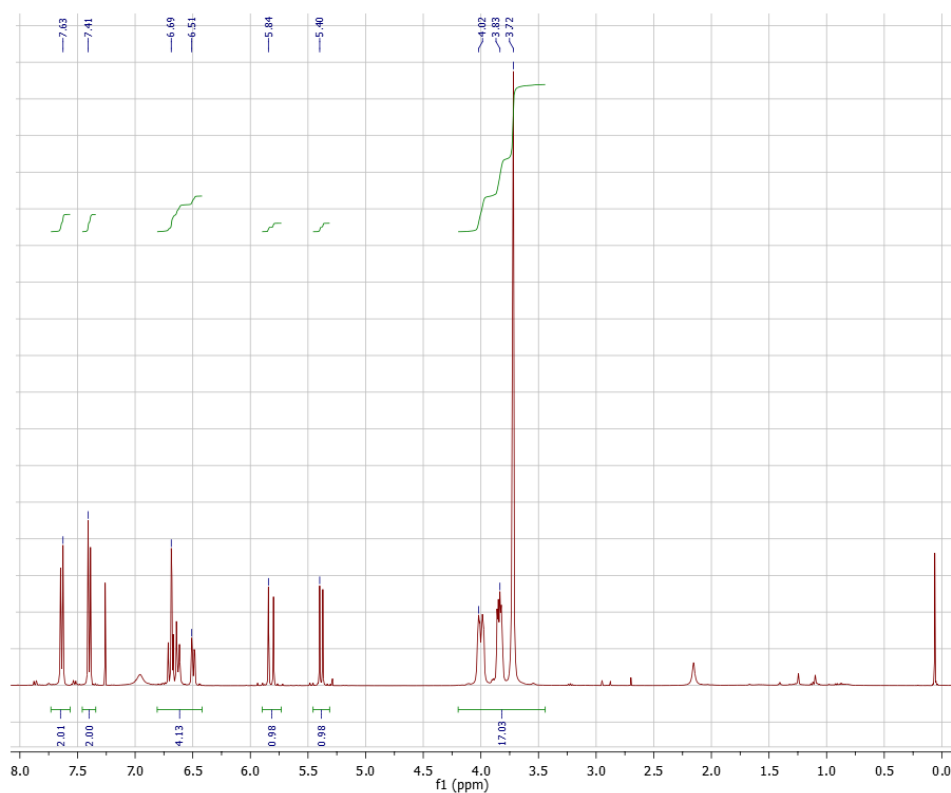
serve as an Insulation/ion barrier. After a post-exposure bake, it was developed according to the manufacturer's specifications to open a well of 16 mm × 5 mm. The final chose was to use a peel-able tape to define the area to be accessible by the electrolyte. PaC was deposited on top of the conductive polymer films to serve as an Insulation/ion barrier. Finally, the films were immersed in deionized water to remove low molecular weight additives.

On some trials was tested a second fabricated set-up, where few changes were introduced. The film was isolated with a parafilm/glass top layer as insulator. They were used two Pt electrodes instead of Ag/AgCl: one of them to applied the bias with respect to the Au electrode, and the second one was placed really close to the beginning of the 1D opening in the film and it was connected to a multimeter to measure the voltage/current leakage, and so the effective voltage in the film.

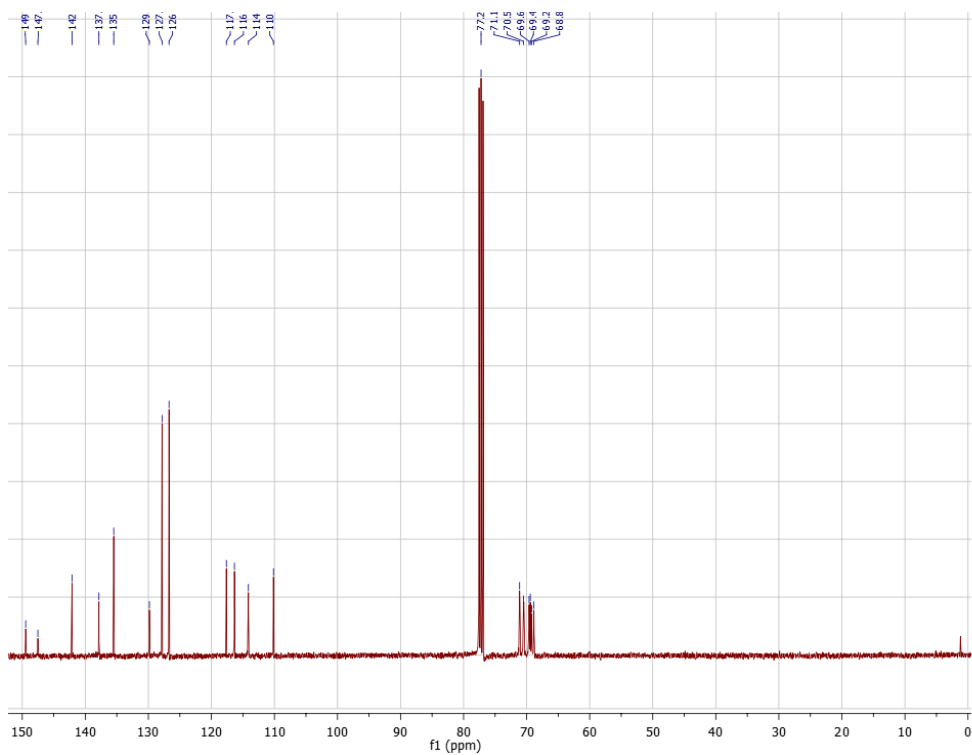
*1D- Ion mobility characterization:* Characterization was carried out using a polydimethylsiloxane (PDMS) well, placed on top of the insulator (SU-8/PaC) opening, confining 1.5–2 mL of electrolyte. A Ag/AgCl electrode was immersed in the electrolyte. The device-to-device reproducibility was found to be better than 15%, which permitted a pristine device to be used for each type of electrolyte. The electrolyte solutions were freshly made using 0.1 M aqueous solution of KCl /NaCl/ ZnCl<sub>2</sub> in deionized water. Dedoping was achieved by applying a positive bias to the Ag/AgCl electrode. The dedoping front was not allowed to reach the Au electrode. Dedoping front movement in the sample was recorded with a confocal microscope (Axio Observer Z1, Zeiss, Germany) and time lapse images were recorded in the bright-field mode with a 1x objective. The images were corrected to assure uniform light intensity throughout the field of view. Repolarization have been done applying the opposite voltage. Analysis of the grey level profile and quantification of the data was done using Fiji and Origin software.

### 6.3 NMR Spectrum

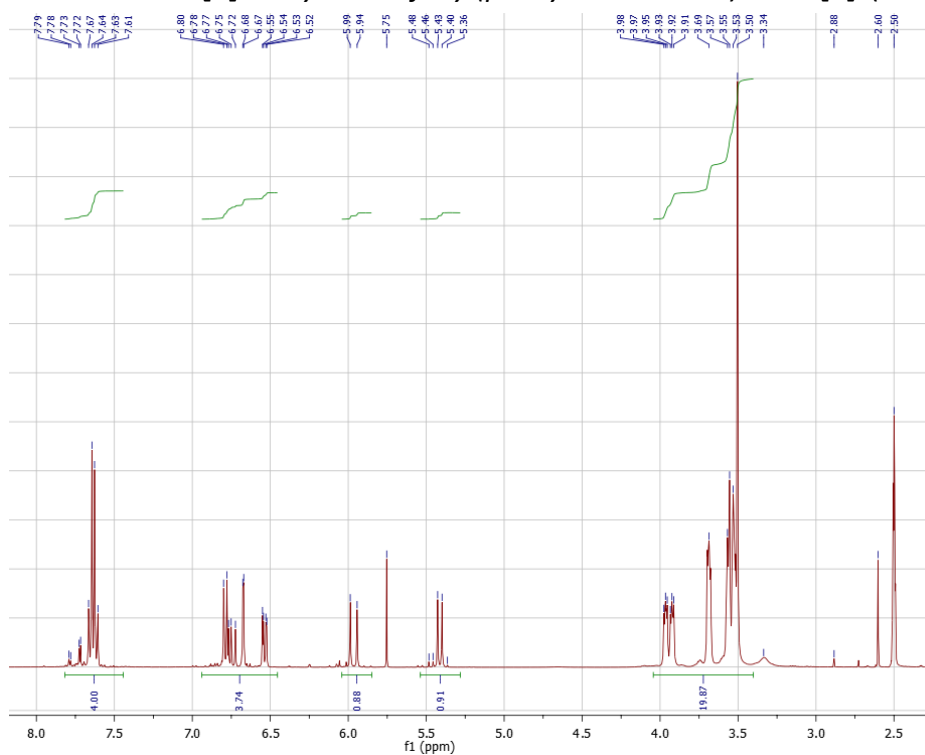
S- 1:  $^1\text{H-NMR}$  of monomer [1]: 4-styrenesulfonyl(phenyl-15-crown-5) imide [1] (400 MHz,  $\text{CDCl}_3$ )



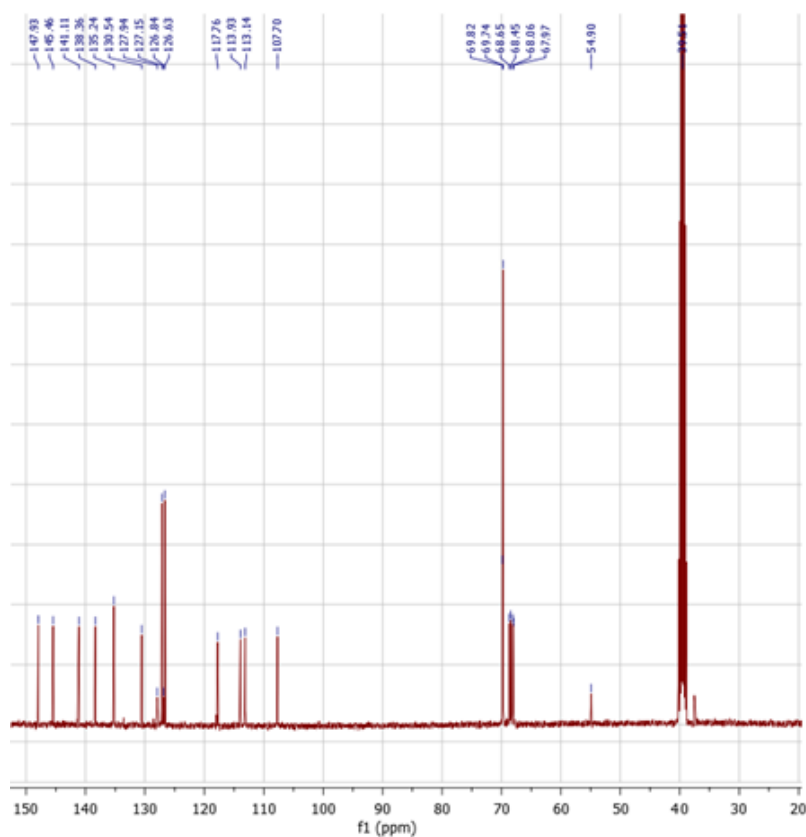
S- 2:  $^{13}\text{C-NMR}$  of monomer [1]: 4-styrenesulfonyl(phenyl-15-crown-5) imide [1] (400 MHz,  $\text{CDCl}_3$ )



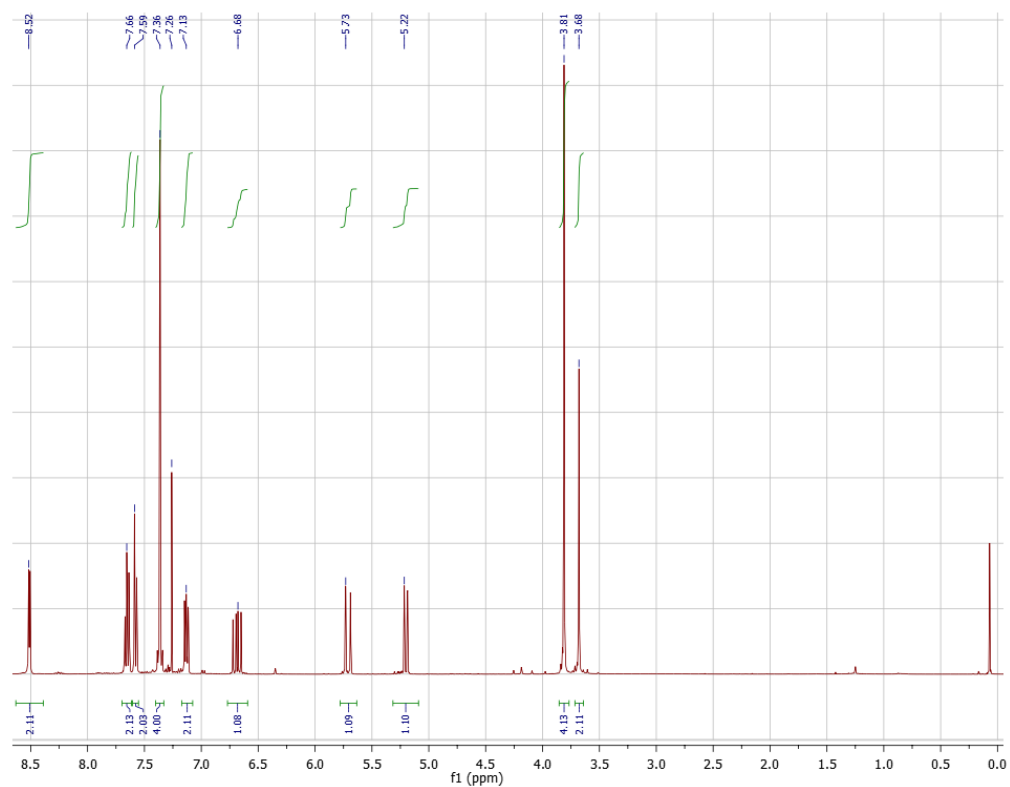
**S- 3:  $^1\text{H-NMR}$  of monomer [2]: 4-styrenesulfonyl(phenyl-18-crown-8) imide[2] (400 MHz; DMSO)**



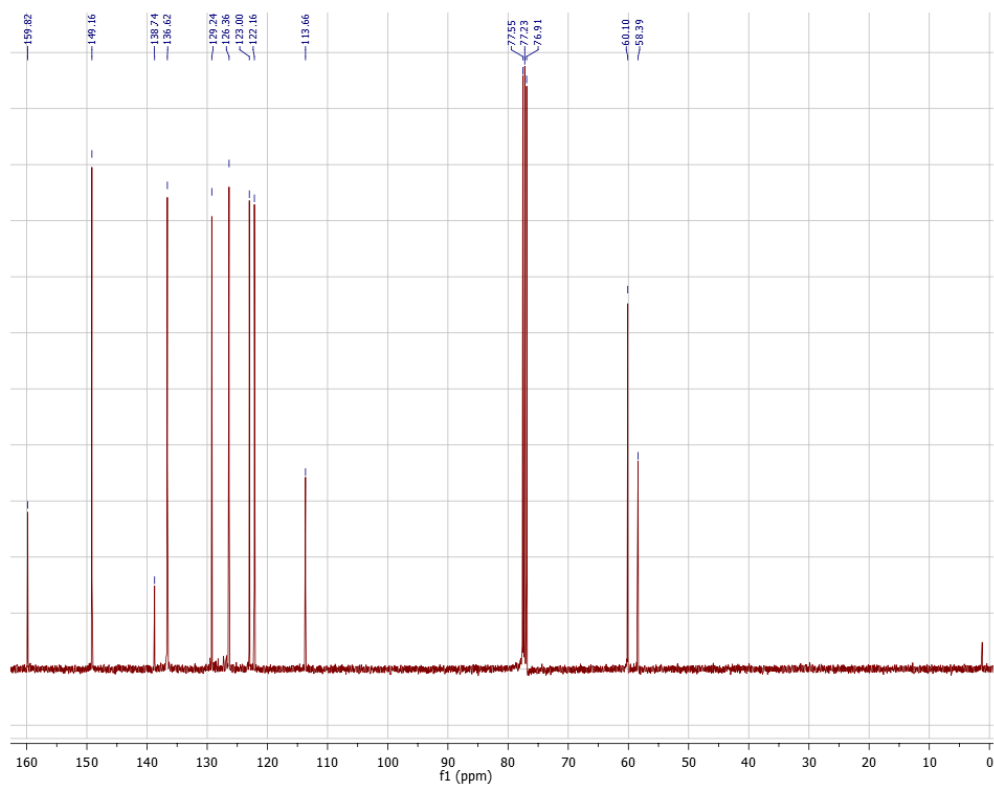
**S- 4:  $^{13}\text{C-NMR}$  of monomer [2]: 4-styrenesulfonyl(phenyl-18-crown-6) imide [2] (75 MHz, DMSO)**



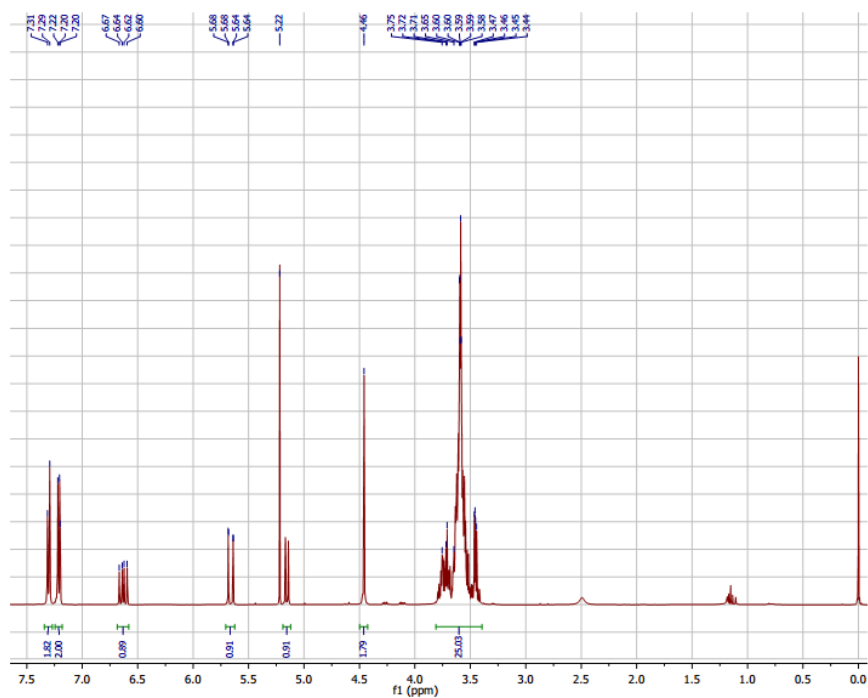
S- 5:  $^1\text{H-NMR}$  of monomer **[3]**: *N*-(4-vinylbenzyl)-di-(2-picoly) amine **[3]** (400 MHz,  $\text{CDCl}_3$ ).



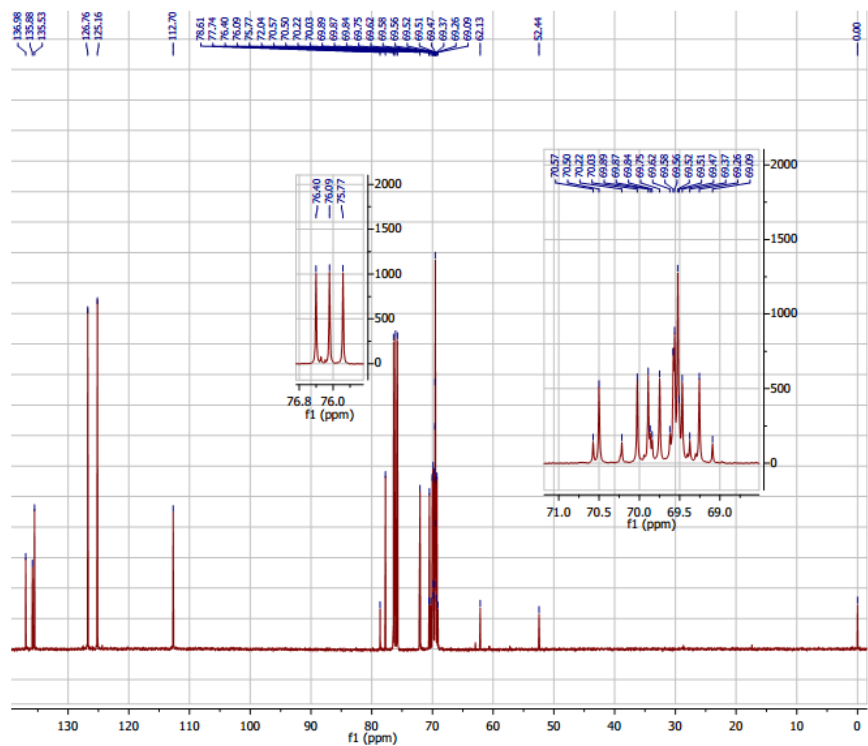
S- 6:  $^{13}\text{C-NMR}$  of monomer **[3]**: *N*-(4-vinylbenzyl)-di-(2-picoly) amine **[3]** (400 MHz,  $\text{CDCl}_3$ )

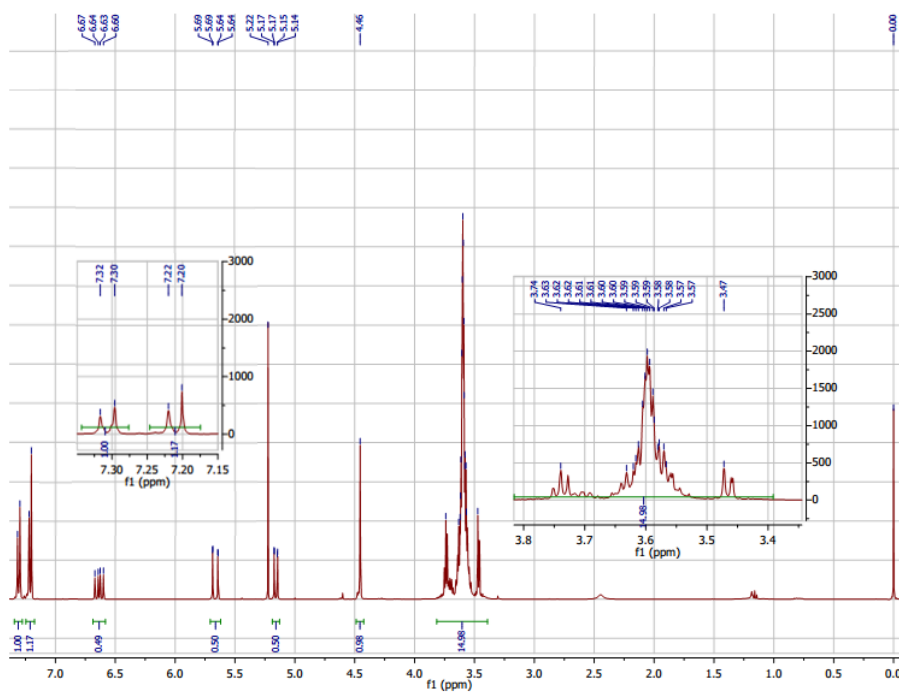
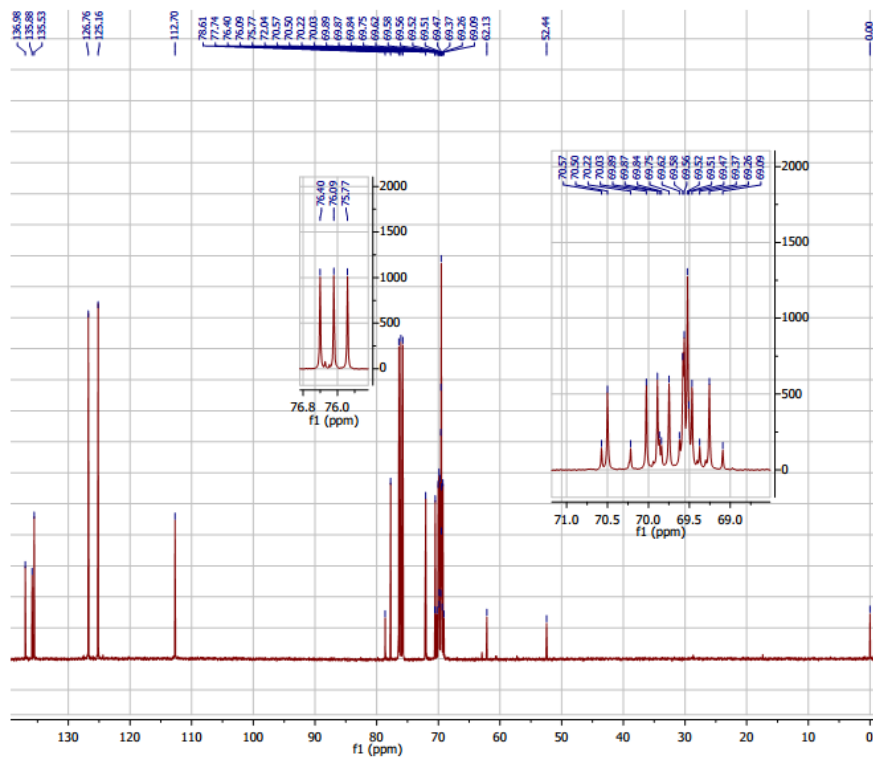


**S- 7:**  $^1\text{H-NMR}$  of monomer **[4]**: 15-crown-5-methyl-(4-vinylbenzyl)-methyl ether **[4]** (400 MHz,  $\text{CDCl}_3$ ).



**S-8:**  $^{13}\text{C-NMR}$  of monomer **[4]**: 15-crown-5-methyl-(4-vinylbenzyl)-methyl ether **[4]** (400 MHz,  $\text{CDCl}_3$ )



S- 9:  $^1\text{H-NMR}$  of monomer [5]: 18-crown-6-methyl-(4-vinylbenzyl)-methyl ether (400 MHz,  $\text{CDCl}_3$ ).S- 10:  $^{13}\text{C-NMR}$  of monomer [5]: 2,3-dihydrothieno[3,4-b][1,4]dioxine-3-aminobenzo-15-crown-5 (400 MHz,  $\text{CDCl}_3$ ).

## 7 BIBLIOGRAPHY

25. Li, D.; Chen, S.; Bellomo, E.A.; Tarasov, A.I.; Kaut, C.; Rutter, G.A.; Li, W. Imaging dynamic insulin release using a fluorescent zinc indicator for monitoring induced exocytotic release (ZIMIR). *Proc. Natl. Acad. Sci. U. S. A.* **2011**, *108*, 21063–21068, doi:10.1073/pnas.1109773109.
92. Shi, H.; Wang, R.; Yang, J.; Ren, H.; Liu, S.; Guo, T. Novel imprinted nanocapsule with highly enhanced hydrolytic activity for organophosphorus pesticide degradation and elimination. *Eur. Polym. J.* 2015, *72*, 190–201.
93. Llanes, P.; Sayalero, S.; Rodríguez-Esrich, C.; Pericàs, M.A. Asymmetric cross- and self-aldol reactions of aldehydes in water with a polystyrene-supported triazolylproline organocatalyst. *Green Chem.* 2016, *18*, 3507–3512.
94. Moad, G.; Rizzardo, E.; Thang, S.H. Living Radical Polymerization by the RAFT Process – A Second Update. *Aust. J. Chem.* 2009, *62*, 1402.
95. Meziane, R.; Bonnet, J.-P.; Courty, M.; Djellab, K.; Armand, M. Single-ion polymer electrolytes based on a delocalized polyanion for lithium batteries. *Electrochimica Acta* 2011, *57*, 14–19.
96. Proctor, C.M.; Rivnay, J.; Malliaras, G.G. Understanding volumetric capacitance in conducting polymers. *J. Polym. Sci. Part B Polym. Phys.* 2016, *54*, 1433–1436.
97. Inal, S.; Malliaras, G.G.; Rivnay, J. Benchmarking organic mixed conductors for transistors. *Nat. Commun.* 2017, *8*.
98. Koutsouras, D.A.; Gkoupidenis, P.; Stolz, C.; Subramanian, V.; Malliaras, G.G.; Martin, D.C. Impedance Spectroscopy of Spin-Cast and Electrochemically Deposited PEDOT:PSS Films on Microfabricated Electrodes with Various Areas. *ChemElectroChem* 2017, *4*, 2321–2327.
99. Stavrinidou, E.; Leleux, P.; Rajaona, H.; Khodagholy, D.; Rivnay, J.; Lindau, M.; Sanaur, S.; Malliaras, G.G. Direct Measurement of Ion Mobility in a Conducting Polymer. *Adv. Mater.* 2013, *25*, 4488–4493.

## *Chapter III.-*

# *Ion-sensitive EDOT and PEDOT derivatives*



## 1 INTRODUCTION

In this approach, functionalization of the referent EDOT monomer was performed with selected cation chelating moieties. These materials were characterized and used *a posteriori* to develop electrochemically ion-sensitive polymer films.

As it can be considered from the state of the art, most of the conjugated polymers today are based on EDOT, PEDOT: PSS dispersions or on derivatives from thiophene, having still more efforts to do on the synthetic side to offer alternatives to these materials, giving an added value to these new EDOT derivatives developed during this PhD.

## 2 MONOMERS

In this approach is described the formation of the second family of monomers based on EDOT derivatives whose chemical structures are illustrated in Figure 36. As in the first route, it can be distinguished the same type of ion-complexing moieties, such as the crown ethers for the alkali metals recognition (18-crown-6 for  $K^+$  and 15-crown-5 for  $Na^+$ ) as well as the dipicolyl moiety, DPA, (see monomer **[8]**, Figure 36) well-known for its affinity for the divalent transition cation  $Zn^{2+}$ . All these EDOT derivatives monomers have been recently filed in a patent, including their synthesis method, their characterization as well as their electrochemical polymerization method.

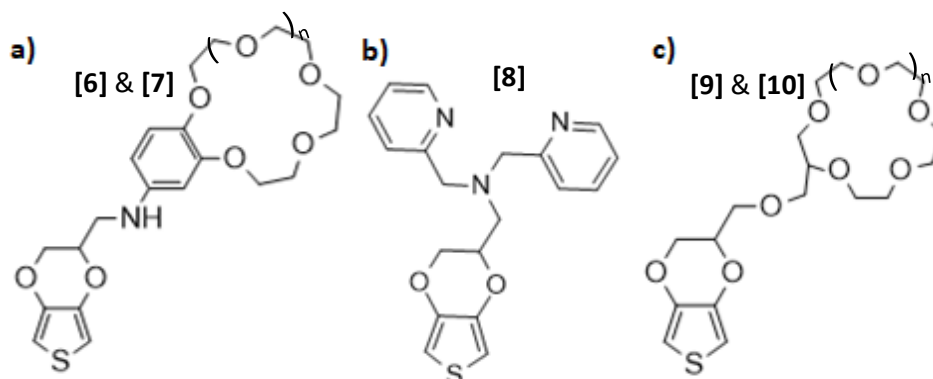


**Figure 36: Scheme of derivatives EDOT monomers synthesized: a)** 2,3-dihydrothieno[3,4-b][1,4]dioxine-3-aminobenzo-15-crown-5 [6] avec  $n=1$  et 2,3-dihydrothieno[3,4-b][1,4]dioxine-3-aminobenzo-18-crown-6 [7] avec  $n=2$ ; **b)** 2'-(Bis(2-picoly)aminomethyl)-3,4-ethylenedioxythiophene [8] **c)** 15-crown-5-methyl-2,3-dihydrothieno[3,4-b][1,4]dioxine ether [9] avec  $n=1$  et 18-crown-8-methyl-2,3-dihydrothieno[3,4-b][1,4]dioxine ether [10] avec  $n=2$ .

In this section, a summary of the synthetic methods used to obtain the different functionalized EDOT derivatives as well as the analysis of their structural characterization is given. For all the experimental details, see the experimental part and the Appendices.

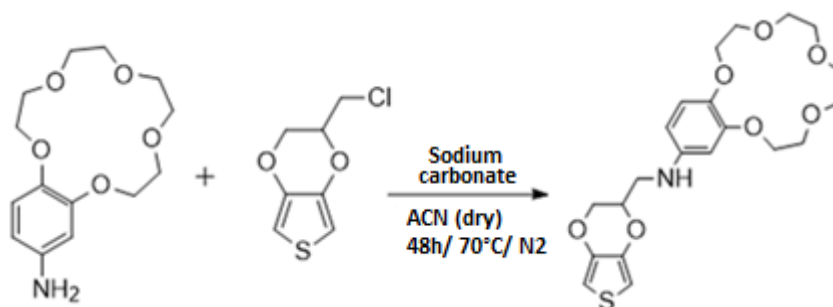


**Figure 37: Reactional Scheme of the synthesis of monomer [6]:** Amination reaction between the 4'-aminobenzo-15-crown-5 ether and the 2'-chloromethyl-3,4-ethylene-dioxythiophene to obtain the 2,3-dihydrothieno[3,4-b][1,4]dioxine-3-aminobenzo-15-couronne-5 [6].

Monomers [6] and [7] (see Figure 36-a) synthesis was achieved in a one-step reaction of nucleophilic substitution between the chloromethyl-EDOT and the 4'-aminobenzo-15 crown-5 to obtain [6] or 4'-aminobenzo-18 crown-6 to obtain [7] in presence of the

sodium carbonate as base (Figure 37, scheme for [6]).  $^1\text{H-NMR}$  spectrum is shown in Figure 38 for monomer [6] as example.

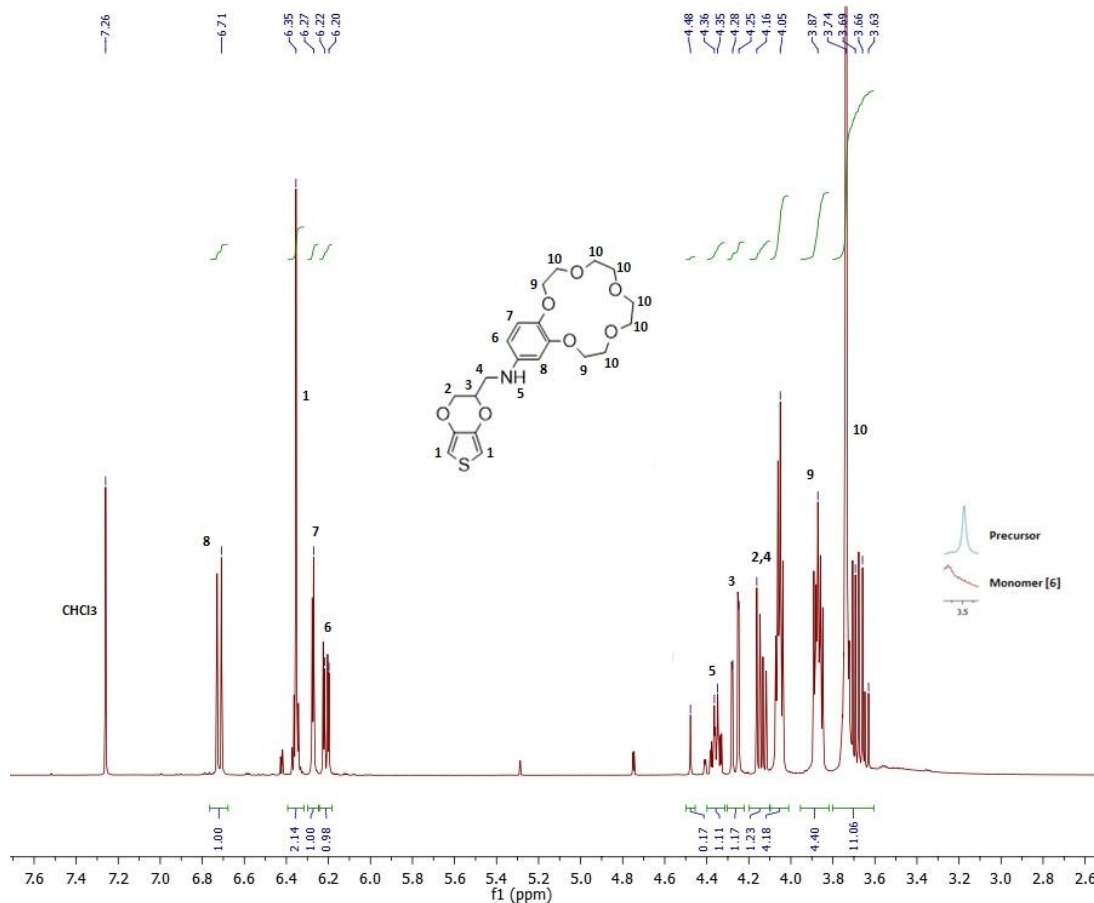
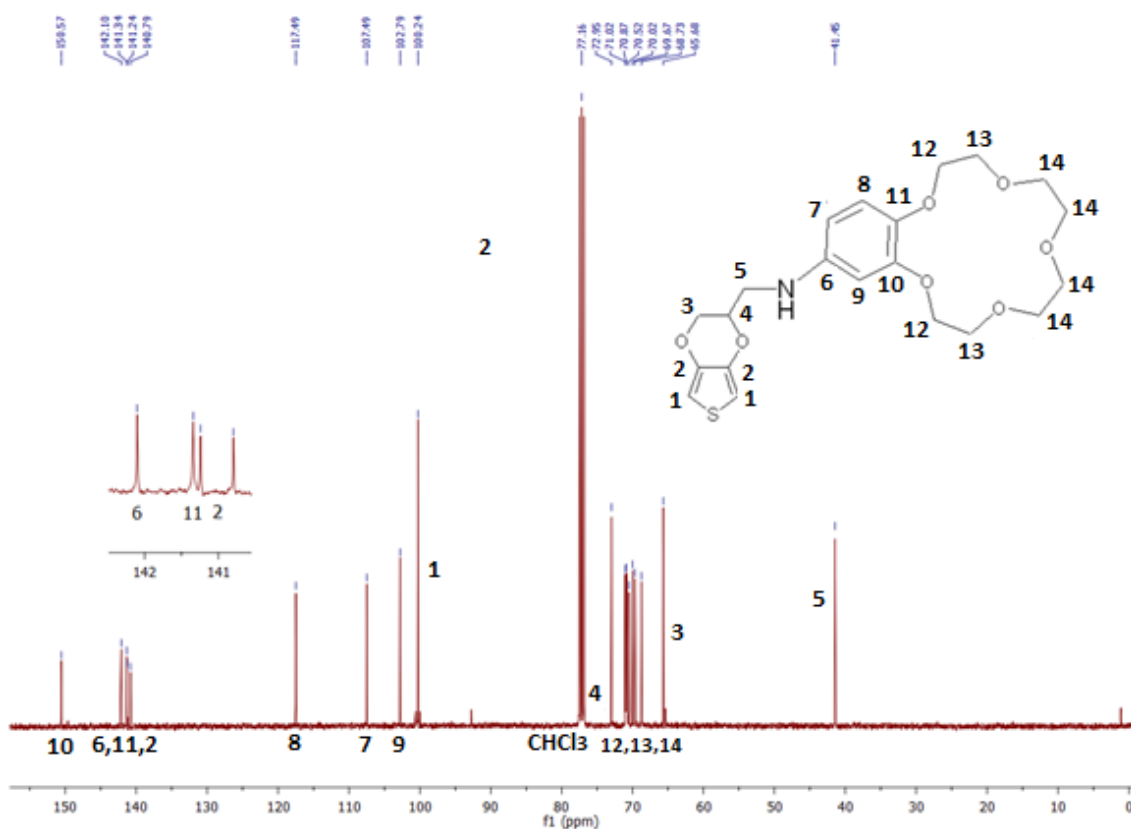


**Figure 38: Structural characterization of monomer [6]:  $^1\text{H-NMR}$  ( $\text{CDCl}_3$ , 400 MHz)**

Proton NMR spectrum (Figure 38) allows us to confirm the structure of the obtained monomer [6]. In fact, both multiplets at 3.87 ppm the larger 3.74- 3.63 ppm with a total integration counting for fifteen protons are consistent with the crown ether protons, appearing more deshielded the four closer to the phenyl ring (named as 9 and 10, respectively). The aromatic protons of phenyl ring next to the amine (*ortho* positions, 6 and 8) shift giving the doublets at 6.21 ppm and 6.71 ppm. The *meta* proton (7) appears at 6.27 ppm integrating for only one proton. Thiophene ring protons (1) are present at 6.35 ppm corresponding to the integral of two protons.

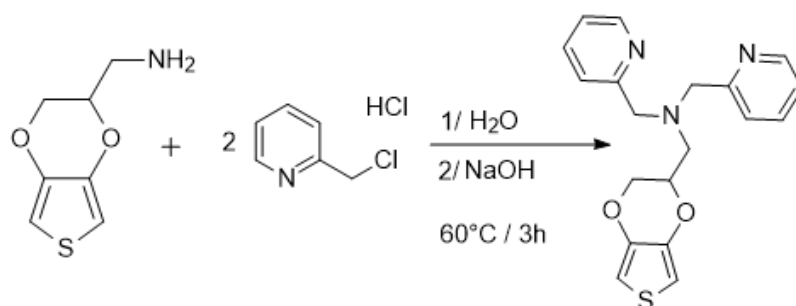
In the alkyl region appear two multiplets corresponding to the ethylendioxy bridge, shifting at 4.05 – 4.16 ppm for protons 2&4 and at 4.28 ppm as a doublet for (3) integrating for one proton. The peak at 4.35 ppm seems to correspond to the secondary amine (5), fact confirmed by the appearance of this peak in the product spectrum as well as the disappearance of the primary amine peak of the reagent shifting at 3.5 ppm (inset in Figure 38).

Carbon NMR is also shown in Figure 39 for the same monomer. The crown ether carbons (12-14) are distinguishable at 72.95 ppm and 68.73 ppm. Aromatic carbons are more dispersed due to the several chemical environments. The most deshielded protons originated on the higher electronic density of the aromatic ring appear at 150.57 ppm (10), 142.10 ppm (6) and 141.34 ppm (11). The other aromatic carbons directly bonded to protons appears at 117.49 ppm (8), 107.49 ppm (7) and 102.79 ppm (9). Thiophene ring carbons shift up to 100 ppm as expected for the aromatic carbons. The ones placed next to the heteroatom (1) are less shielded appearing as a singlet peak at 100.24 ppm, while the others (2) formed two singlets at 141.24 ppm and 140.79 ppm. Finally, the aliphatic carbon atoms appear at 72.95 ppm (4), 65.68 ppm (3) and 41.45 ppm (5).



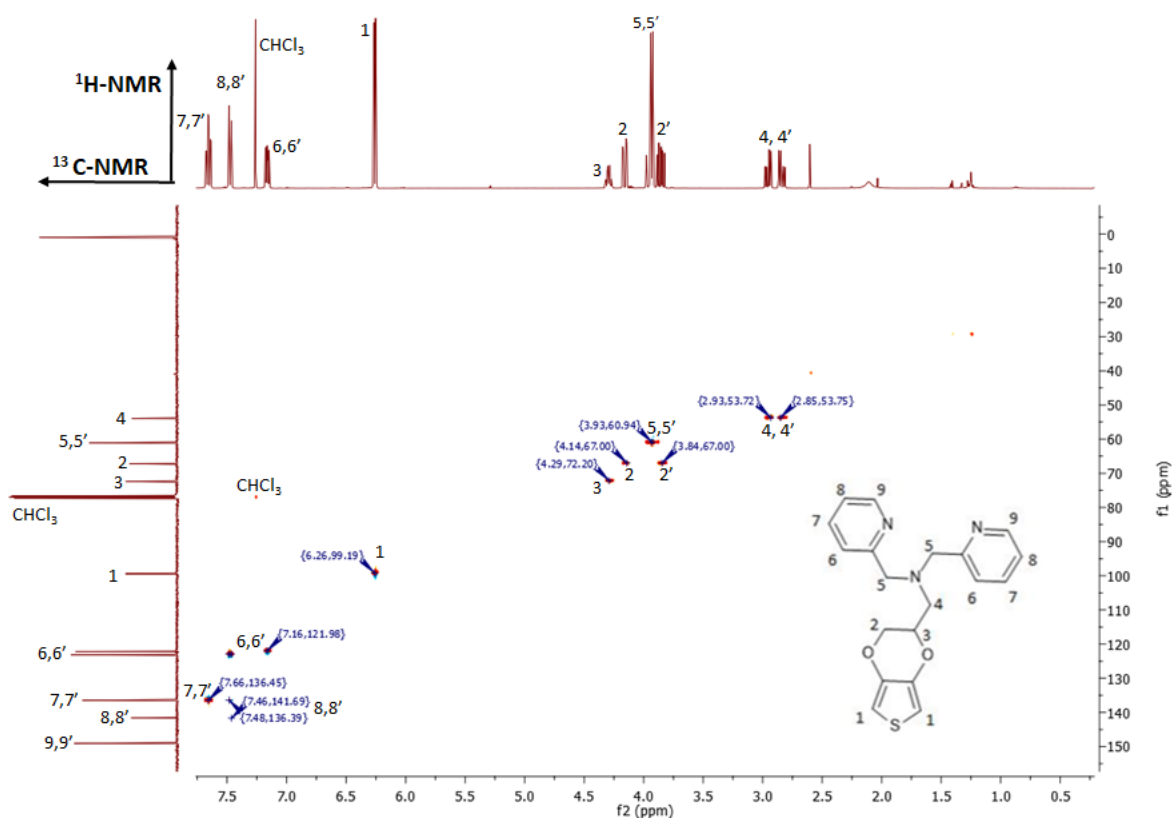
**Figure 39: Structural characterisation of monomer [6]:**  $^{13}\text{C}$ -NMR ( $\text{CDCl}_3$ , 400 MHz)

All the structural spectra confirm the structure of the obtained product, for instance based on the disappearance of the signals corresponding exclusively to the precursor reagent and the good integrations obtained on the product.



**Figure 40: Reactional Scheme of the synthesis of monomer [8]:** Amination reaction between the 2'-aminomethyl-3,4-ethylene-dioxythiophene and the 2-(Chloromethyl)pyridine hydrochloride to obtain the 2'-(Bis(2-picolyl)aminomethyl)-3,4-ethylenedioxythiophene [8].

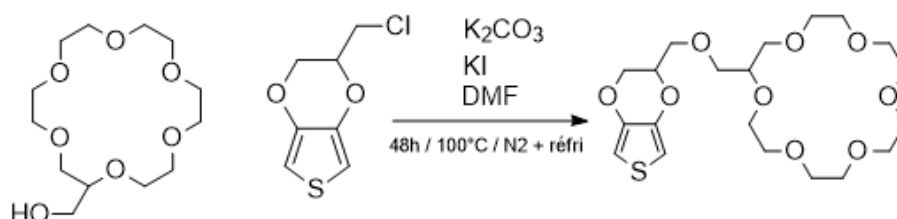
Monomer [8] (see Figure 36-b) synthesis was done by a two steps nucleophilic amination substitution reaction to obtain the *2'-(Bis(2-picolyl)aminomethyl)-3,4-ethylenedioxythiophene* in presence of strong base as shown in the Figure 40. The structural characterization of this monomer is presented in Figure 41.



**Figure 41: HSQC spectrum for structural characterization of [8]:** X-axis:  $^1\text{H-NMR}$  ( $\text{CDCl}_3$ , 400 MHz); Y-axis:  $^{13}\text{C-NMR}$  ( $\text{CDCl}_3$ , 400 MHz).

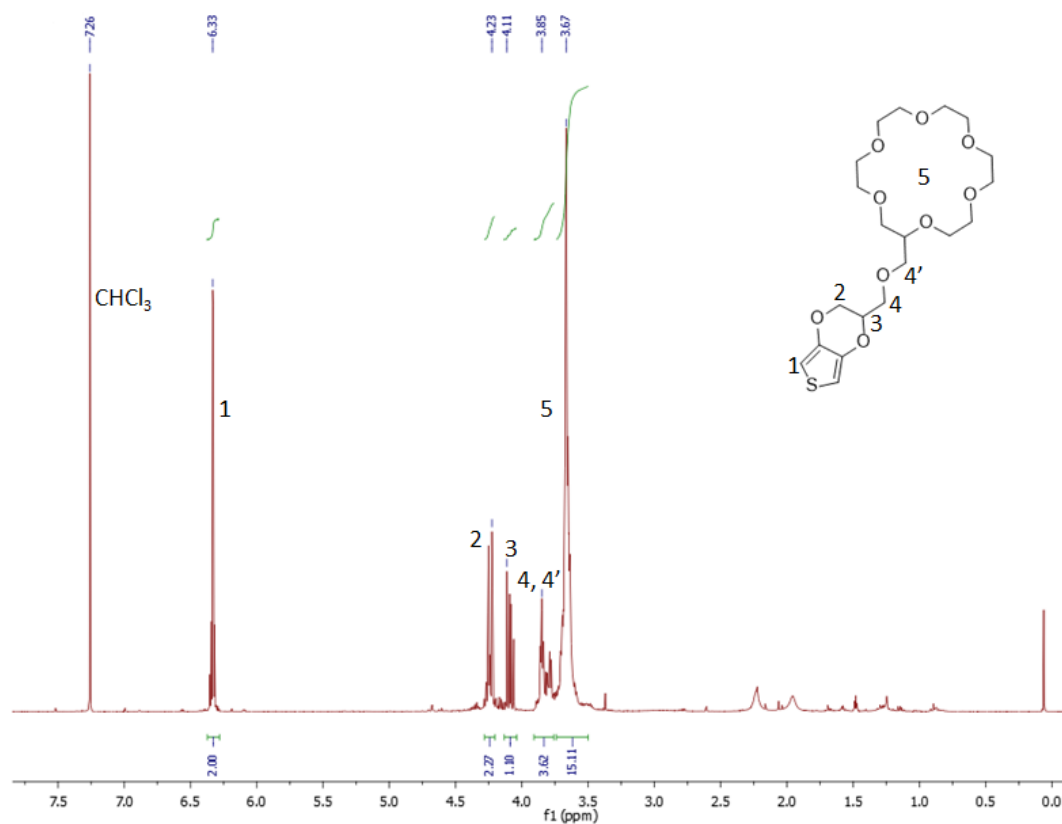
On the HSQC 2D NMR spectrum (Figure 41) one can easily assign all signals corresponding to monomer [8]. It can be clearly differentiating two regions of interactions, the aliphatic one and the aromatic one separated by the thiophene signal (peak 1, shifting at 6.26 ppm in the  $^1\text{H-NMR}$  and 99.19 ppm in the  $^{13}\text{C-NMR}$ ). In the aliphatic region, it can be distinguished the peaks of the ethylenedioxy fraction (peaks 2-4). Moreover, the presence of the dipicolyl moiety (DPA) is confirmed by the appearance of the peak 5, integrating in the proton spectrum for four atoms.

In the case of monomers *15-crown-5-methyl-2,3-dihydrothieno[3,4-b][1,4]dioxine* [9] and *18-crown-6-methyl-2,3-dihydrothieno[3,4-b][1,4]dioxine ether* [10] (see Figure 36-c), synthesis has been done by an etherification reaction (Figure 42).



**Figure 42. Reactional Scheme of the synthesis of monomer [10]:** Etherification reaction between 2-hydroxymethyl-18-crown-6 and 2'-chloromethyl-3,4-ethylene-dioxythiophene to obtain the *18-crown-6-methyl-2,3-dihydrothieno[3,4-b][1,4]dioxine ether* [10]. Monomer [9] was synthesized following the same method. All the experimental details are described in the experimental part.

Proton NMR spectrum of monomer [10] is shown as illustrative example (Figure 43). It allows us to confirm the structure of the obtained monomer [10]. In fact, thiophene ring protons (1) are presented at 6.33 ppm corresponding to the integral of two protons. The protons of the ethylenedioxy fraction appear as two multiplets at 4.23 ppm and 4.11 ppm with integration counting for three protons. Alkyl proton in  $\alpha$  position to the oxygen (4 and 4' peak) appear as multiplet at 3.85 ppm and at 3,67 ppm appears the characteristic large band of the crown-ether protons (peak 5). All the details of the characterization are available in the experimental part (Spectra section).

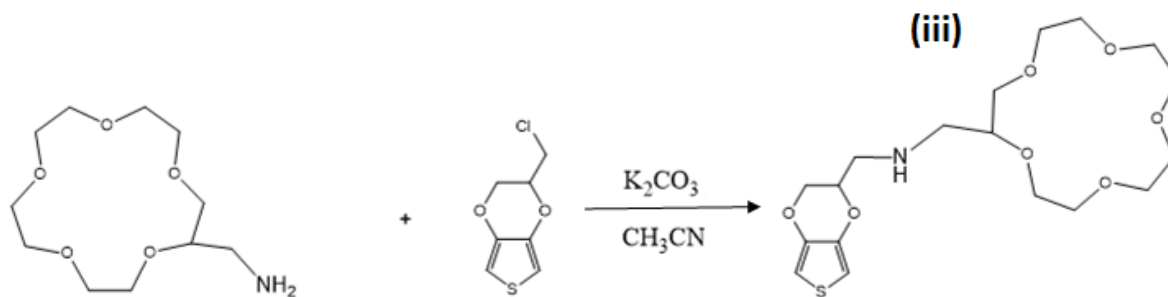


**Figure 43:** <sup>1</sup>H-NMR of monomer [10] (CDCl<sub>3</sub>, 400 MHz), 18-crown-5-methyl-2,3-dihydrothieno[3,4-b][1,4]dioxine ether [10].

## 2.1 Other synthetic routes

Other synthetic routes were evaluated during this project, and some of them have been tested in preliminary experiments. Even, if they were not exhaustively evaluated in the polymers stage, the monomers synthesis will be briefly described here and could be exploited as perspective work.



B- *SN<sub>2</sub> coupling with a non-aromatic amine*

**Figure 45: Reactional scheme of the  $S_N^2$  amination** between the 2-aminomethyl-15-crown-5 and 2'-chloromethyl-3,4-ethylene-dioxythiophene to obtain the 2,3-dihydrothieno[3,4-b][1,4]dioxine-N'-(15-crown-5)-methylamine (**iii**).

We had a great interest on obtaining a similar monomer to **[6]** (Figure 36-a), but testing the coupling with a non-aromatic amine to evaluate the change in the electrochemical properties in the absence of the aniline fraction. For this, the same kind of nucleophilic amination reaction was done using in this case the aliphatic primary amine 4-aminomethyl-15-crown-5 (Figure 45). It was obtained a brownish viscous liquid product with a 37% yield. The  $^1H$ -NMR is given in Figure 46:

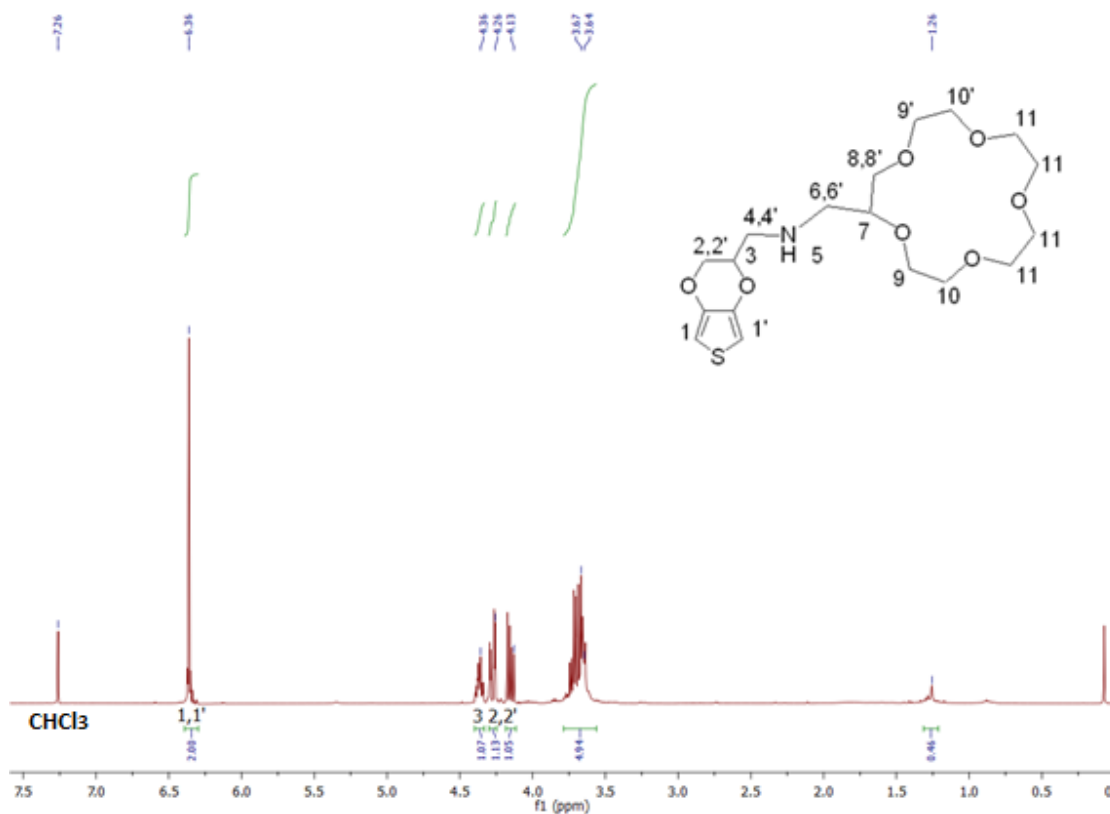


**Figure 46: Structural characterization of the aminomethyl coupling to obtain (iii): <sup>1</sup>H NMR (CDCl<sub>3</sub>, 400 MHz)**

Multiplet at 6.36 ppm integrating for two protons corresponds as already shown to the thiophene ring. The 4.36 ppm multiplet (peak 3) and 4.26 ppm and 4.13 ppm (2,2') are assigned to the more deshielded protons of the ethylenedioxy moiety. At 3.74-3.64 is found a complex multiplet assigned, after comparison with the precursors reagents spectrum, to the alkyl protons (4, 4'). They overlapped with the crown ether protons signals. This shows that coupling could take place, nevertheless integration is much poorer than for the expected product (iii) (see the wrong integration and shape of the crown ether band at 3.64-3.67 ppm, Figure 46). Signal at 1.6 ppm present in the primary amine precursor is absent in the product spectrum, confirming the formation of the product even if in a weak yield. Finally, the 1.26 ppm peak corresponds to a minor impurity already present in EDOT precursor.

Considering the  $^{13}\text{C}$ -NMR spectrum (Figure 47), EDOT characteristic peaks are clearly observed at 141.25 ppm and 140.80 ppm (2,2') as well as at 100.26 ppm (1, 1'). Aliphatic carbons (3-5) are found at 65.69 ppm, 72.97 ppm and 41.46 ppm. However, at 71.07 ppm and 70.49 ppm are present some weak signals, confirming the crown presence, but with a poor integration.

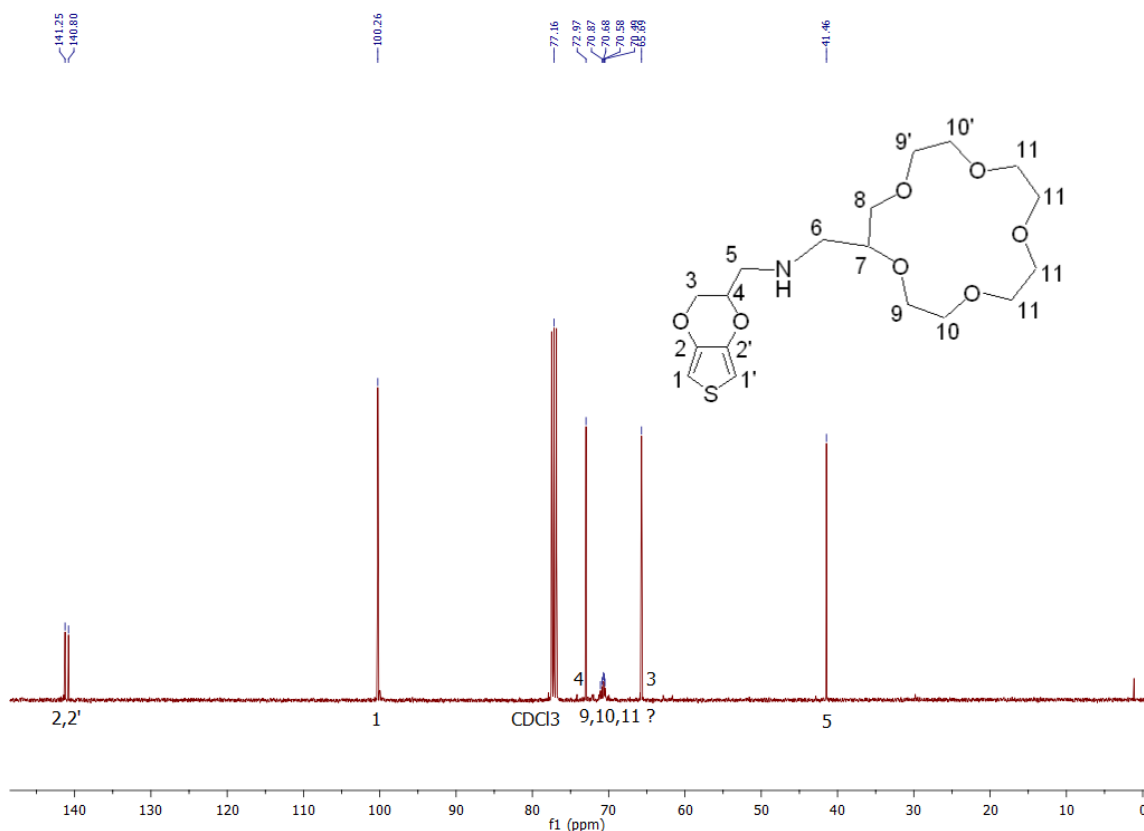


**Figure 47: Structural characterization of (iii):  $^{13}\text{C}$ -NMR ( $\text{CDCl}_3$ , 400 MHz)**

In conclusion, this coupling seems to be less efficient than with the aromatic amines, which was a little bit surprising considering the higher reactivity (nucleophilicity) of the aliphatic amines. Certainly, geometrical stabilization of the position of the substituted amine due to the presence of the aromatic ring is likely a major driving force in the coupling to obtain [6] in a better yield in comparison with this monomer (iii).

### 3 ELECTROCHEMICAL POLYMERS FORMATION

The electrochemical polymerization and characterization of the different EDOT derivatives was performed. Electrochemical profiles of the different monomers, as well as the conditions for the polymerization and copolymerization with EDOT have been devised to obtain the ion-sensitive films.

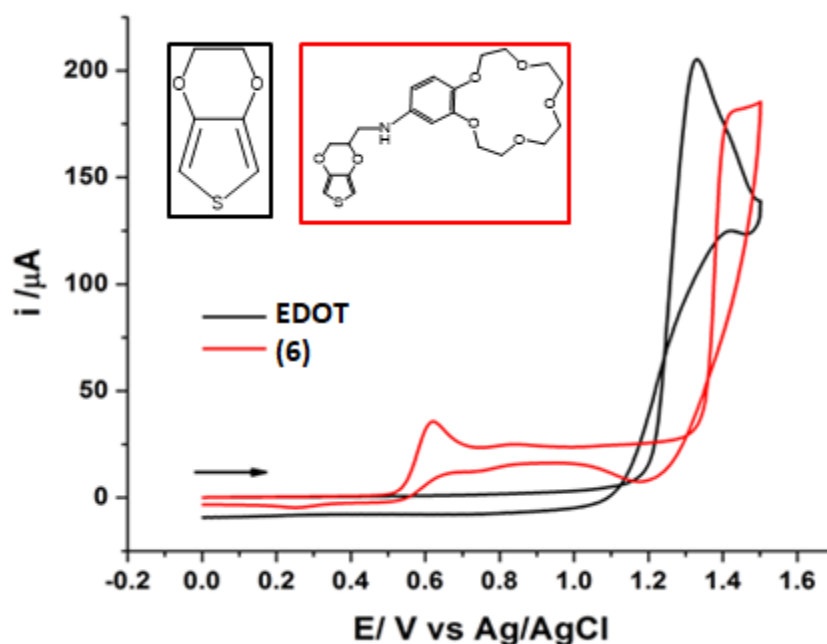


**Figure 48: Potentiodynamic oxidative voltamperogram of [6] vs EDOT:**  
Conditions: 0.1 M LiClO<sub>4</sub>, ACN,  $\nu=25\text{mV}\cdot\text{s}^{-1}$ .

To characterize the oxidation potential of the functionalized monomers, only one cycle of potentiodynamic voltammetry has been done. As example, in Figure 48 is illustrated the comparison of the electrochemical profile of EDOT, black curve, and the 15-crown-5-containing monomer [6], red curve. EDOT and the studied monomers present an irreversible oxidation, showing in the reverse cycle the classical cross-line typically observed during the electrochemical polymerization. This phenomenon is known as a *nucleation loop* (circle at 1.2V), corresponding to the start of the nucleation process of the polymer. This is based on a homogeneous autocatalytic reaction (Annex 8) from an intermediate Oligo<sup>n+</sup> (oligomer of small chain) with the starting monomer (Mon) to

Oligo<sup>(n+1)+</sup> and Mon<sup>+</sup> [101]. A slight shift is observed on the oxidation peak of the modified monomer to more positive potential values in comparison with EDOT (0.12 V), which implies that higher energy is required to achieve the oxidation of EDOT moiety in the functionalized monomer. Moreover, the appearance of a first oxidation peak at lower oxidation potential values ( $E=+0.6$  V) has been observed. This corresponds to the oxidation of the aniline moiety bridge between the EDOT and the crown ether; nevertheless, this oxidation does not let to obtain an aniline polymer, due to a steric hindrance. This oxidation leads to the formation of a radical cation which may be stabilized by resonance or form some  $\sigma$ -couplings[102]. This charge may cause an electron withdrawing effect which leads to an increase in the oxidation potential of the EDOT ring. It is important to note that this aniline signal could be used as internal reference while sensing (trapping) cations in the crown ether moieties directly link to this moiety.

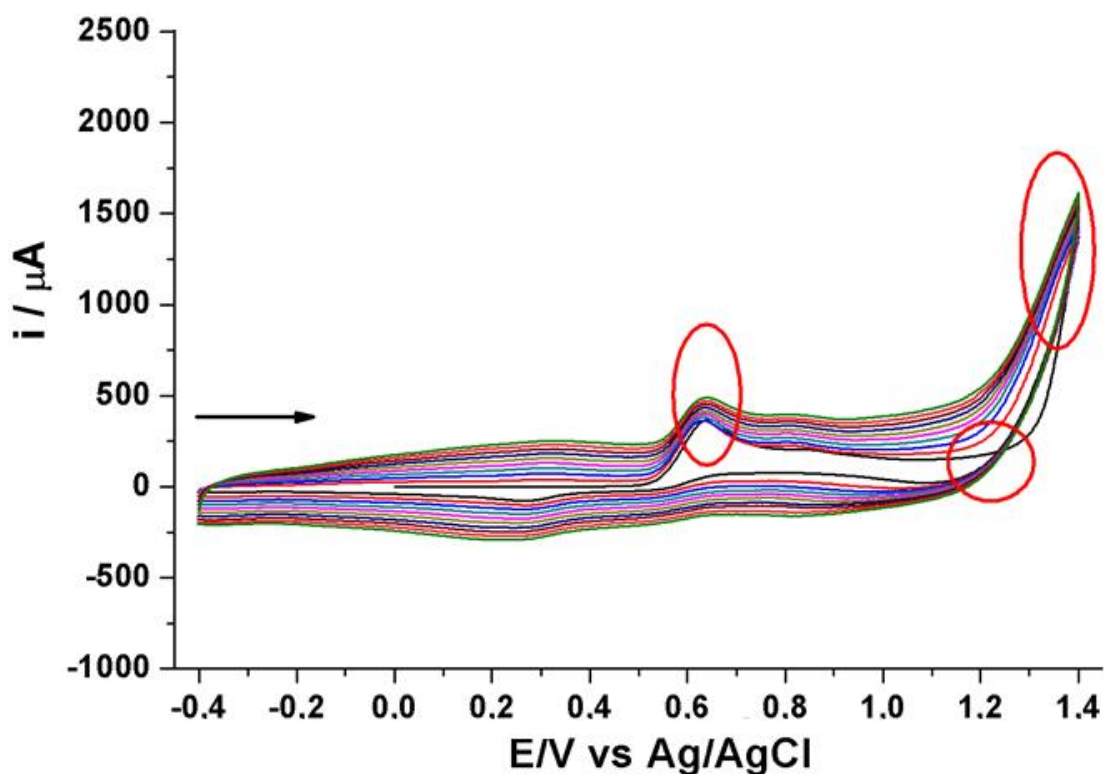


**Figure 49: Electropolymerization of monomer [6] by potentiodynamic voltammetry:** Cycles: one (black curve, interior), last (green curve, exterior). Conditions: 0.1 M LiClO<sub>4</sub>, ACN,  $\nu=25\text{mV}\cdot\text{s}^{-1}$ .

Once the oxidation potential of each monomer was determined (see Table 11 in Appendices chapter), their electropolymerization was evaluated on a potential value where no overoxidation occurs (i.e.  $E_p = 1.43$  V for **[6]**). During the electropolymerization an increase of anodic and cathodic currents at lower potentials than the oxidation of the monomer is observed (Figure 49). This is an evidence of the polymer growth on the electrode surface. In addition, it can be identified the aniline oxidation peak at +0.6V characteristic of the functionalized monomer, demonstrating that the presence of the crown ether moiety is not a steric impediment for the electropolymerization to take place via the oxidation of the EDOT moiety. Nevertheless, the comparison between the electropolymerized EDOT and the crown functionalized EDOT films (Figure 50, black curve and red curve respectively), shows a higher anodic and cathodic current for the PEDOT films (in the charge-discharge potential window), thus the absence of the crown ether group allows a faster electropolymerization, which leads to a thicker film, after the same number of cycles. This is caused by a faster diffusion of the EDOT monomer through the electrode ( $D_{app}=3.48 \cdot 10^{-5}$  cm<sup>2</sup>/s) in comparison with monomer **[6]** ( $D_{app}=3.47 \cdot 10^{-6}$  cm<sup>2</sup>/s). This apparent diffusion coefficient ( $D_{app}$ ) were calculated by a theoretical method which correlates the molecular weight of organic molecules in acetonitrile with the  $D_{app}$ [103]

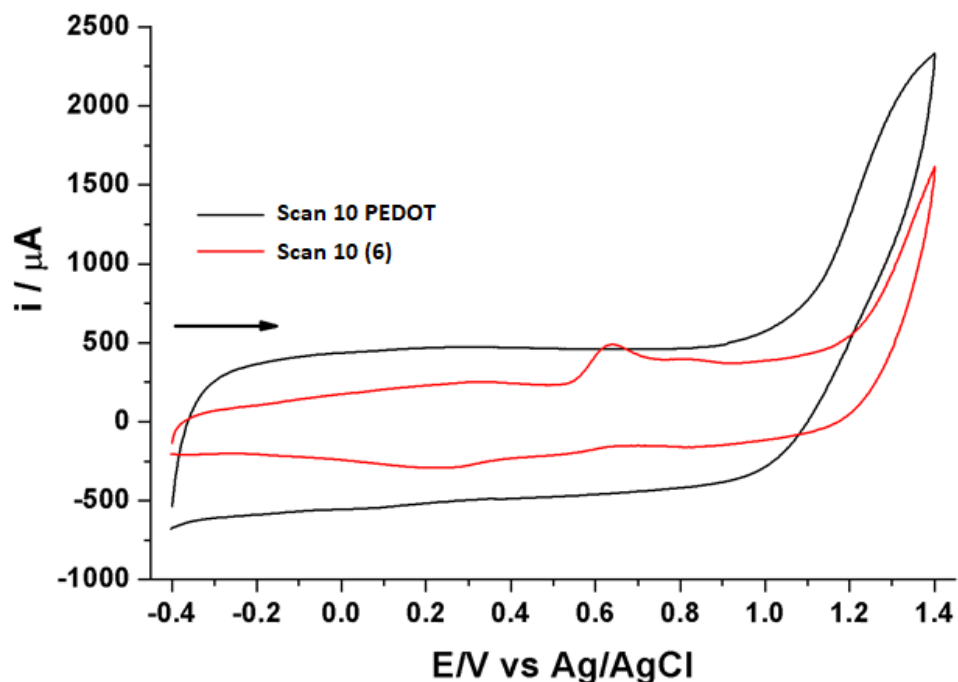


**Figure 50: Electrochemical profile of the electropolymerized films: PEDOT (black curve) vs Poly- (6) (red curve).** Conditions: 0.1 M LiClO<sub>4</sub>, ACN,  $\nu=25\text{mV}\cdot\text{s}^{-1}$ .

To conclude, the aniline crown-ether functionalized monomer [6] has a well-defined electrochemical profile with two oxidation processes corresponding to the aniline and the EDOT structures. Finally, their electropolymerization was achieved, even by the limitation of the sterically hindrance effect of the crown ether-moiety.

A similar study was done for monomer [7] and it was found a similar profile than previously discussed for [6]. In this case, we went further, evaluating the thickness that we could obtain with this kind of functionalized monomers. For this purpose, a long electropolymerization procedure up to twenty cycles was performed to obtain a thick polymer film on a flat gold electrode surface. SEM image of polymer film from [7] present a thickness of  $\sim 20\ \mu\text{m}$  (Figure 51), demonstrating the possibility to obtain very thick films that could be useful in several applications.

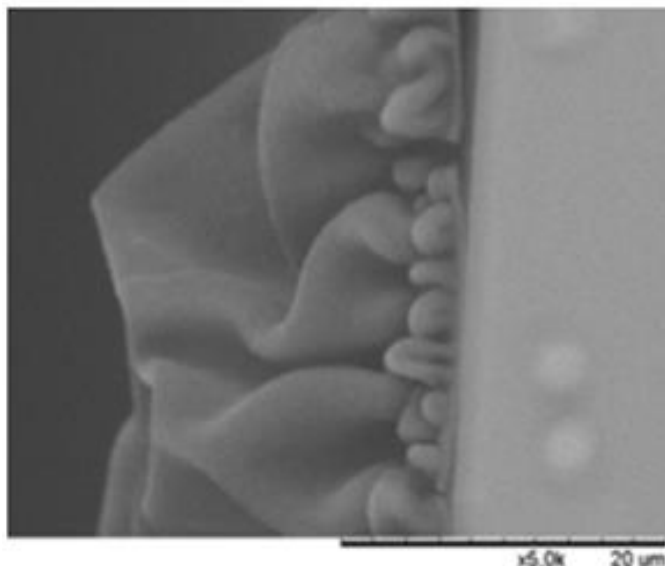


**Figure 51: SEM characterisation of thick electropolymerized homopolymer:** Lateral profile of electropolymerized film from [7]. Thickness: 20  $\mu\text{m}$ .

In order to understand the influence of the binding moiety between crown ether and EDOT ring in the electroactivity of the functionalized monomers, the *charge-discharge* window of polymers films from monomers [7],  $P(7)$ , and [10],  $P(10)$ , obtained by electropolymerization (ten cycles) were characterized by potentiodynamic voltammetry (Figure 52).

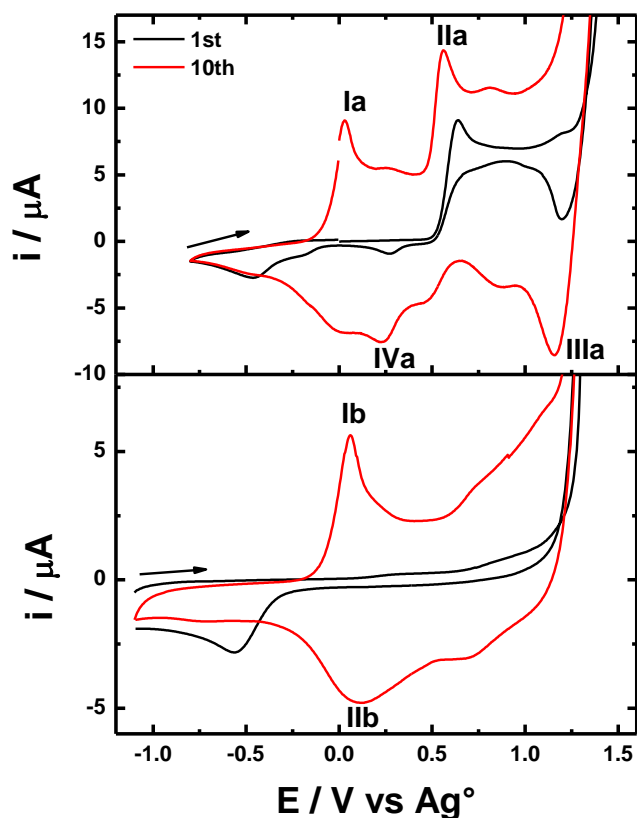


**Figure 52: Influence of EDOT-crown ether binding fraction on the electrochemical activity:** Charge-Discharge window of electropolymerized: *P(7)* with aniline binding (top) and *P(10)* with ether binding (bottom) in the first (black curves) or tenth (red curves) cycles of electropolymerization. Conditions: 0.1 M LiClO<sub>4</sub>, [M]=5 mM, ACN,  $\nu = 25 \text{ mV} \cdot \text{s}^{-1}$

From the oxidation peaks observed in both films, it is evident that peak **Ia** and **Ib**, in *P(7)* and *P(10)* respectively, are associated to the charge of EDOT. In addition, for *P(10)* this anodic peak is coupled to the cathodic peak **IIb** defining the discharge of PEDOT. Peak **IIa** correspond to the aniline oxidation in *P(7)* and very likely **IIIa** is correlated with the reduction of the short chain oligomers at the interface of the polymer electrode. Peak **IVa** could be attributed to the reduction of the PEDOT backbone or to the reduction of the charged aniline inside the polymer structure. Since the aniline oxidation occurs around 1 V before the oxidation of EDOT, the over oxidation of aniline could be reached. Therefore, this overoxidation could produce the crosslinking or decomposition of the polymers. Future experiments changing the kinetic electrochemical parameters, such as

temperature and switching potential may improve the incorporation of EDOT crown ether, and to calculate the real amount of functionalized monomer elemental analysis may be performed.

## Copolymerizations

The possibility to improve the electropolymerization of the bulky functionalized monomers has been carried out by performing the copolymerization with EDOT. Several molar ratio between EDOT and the crown functionalized EDOT (Figure 53, EDOT, black index, and [6], red index, respectively) shows that the increase in the amount of EDOT causes an increase in the current obtained on the charge-discharge potential window (i.e. comparing black curve vs blue curve). Therefore, the presence of EDOT improves the formation of a higher amount of oligomers. However, this relation is not infinitively linear. It seems to arrive to a saturation growth rate regime up to this ratio 3-1. If we compare the difference of current using the double (red curve) or the triple (blue curve) of EDOT vs the crown-containing monomer, it is evident that the charge-discharge region has a similar current value in both cases.

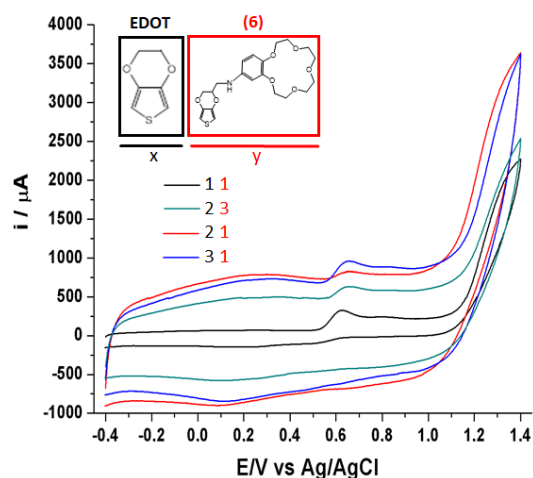


**Figure 53: Potentiodynamic voltammogram of different electrochemically formed copolymers between EDOT and (6):** Inset: Chemical structure of EDOT (black) and [6] monomers. Legend index: Molar ratio used of each monomer, EDOT (black index) vs [6] (red index), to the formation of each copolymer: 1:1 (black curve), 2:3 (green curve), 2:1 (red curve), 1:1 (blue curve). Conditions: 0.1M  $\text{LiClO}_4$ , ACN,  $v=25\text{mV}\cdot\text{s}^{-1}$ .

Moreover, we have evaluated the morphology obtained for the different copolymer films. In most of the cases, they were really rough obtaining a similar *cauliflower* morphology very common for electropolymerized formed PEDOT and their derivatives as it is illustrated in Figure 54.

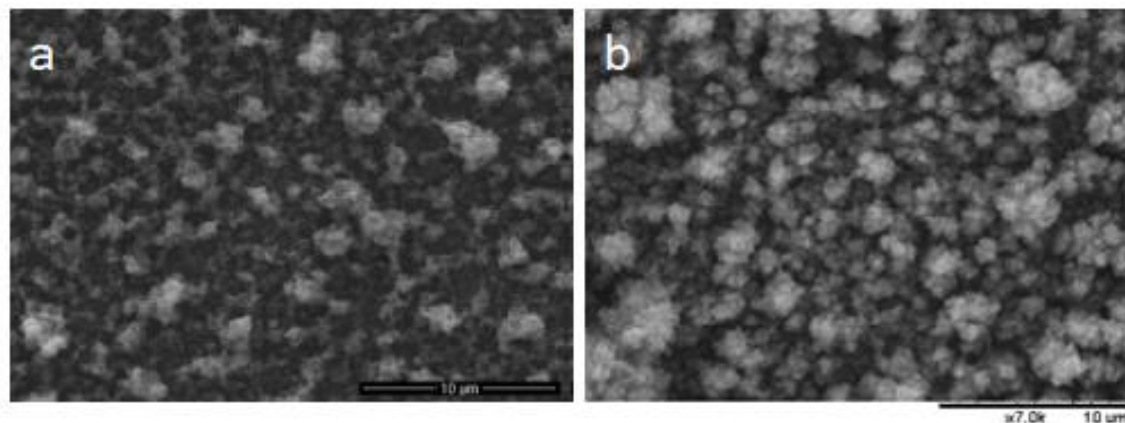


**Figure 54: SEM images of electropolymerized films: a) PEDOT; b) P(6).** Scale: 10 µm

Finally, homopolymer of [8] was not achieved, certainly due to the high oxidation potential of this monomer and some secondary reactions involving the pycolyl units could be inhibiting the polymerization. Thus, we proceed to perform its copolymerization and this was achieved with other non-functionalized monomer, the bithiophene (Annex 9). The interest to try to copolymerize [8] monomer with a non-functionalized monomer was to observe if, as for the copolymerization with the other EDOT functionalized monomers ([1] and [2]) was possible. It was used the bithiophene due to its lower oxidation potential with respect to EDOT. Nevertheless, considering that this little monomer has a lower electroactivity window of charge-discharge, these copolymers have not been explored in the films characterization stage (section 4). Moreover, the interest of copolymers is limited in the final sensing application due to the decrease in ion sensitive moieties and to the increase on the number of parameters to control.

To sum up, the electropolymerization of the different containing crown-ether monomers was shown possible, obtaining even very thick homopolymer films. Moreover, this could be improved by their copolymerization with EDOT.

## 4 ELECTROCHEMICAL CHARACTERIZATION

Once the electropolymerization film formation was optimized and reproducibly obtained, polymer films were characterized to evaluate their electrochemical properties and determine their ion sensitivity. Several electrochemical methods were used in this characterization including multi-sweep voltammetry, potentiometric titrations, as well as *in-situ* conductivity. In this section I describe the most important results obtained with each characterization technique.

### 4.1 Potentiodynamic voltammetry

Potentiodynamic voltammograms obtained for the different polymeric films were obtained in a three-electrodes electrochemical cell as detailed in the experimental part. This technique allows us to gain information about the region of *charge-discharge* of the polymeric film under study. A first characterization in pure water electrolyte was done, followed by the characterization in different electrolytes solutions to study the ionic effect on the electrochemical profile of the film.

As illustrated in the Figure 55, first experiments done with *P(6)* seemed to indicate a higher sensitivity of the polymeric film to sodium cation, presumably due to the good match in size between the complexing cavity (15-crown-5) and this cation as compared with the larger potassium cation. Indeed, the measured current in lower concentration electrolyte (10mM) gives an equivalent *charge-discharge* area for both cations (dot curves). Nevertheless, we observed only with the sodium cation (solid red curve) a

significant increase of this area when the film was exposed to an electrolyte of higher ionic concentration (100 mM).

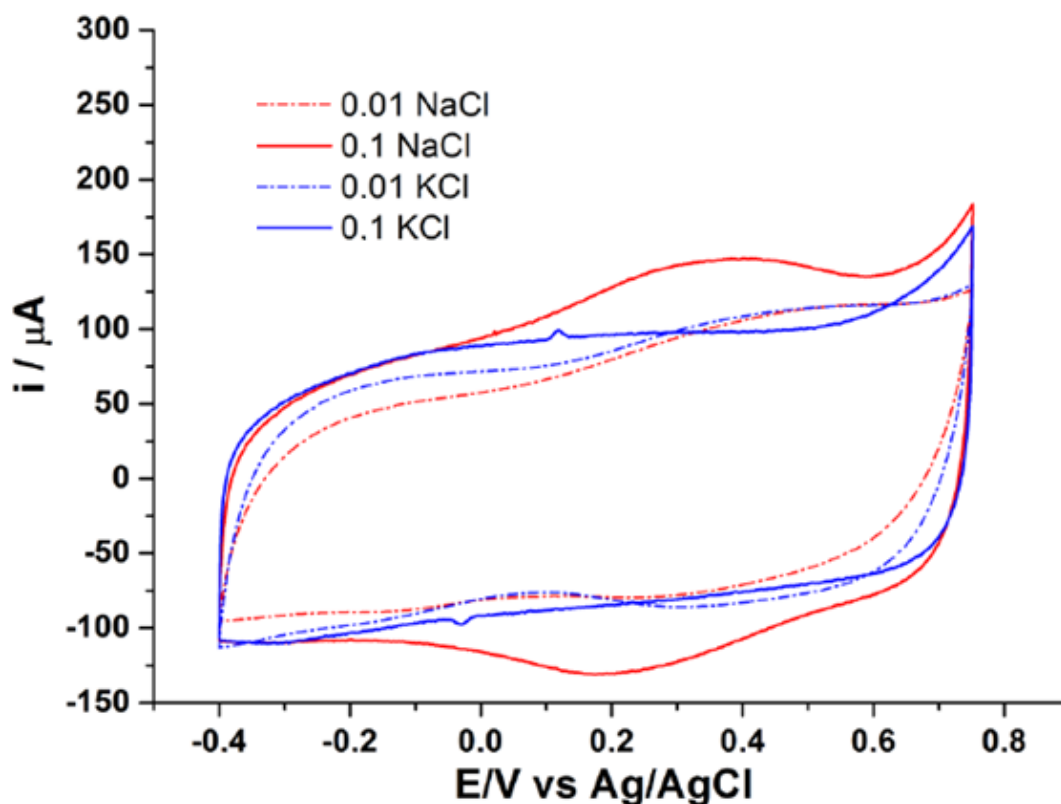


**Figure 55: Ionic Electrolyte effect on the electrochemical profile of 15-crown-5 based film:** Potentiodynamic voltammogram of a polymer film from [6] characterised in different electrolytes: Sodium (red) or Potassium (blue) in low (10 mM, dot) or high (100 mM, solid) concentrations.

We performed many times the quantification and study of the reproducibility of these experiments in order to validate this approach as quantitative method for the ionic sensitivity of the functionalized polymeric films. In Table 6 is given a summary of the quantification of the cathodic/ anodic charge ratio for every polymeric film from [6], *P(6)*, evaluated in different ionic electrolytes ( $n=3$ ). The other polymers were characterized with the following techniques. The explanation will be given further in the discussion of these results.

**Table 6: Summary of the cathodic charge (Qc), anodic charge (Qa) and their ratios (Qc/Qa) for the different electrolytes (NaCl or KCl at the indicated concentrations, 10 or 100 mM).**

| P     | EP | [NaCl]/M | Qa      | Qc      | Qc/Qa | [KCl]/M | Qa      | Qc      | Qc/Qa |
|-------|----|----------|---------|---------|-------|---------|---------|---------|-------|
| P(6)  | 1  | 0.01     | 0.00358 | 0.00321 | 0.90  | 0.01    | 0.0039  | 0.00361 | 0.93  |
|       | 1  | 0.1      | 0.00509 | 0.00474 | 0.93  | 0.1     | 0.0042  | 0.0038  | 0.90  |
|       | 2  | 0.01     | 0.00247 | 0.00234 | 0.95  | 0.01    | 0.00296 | 0.00275 | 0.93  |
|       | 2  | 0.1      | 0.00303 | 0.00296 | 0.98  | 0.1     | 0.00373 | 0.00364 | 0.97  |
|       | 3  | 0.01     | 0.00426 | 0.00388 | 0.91  | -       | -       | -       | -     |
|       | 3  | 0.1      | 0.00395 | 0.00367 | 0.93  | -       | -       | -       | -     |
| PEDOT | 2  | 0.01     | 0.0137  | 0.0132  | 0.96  | 0.01    | 0.0129  | 0.0124  | 0.96  |
|       | 2  | 0.1      | 0.0172  | 0.0171  | 0.99  | 0.1     | 0.0148  | 0.0146  | 0.98  |

For a more clear visualisation, this information is represented in Figure 56. In the red framed graph, three different films (n=3) are represented which were formed from the 15-crown-5 containing monomer [6] and they were compared to a PEDOT film (grey framed). It can be noticed that at higher ionic concentration (right side vs left side of the red framed) an increase in the reduction/oxidation charge ratio appears, also observed in PEDOT films. However, it is clear that there is a certain variability in the cation relations (red for sodium and blue for potassium) which may reflect the accessibility of the ions to the functional groups of the different polymer film.

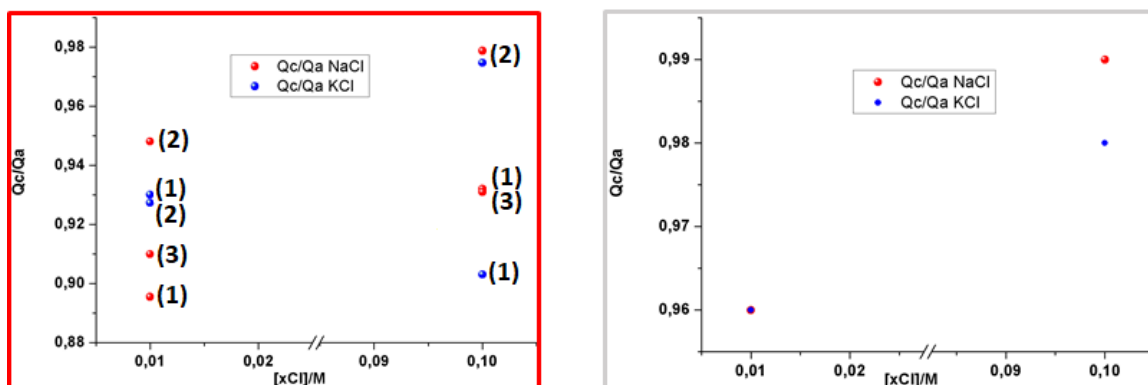


**Figure 56: Quantification of potentiodynamic voltammetry experiments: Ratios Qc/Qa vs Cation concentration (n=3). Sodium cation (red dots), potassium (blue dots) and number of experiment (index number). Red frame: 15-crown-5 containing films from monomer [6]. Grey frame: PEDOT film (control).**

Taking this into account, and considering that acidic conditions are usually used as the state of the art for analytical purposes[104], we went further in our analysis studying the electrochemical profile of the films in acetic aqueous electrolytes (pH=4). In the same manner as before, a sequential characterization in different electrolytes was done to evaluate the effect of cation concentration and nature. For example, Figure 57 shows the potentiodynamic sweep for the different acidic electrolytes. It is represented the second cycle in every condition from the charge-discharge of the polymer film. It should be noticed, that the aniline peak of the functional group sterically placed next to the complexing moiety could be followed under these conditions (at  $t=0$ ,  $E_{ox}= +0.3$  V and  $E_{red}= +0.25$  V). This peak is due to the acid doping of the aniline, confirmed due to the absence of this peak in organic medium. As it could be observed, this peak undergoes a more or less reversible shift depending on the electrolyte used.

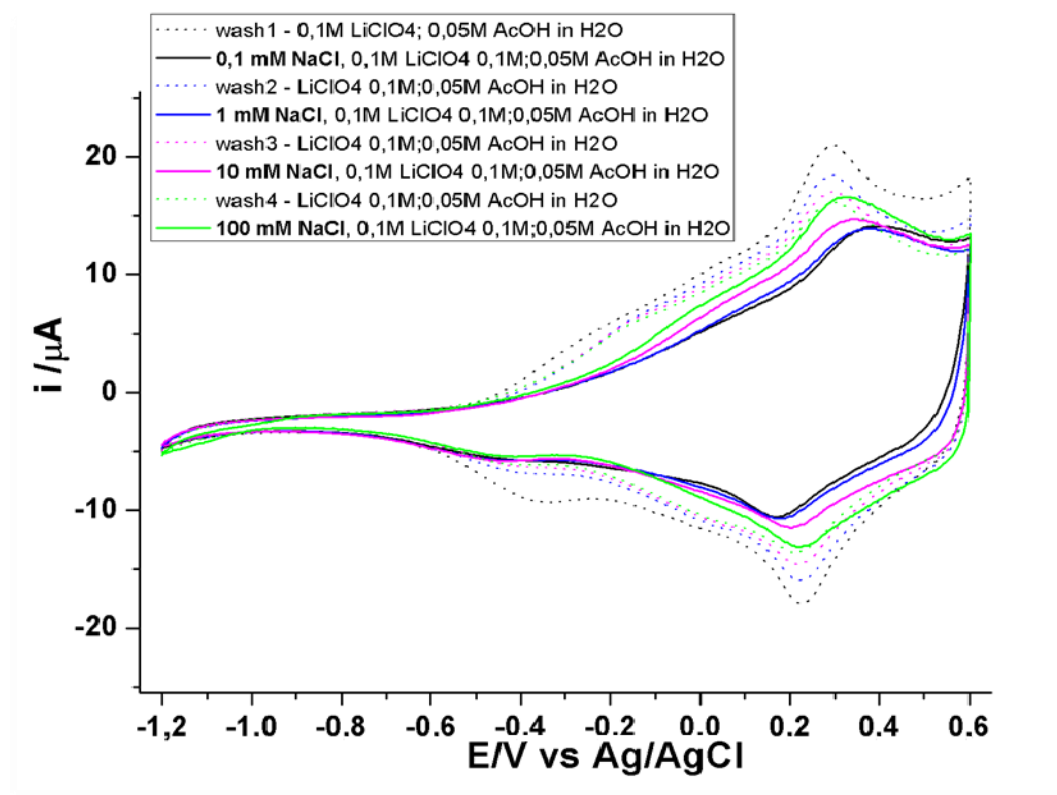


**Figure 57: Concentration effect on the electrochemical profile of *P(6)*, a 15-crown-5 based film:** Potentiodynamic voltammogram of a polymer film from [6] characterised in different concentration electrolytes: Solid curves: NaCl concentration from 0.1 mM (black) to 0.1 M (green). Dot curves: Voltammogram of the film on washing electrolyte (0.1M LiClO<sub>4</sub>, H<sub>2</sub>O, pH=4).

At low concentrations of NaCl (black and blue curves), we observed the maximum shift of the peaks and the process of *charge-discharge* of the film was reproduced in a less reversible way. This is evident by the larger separation between the oxidation and the reduction peaks ( $\Delta E=200$  mV). In the case of high cation concentrations (pink and green curves), it is observed that the process of charge-discharge becomes more reversible ( $[E_{ox} - E_{red}] = 80-120$  mV). This was the first evidence that could confirm that this polymeric surface could have an ionic concentration sensitivity and could work as active transductor material to be integrated into devices.

For studying the ion affinity and sensitivity of these films  $P(6)$ , the same kind of systematic study has been performed with potassium and electrolytes were present in the same concentrations as described for sodium. Figure 58 represents the comparison of the difference of anodic and cathodic potential:

$$\Delta E_p = E_{p,a} - E_{p,c}$$

between the oxidation and the reduction peaks obtained when the characterization was done in the different electrolytes for each set of experiments.

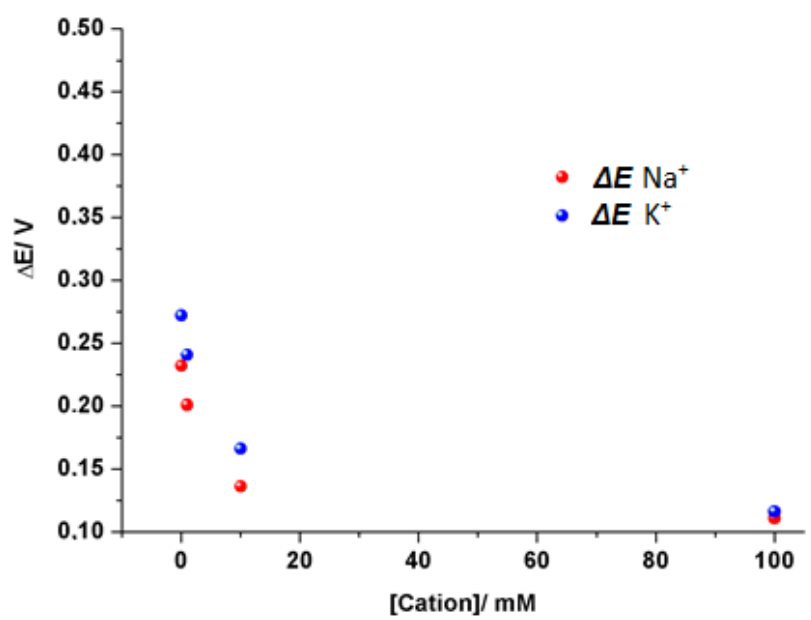


**Figure 58: Comparison of the effect on the reversibility of the *charge-discharge* process in presence of alkaline cations:** Difference of potential,  $\Delta E$ , between the oxidation and reduction peaks for the different electrolytes: 1, 10 or 100 mM of sodium (red) or potassium (blue) cations.

It is observed that the *charge-discharge* process is always more reversible in presence of the sodium cation, except at high concentrations. Thus, the difference between the oxidation potential and the reduction potential are always larger for the potassium peaks. This could indicate an interaction of the cation with the polymeric film structure in a reversible (sodium) vs a less-reversible or at least a slower process (potassium). However, once again in the reproducibility study, some variability was observed in the tendencies that were certainly dependant on the surfaces directly interacting with the electrolyte.

In conclusion, in the potentiodynamic voltammetry characterization in neutral aqueous conditions we observed a larger sensitivity at higher concentrations of the target cations sodium with respect to potassium, as expected from the monomer [6] structure. Under acidic conditions, it is possible to follow the change of the characteristic aniline peak, the group sterically close to the ion-sensitive moiety in monomers [6] and [7]. Note that the reversibility was affected in function of the concentration and nature of the cation present on the electrolyte, being more reversible for sodium in the preliminary experiments. However, it is clear that a surface accessibility to the groups or interface processes with the electrolyte plays an important role that affects to the experimental reproducibility. For this reason, stability of the films was evaluated and potentiostatic experiments were performed to determine potentials related to surface phenomena.

### Stability of the films

To have a better knowledge about the stability of the films during the electropolymerization process and along the exposure of the films to demanding conditions, we evaluated the influence of the scan rate in the *charge-discharge* process, as well as assess the limiting process during these cycles, either the electronic transfer or the ionic mobility.

Firstly, for the evaluation of the influence of the scan rate in the *charge-discharge* process, the electropolymerization of the polymer films was done at scan rates between 10 and 200 mV under the same conditions as the potentiodynamic titrations. For all the crown-ether containing films evaluated ( $P(7)$  is shown in Annex 10), we found a logarithmic regression between the current peak ( $i_p$ ) and the scan rate ( $v$ ). This allows us to confirm, firstly that the polymer films adhered well to the electrode, and, secondly, that the redox process is occurring at the polymer-electrode interface. In Figure 59, it is shown as illustrative example the evaluation for polymer from monomer [6],  $P(6)$ .

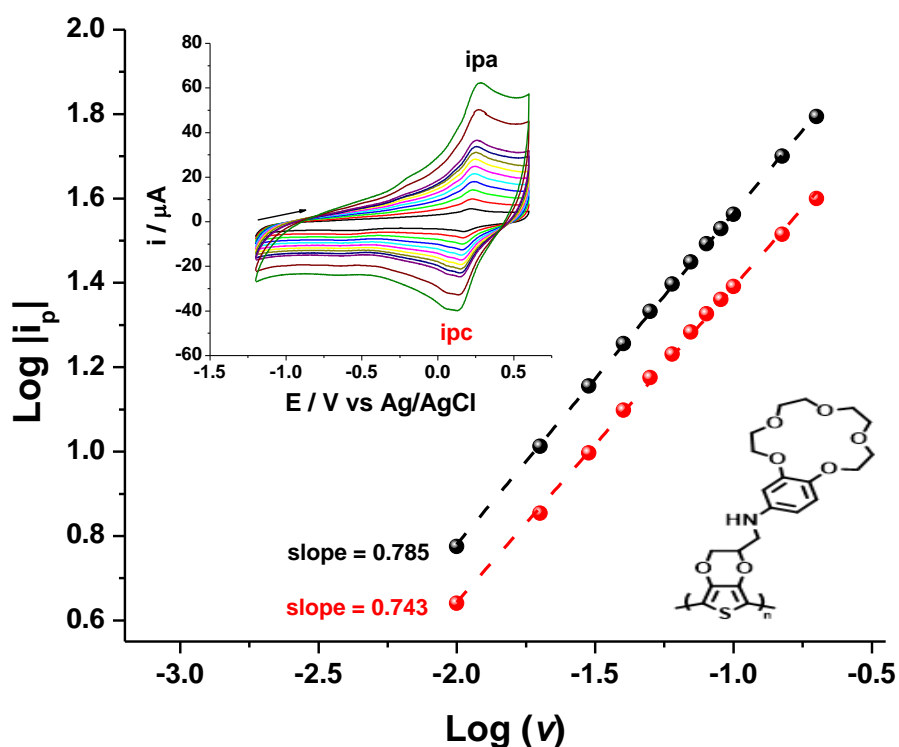


**Figure 59: Influence of the scan rate on the *charge-discharge* process:** Variation of  $\log(i_p)$  vs  $\log(v)$  for the polymer film  $P(6)$ . *Inset:* Variation of the current with the scan rate. *ipa*: anodic peak current, *ipc*: cathodic peak current. Scan rate ( $v$ ): 10 to 100; 150 and 200 mV/s (from black to green curves). Conditions: 0.1 M  $\text{LiClO}_4$  in ACN, AcOH (pH=4).

To evaluate the limiting process during the *charge-discharge* cycles, we also plotted the  $\log(i_p)$  vs the  $\log(v)$ . The slopes of these linear regressions allow us to determine quantitatively what is the limiting process during these cycles, either the ion mobility of

the anions present in the electrolyte (if  $m=1$ ) or the rate of the electronic transfer in the conjugated polymer (if  $m=0.5$ )[105]. For all the aniline crown-ether containing films evaluated (see Annex 10), the slopes have values of  $m=0.7-0.8$ . This indicates an intermediate situation where the *charge/discharge* process is limited by both processes. This occurs probably due to the sterical hindrance of the crown ether moieties, but specially by the ionic mobility in the polymeric matrix. This phenomenon has been already observed in PEDOT and other PXDOT derivatives due to the compact structures formed.

Secondly, to study the temporal stability of the film along the subsequent series of *charge-discharge* process, we evaluated the evolution of cathodic and anodic charge by chronoamperometry of double pulse for 100 cycles, and the electrochemical profile of the film by cyclic voltammetry characterization before and after the 100 cycles of redox process.

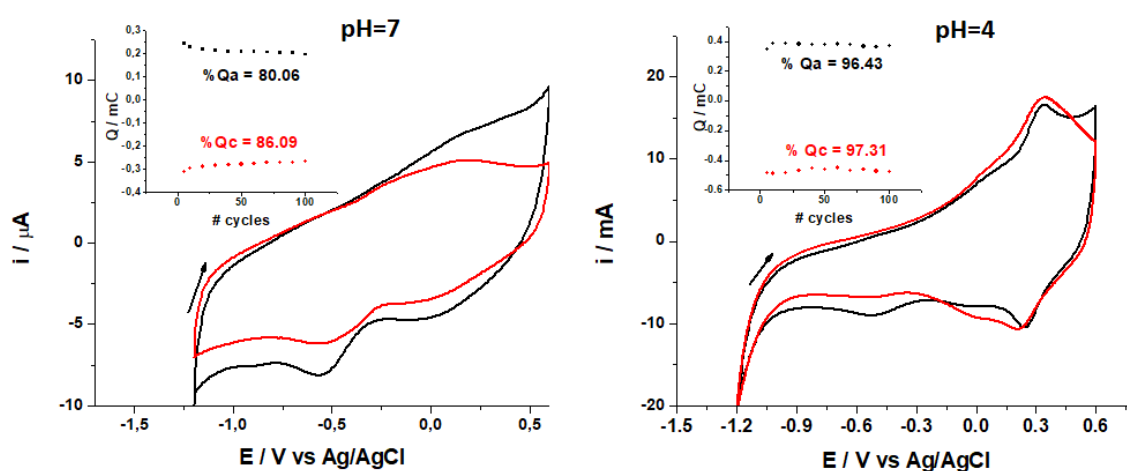


**Figure 60: Stability of film of P(7) after 100 cycles of charge-discharge process:** Potentiodynamic oxidative voltammogram before (black curves) and after (red curves) the 100 cycles. Conditions: 0.1M LiClO<sub>4</sub>, ACN,  $v=25\text{mV}\cdot\text{s}^{-1}$ ; pH=7 (left), pH=4 (right).

As we can observe in the insets of Figure 60, the charge related to the number of cycles confirmed that the films are stable in neutral and soft acid conditions ( $Q_a$  and  $Q_c > 80\%$  in both cases), keeping their electroactivity. This confirms also the presence of an efficient

charge transfer based on the high ratio  $Q_c/Q_a$  obtained. The change of current observed in the voltammogram performed after the cycles (red curves) could be explained as a rearrangement of the oligomer chains or, in the case of the discharge current (effect observed in the reduction at both pH), it could be explained by the dissolution of some oligomers and charge trapping phenomenon.

In conclusion, aniline crown-ether containing films result to be stable films after several cycles of charge-discharge process, being more efficiently the charge transport in softly acidic conditions, meaning that loose of material or instability is not the main reason of the variability observed before. This lead us to explore other techniques.

## 4.2 Potentiometric titrations

To have a better understanding about the influence and detection of the ion interaction with the surface electrode functionalized with the ion-sensitive conducting polymers under study, we oriented our work to a classical analytical method, the potentiometric measurement. This technique results attractive for the research on conducting polymers with covalently bound ion-recognition moieties and it stays still unexplored as potentiometric sensor in comparison with other methods, such as spectroscopic or conductometric measurements.

Figure 61 illustrates the comparison of the potentiometric titrations done of conducting polymer films growth on glassy carbon electrodes: *PEDOT* (blue inset) on the left and *P(7)* (green inset) on the right. Given is the difference of potential between the functionalized electrodes (with the respective CP) vs a Ag/AgCl reference electrode when the concentration of the analyte, sodium (red curves) or potassium (black curves) were changed.

In both graphs, we can distinguish between two and three regimes. The first one could correspond to the changes in the interface until arrived to the limit of detection of the electrode. The second regime, linearly dependant on the ion concentration, gives us information about the affinity with the analyte, as the slopes of the curves are in relation with the sensitivity to the cations. The third regime seems to be related with saturation or ionic force depending mechanisms. Thus, analysis of the second regime has been evaluated for the different conductive materials.

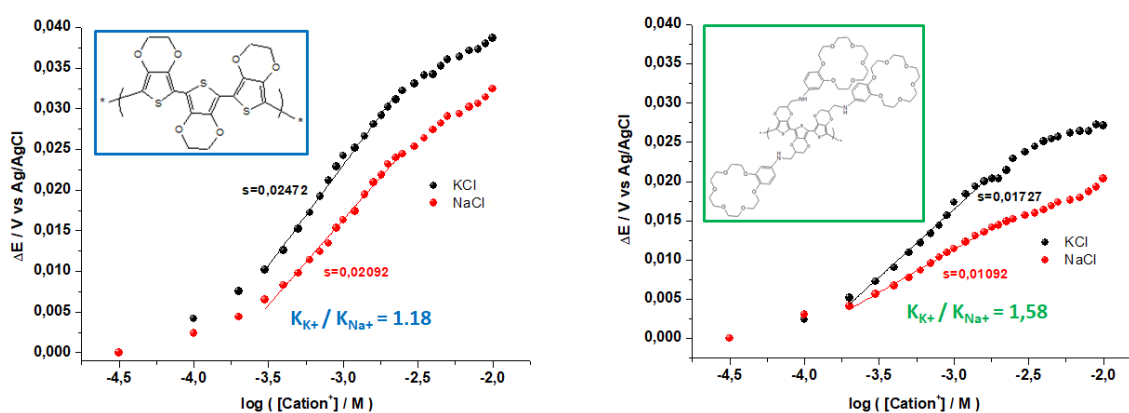


**Figure 61: Comparison of potentiometric titrations of: PEDOT (left) and P(7) (right).**

On the one hand, considering the absolute values, it appears that PEDOT have steeper slopes for both cations than the functionalized polymer. This fact that may be related to the easier access of the cations to the polymer or the better charge transfer in these films. However, a small distinction between the alkaline cations is present, obtaining a ratio between both slopes close to 1 for PEDOT ( $K_{K^+} / K_{Na^+} = 1.18$ ). On the other hand, P(7) shows very distinct difference of potential when the titration is done with potassium or with sodium cations, presenting a ratio of 1.58. These results could suggest a larger affinity for potassium and is confirmed by the larger slope in the linear regime, even if the absolute values of the slopes are lower than in the case of PEDOT ( $n=2$ ). This result is in agreement with expected behaviour for 18-crown-6 containing polymers P(7).

To conclude, potentiometric measurements of the referent material, PEDOT, and their derivatives with ion-sensitive moieties were explored, and the results indicate a higher ionic discrimination in the case of the crown-ether containing polymers.

### 4.3 In-situ Conductivity Spectroscopy

In order to corroborate the previous results, simultaneous measurement of the conductance *in-situ* with the electrochemical measurements was performed. This method is very interesting because of the reproducible and reliable conductivity results obtained [106].

Electropolymerization of the monomers [6] and [7] presents the oxidation peak of the aniline moiety which is associated to an increase of conductance ( $G$ ) of  $2.5 \mu\text{S}$  ( $E = 0.8 \text{ V}$ ), see Figure 62-a. This increase of conductance is attributed to the possible formation of some small oligomer chains of polyaniline deposited between the combs of the Pt interdigital microarrange electrode, IDME (Figure 64 in the experimental part). After this point the conductance decrease ( $E = 0.8 - 1.45 \text{ V}$ ), due to the possible overoxidation of the small oligomer chains. When the oxidation potential of the EDOT moiety is reached ( $E = 1.55 \text{ V}$ ), an increase of conductance is observed which is attributed to the deposit of charged oligomers deposited between the combs of the IDME. During the cathodic sweep a maximum of conductance is observed, which is due to the conductance of the deposited film. This behaviour is observed all along the five electropolymerization cycles.

For the monomers [9] and [10] the absence of the oxidation peak of aniline is observed (Figure 62-b). Therefore, the only oxidation process is the one due to the EDOT moiety ( $E = 1.5 \text{ V}$ ), at this point an increase of conductance is observed which is attributed to the deposit of charged oligomers between the combs of the IDME. During the cathodic sweep a maximum of conductance is observed. The electropolymerization kinetic and *charge-discharge* process of polymer *p(10)* is similar to the one observed for PEDOT (Annex 11).

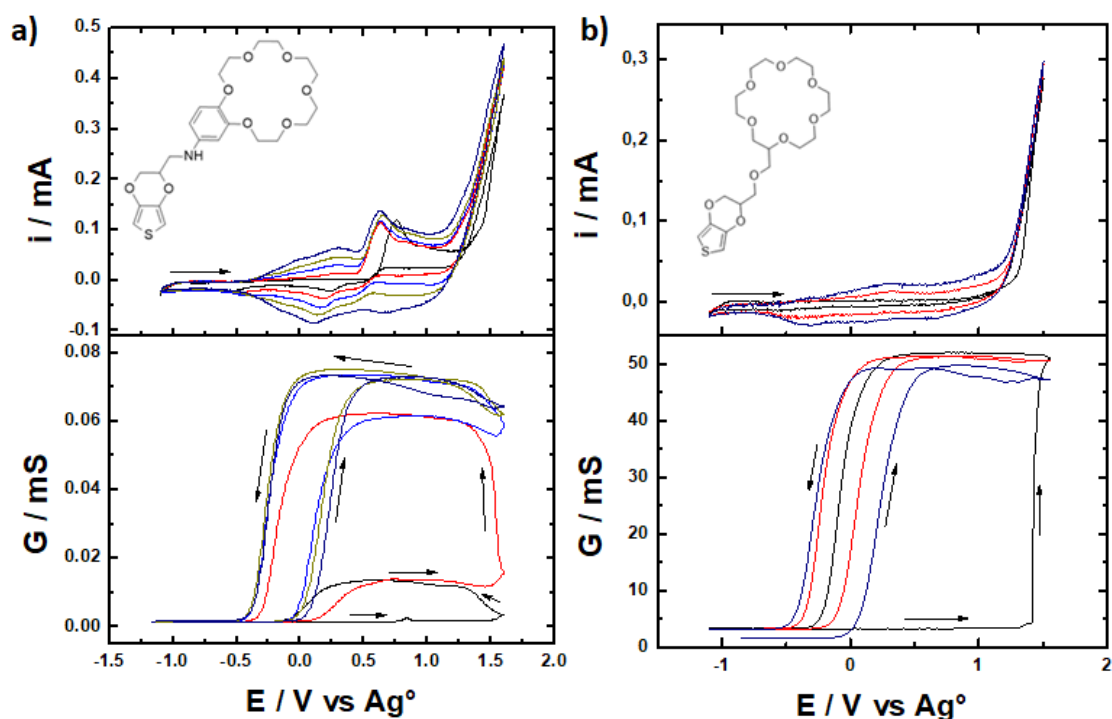


**Figure 62: *In-situ* conductivity measurements:** Top: Electropolymerization of *p*(7) (aniline linking) from monomer [7] (a) and *p*(10) (ether linking) from monomer [7] (b) for five and three cycles, respectively. Bottom: Related conductance ( $G$ ) recorded during the electropolymerization.

After the electropolymerization, the films were dipped in a free monomer 0.1 M  $LiClO_4$  aqueous solution and an *in-situ* electrochemical conductance experiment was performed in a potential window where the polymer does not suffer overoxidation (0.7 V vs  $Ag^{\circ}$ ) and the reduction of water is not reached (-0.3 V vs  $Ag^{\circ}$ ). With this result, the initial conductance in function of time was obtained ( $G_0$ ). Subsequently, the same experiment was performed in a 0.1 M NaCl or KCl aqueous solutions to study the influence of the cation in the conductance of the polymer ( $G$ ). These results allowed to evaluate the quotient  $G/G_0$  (Figure 63).

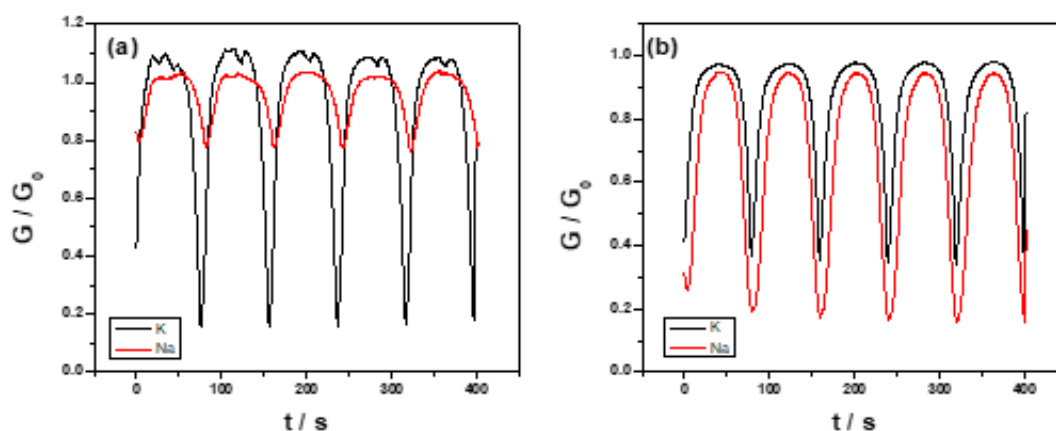


**Figure 63: Influence of the cation affinity of the ion-sensitive polymers on the conductance during the doping/dedoping of the previously electropolymerized films:** Polymer films *P(6)* and *P(7)*, left and right respectively, exposed to 0.1M of KCl or NaCl aqueous electrolytes.

The presence of  $K^+$  in the solution causes a slight increase of conductance for *P(6)* ( $G/G_0 = 1.1$ ) and a small decrease ( $G/G_0 = 0.97$ ) for *P(7)*. This is attributed to the low affinity of *P(6)* to  $K^+$ , due to the fact that the cation is not trapped in the 15-crown-5 ether moiety which improves the charge mobility. In contrast, in the case of *P(7)* the  $K^+$  may be trapped inside the crown-ether moiety which causes a decrease in the charge mobility (conductance) due to a charge repulsion.

The presence of  $Na^+$  causes no change on the conductance for *P(6)* ( $G/G_0 = 1.0$ ) and a small decrease for *P(7)*, ( $G/G_0 = 0.9$ ) as illustrated in Figure 63 (red curves). This decrease may be attributed to the size of the crown ether moiety of *P(7)* that allows both cations to be trapped. This allows to conclude that there is a small selectivity of *P(6)* to  $Na^+$ , whereas *P(7)* does not show a selectivity for either of the cations.

This result is contrary to the tendency obtained in potentiometric measurements, indicating probably some variability in the formation of the films. Nevertheless, this selectivity is in total agreement with the association constants obtained for monomers [6] and [7] obtained by  $^1H$ -NMR titrations, showing a higher affinity of [6] for sodium

cation while an unclear distinction of [7] toward these two cations (see Table 10, monomer [6] and [7] on *Appendices* chapter). Note that these results may not be conclusive since the difference of conductance may be inside the statistical bar error.

## 5 CONCLUSION

Synthesis and characterization of a series of functionalized EDOT derivatives with ion-sensitive moieties [6] to [10] were performed. The study of the structure-properties relationship of the different materials by different techniques was presented and discussed in this chapter.

The electropolymerization and generation of homopolymer films of these monomers was feasible, except for monomer [8], and these polymer films show a good stability over the cycling characterization. In addition, their copolymerization with well-known conjugated monomers (EDOT or even bithiophene) was possible and improves the film formation, at the expenses of a diminished cation affinity due to a decrease in the percentage of sensing monomer (functionalized monomers). Evidence for a difference on the film formation and *charge-discharge* profiles was found between the aniline, present in *P(6)* and *P(7)*, and the ether link, found in *P(9)* and *P(10)*. They were assigned the characteristic peaks corresponding to the *charge/discharge* of the EDOT moiety and the aniline characteristic peak. In addition, it was observed the formation of short oligomer chains during the polymerization of the aniline containing monomers, suggesting an influence of this fraction in the autocatalytic oxidation process.

Moreover, due to the chelating modifications introduced in these polymers, their ion sensitivity and the evaluation of the changes in their electrochemical properties were discussed. Study of the structure-properties relationship was performed by different techniques. To sum up, these films appear to have an ion affinity for alkaline cations. Problems of reproducibility were encountered in the characterization of films by potentiodynamic methods or potentiometric titrations. To validate these results, characterization of conductivity *in-situ* while the film was forming were performed, showing a selectivity of *P(6)* and *P(7)* in accordance with affinities extract from

associations constants of the corresponding monomers, [6] and [7], obtained by  $^1\text{H-NMR}$  titrations.

## 6 EXPERIMENTAL PART

### 6.1 SYNTHESIS OF MATERIALS

#### 6.1.1 MONOMERS

- **2-phenyl-18-crown-6-(3,4-ethylene-dioxythiophene)-amine [7] (GENERAL PROCEDURE):**

A three necked round bottom flask, previously flame-dried, and kept under inert conditions was charged with Chloromethyl-EDOT (5.91 g, 46.6 mmol, 1.0 eq.), 2'-Aminobenzo-18-crown-6 (5.91 g, 46.6 mmol, 1.0 eq.) and sodium carbonate (5.91 g, 46.6 mmol, 3.0 eq.) solubilizing everything with dry and degassed Acetonitrile (V=40 mL). The mixture was stirred for 48h at 70°C. The solvent was removed under reduced pressure, and after solubilize in dichloromethane, the product was washed with water and dried over magnesium sulfate. Solvent was removed after and a brownish oil was obtained (72 % yield). <sup>1</sup>H NMR (400 MHz, CDCl<sub>3</sub>) δ(ppm): 6.71 (d, 1H), 6.36 (s, 2H); 6.29 (s, 1H); 6.23 (dd, 1H); 4.35 (m, 1H); 4.26 (dd, 1H); 4.17-4.08 (m, 5H); 3.87 (dt, 4H); 3.68 (m, 15H). <sup>13</sup>C-NMR (CDCl<sub>3</sub>, 150 MHz): δ(ppm)= 150.4; 142.1; 141.3; 140.9; 117.4; 107.7; 103.1; 100.32; 73.03; 71.0; 70.8; 70.6; 70.2; 69.9; 69.0; 65.76.

- **2-phenyl-15-crown-5-(3,4-ethylene-dioxythiophene)-amine [6]:**

Same procedure as describes before (2-phenyl-18-crown-6-(3,4-ethylene-dioxythiophene)-amine) (72 % yield). <sup>1</sup>H-NMR (400 MHz, CDCl<sub>3</sub>) δ(ppm): 6.72 (d, 1H), 6.36 (q, 2H); 6.28 (d, 1H); 6.23 (dd, 1H); 4.36 (m, 1H); 4.26 (dd, 1H); 4.17 (q, 1H); 4.06 (m, 4H); 3.88 (m, 4H); 3.74-3.68 (m, 11H). <sup>13</sup>C-NMR (CDCl<sub>3</sub>, 150 MHz): δ(ppm)= 150.6; 142.3; 141.3; 140.9; 117.5; 107.7; 102.9; 100.3; 77.1; 71.1; 71.0; 70.9; 70.6; 70.1; 69.8; 68.8; 65.8; 41.5.

- **2'-(Bis(2-picolyl) aminomethyl)-3,4-ethylenedioxythiophene [8]**

Step 1- Synthesis of 2-aminomethyl-3,4-ethylenedioxythiophene:

2'-azidomethyl-3,4-ethylene-dioxythiophene (1.5 g, 7.2 mmol) in 10 ml of THF, was added dropwise to a suspension of LiAlH<sub>4</sub> (0.432 g, 10.8 mmol) in 20 mL of THF cooled at 0°C under nitrogen, equipped with refrigerant. The reaction mixture was stirred for 2.5 h at 0-8°C under nitrogen. After slow, cautious addition of H<sub>2</sub>O (1.2 ml), the grey mixture was stirred at 0°C for 20 min and filtered over a pad of Celite. The solvent was removed, yielding a colorless oil of 2,3-dihydrothieno[3,4-b][1,4]dioxin-2-yl)methanamine (yield 98%). <sup>1</sup>H-NMR (CDCl<sub>3</sub>, 400 MHz): δ= 6.25 (d, 2H), 4.12 (dd, 1H), 4.03 (m, 1H), 3.92 (q, 2H), 2.98 (q, 2H). <sup>13</sup>C-NMR (CDCl<sub>3</sub>, 150 MHz): δ= 141.6, 141.6, 140.71, 99.5, 75.2, 66.6, 42.3

Step 2- Synthesis of 2'-(Bis(2-picolyl) aminomethyl)-3,4-ethylenedioxythiophene:

2'-aminomethyl-3,4-ethylene-dioxythiophene (1.29 g, 75 mmol) and 2-picolylchloride hydrochloride (2.54 g, 15 mmol) were dissolved in 20 mL of water and heated to 60°C in an oil bath. To the stirring mixture was added 9 mL of 5 N aqueous NaOH drop-wise, after which the mixture was stirred at 60°C for one hour. A solution of 2-picolylchloride hydrochloride (0.83 g, 5 mmol) in 5 ml of THF, was added to the mixture and stirred at 60°C for further two hours. The mixture was cooled to room temperature and then extracted with 3x20 mL Et<sub>2</sub>O. The combined extracts were dried (Na<sub>2</sub>SO<sub>4</sub>) and then evaporated to give a brown oil. The crude product was purified by silica gel chromatography, using DCM/EtO<sub>2</sub> (10:1) as the eluent. The purified product (2.7 g, 92% yield) was obtained as a yellow oil. <sup>1</sup>H-NMR (400 MHz, CDCl<sub>3</sub>): δ (ppm)= 8.44 (2H, m); 7.55 (2H, m); 7.38 (2H, m); 7.06 (2H, m); 6.19 (2H, m); 4.20 (1H, m); 4.10&3.90 (2H, m); 3.85 (4H, m); 2.81 (2H, m). <sup>13</sup>C-NMR (150 MHz, CDCl<sub>3</sub>): δ=159.0; 149.1; 141.6; 136.4; 123.1; 122.2; 73.3; 72.3; 67.1; 67.0; 61.1; 55.1; 53.9; 49.2.

- ***2-methyl-(3,4-ethylene-dioxythiophene)-18-crown-6-methyl ether [10]***  
**(GENERAL PROCEDURE) [10]:**

A three necked round bottom flask, previously flame-dried, was charged with Chloromethyl-EDOT (5.91 g, 46.6 mmol, 1.0 eq.), hydroxymethyl-18-crown-6 (5.91 g, 46.6 mmol, 1.0 eq.), potassium carbonate (5.91 g, 46.6 mmol, 2.0 eq.), a catalytic amount of potassium iodide (5.91 g, 46.6 mmol, 0.1 eq.) and dry and degassed DMF (V=40 mL). The mixture was stirred and heated to 100°C for 24h under inert conditions. After 24h, one extra equivalent of Chloromethyl-EDOT was added and the reaction was continued for a further 24h under the same conditions. The mixture was allowed to reach room temperature and was then extracted with dichloromethane (3x20mL). The combined organic layers were then washed with water (20mL) and dried over anhydrous magnesium sulfate. The solvent was then evaporated under vacuum and the residue was purified on alumine chromatography (DCM/EtOAc/MeOH) obtaining a viscous brown oil (56 % yield). <sup>1</sup>H-NMR (400 MHz, CDCl<sub>3</sub>): δ (ppm)= 6.36 (q, 2H), 4.25-4.23 (m, 2H); 4.11-4.06 (q, 1H); 3.85-3.67 (m, 18H). <sup>13</sup>C-NMR (CDCl<sub>3</sub>, 150 MHz): δ(ppm)= 141.7; 99.9; 100.0; 74.2; 70.8; 66.0; 61.7.

- ***2-methyl-(3,4-ethylene-dioxythiophene)-15-crown-5-methyl ether [9]:***

Same procedure as describes before (see 2-methyl-(3,4-ethylene-dioxythiophene)-18-crown-6-methyl ether).

<sup>1</sup>H-NMR (400 MHz, CDCl<sub>3</sub>): δ (ppm)= 6.36 (q, 2H), 4.36-4.17 (m, 4H); 3.67 (m, 8H). <sup>13</sup>C-NMR (150 MHz, CDCl<sub>3</sub>, 298K): δ(ppm)= 141.32; 140.87; 100.34; 73.0; 70.1; 65.8; 41.3.

### 6.1.2 Electrochemical polymerizations

A typical three electrode cell containing a 0.1M LiClO<sub>4</sub> in ACN solution with different monomer concentrations was used for the electropolymerization. During the electrocopolymerization, both monomers were added in the necessary concentrations to obtain a desired ratio to keep a global constant concentration (10 mM). After all the electrochemical characterization the glassy carbon electrode, was polished with alumina

to achieve reproducibility. Previously each electropolymerization, the oxidation of the monomer was evaluated in a potential window from 0 V to 1.5 V ( $\nu = 25 \text{ mV s}^{-1}$ , 1 cycle). To carry out the electropolymerization the peak potential of each monomer was selected ( $E_p$ ) using 10 cycles and  $\nu = 25 \text{ mV}\cdot\text{s}^{-1}$ , in a potential window where the whole charge/discharge process of the film was observed (i.e. for EDOT from -1.2 V to 1.4 V). Prior each electrochemical experiment an equilibrium time was applied (10 s) to reach the thermodynamic equilibrium of the electrode.

## 6.2 Characterization methods

### 6.2.1 Potentiodynamic Characterization

All electrochemical characterizations were performed in a free monomer cell containing a 0.1 M  $\text{LiClO}_4$ , in two different solvents; ACN and  $\text{H}_2\text{O}$ . Through the aqueous solution studies a different concentration of NaCl and KCl was used (from 10 to 100 mM).

### 6.2.2 Potentiometric Characterization

Open circuit potentiometric experiments were done using an PalmSense potentiostat instrument controlled by PS Trace 5.2 software (PalmSense BV, Netherlands). The polymeric films were grown by electropolymerization on glassy carbon working electrodes as explained before. Then, the evolution of the difference of potential at the open-circuit voltage between this covered working electrode and a Ag/ AgCl reference electrode was evaluated during the titration with different salts. At the beginning was measured the OCV during at least 3 cycles of 10 min to stabilize the potential measured between the 2 electrodes. Once stabilized, addition of the volume need of the salt solution was added to the cell, 30 s of stirring was applied and stopped, and further measured of the OCV was run during 5 minutes. Analysis and Quantification of data was done with Origin software.

### 6.2.3 *In-situ* conductivity measurements

All the electrochemical experiments were performed with a two potentiostat system where potentiostat (1) generates the electrical perturbation signal (lineal potential sweep), while potentiostat (2) keeps a constant potential ( $\Delta V$ ), between both parts of an Pt interdigital microarrange electrode (IDME) and simultaneously reads the drain current ( $i_d$ ) that flows through the deposited films. In order to separate the working electrode from potentiostat (1) and to apply the  $\Delta V$  with the potentiostat (2) in an adequate manner, a series of resistances was made[107]. A single compartment three-electrode cell, equipped with an IDMAE of 1 cm x 0.5 cm, featuring separated Pt bands (10  $\mu\text{m}$ ) as working electrode, a Pt foil separated 0.5 cm from the working electrode (parallel and of the same size of the working electrode) as counter electrode and an Ag wire as quasi-reference electrode was used. A constant potential difference of 10 mV ( $\Delta V$ ) provided by one potentiostat was applied between the IDMAE branches to generate the drain current that circulates through the polymer during conductance determinations. The conductance of the electropolymerization and the grown films was measured in real time during all the experiments. Conductance was calculated according to Ohm Law, which is directly related with specific conductivity. More details about this technique and examples of the use of conductance measurements in conducting polymers can be found elsewhere in the literature[107–109]. The electropolymerization experiments were performed with cyclic voltammetry by using the Pt IDME dipped in a 0.1 M  $\text{LiClO}_4$ , 5 mM monomer solution in ACN,  $\nu = 25$  mV/s, and  $E_\lambda = 1.6$  vs.  $\text{Ag}^\circ$ . All the electropolymerizations were performed under a  $\text{N}_2$  atmosphere. The electrochemical behaviour of the films thus obtained was evaluated in a free monomer aqueous solution,  $\nu = 25$  mV/s,  $E_\lambda = 0.65$  vs.  $\text{Ag}^\circ$  using different supporting electrolytes ( $\text{LiClO}_4$ ,  $\text{NaCl}$  and  $\text{KCl}$ , 0.1 M).

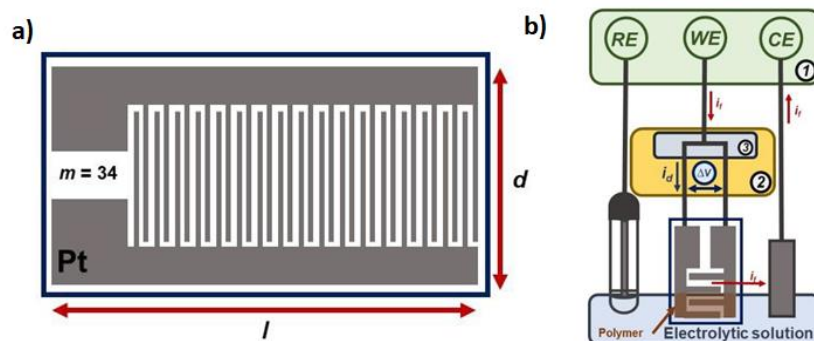
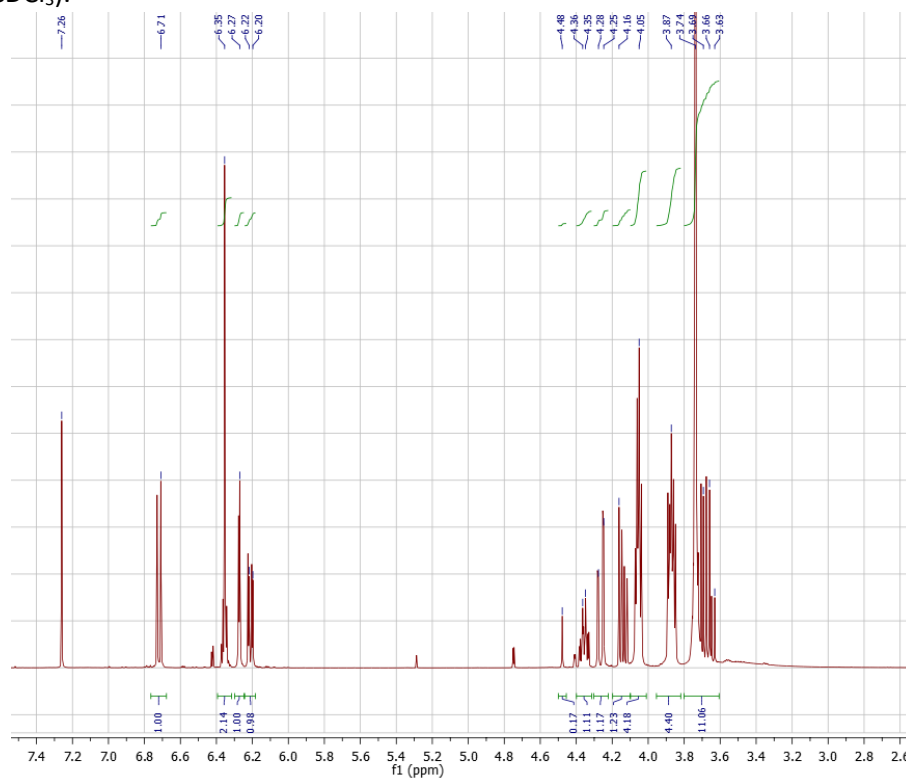


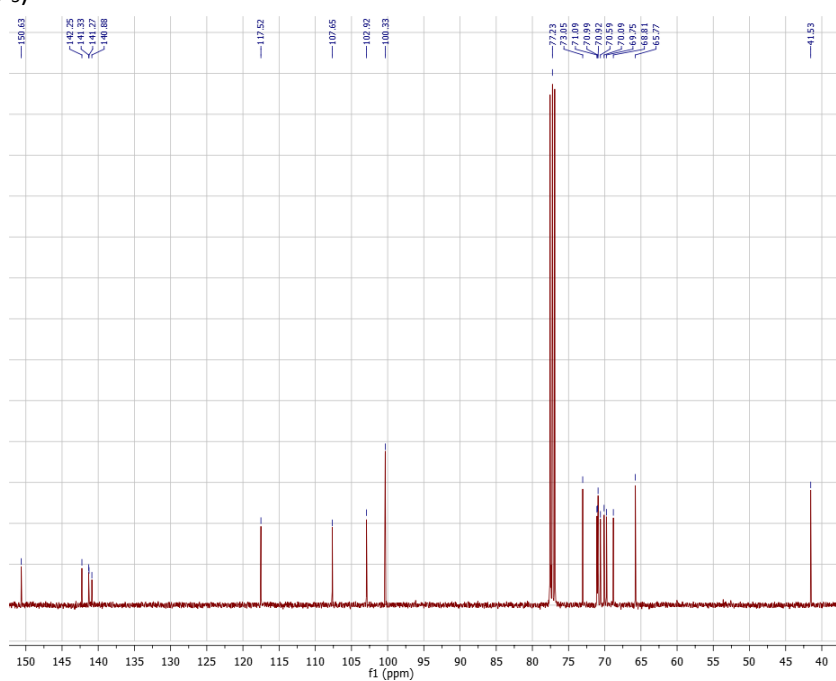
**Figure 64: Scheme of the *In-situ* conductivity measurements set-up:** **a)** Comb type Pt interdigital microelectrode arrangement (IDME) with 34 separation strips; **b)** Schematic diagram of the two potentiostats for *in-situ* electrochemical-conductance method. The potentiostat (1) perform the potentiodynamic experiment, the potentiostat (2) maintains a constant potential ( $\Delta V$ ) during the conductivity experiment and the symmetry unity (3) which applies  $\Delta V$  between both combs of the IDME.

### 6.3 NMR Characterization

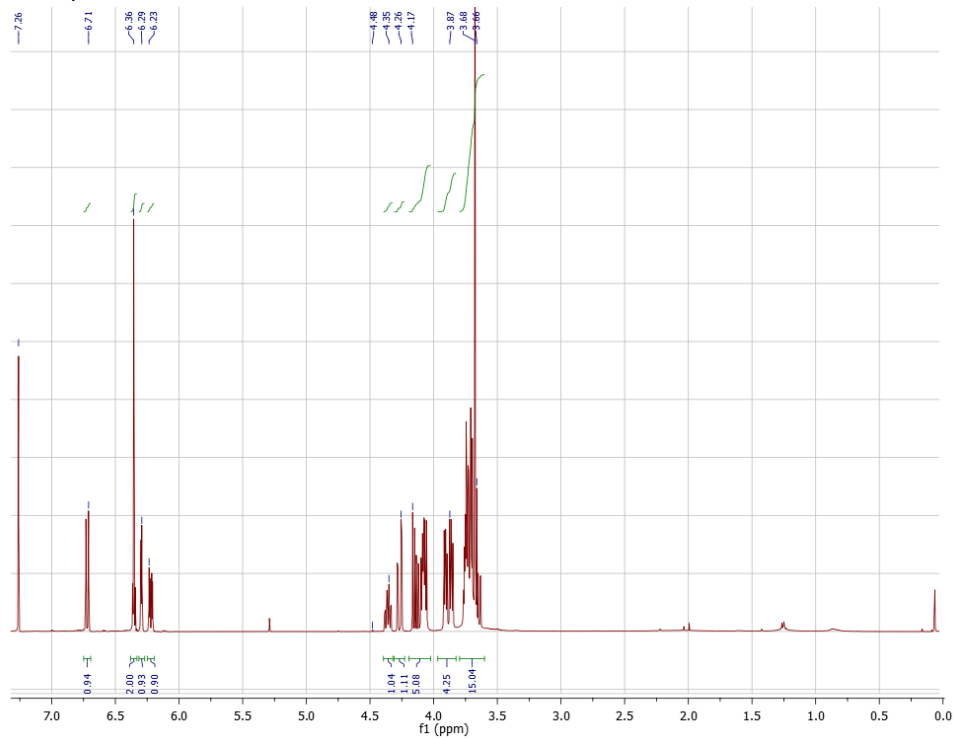
S- 11:  $^1\text{H-NMR}$  of monomer [6]: 2-phenyl-15-crown-5-(3,4-ethylene-dioxythiophene)-amine [6] (400 MHz,  $\text{CDCl}_3$ ).



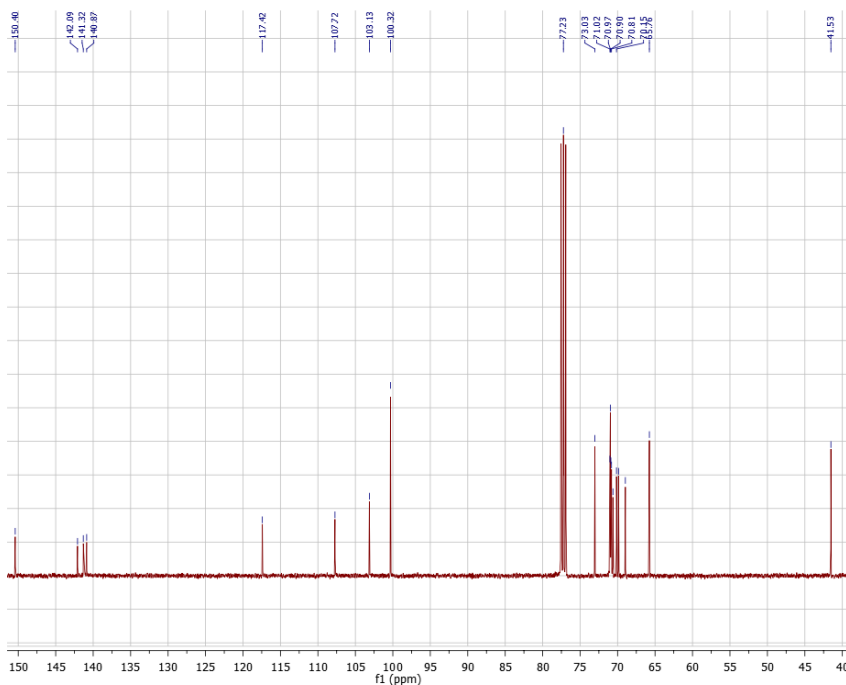
S- 12:  $^{13}\text{C-NMR}$  of monomer [6]: 2-phenyl-15-crown-5-(3,4-ethylene-dioxythiophene)-amine [6] (150 MHz,  $\text{CDCl}_3$ ).



**S- 13:**  $^1\text{H-NMR}$  of monomer [7]: 2-phenyl-18-crown-6-(3,4-ethylene-dioxythiophene)-amine [7] (400 MHz,  $\text{CDCl}_3$ ).

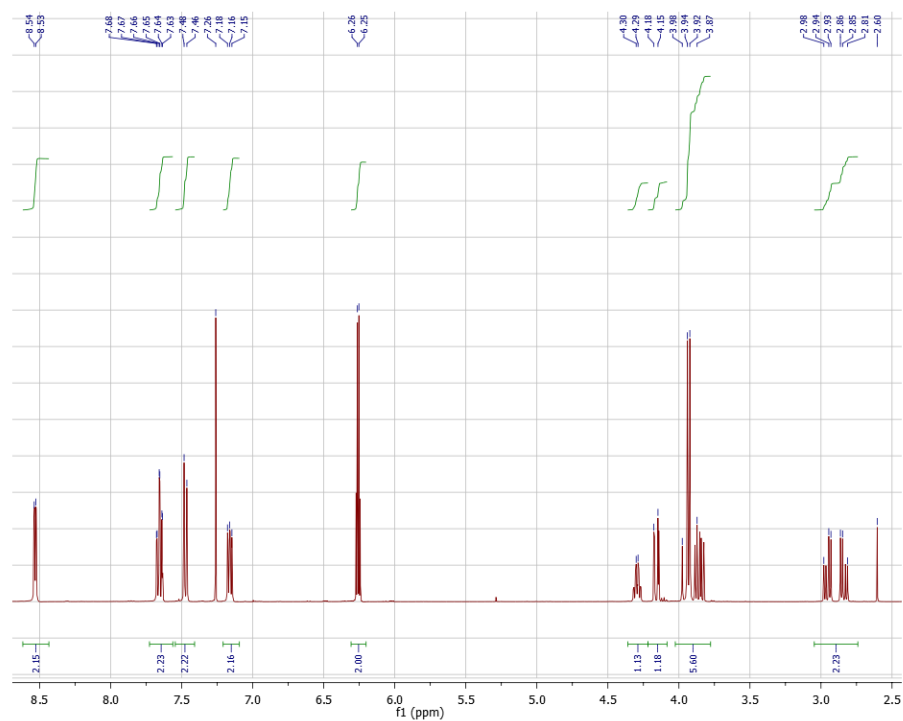


**S- 14:**  $^{13}\text{C-NMR}$  of monomer [7]: 2-phenyl-18-crown-6-(3,4-ethylene-dioxythiophene)-amine [7] (150 MHz,  $\text{CDCl}_3$ ).

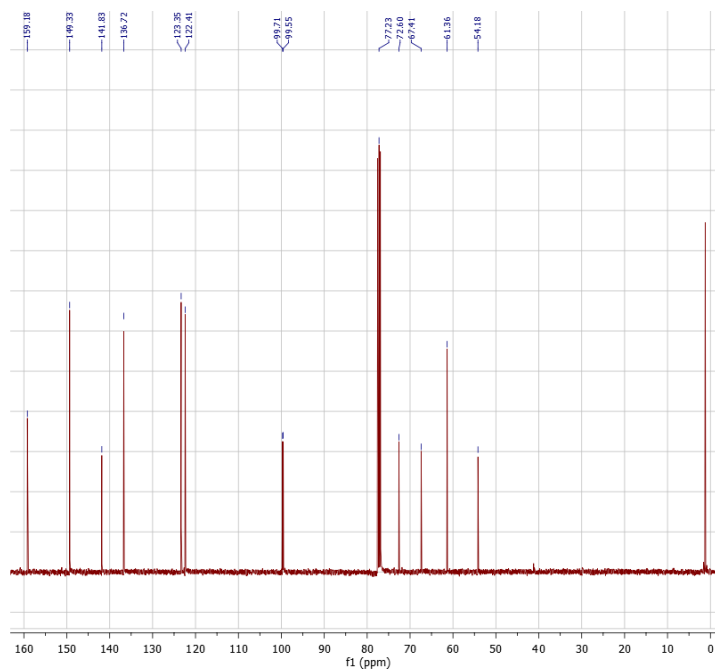


### Chapter III – Ion sensitive EDOT and PEDOT derivatives

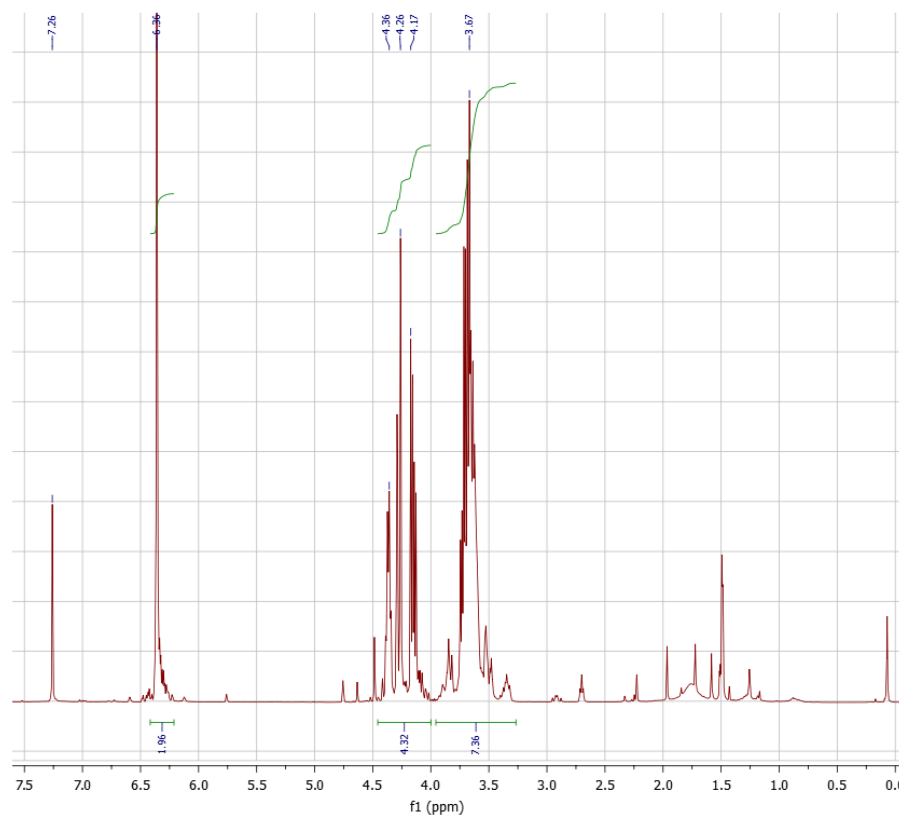
**S- 15:**  $^1\text{H-NMR}$  of monomer **[8]**: 2'-(Bis(2-picolyl) aminomethyl)-3,4-ethylenedioxythiophene **[8]** (400 MHz,  $\text{CDCl}_3$ ).



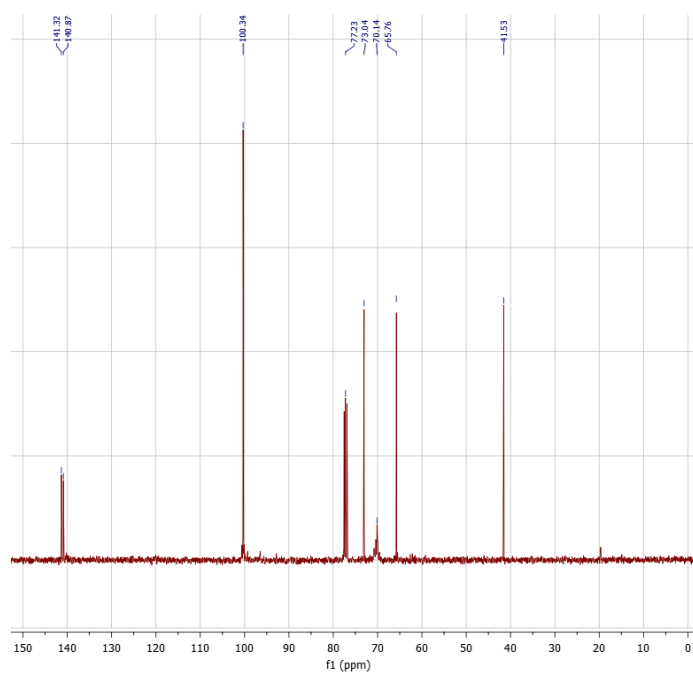
**S- 16:**  $^{13}\text{C-NMR}$  of monomer **[8]**: 2'-(Bis(2-picolyl) aminomethyl)-3,4-ethylenedioxythiophene **[8]** (150 MHz,  $\text{CDCl}_3$ ).



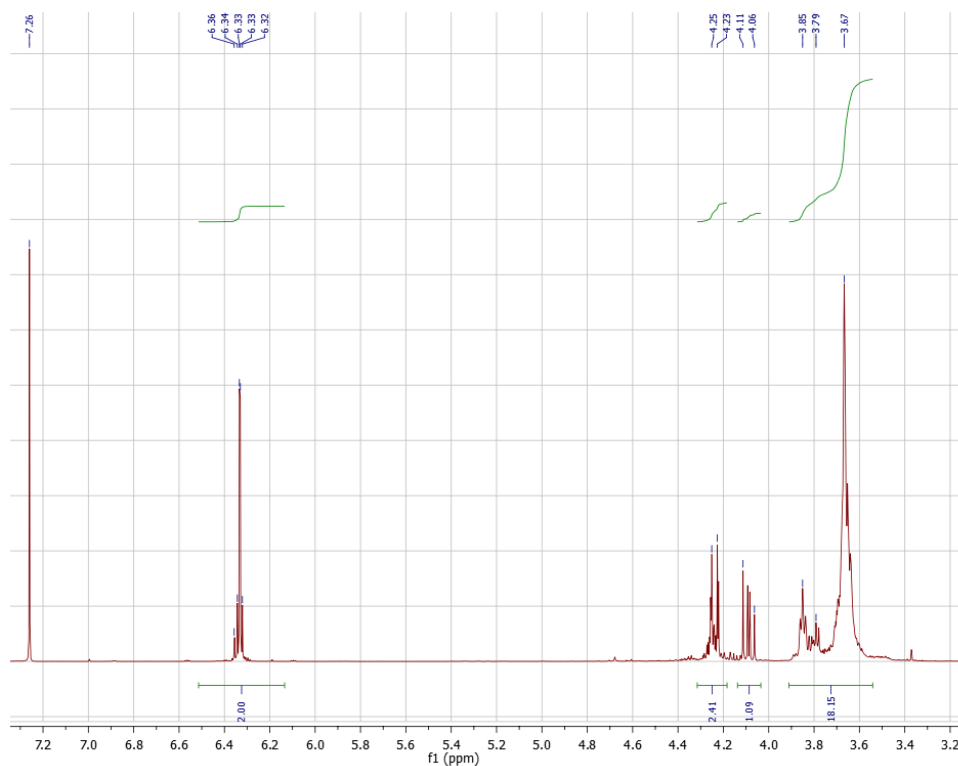
**S- 17:**  $^1\text{H-NMR}$  of monomer [9]: 2-methyl-(3,4-ethylene-dioxythiophene)-15-crown-5-methyl ether [9] (400 MHz,  $\text{CDCl}_3$ ).



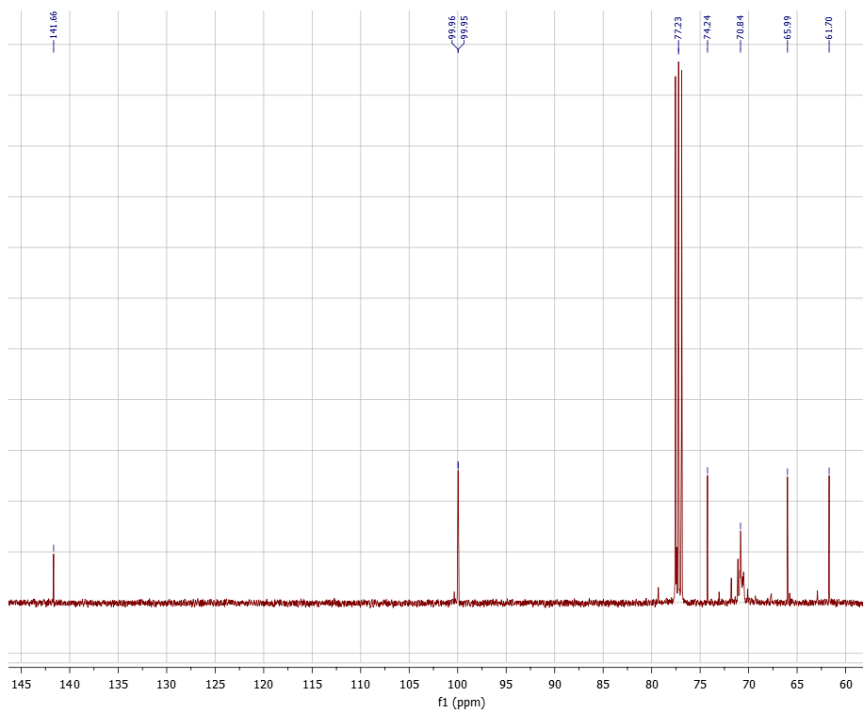
**S- 18:**  $^{13}\text{C-NMR}$  of monomer [9]: 2-methyl-(3,4-ethylene-dioxythiophene)-15-crown-5-methyl ether [9] (150 MHz,  $\text{CDCl}_3$ ).



**S- 19:**  $^1\text{H-NMR}$  of monomer **[10]**: 2-methyl-(3,4-ethylene-dioxythiophene)-18-crown-6-methyl ether **[10]** (400 MHz,  $\text{CDCl}_3$ ).



**S- 20:**  $^{13}\text{C-NMR}$  of monomer **[10]**: 2-methyl-(3,4-ethylene-dioxythiophene)-18-crown-6-methyl ether **[10]** (150 MHz,  $\text{CDCl}_3$ ).



## 7 BIBLIOGRAPHY

100. Degirmenci, A.; Iskenderkaptanoglu, D.; Algi, F. A novel turn-off fluorescent Pb(II) probe based on 2,5-di(thien-2-yl)pyrrole with a pendant crown ether. *Tetrahedron Lett.* **2015**, *56*, 602–607.
101. Heinze, J.; Frontana-Uribe, B.A.; Ludwigs, S. Electrochemistry of Conducting Polymers—Persistent Models and New Concepts †. *Chem. Rev.* **2010**, *110*, 4724–4771.
102. Merz, A.; Kronberger, J.; Dunsch, L.; Neudeck, A.; Petr, A.; Parkanyi, L. Radical Dimerization of 5,5'-Diphenyl-3,3',4,4'-tetramethoxy-2,2'-bipyrrole:  $\pi$  Dimer in the Crystal,  $\sigma$  Dimer in Solution. *Angew. Chem. Int. Ed.* **1999**, *38*, 1442–1446.
103. Valencia, D.P.; González, F.J. Estimation of diffusion coefficients by using a linear correlation between the diffusion coefficient and molecular weight. *J. Electroanal. Chem.* **2012**, *681*, 121–126.
104. Ćirić-Marjanović, G. Recent advances in polyaniline research: Polymerization mechanisms, structural aspects, properties and applications. *Synth. Met.* **2013**, *177*, 1–47.
105. Shimidzu, T.; Ohtani, A.; Iyoda, T.; Honda, K. Charge-controllable polypyrrole/polyelectrolyte composite membranes: Part II. Effect of incorporated anion size on the electrochemical oxidation-reduction process. *J. Electroanal. Chem. Interfacial Electrochem.* **1987**, *224*, 123–135.
106. Aubert, P.-H.; Groenendaal, L.; Louwet, F.; Lutsen, L.; Vanderzande, D.; Zotti, G. In situ conductivity measurements on polyethylenedioxythiophene derivatives with different counter ions. *Synth. Met.* **2002**, *126*, 193–198.
107. Smie, A.; Synowczyk, A.; Heinze, J.; Alle, R.; Tschuncky, P. *i,i*-Disubstituted oligothiophenes, a new oligomeric approach towards the synthesis of conducting polymers. *J. Electroanal. Chem.* **1998**, *9*.
108. Salinas, G.; Del-Oso, J.-A.; Espinoza-Montero, P.-J.; Heinze, J.; Frontana-Uribe, B.A. Electrochemical polymerization, characterization and in-situ conductivity studies of poly-3,4-ortho-xylendioxythiophene (PXDOT). *Synth. Met.* **2018**, *245*, 135–143.
109. Voortman, T.P.; Bartesaghi, D.; Koster, L.J.A.; Chiechi, R.C. Cross-Conjugated *n*-Dopable Aromatic Polyketone. *Macromolecules* **2015**, *48*, 7007–7014.



*Chapter IV.-*  
**APPLICATIONS**

*Ch. V.- Amendices*

## **1 IMPROVING DETECTION OF $\beta$ -CELLS RECORDINGS WITH MEA**

### **1.1 INTRODUCTION**

Islets of Langerhans produce slow field potentials (SP) due to the multicellular activity and fast action potentials (AP) in response to glucose and other stimulus[34,110,111]. To improve detection of APs, PEDOT: PSS covered electrodes were used and compared to classical MEA (TiN and Gold). It was found that both signals were observed, and even with a bigger amplification in the case of the fast signal (AP) when  $\beta$ -cells were recorded with PEDOT: PSS covered MEA. This fact was explained by the better interface of the polymer with the biological material, decreasing the impedance of the electrodes and, increasing so the signal-to-noise ratio allowing better amplification of the signals. This is the first work demonstrating the possibility to extracellularly record  $\beta$ -cell activity measurements with this kind of materials. This work provided the exciting possibility to detect at the same time single cell activity (AP) and coupled activity of cell groups (SP). This approach has indeed been used to describe in detail the unicellular and multicellular events during islet activation (M. Jaffredo and M. Raoux, Ms in preparation) which leads to a better understanding of biphasic secretion. My main contribution to this work have been the physical characterization of MEA to have a complete understanding of PEDOT layer influence in the impedance and capacitance of the studied electrodes. Moreover, I've contributed to MEA recordings, data analysis and Ms preparation.



## 1.1. ELECTROPHYSIOLOGICAL RECORDINGS WITH PEDOT:PSS COVERED MEAs & COMPARISON BETWEEN STANDARD MEAs vs PEDOT:PSS covered MEAs

DOI: 10.1016/j.msec.2017.07.028

Article type: Communication

Title

### Simultaneous monitoring of single cell and of micro-organ activity by PEDOT:PSS covered multi-electrode arrays

Author(s), and Corresponding Author(s)\*

Dimitiros A. Koutsouras<sup>1</sup>, Romain Perrier<sup>2</sup>, Ariana Villarroel-Marquez<sup>2,3</sup>, Antoine Pirog<sup>4</sup>, Eileen Pedraza<sup>2</sup>, Eric Cloutet<sup>3</sup>, Sylvie Renaud<sup>4</sup>, Matthieu Raoux<sup>2</sup>, George G. Malliaras<sup>1</sup>, Jochen Lang<sup>2</sup>

D.A. Koutsouras and G.G. Malliaras,  
Department of Bioelectronics, Ecole Nationale Supérieure des Mines, CMP-EMSE, 13541  
Gardanne, France  
malliaras@emse.fr

R. Perrier, A. Villarroel Marquez, E. Pedraza, M. Raoux and J. Lang  
Chimie et Biologie des Membranes et Nano-Objets (CBMN), UMR CNRS 5248,  
Université de Bordeaux, 18 Av Geoffroy St Hilaire, 33600 Pessac, France  
jochen.lang@u-bordeaux.fr

A. Villarroel-Marquez and E. Cloutet  
Laboratoire de Chimie des Polymères Organiques (LCPO), UMR CNRS 5629, Université de  
Bordeaux, 33600 Pessac, France

A. Pirog and S. Renaud  
Laboratoire d'Intégration de Matériaux aux Systèmes (IMS), UMS CNRS 5218, Institut  
Polytechnique de Bordeaux  
DAK et RP contributed equally

Keywords:

bioelectronics, biosensor, PEDOT: PSS, diabetes, islets

Complete Manuscript

#### Abstract

Continuous and long-term monitoring of cellular and micro-organ activity is required for new insights into physiology and novel technologies such as Organs-on-Chip. Moreover, recent advances in stem cell technology and especially in the field of diabetes call for non-invasive approaches for quality testing of the large quantities of surrogate pancreatic islets to be generated. Electrical activity of such a micro-organ results in single cell action potentials (APs) of high frequency and in low frequency changes in local field potentials (slow potentials or SPs), reflecting coupled cell activity. Each of them is indicative of different physiological stages in islet activation. Action potentials in islets are of small amplitude and very difficult to detect. The use of PEDOT:PSS to coat metal electrodes is expected to reduce noise and results in a frequency

## Ch. V.- Appendices

dependent change in impedance, as shown here. Whereas detection of high-frequency Aps improves, low frequency SPs are less well detected which is, however, an acceptable trade off in view of the strong amplitude of SPs. Using a dedicated software, recorded APs and SPs can be automatically diagnosed and analyzed. Concomitant capture of the two signals will considerably increase the diagnostic power of monitoring islets and islet surrogates.

Continuous long-term monitoring of cell and micro-organ activity is required for Organs-on-Chip or quality testing of therapeutic surrogate organs. The frequency-dependent impedance of PEDOT:PSS permits simultaneous monitoring of single cell and coupled micro-organ activity in pancreatic islets, each of them indicative of defined physiological stages. Together with dedicated software, concomitant capture of the signals considerably increases diagnostic power.

### Keywords

bioelectronics, biosensor, PEDOT:PSS, diabetes, islets

### Authors

Dimitrios A. Koutsouras <sup>1</sup>, Romain Perrier <sup>2</sup>, Ariana Villarroel Marquez <sup>2,3</sup>, Antoine Pirog <sup>4</sup>, Eric Cloutet <sup>3</sup>, Sylvie Renaud <sup>4</sup>, Matthieu Raoux <sup>2</sup>, Georges Malliaras <sup>1\*</sup>, Jochen Lang <sup>2\*</sup>

### Title

Simultaneous monitoring of single cell and of micro-organ activity by PEDOT:PSS covered multi-electrode arrays

Continuous and long-term monitoring of cellular and micro-organ activity is required for new insights into physiology, constitutes a mainstay of novel technologies such as Organs-on-Chip and will also open new therapeutic possibilities in biomedicine. [1] Moreover, with the recent advances in stem cell technology and ensuing de-novo creation of organs, non-invasive approaches are required to improve current protocols. In the same vein, simultaneous monitoring of individual cells as well as organ activity is necessary for quality testing of the large amount of surrogate organs to be generated before their use for therapeutic purposes. These issues have also become important in the diabetes field, especially for type 1 diabetes which is characterized by a loss of islet  $\beta$ -cells.[2]

Ideally, continuous monitoring should be non-invasive and non-destructive, and not require changes in the genetic repertoire or addition of chemical probes. Recording electrical membrane potentials from excitable cells, which include not only neurons and muscle but also endocrine cells, should offer a convenient approach, especially via non-invasive extracellular electrodes.

Electronics avoid heat-generation or bleaching that may damage biological samples, as encountered in optical means. Electric potentials are created by changes in ion fluxes. Their information content is high as changes in membrane potentials are often the first integrative signal of physiological regulations.[3] Excitable organs or cell clusters generate two types of electrical signals: short-lived high frequency action potentials (AP) that reflect single cell depolarization and longer lived changes in field potentials, the low frequency slow potentials (SP). The latter reflects the integrative electrical activity at the organ or micro-organ level. Ideally, both should be recorded to obtain information about the activity of single cells, which may be of different type and behavior, and of the whole (micro) organ that provides information on a higher level of physiological integration.

## Ch. V.- Appendices

APs recorded by extracellular electrodes are of considerable amplitude in neurons or cardiomyocytes. The situation is different in other excitable cells such as in the islets of the endocrine pancreas. In this micro-organ  $\alpha$ - and  $\beta$ -cells produce action potentials, but only  $\beta$ -cells are electrically coupled and generate SPs.<sup>[4]</sup> Whereas SPs are robust, APs are often small and very difficult to detect in endocrine cells when using electrodes in standard materials such as Titanium Nitride (TiN) and Platinum.<sup>[4-5]</sup> Some elegant approaches involving a sophisticated geometry for extracellular electrodes provide some improvement but do not enhance detection of APs.<sup>[6]</sup> Detection can be improved by filtering, but this is ultimately not satisfactory.<sup>[7]</sup> We therefore searched for means to improve detection of islet cells' APs at the electrode level while preserving SP detection. One possibility would be to increase electrode size, but this reduces spatial discrimination and endocrine micro-organs often have a diameter of 50  $\mu\text{m}$ , severely limiting this factor. Conducting polymers such as poly(3,4-ethylenedioxythiophene), complexed with polystyrene sulfonate (PEDOT:PSS) are known to decrease electrode impedance and achieve higher signal-to-noise ratios.<sup>[8]</sup> Clearly, this may favorably influence AP detection.

A corresponding device was assembled (**Figure 1a** for scheme) and its electric characteristics determined in relation to commercial titanium nitride (TiN) electrodes or gold electrodes. As expected, PEDOT:PSS coverage considerably improved the performance of gold electrodes in terms of impedance and the related capacitance (**Figure 1b** and **c**) which is reflected by the known improvement in signal recording. The comparison of TiN- and gold/PEDOT:PSS electrodes revealed a less pronounced difference and was dependent on frequency. Whereas both types of electrodes behaved similarly at frequencies between 1 and 300 Hz, differences were observed below and above this range for impedance and even more marked for capacitance. The expected range for SPs (0.1-1 Hz) and APs (>300 Hz) are shaded in grey in Figure 1 b and c. Thus the behavior of the two types of electrodes predicts an improved signal/noise ratio for PEDOT:PSS covered gold electrodes in the high frequency range, typical for APs, and a less favorable outcome at low frequencies such as those found for SPs.

As SPs are rather robust and of considerable amplitude, we expected the trade-off in the low frequency range to be acceptable in view of an improved recognition of APs. We therefore recorded pancreatic  $\beta$ -cell activity from rodent or human islets in-vitro (**Figure 2**). As shown in **Figure 2a**, these extracellular electrodes record the sum of changes in ion fluxes, mainly  $\text{Na}^+$ ,  $\text{K}^+$  and  $\text{Ca}^{2+}$ , brought upon by the electrical activity of the cells subsequent to changes in ion channel activities. Their activity is regulated in islet  $\beta$ -cells by the ambient glucose concentration and changes in circulating hormones from the gut or stress mediators such as adrenalin. Metabolism of glucose, lipids or certain amino acids leads to the intracellular increase in metabolic coupling factors, such as ATP, that leads to the closure of ATP-sensitive potassium channels and subsequent membrane depolarization with ensuing opening of voltage-dependent calcium channels.<sup>[9]</sup> Electrical activity of islets is biphasic and proceeds first mainly through single cell activity with action potentials and subsequently results in a second phase, vital for physiological glucose homeostasis, which is characterized by pronounced coupling between cells.<sup>[10]</sup> Stress or gut hormones further regulate ion channel activity via classical cAMP or PLC pathways.<sup>[11]</sup> Changes in ion fluxes therefore constitute the first integrative read-out combining nutrient levels and the status of the entire organism, and finally lead to the secretion of the hormone insulin to adapt glucose homeostasis to the physiological needs. **Figure 2b** depicts islet cell clusters seeded on PEDOT:PSS covered gold electrodes and exposed to different stimuli. Representative recordings of an electrode covered by islets (electrode 1) are given in **Figure 2c**. Changing glucose levels from a low normoglycemic concentration of 3 mM to a hyperglycemic level of 15 mM induces a strong electrical response. Addition of the stress hormone adrenalin to 15 mM glucose reduces transiently the islet activity as expected. An even stronger level of activity can be elicited by the subsequent addition of the drug glibenclamide, used in the treatment of type 2

## Ch. V.- Appendices

diabetes and known to directly close  $K_{ATP}$  channels. The addition of nifedipine, a blocker of voltage dependent calcium channels, strongly inhibits the electrical activity evoked by 15 mM glucose indicating that calcium ion fluxes contribute considerably to the changes in field potentials. These observations are in line with the activities described previously by us using TiN or platinum electrodes.<sup>[4, 5b]</sup> To further illustrate the nature of the electrical signals recorded, magnifications of the recording are given in the lower panel of Figure 2c. They demonstrate the presence of low frequency waves, the SPs, and small superimposed activities of high frequencies, the APs. To better demonstrate the presence of the two types of events, we have done some filtering on the traces in presence of glucose and glibenclamide. Whereas a 2 Hz low-pass filter sorts mainly the SPs (red), a 2-700 Hz band pass filter cuts out the SPs and demonstrates the presence of APs (blue). Figure 2d shows the activity recorded from another electrode (electrode 2) that was not covered by islets and consequently no specific signal was recorded. Although mouse islets provide a useful model, it has become clear recently that human islets show a number of differences also in terms of electrophysiology.<sup>[12]</sup> We have therefore also tested human islets, obtained post-mortem from donors, and some results are shown in **Figure 2e**. Recordings shown were obtained from two different donors. Islets of donor 1 exhibit prominent SPs with some APs and activity can be blocked by the use of adrenalin. Islet activity of donor 2 was characterized by the presence of very marked APs that were fully sensitive to nifedipine. Also both responded to glucose and inhibitors, this suggests a marked heterogeneity between donors. Indeed considerable variances have been described for a number of biological responses of human islets and reflect probably their diverse genetic background and history as compared to inbred rodent strains.<sup>[13]</sup> Collectively these experiments suggest that APs may be easier to capture using PEDOT:PSS covered electrodes. We therefore directly and quantitatively compared those electrodes with classical TiN electrodes. To avoid bias and provide a rapid mean we devised an offline Matlab routine as current commercial programs are rather time consuming and not able to reliably distinguish between SPs and APs of small amplitude. We have previously described approaches that determine frequencies of APs or SPs, but not amplitudes. As depicted in **Figure 3a**, input data are filtered, detection thresholds are set and the read-out provides frequency and amplitude for both types of events. As demonstrated in **Figure 3b**, this allows rapid detection of SPs and APs from traces, such as here during stimulation by glucose. Statistical evaluation of TiN vs Au/PEDOT:PSS recordings revealed interesting differences (**Figure 3c**). Au/PEDOT:PSS clearly captured a higher number of APs but lost some SPs. Interestingly, amplitudes of APs were comparable between TiN and Au/PEDOT:PSS indicating the increase in captured events does not reflect an artefact and are most likely due to lower noise levels. In contrast, amplitudes of SPs were largely reduced. The initial characterization of impedance and capacitance (Figure 1) was done under ideal conditions, without culture solutions and additional noise generated by the complete recording set-up including heating systems, amplifiers etc. To evaluate whether this seemingly frequency dependent behavior of the electrodes can be found also under real working conditions, we determined the power spectrum of the two types of electrodes using recordings from electrodes that had not been covered by islets. As can be seen in Figure 3c, we have again similar frequency-dependent characteristics indicating that indeed noise is more prominent at low frequencies in Au/PEDOT:PSS electrodes but more favorable at high frequencies. In conclusion, the frequency-dependent behavior of PEDOT:PSS permits simultaneous recording of single cell and micro-organ activity in the rodent and human endocrine system in a non-invasive system using native biological preparations. As shown, the two types of signals can be reliably distinguished by a novel software script under Matlab, and amplitudes as well as frequencies can be determined automatically. The concomitant capture of the two signals considerably increases the diagnostic power of such an approach in pharmacological screening or the control of stem-cell derived islet surrogates. Moreover, such a detection module may increase the accuracy of bioinspired sensors for the demand of insulin.<sup>[14]</sup>

## **MATERIALS AND METHODS**

**Device Fabrication:** Devices were fabricated as previously reported.<sup>[15]</sup> A 26 mm x 76 mm glass slide was used as a substrate after thorough cleansing in a 1:1 (vol/vol) acetone/isopropanol solvent. The gold electrodes were patterned on top of the glass slide in a standard photolithographic technique with the use of S1813 photoresist, subsequent UV light exposure and development in MF-26 developer. The resulting gold electrodes were 100 nm thick while a 10 nm thick Cr layer between them and the substrate was chosen to act as an adhesive promoter. Both metals were deposited via standard metal evaporation. Thereafter, two layers of Parylene C (with the second serving as a sacrificial one in a later stage) were deposited for the device encapsulation with an antiadhesive soap layer in between. A second photolithography step was used to pattern the electrode active area with the use of AZ 9260 photoresist and development in AZ developer. Reactive Ion Etching with O<sub>2</sub> plasma created openings in Parylene C before the PEDOT: PSS suspension was spun on the device. A final peel-off step defined the conducting material-covered electrode area by the removal of the second sacrificial Parylene C layer. The devices were hard baked for 60 minutes at 140° C and immersed in bidistilled water overnight for the removal of any low molecular weight compounds of the PEDOT:PSS dispersion. The PEDOT: PSS formulation used is as follows: 38 mL of PEDOT:PSS aqueous dispersion (Clevios PH -1000) were mixed with 2 mL of ethylene glycol (for conductivity enhancement), 50 µL of 4- dodecylbenzenesulfonic acid (DBSA) that helps the film formation and 0,4 mL of 3- methacryloxypropyltrimethoxysilane (GOPS) which is a surface adhesion promoter and a polymer cross-linking agent that enhance film stability in aqueous environments. Commercial devices were obtained from Multichannel Systems (Tübingen, Germany).

**Islet isolation and cell culture:** Islet cells were obtained from mice as published.<sup>[7, 16]</sup> Before cell culturing the devices were plasma treated for 2 minutes to render them hydrophilic (the plasma treatment was 9.82 W/L-27.5 W in a 2.8 L chamber) as described <sup>[5b]</sup> and islets seeded as described <sup>[4]</sup>. Human islets were isolated from non-diabetic donors at the Cell Isolation and Transplantation Center (Geneva University Hospital) and handled as described. <sup>[4]</sup>

**Device characterization and electrophysiological recordings:** Devices were characterized with a potentiostat (Autolab PGSSTAT128N) in a three electrode configuration in 0.1 M NaCl solution. The PEDOT:PSS covered electrodes served as the working electrode while a Pt and Ag/AgCl electrode were used as counter and reference electrode, respectively. Measurements were performed with an INTAN RHD2132 32-channels amplifier chip with unipolar inputs (Intan Technologies) at a sampling rate of 10kS/s.

**Data processing and spectral analysis:** Processing was performed offline using a custom Matlab program (Mathworks, Cambridge, UK). It covers AP and SP detection, frequency and amplitude measurements and generates processed data and image files for visual control. Regarding AP detection, a band-pass Butterworth filter was used to isolate AP waveforms. Traditionally, wavelet filters are used for this purpose, since they increase the signal-to-noise ratio of the AP signal, but they also tend to modify the APs' amplitudes, which would have altered our measurements. APs were detected when the band-pass filtered signal exceeded a threshold set at 2.9 times the standard deviation of the high-pass part of the signal for each electrode. Digital blanking was used to avoid multiple detections of the same AP: subsequent detections were ignored for 75 ms. Each AP's peak-to-peak amplitude was individually measured from the filtered signal, in a 50ms window, starting 10ms before the detection. In parallel, SPs were isolated using a third-order band-pass 0.1-1Hz Butterworth filter. SPs were detected by finding their individual maxima and minima, discriminated using an amplitude tolerance of 8 µV that avoided the detection of small ripples in the filtered signal. The extrema values were stored and used to measure the peak-to-peak amplitude of each SP. Frequency measurements on both APs and SPs were performed using second order IIR filters with a time constant of 25.6 s. The total number of events

## Ch. V.- Appendices

detected here were for APs 12563 (TiN, 61 electrodes) and 4364 (PEDOT:PSS, 14 electrodes); for SPs 5286 (TiN, 59 electrodes) and 891 (PEDOT:PSS, 14 electrodes). Frequency repartition of noise was estimated by applying Fast Fourier Transforms on 600 s recordings of uncovered electrodes for both PEDOT:PSS and TiN technologies. This yielded the power spectral density of the noise in dB $\mu$ V/Hz, which indicates how noise is distributed frequencywise and consequently which portions of the biological signal are more impacted by noise.

### **Acknowledgements**

*This work was supported by grants from LABEX Amadeus, SATT Aquitaine and Curie ITN OLIMPIA. The authors D.A. Koutsouras and R. Perrier contributed equally.*

*Received:*

*Revised:*

*Published online:*

### **References**

- [1] C. Luni, E. Serena, N. Elvassore, *Curr Opin Biotechnol* **2014**, *25*, 45-50.
- [2] D. A. Melton, *Curr Top Dev Biol* **2016**, *117*, 65-73.
- [3] P. E. MacDonald, *Am J Physiol Endocrinol Metab* **2011**, *301*, E1065-1069.
- [4] F. Lebreton, A. Pirog, I. Belouah, D. Bosco, T. Berney, P. Meda, Y. Bornat, B. Catargi, S. Renaud, M. Raoux, J. Lang, *Diabetologia* **2015**, *58*, 1291-1299.
- [5] a Q. V. Nguyen, A. Caro, M. Raoux, A. Quotb, J. B. Floderer, Y. Bornat, S. Renaud, J. Lang, *Conf Proc IEEE Eng Med Biol Soc* **2013**, *2013*, 172-175;  
b E. Pedraza, A. Karajic, M. Raoux, R. Perrier, A. Pirog, F. Lebreton, S. Arbault, J. Gaitan, S. Renaud, A. Kuhn, J. Lang, *Lab Chip* **2015**, *15*, 3880-3890.
- [6] N. Rabieh, S. M. Ojovan, N. Shmoel, H. Erez, E. Maydan, M. E. Spira, *Scientific reports* **2016**, *6*, 36498.
- [7] M. Raoux, Y. Bornat, A. Quotb, B. Catargi, S. Renaud, J. Lang, *The Journal of physiology* **2012**, *590*, 1085-1091.
- [8] G. Cellot, P. Lagonegro, G. Tarabella, D. Scaini, F. Fabbri, S. Iannotta, M. Prato, G. Salviati, L. Ballerini, *Front Neurosci* **2015**, *9*, 521.
- [9] P. E. MacDonald, J. W. Joseph, P. Rorsman, *Philosophical transactions of the Royal Society of London. Series B, Biological sciences* **2005**, *360*, 2211-2225.
- [10] N. R. Johnston, R. K. Mitchell, E. Haythorne, M. P. Pessoa, F. Semplici, J. Ferrer, L. Piemonti, P. Marchetti, M. Bugliani, D. Bosco, E. Berishvili, P. Duncanson, M. Watkinson, J. Broichhagen, D. Trauner, G. A. Rutter, D. J. Hodson, *Cell Metab* **2016**, *24*, 389-401.
- [11] J. E. Campbell, D. J. Drucker, *Cell Metab* **2013**, *17*, 819-837.
- [12] P. Rorsman, M. Braun, *Annu Rev Physiol* **2013**, *75*, 155-179.
- [13] D. M. Blodgett, S. D. Redick, D. M. Harlan, *Cell Syst* **2016**, *3*, 330-332.
- [14] S. Renaud, B. Catargi, J. Lang, *IEEE pulse* **2014**, *5*, 30-34.
- [15] M. Sessolo, D. Khodagholy, J. Rivnay, F. Maddalena, M. Gleyzes, E. Steidl, B. Buisson, G. G. Malliaras, *Advanced Materials* **2013**, *25*, 2135-2139.
- [16] M. Raoux, P. Vacher, J. Papin, A. Picard, E. Kostrzewa, A. Devin, J. Gaitan, I. Limon, M. J. Kas, C. Magnan, J. Lang, *Diabetologia* **2015**, *58*, 749-757.

## 2 STUDY OF THE CYTOTOXICITY OF GENERATED ION-SENSITIVE INKS

### 2.1 INTRODUCTION

As it could be understood from the introductory section of electrophysiology methods (Chapter I), the active material in devices used for extracellular recordings configuration are in direct contact with the biological material, in our case the  $\beta$ -cells or the non-dissociated *Islets of Langerhans*. For this reason, biocompatibility between the ion-sensitive materials and this type of cells is a major requirement, demanding the absence of any interference with their metabolism by the interfacing with the inks. Accordingly, we have done cytotoxicity studies of some samples of the Ion sensitive dispersions to evaluate the morphology and state of the cells in their presence. Results of these studies are presented in this section.

### 2.2 CELL CULTURE & MORPHOLOGICAL STUDY

In the case of study presented in Figure 65, I evaluated the cytotoxicity of a PEDOT based ink containing 18-crown-6 moieties (*Ink 4* in Table 3, Chapter II). As it can be noted, growth of cells is not affected in the ink-covered coverslips (Figure 65-c). In the control (non-covered coverslip, Figure 65-a) cells present several morphologies (stars, elongated...) and there is also the beginning of tile formation by the normal growth and interaction between the cells in the culture. If we compare these results with film covered-coverslips (Figure 65-b), morphologies are comparable and growth of the cells seems not to be affected. This suggests that cells can be cultured without inconvenience on these materials and that their use as active materials for the biosensors is possible. Nevertheless, it is useful to do a more exhaustive evaluation about the state of the cells.

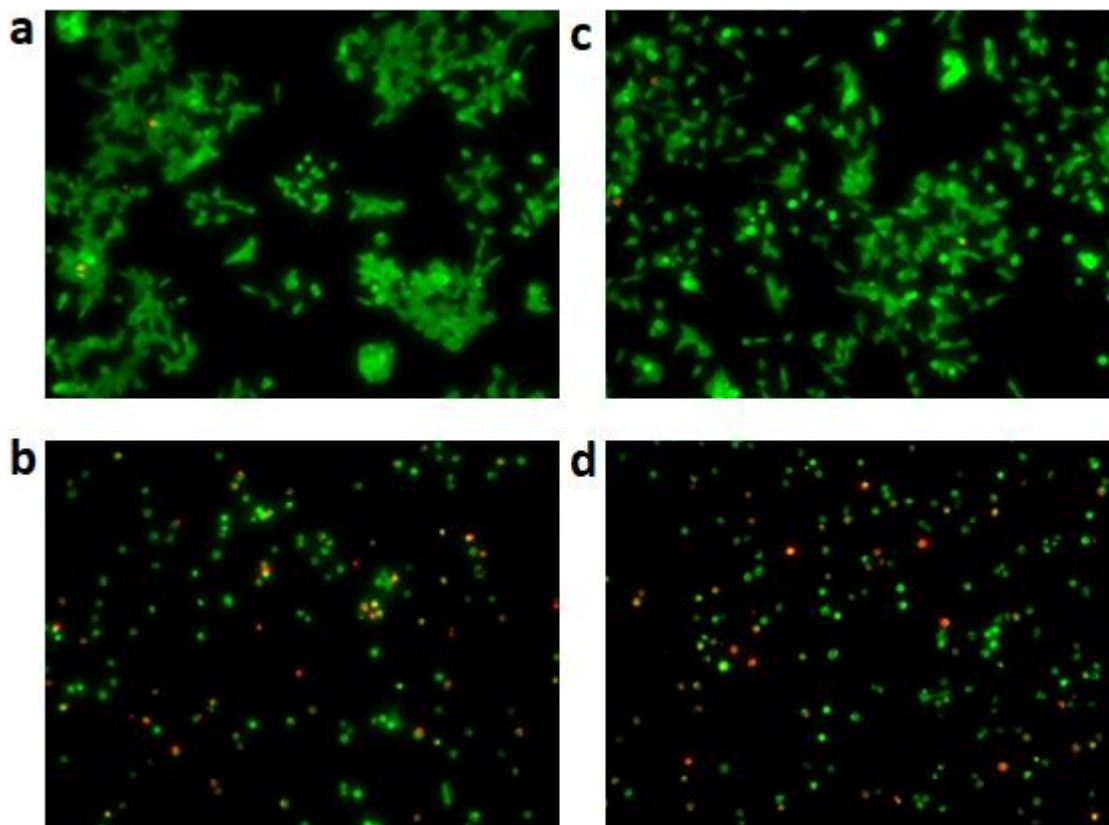


**Figure 65: Cytotoxicity study of the Ion Sensitive Inks:** Clonal  $\beta$  cells (INS832-13) were cultured for 24h on control coverslips (**a** and **b**) or coverslips covered with the studied ink (**c** and **d**) (*Ink 4* in Table 3, Chapter II). *Effect of thapsigargin* (apoptosis) was evaluated: control (**b**) vs film-covered coverslips (**d**). Merge images are presented. Experimental conditions: **Green:** FYTC filter (live cells); **Red:** YFP filter (dead cells).

### 2.3 APOPTOSIS STUDY: Live/Dead Cell Imaging and Thapsigargin effect

After observation that the morphology of the  $\beta$  cells is unchanged in presence of the polymer film, one important question remains, the evaluation of cell survival: do the cells continue to work properly and do the cells remain undamaged?

One method to evaluate this is to measure apoptosis, meaning the programmed cell death as response to a stimulus. A small rate of apoptosis is always observed during cells growth in culture medium and it is comparable in control vs film-covered coverslips

## *Ch. V.- Appendices*

(Figure 65-a and c, respectively), meaning that the cells growth is normal and mortality of cells is negligible (small percentage of “red” (dead) cells).

But does any of the films increases the rate of apoptosis? As positive control, to confirm that we detect an increase in the cellular death, thapsigargin was added. This is a non-competitive inhibitor of the sarco/endoplasmic reticulum  $\text{Ca}^{2+}$  ATPase (SERCA). The latter raises intracellular calcium concentration by blocking the ability of the cell to pump calcium into the endoplasmic reticulum, provoking the cell death.

In the case studied and presented in Figure 65 (*Ink 4* in Table 3, Chapter II), it can be noted that cell growth is as comparable in the ink-covered coverslip (Figure 65-d) to the control coverslip (Figure 65-b). Morphology reflecting the state of the cells is strongly affected when cells are cultured in presence of thapsigargin. If we compare both controls, the negative (-) in normal culture medium (Figure 65-a) and the positive (+) in thapsigargin (Figure 65-b), the clear-cut effect of the drug is apparent.

Subsequently, we quantified the ratio between alive cells (in green) and dead cells (in red). In both cases it is evident that the number of dead cells increased considerably due to the action of thapsigargin (Figure 66, a vs b). In the equivalent comparison between films-covered coverslips with/without thapsigargin (Figure 65-c/d and Figure 66-a/b, respectively), a change from an elongated or star morphology (Figure 65-c) to small round cells is apparent in the case of treatment with the inhibitor (Figure 65-d).

## Ch. V.- Appendices

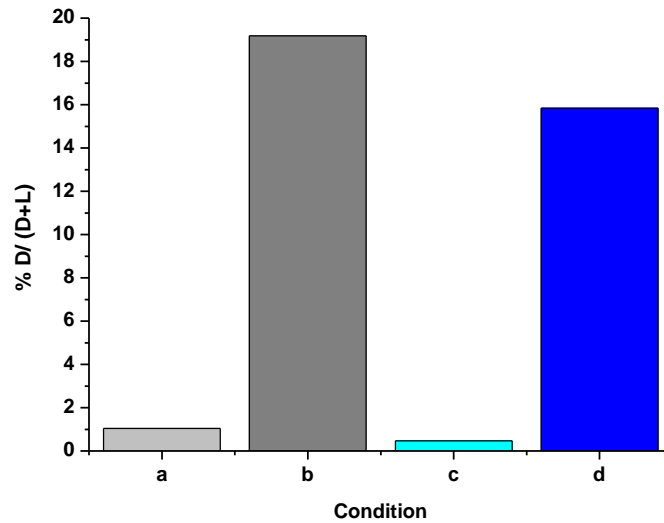


**Figure 66: Quantification of apoptosis effect by inks and exposure to thapsigargin:** Cells cultured on coverslips (CS): **a)** Non-covered CS in medium culture (- control) in light grey; **b)** Non-covered CS under *thapsigargin* effect (+ control) in dark grey; **c)** Film-covered CS in culture medium in light blue; **d)** Film-covered CS under *thapsigargin* effect in marine blue.

In addition, the quantification of the ratio dead/ total (dead + alive) cells grown on ink is comparable to the one in control conditions (Figure 66, a vs c in normal conditions, and b vs d under thapsigargin effect). This suggest that an unchanged growth of  $\beta$  cells on films-covered coverslips. The think therefore does not exert a cytotoxic effect under the conditions tested.

### 3 I/V CONVERSION CARD: an OECT recording system adapted to $\beta$ -cell

#### 3.1 INTRODUCTION

As already introduced, the characteristic signals of the *Islets of Langerhans* are slow field potentials (SP) due to the multicellular activity and fast action potentials (AP) in response to glucose and other stimulus. To improve detection of AP, PEDOT: PSS covered MEA recordings demonstrated a better recording of both signals in comparison with traditional materials[37]. Nevertheless, still the S/N is not really suitable for the discrimination of AP from SP before the tedious signal treatment and analysis. For that reason, the objective was to use for the first time OECTs based on classical PEDOT: PSS to record with higher S/N ratio the electrical activity of  $\beta$ -cells. As amplifiers and circuits used in classical electrophysiology are not compatible with this new approach, and moreover, neither any commercial solution is available and only one experimental setup has been published (without details), the circuit properties had to be established and a corresponding card had to be designed for the OECTs. In collaboration with the EliBio team of IMS (University of Bordeaux), we fabricated an I/V conversion card. Preliminary tests and simulation of cellular activity were done and are presented in this section.

#### 3.2 I/V CONVERSION CARD: Installation and Testing

A current to voltage conversion card (I/V) was fabricated to couple the output signals of the transistors (in current) with the electrophysiological components, like amplifiers (reading signals in voltage). Firstly, the connections of the circuit between the conversion card and the OECT array were tested recording the physical characteristics ( $V_{DS}$  and  $V_{GS}$ ) and the working conditions were chosen to obtain the maximal transconductance (blue curve in Figure 67).

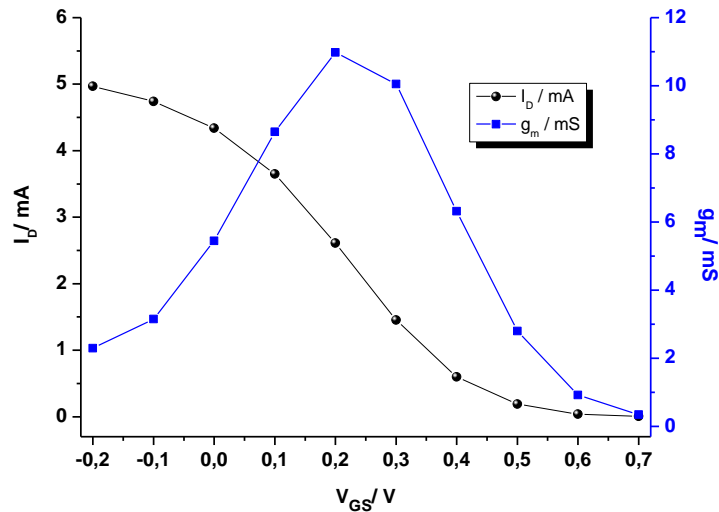


**Figure 67: Physical characterization of a classical PEDOT:PSS vertical OECT[112]:** Transfer curve (black spheres) and transconductance curve (blue squares).

Once characteristic curves were obtained, the cellular behaviour was simulated with the same conversion set-up, but in a modified configuration incorporating filters and a low-frequencies generator on the gate electrode to obtain an oscillatory output signal. An illustration is presented in Figure 68.

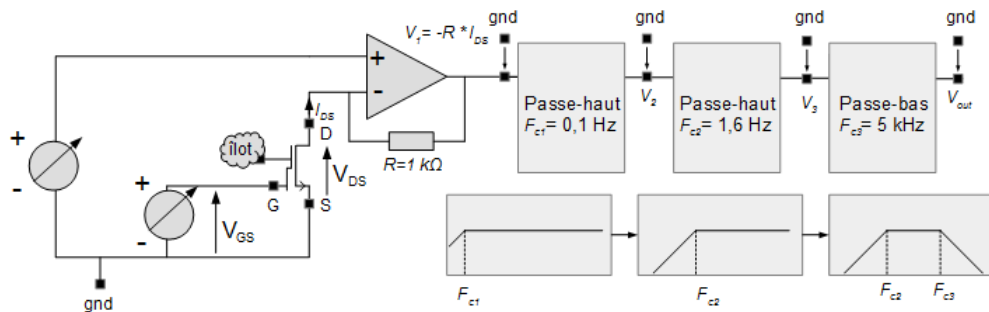


**Figure 68: Scheme of I/V conversion card on the cell activity simulation configuration:** Three filters (2 highpass, HP, and 1 lowpass, LP) are incorporated to the basic configuration presented in Annex 12.

Signals obtained are oscillatory voltage variations reflecting the sinusoidal signals applied on the gate of 200 mV of amplitude (peak to peak). It can be noted from Figure 69 that

## Ch. V.- Appendices

the first filter (HP<sub>1</sub>-F,  $f_c = 0.1$  Hz, yellow curve) removes the offset, the second one (HP<sub>2</sub>-F,  $f_c = 700$  Hz, green curve) removes the high frequency signals, but increases the recording noise and the last filter (BP-F,  $f_c = 5$  KHz, pink curve) reduced this undesired noise for high frequencies. This simulation is a preliminary proof of concept that this system (which could be replicated n times taking into account the number of transistors per device) could allow us to record the electrical activity of  $\beta$  cells cultured on the top of OECT arrays. This part of the project is currently under progress.

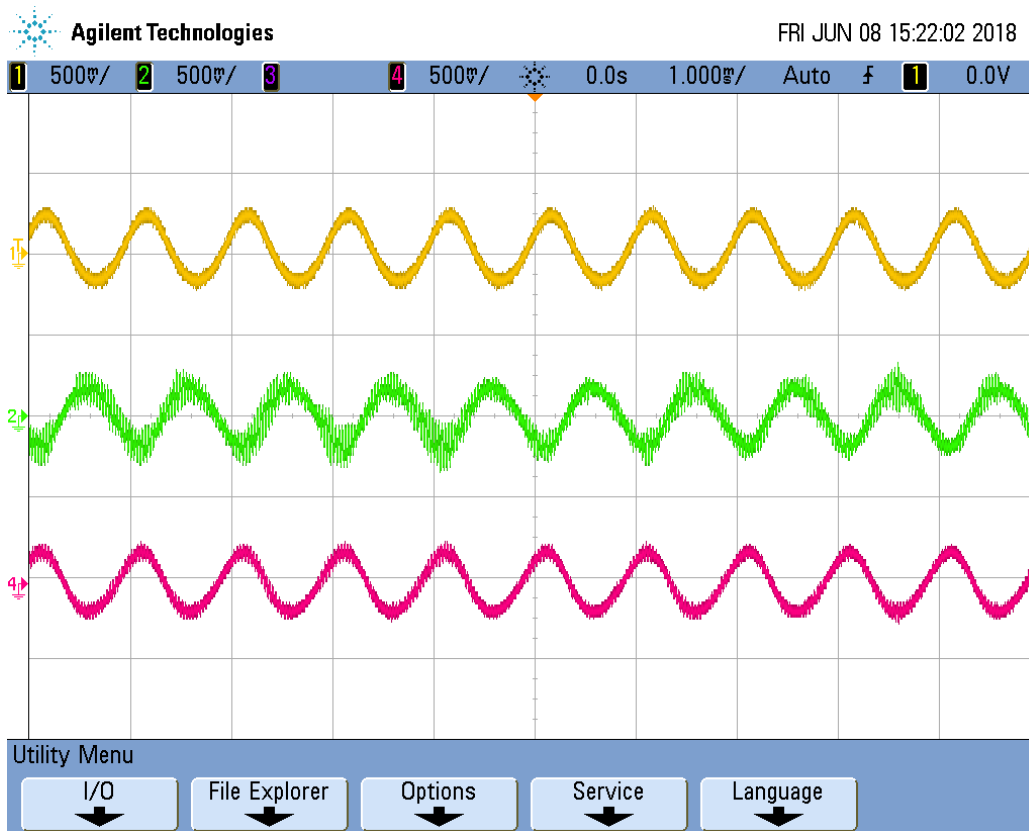


**Figure 69: Illustration of the sinusoidal signals obtained from the electrical activity simulation:** Signal corresponding to a sinusoidal stimulation on gate at a frequency of 1000Hz. Yellow (top curve): Signal corresponding to V<sub>2</sub> in Figure 68, obtained after passing raw signal by the first HP<sub>1</sub>-F; Green (middle curve): Signal corresponding to V<sub>3</sub> in Figure 68, obtained after passing by the second HP<sub>2</sub>-F; Pink (bottom curve): Signal corresponding to V<sub>OUT</sub> in Figure 68, obtained after passing by the last filter LP-F.

## 4 ION-SENSITIVE OECT

### 4.1 INTRODUCTION

The final objective of the overall project within this PhD thesis is the modification of the active material and their integration into OECT devices. Analysis of the ability of the developed materials to act as mixed conductors and physical characterization of these fabricated devices was the first goal. Evaluation of the ion sensitivity and of the changes in the physical properties of the fabricated devices due the chelate modifications introduced in these polymers was the secondary objective. This was carried out through characterization with a variety of electrolyte ion compositions and the results are presented in this section.

### 4.2 INTEGRATION OF THE ION-SENSITIVE INKS ON OECT

The microfabrication process of ion-sensitive OECT (IS-OECT) was based on methods previously reported [37,89] and is detailed in the experimental part. A summary list of the fabricated devices is presented in Table 7. Devices were fabricated at Ecole de Mines de Saint Etienne (EMSE) at Gardanne under the supervision of Dr. M. J. Donahue and according to a layout developed by Dr. Donahue.

**Table 7: Summary of OECT arrays fabricated with the Ion-sensitive inks (IS-OECTs):** OECTs fabricated with inks containing 15-crown-5 (samples 1-2, orange), 18-crown-6 (samples 3-6, blue) and DPA (samples 7-8, green) moieties. Control: Devices based on inks with PSTFSI as polyelectrolyte were also fabricated (samples 9-10, grey).

| sample | #Ink used | $\rho_{V=0} / \Omega$<br>(10um/100 um) |
|--------|-----------|--|
| 1      | ①         | 2000                                   |
| 2      | ②         | 1900                                   |
| 3      | ③         | 150                                    |
| 4      | ④         | 600                                    |
| 5      | ⑤         | 0                                      |
| 6      | ⑥         | 260                                    |
| 7      | ⑦         | 2000                                   |
| 8      | ⑧         | 0                                      |
| 9      | ⑨         | 116                                    |
| 10     | ⑩         | 140                                    |

## Ch. V.- Appendices

For most of the inks, the fabricated devices were functional and their electrical characteristics could be evaluated. It is important to note that, as expected, the characterization of the device based on ink (8) was not possible due to the absence of electrical conductivity. This fact could be explained for the low dispersion of the monomer (8) during the aqueous polymerization. However, the same happened with Ink (5), which was more surprising taking into account the several electrochemical characterizations previously done with this ink, presenting even one of the higher conductivities (Chapter II, Table 3). Thus, it would be necessary to carry out a more exhaustive and thorough fabrication and testing of devices with these inks to validate these observations.

Every device is constituted by twelve OECTs, separated into two groups of six on two sides, left (L) and right (R). Each side contains six OECTs with three different channel dimensions:  $10\mu\text{m}\times 10\mu\text{m}$  (2),  $100\mu\text{m}\times 10\mu\text{m}$  (2) and  $50\mu\text{m}\times 50\mu\text{m}$  (2). As an example, a microscope image of a microfabricated OECT channel is shown in Figure 70.

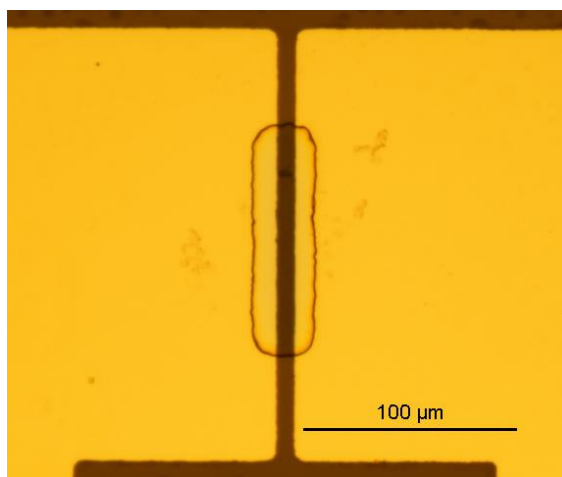


**Figure 70: Micrograph of micro-fabricated IS-OECT with Ink 3**, containing 18-crown-6 moieties (see Table 3 in Chapter II and Table 7). A film of PaC coats the entire surface with the exception of the channel area where the ink was deposited (rectangle of  $100\mu\text{m}\times 10\mu\text{m}$  between the gold electrodes, source and drain).

Electrical characterization and a comparative study between the different ion-sensitive OECT fabricated was done on the transistors with channel dimensions  $100\ \mu\text{m} \times 10\ \mu\text{m}$  and is presented in next section. The approximate thickness of the film forming the channel of the devices is estimated to  $100\ \text{nm}$ , extracted for previous thickness measurements done in the deposition and lithography fabrication method for referent PEDOT:PSS ink. Nevertheless, it was not measure in the IS devices to avoid the deterioration of the device previous to the electrical characterization.

### **4.3 ELECTRICAL CHARACTERIZATION AND ION SENSITIVITY STUDY**

After the electrochemical impedance characterization and biocompatibility study of the ion-sensitive inks synthesized during my PhD, the fabricated IS-OECT arrays were electrically characterized and their ion-sensitivity behaviour was studied.

As an example, the output characteristics of the transistor presented in Figure 70 based on *Ink 3* show the decreasing of the drain current with the increase of the gate voltage (Figure 71-a). In addition, the transfer curve ( $V_{DS} = -0.4\ \text{V}$ ) and the resulting transconductance of the OECT are given in Figure 71-b. The transfer curve (black) reflects the typical profile for depletion operation, where application of positive gate bias causes cations to enter the channel, decreasing hole density and reducing the drain current. The transconductance reaches its highest value around zero gate bias, meaning that the OECT can be used with the gate electrode directly connected with the source[113]. The maximal transconductance is  $1.8\ \text{mS}$ , a very good value for a thin film transistor.

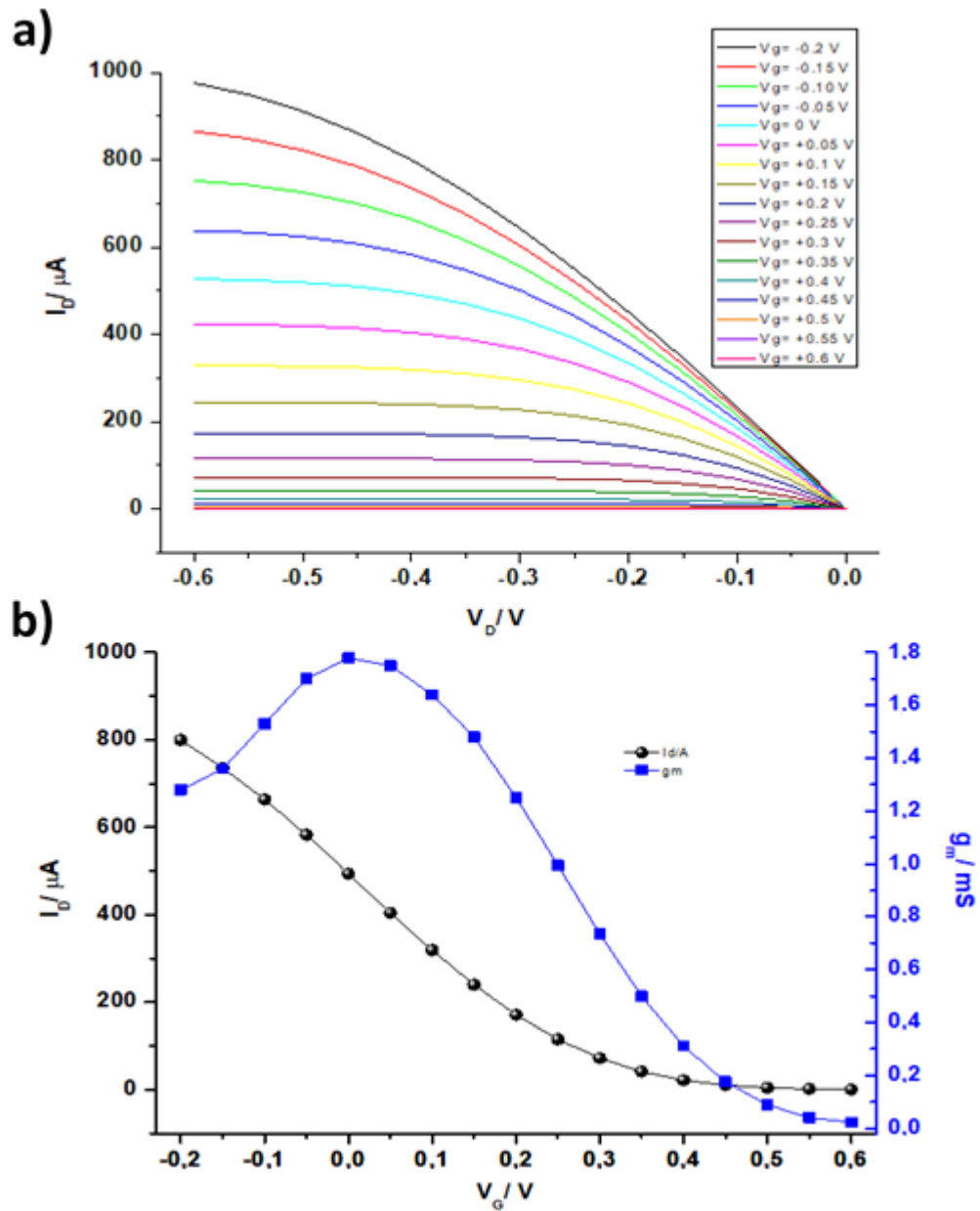


**Figure 71: Electrical characterization of IS-OECT fabricated with Ink 3: a)** Output characterization; **b)** Transfer curve at  $V_{DS}=-0.4\text{V}$  (black curve) and corresponding transconductance (blue curve). The device dimensions are  $W=10\ \mu\text{m}$ ,  $L=100\ \mu\text{m}$  and film thickness  $t=100\text{nm}$ .

## Ch. V.- Appendices

To determine the ion-sensitivity of the different materials in the OECT configuration, electrical characterization of all the 100  $\mu\text{m}$  x 10  $\mu\text{m}$  transistors was systematically done in different electrolyte conditions with 0.01 M solutions of NaCl, KCl and/or ZnCl<sub>2</sub>.

A summary of the transconductance obtained from the transfer curves of the different devices is shown in Table 8.

**Table 8: Summary of the Transconductance of the IS-OECTs devices:** Characterization was done with 0.01 M NaCl, KCl and/or ZnCl<sub>2</sub> aqueous electrolytes. Inks with 15-crown-5 moieties (orange), 18-crown-6 moieties (blue) or DPA moieties (green). Ctrl: Ink based on PSTFSI. OECT: 4 transistors per device: 2 channels (Top and Bottom) per side (left, L, and right, R) (\*) Value in mS instead of  $\mu\text{S}$ .

| sample | Ink | OECT (Channel) | $(g_m)_{\max} / \mu\text{S}$ |                |                  |  |
|--------|-----|----------------|------------------------------|----------------|------------------|--|
|        |     |                | Na <sup>+</sup>              | K <sup>+</sup> | Zn <sup>+2</sup> |  |
| 1      | ①   | L              | Top                          | 29.0 (*)       | 61.5 (*)         |  |
|        |     |                | Bottom                       | -              | 40.4 (*)         |  |
|        |     | R              | Top                          | -              | -                |  |
|        |     |                | Bottom                       | -              | -                |  |
| 2      | ②   | L              | Top                          | 35.4           | 29.3             |  |
|        |     |                | Bottom                       | 10.9           | 9.9              |  |
|        |     | R              | Top                          | 64.3           | 71.6             |  |
|        |     |                | Bottom                       | 63.2           | 64.8             |  |
| 3      | ③   | L              | Top                          | -              | 1.5 (*)          |  |
|        |     |                | Bottom                       | -              | 1.6 (*)          |  |
|        |     | R              | Top                          | 617.5          | 176.4            |  |
|        |     |                | Bottom                       | 1.8 (*)        | 1.0 (*)          |  |
| 4      | ④   | L              | Top                          | 56.2           | -                |  |
|        |     |                | Bottom                       | 704.3          | 643.4            |  |
|        |     | R              | Top                          | 101.2          | 109.8            |  |
|        |     |                | Bottom                       | 67.0           | 65.9             |  |
| 5      | ⑥   | L              | Top                          | 1.2 (*)        | 1.3 (*)          |  |
|        |     |                | Bottom                       | 318.7          | 210.3            |  |
|        |     | R              | Top                          | -              | -                |  |
|        |     |                | Bottom                       | 1.7 (*)        | 798.0            |  |
| 6      | ⑦   | L              | Top                          | 87.3           | 67.9             |  |
|        |     |                | Bottom                       | 124.5          | 115.9            |  |
|        |     | R              | Top                          | 77.6           | 82.6             |  |
|        |     |                | Bottom                       | 86.8           | 92.5             |  |
| 7      | ⑨   | L              | Top                          | 2.5 (*)        | 2.5 (*)          |  |
|        |     |                | Bottom                       | 2.5 (*)        | 2.6 (*)          |  |
|        |     | R              | Top                          | 1.9 (*)        | 1.8 (*)          |  |
|        |     |                | Bottom                       | 1.8 (*)        | 1.6 (*)          |  |

## Ch. V.- Appendices

We can notice that the transconductances ( $g_m$ ) values obtained depend on the ink composition. The more the chelate content (crown ether or DPA) is increased, the lower is the conductivity, and the transconductance subsequently decreases. For example, we observed similar  $g_m$  values in the mS range for a 5% wt. content on 18-crown-6 (sample 3) and in devices based on PSTFSI inks (sample 9). Whilst, the increase content of chelates in the polyelectrolytes structures is at the origin of lower electrical conductivities, and subsequently lower orders of magnitude of transconductance (samples 2, 4 and 7). There are some exceptions, presenting even a much higher transconductance than reference (sample 1, based on a 20% of 15-crown-5 moieties contain polyelectrolyte, *ink 1*).

The evaluation of the ion-sensitivity of the different materials in the OECT configuration, allows to make the following observations:

On the one hand, the control devices with PSTFSI electrolytes, without chelate moieties, present no significant cation distinction (sample 9). On the other, an increase of chelate content does not seem to have an important impact in the maximal value of transconductance, obtaining not a large variation on the  $(g_m)_{\max}$  when characterized with no matter which cation (the target cation or any of the competitor ions).

However, considering that the transconductance gives information about the maximum change in current when a change in voltage is applied, *equation 2*:

$$g_m = \frac{\partial I_D}{\partial V_G} \quad \text{Equation 2}$$

A linear regression could fit the linear regime of the transfer curve (see black curve in Figure 71-b); it means, in the decreased of current when the applied gate voltage is swept around 0 V ( $V_G = [-0.1V, 0,1 V]$ ). The slopes related to this regression obtained from the

## Ch. V.- Appendices

characterisation with each electrolyte give us information about the influence of the cation nature on the transconductance, and thus the influence on the working properties of the transistor.

Table 9 presents a correlation summary of the slope values obtained for the evaluated devices. It was chosen at least one device with the ink designed to target the cations of interest and with the characterization performed in all the comparative conditions. For example, the device fabricated with the ink based on  $Zn^{2+}$  sensitive moieties, *DPA*, was evaluated with  $Zn^{2+}$  (target cation, A) and with sodium (alternative cation, B, called “competitor”). The same procedure was followed for the other inks: Inks targeting  $K^+$ , which contain *18-crown-6 moieties*, was evaluated with  $K^+$  (cation A) and also with  $Na^+$  (cation B); for the *15-crown-5* ink, the same cations were used being  $Na^+$  the targeted cation (Cation A) and  $K^+$  (cation B). It was traced the transfer curves (example in Figure 71, black curve) for all the devices and conditions. Furthermore, a ratio has been calculated between the slopes fits to the linear regime of the curve (transconductance) which were obtained when the transistors were characterized with the different cations.

**Table 9:** Summary of ratios of  $g_m$  obtained by linear regression fitting applied to transfer curves.

| Inks target<br>(%Sensing Moiety) | Sample | Cation        | A: target cation<br>B: competitor |            |
|----------------------------------|--------|---------------|-----------------------------------|------------|
|                                  |        |               | b (slope)                         | ratio A/ B |
| $Zn^{2+}$                        | 7      | $Zn^{2+}$ (A) | -5.25E-08                         | <b>0.9</b> |
|                                  |        | $Na^+$ (B)    | -6.16E-08                         |            |
| $Na^+$                           | 2      | $Na^+$ (A)    | -1.05E-08                         | <b>1.1</b> |
|                                  |        | $K^+$ (B)     | -9.27E-09                         |            |
| $K^+$ (15%)                      | 4      | $K^+$ (A)     | -1.09E-07                         | <b>1.9</b> |
|                                  |        | $Na^+$ (B)    | -5.60E-08                         |            |
| $K^+$ (5%)                       | 6      | $K^+$ (A)     | -7.40E-07                         | <b>0.5</b> |
|                                  |        | $Na^+$ (B)    | -1.64E-06                         |            |
| Ctrl (PSTFSI)                    | 9      | $Na^+$ (A)    | -2.45E-06                         | <b>1.0</b> |
|                                  |        | $K^+$ (B)     | -2.57E-06                         |            |

## *Ch. V.- Appendices*

These results suggest that the increase in 18-crown-6 ether content (from 5% to 15%, samples 6 and 4, respectively) produces a larger change in the transconductance that could be related to an enlarged sensitivity of the device to the target potassium cation ( $K_{K^+}/K_{Na^+}$  change from 0.5 vs 1.9). In the case of sodium (sample 2), sensitivity seems to be similar to the control. This is not surprising considering the low discriminative power which the starting 15-crown-5 functionalized monomer [1] demonstrated for both cations (NMR titration, Chapter II). In the case of DPA, the small “preference” for sodium cation instead of zinc (sample 7), may be explained by the restricted mobility of the pycolyl moieties when present in the cross-linked polymer network. It is likely the smaller cation could have better accessibility to the binding sites, which could explain this result. Depth bulky structural studies should be performed on these thin films to confirm this hypothesis. Thus, a more exhaustive study and optimization of the composition (content in ion-sensitive scavengers) to obtain the target ion – sensitivity in device (OECT) is required.



## 5 CONCLUSION

In this chapter has been presented a summary on the advances done during my PhD project in different aspects towards the  $\beta$ -cells recordings with OECT challenge. Firstly, does *PEDOT*, the normal *PEDOT:PSS*, works to extracellularly record the  $\beta$ -cells activity? The answer was yes, but first promising results bring us to do some characterisations in impedance and capacitance studies to validate the results obtained. We have demonstrated that the increase of the *S/N* was clearly due to the presence of the conductive polymer layer, subsequently, allowing an improved detection of the low amplitude characteristic signals.

Secondly, even if MEAs are really standardized and have been really interesting to have a bigger knowledge on metabolic mechanisms on  $\beta$ -cells, the main challenge is the detection of the signals of interest with a better *S/N*. For this reason, we have oriented to OECT. By one side its amplification power looks very promising for the biosensing, but in the other, these technology remains still very challenging to record, in the case of  $\beta$  cells, signals of low and high frequency at the same time. Thus, the first step in this approach, has been the design, testing and improvement of an adapted I/V translation card in collaboration with partners at IMS (University of Bordeaux). Preliminary results of detection of simulated signals are very promising for the detection of  $\beta$  cells signals. This route continues under progress through the national research agency (ANR) funding.

Finally, test of the alternative materials synthesized were performed. Having in mind the interfacing of  $\beta$  cells with the polymer inks, cell viability was evaluated by a Live/Dead assay. The quantification of the ratio between dead / total cells (dead + alive) grown on ink films was comparable to the one in control conditions, suggesting an unchanged growth of  $\beta$  cells on the films-covered coverslips. It means that the polymer material does not exert a major cytotoxic effect under the conditions tested. *But have the materials*

## *Ch. V.- Appendices*

*synthesized the ion-sensitivity expected?* To reply to this question, integration of some of the inks into OECT devices was performed by microfabrication at EMSE (Gardanne, under the supervision of Dr. Donahue and Pr. O'Connor). 80% of the fabricated devices were working and had similar characteristics than traditional mixed conductors' materials. With respect to the ion sensitivity, the electrical characterization of these IS- OECT were done in different ion electrolytes. It was observed, as promising result, that the increase in 18-crown-6 ether content (from 5% to 15%) brings a larger change in the transconductance. This could be related to an enlarged sensitivity of the device to the target potassium cation ( $K_{K^+}/K_{Na^+}$  change from 0.5 vs 1.9). Nevertheless, these are very preliminary results and statistically study and formulation of the materials in function of the results obtained is needed.

## **6 EXPERIMENTAL PART**

### **6.1 Impedance and Capacitance characterization of MEA**

The working and counter electrodes were electrically contacted with metallic needles and were used to position needles on the electrode. Impedance and capacitance measurements were measured using dielectric interface (model 1296, Solartron, UK) connected to a frequency response analyzer (model SI 1260, Solartron, UK) and data were collected in the frequency range of  $10^5$  to  $10^{-1}$  Hz. Impedance and Capacitance measurements were conducted by mounting microelectrodes arrays (MEAs) on a two electrode stage connected to the Solartron. An Ag/AgCl electrode submerged into the aqueous electrolyte (0.1mM NaCl) was used as reference electrode in the fabricated Au-MEA and Pedot:Au-MEA. On the commercial TiN-MEA (MCS, Germany) a TiN electrode (E15) was used as the reference electrode.

### **6.2 Cytotoxicity Evaluation: Apoptosis test-Thapsigargin effect**

Apoptosis studies (evaluation of the programmed cell's death in response to a stimulus) and the effect of Thapsigargin have been performed by the use of a LIVE/DEAD Kit (ThermoFisher Scientific, USA). This is a sensitive two-colour fluorescence cell viability assay that allows discrimination between live and dead cells with two probes that measure established parameters of cytotoxicity and cell viability—intracellular esterase activity and plasma membrane integrity. Deposition of polymer films (with the different ion-sensitive inks) was done on coverslips (CS, d=18 mm). Previous to use, they were washed (by sonication on acetone, ethanol and isopropanol baths), dried (with air flux) and activated (Surface Plasma cleaning, 15min). Film formation was done by spin-coating of the ink (previously formulated) at the optimal speed to obtain a maximal film coverage (generally a first slow step, 30 s at 500-800 rpm, followed by a faster cycle, 1200-1800 rpm). Curing was done at 50°C for 10 min to finish by a 120°C cooking for one hour in total. After cooling, films were placed in a 12 well slab and used for the following biological procedure. Previously to the cell cultured, the coverslips slab was sterilized by

## *Ch. V.- Appendices*

UV treatment ( $\lambda=254$  nm, 30 min). Then, every coverslip was rinsed with a PBS+/+ buffer (1.5 mL/ well) and they were kept drying overnight. 50,000 cells/CV were cultured and kept until adhesion for 3 days under incubation. Thapsigargin (0.1  $\mu$ M) was added in the INS culture medium and added in the CV where the thapsigargin effect wanted to be observed. In coverslips where this effect didn't want to be evaluated, replacement of culture medium was done. Cell observations were often done (2, 6, 12, 24h). Live/Dead Cell Kit Imaging was used after de-freeze (Datasheet presented in Annexe X). Working solution was prepared by transfer of Live green (1 mL) into the Dead Red (1  $\mu$ L lyophilized). 150  $\mu$ L/coverslip were added and after 15 min of incubation, cells were observed under the microscope.

### **6.3 OECT CHARACTERIZATION AND TRANSLATION**

#### **6.3.1 OECT Characterization**

OECT arrays with four sections and twelve channels (transistors) per side were used for the development of the translation I/V set-up. Previous and after experiments, the electrical characterization of the devices was done to evaluate the state of the transistors. A Keithley 2450 dual source-meter (Tektronics, USA) commanded by a personal computer through a customized LabView VI (National Instruments, USA). The window of voltage applied to bias the devices immersed in an aqueous electrolyte was optimized to record the maximum of transconductance. Generally, sweeping  $V_{GS} = [-0.2, 0.6]$  V keeping constant  $V_{DS} = -0.1$  V for the transfer curve, while sweeping  $V_{DS} = [0, -0.4]$  V and  $V_{GS} = [-0.1, 0.8]$  V for the output curves. Physical characterization curves were traced using Origin software.

#### **6.3.2 I/V Conversion card (in coll. with IMS, University of Bordeaux)**

The equivalent electrical circuit is illustrated in Annex 12. Electrical scheme, designed with Multisim (NI, US), and fabrication of the card was done by collaborators of my host laboratory, CBMN, at IMS (University of Bordeaux). Testing of the card and circuit

connection with the devices were done by the monitoring of the physical characteristics (output and transfer curves) to determine the better bias drain-source and gate voltage to obtain the higher transconductance for different transistors on the device. Test in one by one OECT was done, controlling firstly the connections, grounding the source and connecting the OECT to the non-inverting entry to the OAP (Scheme of the set-up in Figure 72). Oscillatory output signals were done with the same set-up integrating a first band filter with a cut-off frequency of 0.1 Hz to remove the offset, a second high-pass filter cutting at 700 Hz (to remove the slow waves if necessary) and a low-pass cutting at 5 KHz to reduce the noise. A sinusoidal signal with amplitude of 200 mV (peak to peak) with offset and frequency changing from 0.1 Hz to 10 KHz was applied on the gate voltage between each filter and the output was observed through an oscilloscope.

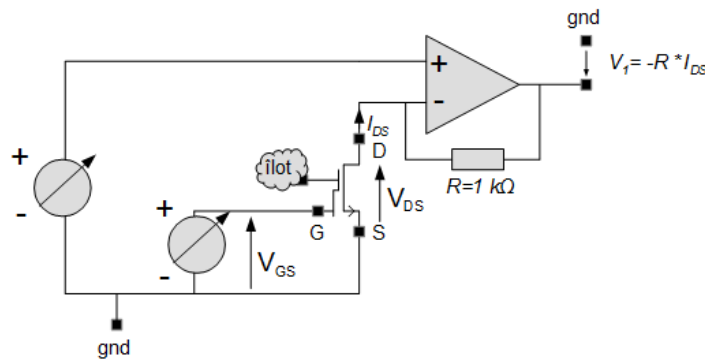


Figure 72: Scheme of the OECT- I/V card connections

## 6.4 OECT DEVICES FABRICATION

### 6.4.1 "Homemade" OECT

Preliminary tests were done at LCPO (University of Bordeaux) following standard methods. Metal interconnects were patterned by thermal evaporation (ME400B evaporator, PLASSYS, France) of gold ( $t=120$  nm) on glass substrates using metallic masks to define the channel geometry. After standard cleaning and plasma activation of the surface, masked of the gold contacts was done by covering with polyimide adhesive film (Kapton, Dupont, USA). The channel formation was done by spin-coating deposition of

## Ch. V.- Appendices

the formulated inks, followed by the film curing for one hour (soft baking at 50°C, followed by a stronger curing at 140°C). Separation of the different channels was done physically removing the excess of polymer present between the gold contacts. Electrical characterization of the OECT devices was done with a Keithley 2450 dual source-meter (Tektronics, USA) commanded by a personal computer through a LabView customize VI (National Instruments, USA). The window of voltage applied to bias the devices immersed in an aqueous electrolyte was optimized to record the maximum of transconductance. Generally, sweeping  $V_{GS} = [-0.2, 0.6]$  V keeping constant  $V_{DS} = -0.1$  V for the transfer curve, while sweeping  $V_{DS} = [0, -0.4]$  V and  $V_{GS} = [-0.1, 0.8]$  V for the output curves. Physical characterization curves were traced using Origin software.

### 6.4.2 OECT arrays

The fabrication process was done in collaboration with our partners at EMSE (Gardanne, France) based on methods reported previously [37]. Metal interconnects were photolithographically patterned on glass microscope slides using a positive photoresist (Shipley 1813), a SUSS MJB4 UV broadband contact aligner and MF26 developer [112]. A 2 nm chromium adhesion promoting layer and 100 nm of gold were thermally evaporated onto the substrates and interconnects were then defined through lift-off. Insulating and sacrificial layer PaC film were subsequently deposited, both to thicknesses of 2  $\mu\text{m}$ . Prior to the sacrificial PaC layer, a dilute solution of Micro-90 industrial cleaner was spin-coated onto the insulating PaC. This allowed the sacrificial layer to later be peeled from the substrate, defining the OECT channel. The PaC layers were etched by reactive ion etching (Oxford 80 Plasmalab plus, ClassOne equipment, USA) with  $\text{O}_2/\text{CHF}_3$  plasma to open contact pads and to create an opening down to the source/drain electrodes. AZ9260 photoresist was utilized as an etch mask, using the UV contact aligner and AZ developer to pattern (MicroChemicals GmbH, Germany). A dispersion of PEDOT:PSS (Clevios PH1000, Heraeus Holding GmbH, Germany), 5 vol% ethylene glycol, 0.1 vol% dodecyl benzene sulfonic acid and 1% wt% of 3-(glycidylxypropyl)-trimethoxysilane was spin-

## *Ch. V.- Appendices*

coated onto the substrates to attain a thickness of 70-180 nm, creating the transistor channel area. For the planar ion-sensitive OECT (IS-OECT), the formulation used of the ink was the same than for PEDOT:PSS, but spin coating speed was slowed down to optimize the film formation (speed rates:  $v_1=500$  rpm,  $v_2=1200$  rpm). The sacrificial PaC layer was peeled off removing superfluous ink and defining the OECT channels. The devices were baked for 1h at 140°C to crosslink the film. Finally, the devices were immersed in deionized water to remove low molecular weight compounds.

*OECT characterization:* All the transistors of the OECT arrays were electrically characterized in 0.1 M NaCl aqueous solution (if other, electrolyte composition is indicated) with an Ag/AgCl pellet (Warner Instruments, USA) gate electrode. A PXIe-4145 source-meter (PXIe-1062Q system, National Instruments, USA) was used along with custom LabVIEW software to carry out steady-state and transient measurements. This provided OECT output (sweeping the drain-source bias,  $V_D$ , from 0 to -0.6 V and stepping the gate-source bias,  $V_G$ , from -0.2 to 0.6 V) and transfer (sweeping  $V_G$  from -0.2 to 0.6 V with  $V_D = -0.6$  V) characteristics.

## 7 BIBLIOGRAPHY

110. Pedraza, E.; Karajić, A.; Raoux, M.; Perrier, R.; Pirog, A.; Lebreton, F.; Arbault, S.; Gaitan, J.; Renaud, S.; Kuhn, A.; et al. Guiding pancreatic beta cells to target electrodes in a whole-cell biosensor for diabetes. *Lab. Chip* **2015**, *15*, 3880–3890.
111. Perrier, R.; Pirog, A.; Jaffredo, M.; Gaitan, J.; Catargi, B.; Renaud, S.; Raoux, M.; Lang, J. Bioelectronic organ-based sensor for microfluidic real-time analysis of the demand in insulin. *Biosens. Bioelectron.* **2018**, *117*, 253–259.
112. Donahue, M.J.; Williamson, A.; Strakosas, X.; Friedlein, J.T.; McLeod, R.R.; Gleskova, H.; Malliaras, G.G. High-Performance Vertical Organic Electrochemical Transistors. *Adv. Mater.* **2018**, *30*, 1705031.
113. Rivnay, J.; Leleux, P.; Sessolo, M.; Khodagholy, D.; Hervé, T.; Fiocchi, M.; Malliaras, G.G. Organic Electrochemical Transistors with Maximum Transconductance at Zero Gate Bias. *Adv. Mater.* **2013**, *25*, 7010–7014.

## ***-General Conclusion & Perspectives-***

In this work, a two track approach of chelates functionalized materials was developed to gain new active components to constitute the channel of OECT devices and interface with pancreatic  $\beta$  cells for electrophysiological recordings. Structural-properties relationship of these materials was presented and discussed along the thesis.

In **Chapter I** were reviewed some fundamental notions of electrophysiology and the role of pancreatic  $\beta$ -cells in diabetes, a brief summary of current methods used to monitor and treat this disease. Moreover, description of the most important classes of materials developed in conducting polymers as well as in the supramolecular chemistry fields during last decades was overviewed, to come to our general strategy applying the combination of these materials to integrate into sensing devices.

The development of a first route was presented in **Chapter II**, performing the synthesis of functionalized styrene derivatives monomers and subsequent polyelectrolytes, used as stabilisers for the chemical oxidative polymerization of EDOT in water dispersions to obtain different inks containing the ion-sensitive groups. The structural and ion-sensitivity of these materials was evaluated and preliminary results show that some of these materials preserve the advantages of traditional PEDOT:PSS inks, presenting even a higher volumetric capacitance, and possess an ion-sensitivity towards the targeted cation due to the chelating groups incorporated in their structures

A second route of EDOT functionalization was explored in **Chapter III** where the chelating groups were directly attached to the “conductive” monomer. The structure-properties relationship study of the different monomers and electropolymerized polymers obtained from these EDOT derivatives was performed. Mainly two linking fractions between the EDOT and ion-chelating moieties were evaluated, an aniline and an ether binding,

showing a lower *charge-discharge* profile for the aniline compounds. Nevertheless, they have the advantage of presenting a characteristic peak that could be used as internal reference to detect the ion-affinity of the polymer films. Their ion-sensitivity was evaluated and it was found that these films have an alkaline affinity, but reproducibility issues were encountered with potentiodynamic or potentiometric methods. Film selectivity to target cation, in accordance to the starting monomers affinities, were put in evidence by *in situ* conductivity measurements and the formation of short oligomer chains during the polymerization of the aniline containing monomers was observed, suggesting the influence of this fraction in the autocatalytic oxidation process which could explain the variability observed with the other techniques.

**Chapter IV** is the reflection of the interdisciplinary advances done during this thesis to obtain more adapted  $\beta$ -cells recordings with the compilation of:

- The improved S/N for biological signals detection with MEA recordings due to the electrodes covering with PEDOT:PSS film.
- The design and testing of an adapted I/V translation card to couple OECT devices (output in current) with standard electrophysiological recording (input in voltage) to detect, simultaneously, fast and low frequency signals typical of pancreatic  $\beta$ -cells.
- The integration and test of the inks synthesized during this thesis into OECT devices. Preliminary results showed an enlarged relative transconductance with respect to alkaline stimulus, fact that could be related to the sensitivity of the device.

For future work, could be of great interest to do a “feedback control” loop combining the simultaneous material development and OECT performance testing to determine the most optimized material and synthesis and/or treatment method to the targeted sensing application. Moreover, more exhaustive work on structural study of the polymer films, as well as their nanostructuration, could allow to clarify the effect of the chelating groups in their functionality and ion sensing ability. To conclude, more intensive and

## *Ch. V.- Appendices*

interdisciplinary exchange is needed to gain the final  $\beta$ -cells adapted recording system, but this work is already under progress in the MULTISPOT framework.



*Chapter V.-*  
**APPENDICES**



## 1 MATERIALS AND INSTRUMENTATION

### 1.1 CHEMICALS:

2-(Dodecylthiocarbonothioylthio)-2-methylpropionic acid; 2,6-di-tert-butyl-4-methylphenol (99%); 2'-azidomethyl-3,4-ethylene-dioxythiophene; 2-hydroxymethyl-15-crown-5; 2-hydroxymethyl-18-crown-6; 2-picolychloride hydrochloride; 3,4-dimethoxythiophene 97%; 3-chloro-1,2-propanediol 98%; 4'-aminobenzo-15-crown-5; 4'-aminobenzo-18-crown-6; 4-styrene sulfonic acid sodium salt; 4-vinylbenzyl chloride; azobisisobutyronitrile; 2'-chloromethyl-3,4-ethylene-dioxythiophene; celite; di-(2-picoly)amine; dichloromethane; diethyl ether; ethyl acetate; hydrochloric acid; lithium aluminium hydride; magnesium sulphate; methanol; oxalyl chloride; p-(chloromethyl)-styrene 90%; potassium carbonate; potassium iodide; p-toluensulfonic acid 99%; silica gel; sodium carbonate; sodium hydride; sodium hydroxide; toluene; triethylamine were used as received if it is not indicated more details from Sigma Aldrich (France). Dimethylformidimide (DMF) was distilled from calcium hydride prior to use. Acetonitrile, was also distilled prior to use or dried by a Solvent machine. Tetrahydrofuran was distilled from benzophenone/ sodium prior to use.

### 1.2 TECHNIQUES AND INSTRUMENTATION:

*Nuclear magnetic resonance (NMR) spectroscopy:*  $^1\text{H}$ -NMR and  $^{13}\text{C}$ -NMR spectra for structural characterizations and titrations experiments were recorded on Bruker Avance (300 MHz) and Bruker Prodigy (400MHz) spectrometers, respectively, at 300K and the residual proton signal of the solvent was used as the internal standard. The *Heteronuclear single quantum correlation (HSQC) spectroscopy* is a type of NMR experiment where the spectrum obtained is two dimensional (2D) with one axis for proton spectrum (X- axis) and the other for an heteronucleus (other than H, usually N or C), in this case the carbon NMR spectrum (Y- axis). In this spectrum are shown the interactions originated from the spin of each proton attached directly to the heteronucleus being considered.

## *Ch. V.- Appendices*

*Size exclusion chromatography (SEC)* were used to determined molar masses and dispersity of the copolymers synthesized. The system used an Agilent GPC220HT instrument with detectors UV and RI and is constituted by a pre-column GF-1G-7B and two columns Asahipack GF-7MHSi (DMF + 0.1M LiBr, T=75°C, flow rate=0.6mL·min<sup>-1</sup>). Polystyrene standards were used for calibration. *UV-Vis spectroscopy*: Absorption spectra in films and solution were recorded using a UV Vis-3600 spectrophotometer (Shimadzu, Japan). The styrene derivatives polyelectrolytes will be an *addendum* later on.

*Potentiodynamic experiments* were done using an  $\mu$ Autolab (Metrohm) instrument controlled through a GPES software. For all the electrochemical experiments a Ag/AgCl electrode and a Pt mesh as reference and counter electrode respectively. A glassy carbon electrode (d = 3.0 mm; BASi®), Au plates (thickness= 120 nm deposit by thermal evaporation on glass substrates) electrode or ITO films were used as working electrodes.

*Potentiometry measurements at open circuit potential (OCP)* were performed using a PalmSense® potentiostat controlled by PS Trace 5.2 software.

*Impedance and capacitance measurements* were measured using dielectric interface (model 1296, Solartron, UK) connected to a frequency response analyzer (model SI 1260, Solartron, UK).

## 2 TABLES

**Table 10:** Summary of the monomers and the binding constants obtained from NMR titrations with different target cations ( $\text{Na}^+$ ,  $\text{K}^+$ ,  $\text{Zn}^{2+}$ ). Mix solvent: DMSO (20%)/  $\text{H}_2\text{O}$  (80%). Tit: Titration. Std ( $K_A$ ): Standard error of the binding constant. GoF: Goodness of Fit.

|                    | Monomer     | Name         | Tit             | $K_A$ ( $\text{M}^{-1}$ ) |              |                 |              |                 |              |
|--------------------|-------------|--------------|-----------------|---------------------------|--------------|-----------------|--------------|-----------------|--------------|
|                    |             |              |                 | $\text{NaClO}_4$          | Std( $K_A$ ) | $\text{KClO}_4$ | Std( $K_A$ ) | $\text{ZnCl}_2$ | Std( $K_A$ ) |
| Route I (Ch. II)   | 1           | StySOph15cr5 | D               | 3,50E+00                  | 8,80E-01     | 5,49E+01        | 2,74E+00     |                 |              |
|                    | 2           | StySOph18cr6 | C               | 1,22E+02                  | 6,89E+00     | 1,03E+03        | 1,18E+02     |                 |              |
|                    |             |              | E (mix solvent) |                           |              | 1,22E+02        |              |                 |              |
|                    | 3           | StyDPA       | A+B             | 2,46E+01                  | 4,63E+00     |                 |              | 2,54E+03        | 1,83E+01     |
|                    | 4           | Sty-o-15cr5  | -               |                           |              |                 |              |                 |              |
| 5                  | Sty-o-18cr6 | -            |                 |                           |              |                 |              |                 |              |
| Route II (Ch. III) | 6           | EDOTph15cr5  | H               | 3,59E+03                  | 2,32E+02     | 1,96E+02        | 3,03E+00     |                 |              |
|                    | 7           | EDOTph18cr6  | G               | 3,77E+02                  | 5,90E+01     | 3,23E+02        | 6,60E+00     |                 |              |
|                    | 8           | EDOTDPA      | -               |                           |              |                 |              |                 |              |
|                    | 9           | EDOT-o-15cr5 | J               | 1,96E+02                  | 2,26E+00     | 2,09E+02        | 3,11E+00     |                 |              |
|                    | 10          | EDOT-o-18cr6 | I               | 5,05E+03                  | 1,54E+03     | 2,44E+02        | 4,01E+01     |                 |              |

**Table 11:** Summary of Oxidation potentials of the functionalized EDOT derivatives synthesized during this thesis. M: Monomer.  $E^\circ$ : Oxidation potential vs Ag/AgCl or (\*) vs  $\text{Ag}^\circ$ .

| M    | $E_0 / \text{V}$ |
|------|------------------|
| [6]  | 1.48*            |
| [7]  | 1.49*            |
| [8]  | 1.55             |
| [9]  | -                |
| [10] | 1.35*            |
| EDOT | 1.45             |

### 3 Supplementary Information

#### Annex 1: Summary of equations related to 1:1 equilibria

##### 1:1 Equilibria

*General expression for equilibrium constant*

$$K_a = \frac{[HG]}{[H][G]}$$

*Expression for free guest concentration*

$$[G] = \frac{1}{2} \left( G_0 - H_0 - \frac{1}{K_a} \right) - \sqrt{\left( G_0 - H_0 - \frac{1}{K_a} \right)^2 + 4 \frac{G_0}{K_a}}$$

*Expression for complex guest concentration*

$$[HG] = \frac{1}{2} \left( G_0 + H_0 + \frac{1}{K_a} \right) - \sqrt{\left( G_0 + H_0 + \frac{1}{K_a} \right)^2 + 4[H_0][G_0]}$$

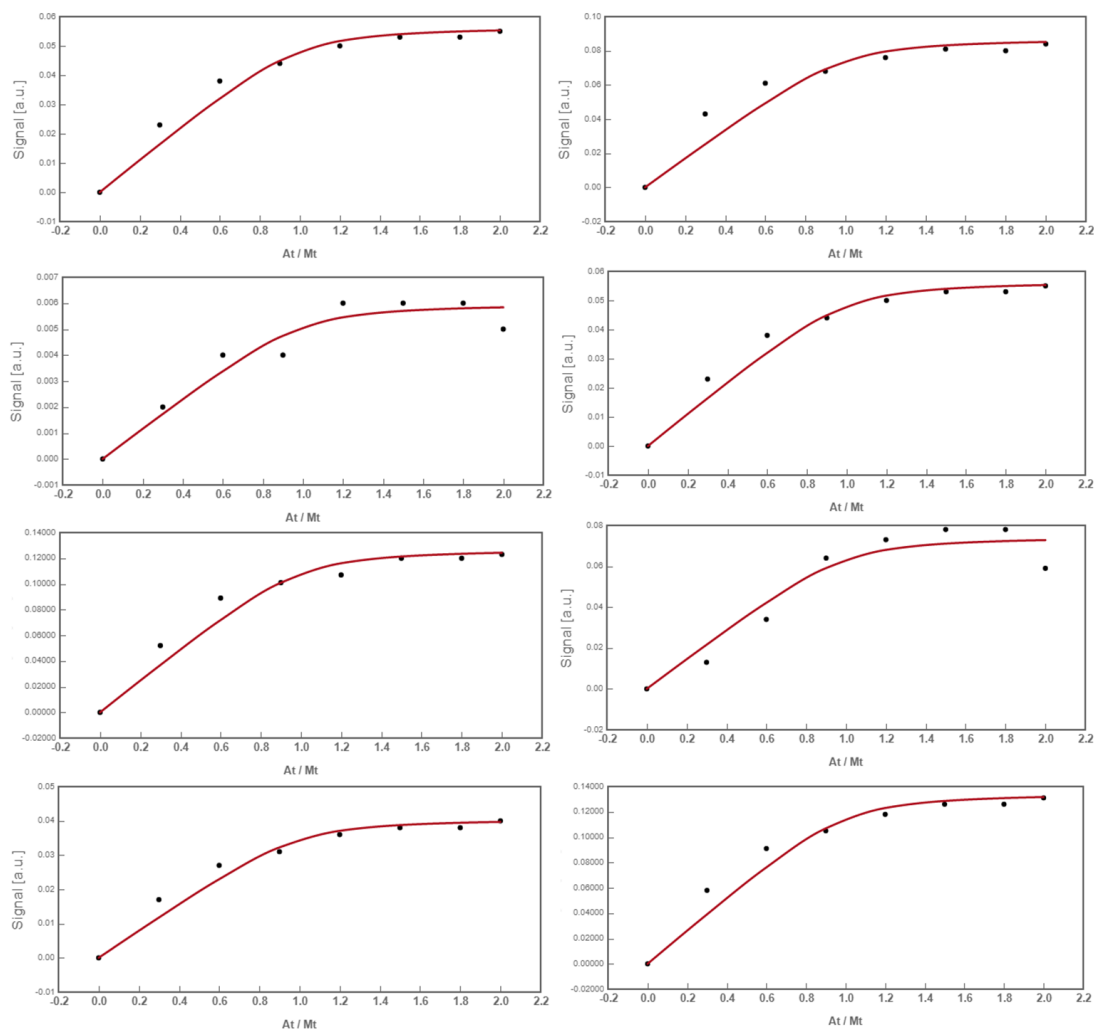
#### Annex 2: Quadratic equations for Non-linear fittings

$$G^2 - [G] \left( G_0 - H_0 - \frac{1}{K_a} \right) - \frac{G_0}{K_a} = 0$$

$$[HG]^2 - [HG] \left( G_0 + H_0 + \frac{1}{K_a} \right) - [H_0][G_0] = 0$$

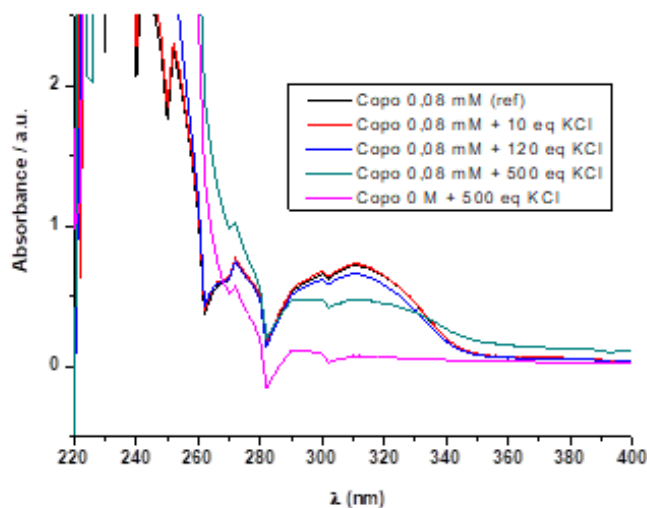
## Ch. V.- Appendices

**Annex 3: Binding Isotherms and fitting to a 1:1 binding model of the experimental data from titration  $^1\text{H-NMR}$  of monomer [2].** Scatter dots: Experimental data obtained from the difference in NMR shift (ppm) with respect to initial monomer spectra (y-axis – “Signal”) vs the increasing concentration of the cation used for the titration,  $A_t$ , in this case  $\text{KClO}_4$ , for a constant monomer concentration,  $M_t$  (x-axis – “ $A_t / M_t$ ”). Red curves: Fitting to the different binding isotherms with a 1:1 binding model to obtain the global binding constant ( $K_A$ ).

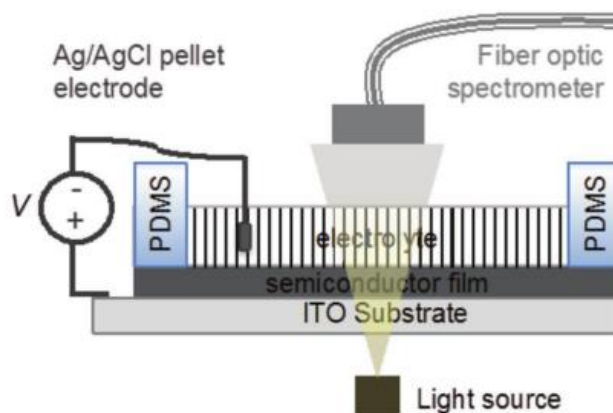


## Ch. V.- Appendices

**Annex 4: UV-Vis titration of P2-X with KCl (target cation):** The maximum of Absorption of the polymer decrease with the increasing concentration of KCl (black, red, blue and green curves). Control: The non-absorption at this wavelength of an alkaline solution (absence of polymer) is also shown (pink curve).

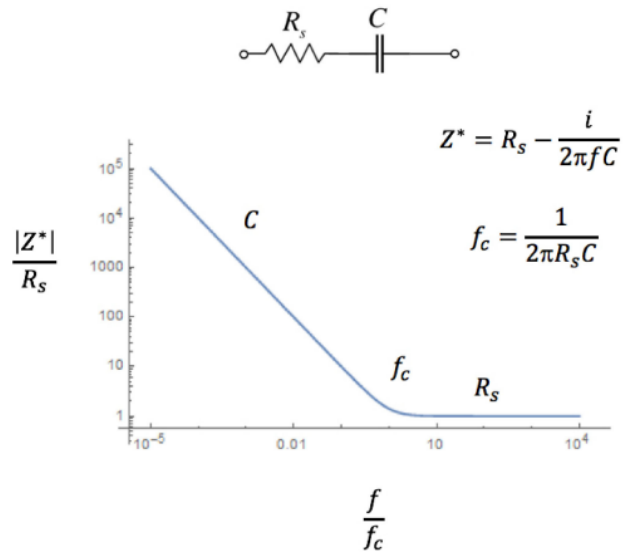


**Annex 5: Electrochromic set-up for 2D dedoping recordings**

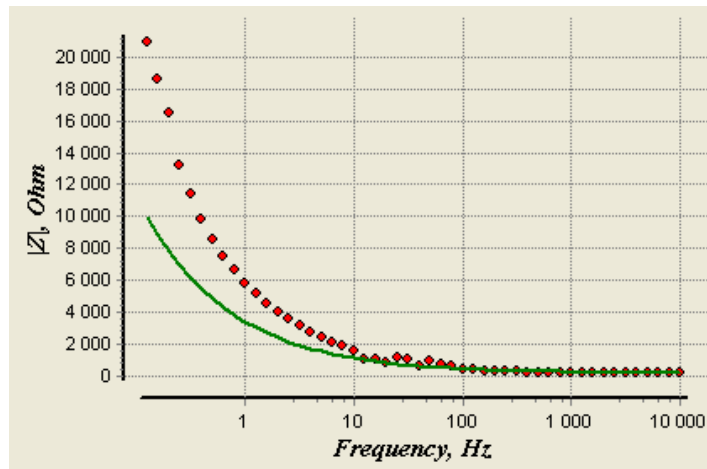


## Ch. V.- Appendices

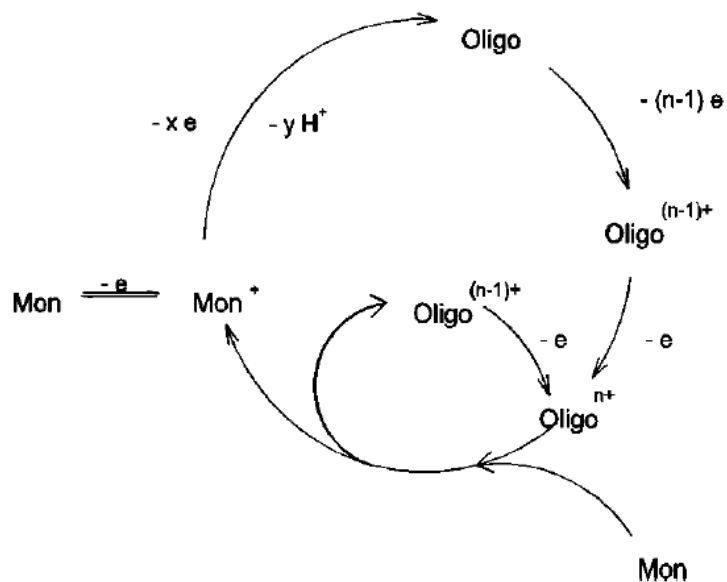
**Annex 6:** RC model used for the EIS fitting (taken from [98]).



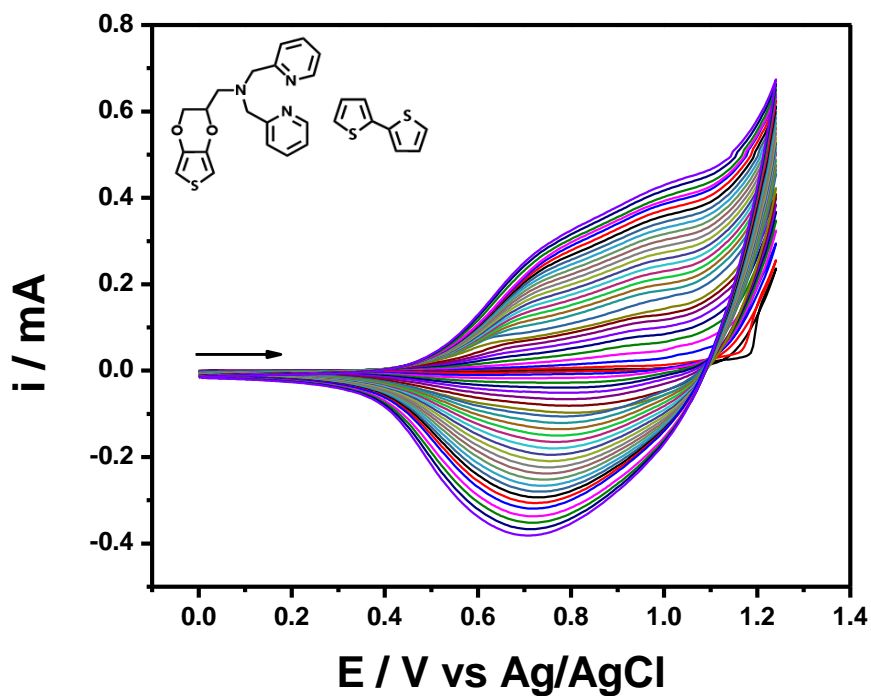
**Annex 7:** Poor Impedance fitting on thicker films ( $t=350$  nm) to extraction of the volumetric capacitance ( $C^*$ ).



**Annex 8: Scheme of the general reaction during the autocatalytic oxidation of monomeric starting species during electropolymerization (reproduced from [101]).**

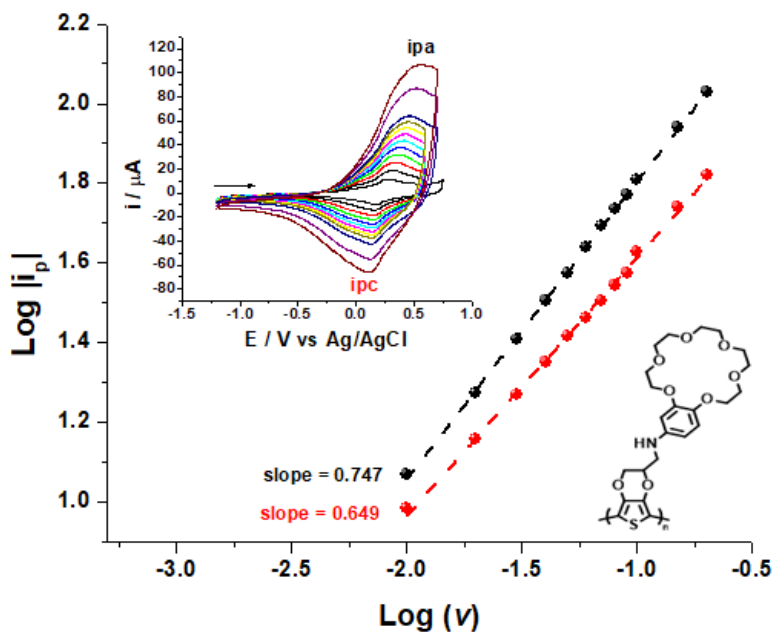


**Annex 9: Electropolymerization of monomer with [8] with bithiophene (Bth) after 20 cycles of potentiodynamic voltammetry. Conditions: 0.1M LiClO<sub>4</sub>, ACN,  $v=25\text{mV}\cdot\text{s}^{-1}$ .**

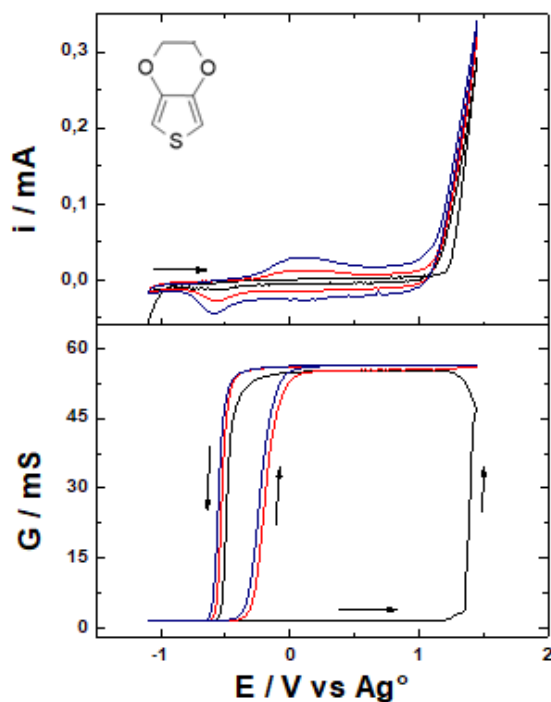


## Ch. V.- Appendices

**Annex 10: Influence of the scan rate on the charge-discharge process:** Variation of  $\log(i_p)$  vs  $\log(v)$  for the polymer film *P(7)*. Conditions: 0.1 M LiClO<sub>4</sub> in ACN, AcOH (pH=4).

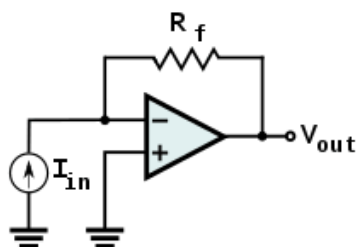


**Annex 11: In-situ conductivity of PEDOT:** Top: Electropolymerization of PEDOT for three cycles. Bottom: Related conductance ( $G$ ) recorded during the electropolymerization.

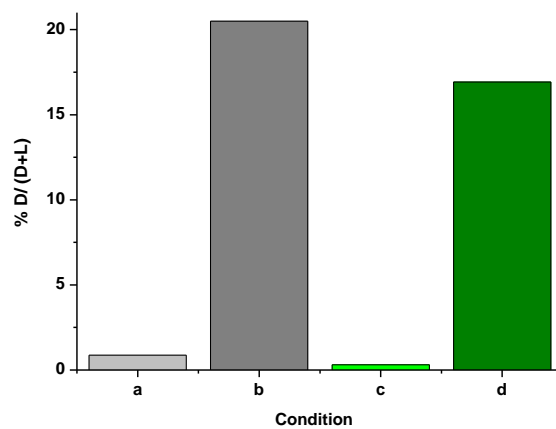


## Ch. V.- Appendices

**Annex 12:** Equivalent circuit of the I/V conversion card



**Annex 13: Cytotoxicity study of Ink 7 (containing Zn chelate moiety, DPA):** Thapsigargin effect. Same conditions as Figure 66.



## 4 Table of Figures

|   |    |
|---|----|
| <b>Figure 1: Scheme of ion channels of the cell membrane:</b> $K^+$ / $Na^+$ Pump and $Na^+$ and $K^+$ ion channels (taken from <a href="https://blausen.com">https://blausen.com</a> ).....  | 11 |
| <b>Figure 2: Scheme of AP formation:</b> <b>1)</b> A Stimulus arrives at the cell, for example a change in voltage. If it has the intensity needed to overcome the threshold voltage of depolarizing voltage-gated channels ( $Na^+$ in this case), the latter open; <b>2)</b> This induces a depolarization of the plasma membrane; <b>3)</b> The inactivation of depolarizing channels and the opening of repolarizing ion channels permeable to $K^+$ repolarizes the plasma membrane <b>4)</b> In some cells the membrane potential goes beyond the desired potential producing a hyperpolarization. <b>5)</b> The membrane recovers its resting state until the arrival of a new stimulus. (Reproduced from <a href="https://www.moleculardevices.com">https://www.moleculardevices.com</a> ).....   | 13 |
| <b>Figure 3: Histological comparison of Human and Mouse Pancreas:</b> $\beta$ -cells (in red), secreting insulin; $\alpha$ -cells (in green), secreting glucagon, a hormone that increases blood glucose such as in between meals; $\delta$ (in blue), secreting somatostatin (adapted from [11]).....  | 15 |
| <b>Figure 4: Insulin secretion triggered by the glucose-induced electrical activity:</b> Biphasic profile of the AP bursts and the insulin secretion (adapted from [11]). ....  | 16 |
| <b>Figure 5: Scheme of the model of GIIS:</b> The signs (+) indicate a stimulation and (-) an inhibition. And the arrows ( $\uparrow$ $\downarrow$ ) indicate an increase or a decrease of the indicated parameter (reproduced from [11]). ...  | 17 |
| <b>Figure 6: Electrical signals due to individual cell activity or to different types of coupling between cells.</b> <b>Left:</b> Scheme of an electrode covered with pancreatic islet ( $\beta$ -cell in blue, $\alpha$ -cell in orange). <b>Right: a)</b> $\beta$ -cell signalling, presenting high frequency signals, the characteristic action potentials (AP) overlapping with the slow potentials (SP), lower frequency wavy multicellular signals due to coupling with other $\beta$ -cells under high glucose concentration (stimulus); <b>b)</b> Suppression of junctions on $\beta$ -cells doesn't allow the couplings, recording only individual cell signals, the AP; <b>c)</b> $\alpha$ -cell signalling, presenting characteristic AP only under low concentration of glucose or adrenaline stimulation, not appearing overlap with the SP at high glucose concentration (taken from [33])..... | 23 |
| <b>Figure 7: Microelectrode Array (MEA): a)</b> MEA device (32 electrodes, MCS) (top) and the same device with cultured of pancreatic islets on it (bottom); <b>b)</b> Scheme of the $\beta$ -cells cultured on one electrode of the MEA; <b>c)</b> Electrophysiological recording of the electrical activity with MEA: no activity at low concentration of Glucose (G3, [Glucose]=3 mM) and high intensity of activity under glucose stimulation (G15, [Glucose]=15 mM); <b>d)</b> Characteristics signal of the electrical activity of $\beta$ -cells: Actions Potentials (AP) corresponding to individual cells activity and Slow Potentials (SP) giving information of global response of the islet. ....   | 25 |
| <b>Figure 8: Scheme of an organic electrochemical transistor (OECT):</b> A bias is applied between two electrodes, source and drain, which are connected by a channel, constituted of an organic semi-conductor, usually PEDOT:PSS. This channel is in direct contact with an electrolyte where is immersed a third electrode, the gate electrode (i.e. Ag/AgCl electrode). ....  | 26 |
| <b>Figure 9: Scheme of the working mechanism of an OECT: Left:</b> No application of a gate voltage. <b>Right:</b> Application of positive gate voltage [39] .....  | 27 |
| <b>Figure 10: Summarize of structure and characteristics of OECT vs other devices: a)</b> Image of a "multidevice" platform. The image reflects the flexibility and mechanical resistance of the devices. Inset: Zoom to one OECT (S: source electrode; D: drain electrode, E: Electrode); <b>b)</b> Scheme of the electrode (left) and the transistor (right) showed in a). Both devices have similar dimensions[42]; <b>c)</b> Comparison of the amplification power of an OECT (light blue) against an OFET (dark blue) (adapted from [43]). ....  | 28 |
| <b>Figure 11: Chemical structures of some crown ethers often used in the literature</b> .....   | 36 |

## Ch. V.- Appendices

- Figure 12: Scheme of the different complexation hosting modes of a crown-ether with a ligand:** nest (left), perched (centre) or sandwich (right) [62]. ..... 37
- Figure 13: Scheme summarizing the families of most used electronically conducting polymers (ECP):** Polyanilines (PANis), polythiophenes (PThs) and polypyrroles (PPys) (adapted from [71]). ..... 40
- Figure 14: Scheme of the chemical structures of thiophene (left) compare to its derivative EDOT (right).** ..... 41
- Figure 15: Electrochromic property of PEDOT based inks:** a) Oxidized state; b) Reduced state ..... 42
- Figure 16: Chemical structure of polymer complex PEDOT:PSS.** In red, a polaron is represented in the conjugated chain of PEDOT. In blue a counterbalance charge of the sulfonate group is represented as a pending group in the PSS backbone. .... 43
- Figure 17: Summary of the double route of functionalization developed during this PhD:** Top: Styrene derivatives with binding moieties (monomers), their copolymers to gain new ion-sensitive polyelectrolytes used to stabilize the water dispersed PEDOT based inks. Bottom: EDOT derivatives with the ion-sensitive fractions and their electropolymerization to obtain ion-sensitive films. .... 47
- Figure 18: Scheme of targeted monomers designed to recognize the cations of biological interest:** 18-crown-6 moiety for  $K^+$  (blue), 15-crown-5 moiety for  $Na^+$  (red), dipicolyl (DPA) for  $Zn^{+2}$  (green). ..... **Error! Bookmark not defined.**
- Figure 19: Summary of the chemical structures of the monomers synthesized:** a) 4-styrenesulfonyl(phenyl-15-crown-5) imide [1] when  $n=1$  and 4-styrenesulfonyl(phenyl-18-crown-6) imide [2] when  $n=2$ ; b) N-(4-vinylbenzyl)-di-(2-picolyl) amine [3]; c) 15-crown-5-methyl-(4-vinylbenzyl)-methyl ether [4] when  $n=1$  and 18-crown-6-methyl-(4-vinylbenzyl)-methyl ether [5] when  $n=2$ . ..... 58
- Figure 20: Reactional Scheme of the synthesis of monomer [1]:** Step 1: Vilsmeier-Haack to form the styrenesulfonyl chloride. Step 2: Amination and formation of 4-styrenesulfonyl(phenyl-15-crown-5) imide [1]. ..... **Error! Bookmark not defined.**
- Figure 21: Structural characterization of 4-styrenesulfonyl(phenyl-15-crown-5) imide (1):**  $^1H$ -NMR ( $CDCl_3$ , 400 MHz, 128 scans) ..... **Error! Bookmark not defined.**
- Figure 22: Reactional Scheme of the synthesis of monomer [3]:** Amination reaction between the 4-vinylbenzylchloride and the di-(2-picolyl)amine to obtain the 4-vinylbenzyl-di-(2-picolyl)-amine or Styrene-DPA [3]. ..... 60
- Figure 23: Reactional Scheme of the synthesis of monomer (4):** Etherification reaction between 2-hydroxymethyl-15-crown-5 and 4-vinylbenzylchloride to obtain the 15-crown-5-methyl-(4-vinylbenzyl)-methyl ether [4]. ..... 60
- Figure 24: Binding ability evaluation by  $^1H$ -NMR titration of monomer [3]:**  $^1H$ -RMN Spectrum (TDF, 400 MHz) obtained for the titration of the monomer [3] under variable concentrations (from 0 to 10 molar equivalents) of zinc chloride (II). ..... 61
- Figure 25: Ion-specific changes in Absorption of 4-styrenesulfonyl(phenyl-18-crown-6)imide (SP18Cr6)(2).** Absorbance spectra were measured for SP18Cr6 (50  $\mu$ M) at different KCl or NaCl concentrations (10 mM steps from 0 to 60). Upper panel: spectra; Lower panel, Absorption maxima at 240 or 260 nm. .... 64
- Figure 26: Scheme of the RAFT polymerisation of P3 Copolymers family between STFSI and [3]:** CTA: Control transfer reagent; AIBN: Initiator 2,2'-Azobis(2-methylpropionitrile); m: fraction of STFSI; n: fraction of DPA functionalized monomer [3]. ..... 66

## Ch. V.- Appendices

- Figure 27: Structural characterization of copolymer P1-C (see Table 2):**  $^1\text{H}$ -RMN Spectrum (d-DMF, 400 MHz) of a copolymer P1-C synthesized from STFSIK (65% wt.) and 15-crown-funtionalized monomer [1] (35 %wt.). ..... 68
- Figure 28: Size exclusion chromatogram of a P2-G (18-crown-6 family)** showing a monomodal distribution (Mw: 96 KDa. Obtained from SEC calibrated with polystyrene standards. DMF, LiBr, 70°C). ..... 69
- Figure 29: Integration of DPA in copolymers of the serie P3 (see Table 2-serie P3):** Ratio between the integration area under the NMR peaks (**Int A**) related to monomer [3] ( $m_{\text{DPA}}$ ) vs STFSI ( $m_{\text{STFI}}$ ) with respect to the weight percentage added of [3] (**%wt. mon StDPA [3]**). ..... 70
- Figure 30: Oxidative polymerization of EDOT** in the presence of oxidants (iron chloride (III) and ammonium persulfate) and stabiliser in water (example of PSS)..... 71
- Figure 31: Aqueous dispersion formation of the ion-sensitive PEDOT based inks:** Reactors of water dispersions of the polyelectrolyte: **a)** Before the addition of the oxidants, brownish colour polyelectrolyte solution; **b)** After addition of the oxidants, formation of the PEDOT based ink. .... 71
- Figure 32: PEDOT based inks. a)** Some examples of the stable aqueous dispersions synthesized containing crown-ether moieties; **b - c)** Electrochromic behaviour of these inks showing their doped (transparent) and dedoped state (light blue);,  $V=-0.75\text{mV}$ : **b)** PEDOT: PSS (commercial); **c)** PEDOT ink with 18-crown-6 moieties (Ink 4, Table 3). Conditions: electrolyte 0.1 M NaCl (aq.) ..... 73
- Figure 33: Electrochromic response of thin films (150 nm) of referent vs 18-crown-6-functionalized ink:** Electrochemical rates of PEDOT based inks in different aqueous electrolytes: Ink containing 15 wt% of 18-crown-6 (Ink 4 of P2-C) in 0.1M NaCl (aq.) (**a**) and 0.1M KCl (aq.)(**b**); PEDOT:PSS in 0.1M NaCl (aq.) (**c**) and 0.1M KCl (aq.)(**d**). ..... 74
- Figure 34: Electrochemical impedance fitting and capacitance extraction:** Bode plot ( $|Z^*|$  vs.  $f$ ) of a film of Ink 4, based on a polyelectrolyte PSTFSI<sub>85%</sub>-PS18cr6<sub>15%</sub> (P2-C), (red scatter) and its fitting (green line)..... 76
- Figure 35: Molecular weight effect on the electrochemical impedance profile:** Bode plots of inks films constituted by the same polyelectrolyte composition as Figure 34 (PSTFSI<sub>85%</sub>-PS18cr6<sub>15%</sub>) with different Molecular weights: 100 KDa (Film1) and 250 KDa (Film 2). Control: ITO substrate (Black curve). ..... 78
- Figure 36: Scheme of derivatives EDOT monomers synthesized: a)** 2,3-dihydrothieno[3,4-b][1,4]dioxine-3-aminobenzo-15-crown-5 [6] avec  $n=1$  et 2,3-dihydrothieno[3,4-b][1,4]dioxine-3-aminobenzo-18-crown-6 [7] avec  $n=2$ ; **b)** 2'-(Bis(2-picolyl)aminomethyl)-3,4-ethylenedioxythiophene [8] **c)** 15-crown-5-methyl-2,3-dihydrothieno[3,4-b][1,4]dioxine ether [9] avec  $n=1$  et 18-crown-8-methyl-2,3-dihydrothieno[3,4-b][1,4]dioxine ether [10] avec  $n=2$ . ..... 96
- Figure 37: Reactional Scheme of the synthesis of monomer [6]:** Amination reaction between the 4'-aminobenzo-15-crown-5 ether and the 2'-chloromethyl-3,4-ethylene-dioxythiophene to obtain the 2,3-dihydrothieno[3,4-b][1,4]dioxine-3-aminobenzo-15-couronne-5 [6]..... 96
- Figure 38: Structural characterization of monomer [6]:**  $^1\text{H}$ -NMR ( $\text{CDCl}_3$ , 400 MHz) ..... 97
- Figure 39: Structural characterisation of monomer [6]:**  $^{13}\text{C}$ -NMR ( $\text{CDCl}_3$ , 400 MHz) ..... 99
- Figure 40: Reactional Scheme of the synthesis of monomer [8]:** Amination reaction between the 2'-aminomethyl-3,4-ethylene-dioxythiophene and the 2-(Chloromethyl)pyridine hydrochloride to obtain the 2'-(Bis(2-picolyl)aminomethyl)-3,4-ethylenedioxythiophene [8]..... 99
- Figure 41: HSQC spectrum for structural characterization of [8]:** X-axis :  $^1\text{H}$ -NMR ( $\text{CDCl}_3$ , 400 MHz); Y-axis :  $^{13}\text{C}$ -NMR ( $\text{CDCl}_3$ , 400 MHz). ..... 100
- Figure 42: Reactional Scheme of the synthesis of monomer [10]:** Etherification reaction between 2-hydroximethyl-18-crown-6 and 2'-chloromethyl-3,4-ethylene-dioxythiophene to obtain the 18-crown-6-

## Ch. V.- Appendices

|  |     |
|--|-----|
| methyl-2,3-dihydrothieno[3,4-b][1,4]dioxine ether [10]. Monomer [9] was synthesized following the same method. All the experimental details are described in the experimental part.....  | 101 |
| <b>Figure 43: <math>^1\text{H-NMR}</math> of monomer [10] (<math>\text{CDCl}_3</math>, 400 MHz), 18-crown-5-methyl-2,3-dihydrothieno[3,4-b][1,4]dioxine ether [10].</b> .....  | 102 |
| <b>Figure 44: Reactional Scheme of crown-ether functionalized thio-pyrrole ter-monomers:</b> Step 1: Friedel-Craft reaction to obtain (i); Step 2: Paal Knorr coupling to obtain (ii). .....   | 103 |
| <b>Figure 45: Reactional scheme of the <math>\text{S}_\text{N}^2</math> amination</b> between the 2-aminomethyl-15-crown-5 and 2'-chloromethyl-3,4-ethylene-dioxythiophene to obtain the 2,3-dihydrothieno[3,4-b][1,4]dioxine-N'-(15-crown-5)-methylamine (iii). .....   | 104 |
| <b>Figure 46: Structural characterization of the aminomethyl coupling to obtain (iii): <math>^1\text{H NMR}</math> (<math>\text{CDCl}_3</math>, 400 MHz)</b> .....   | 105 |
| <b>Figure 47: Structural characterization of (iii): <math>^{13}\text{C-NMR}</math> (<math>\text{CDCl}_3</math>, 400 MHz)</b> .....   | 106 |
| <b>Figure 48: Potentiodynamic oxidative voltamperogram of [6] vs EDOT:</b> Conditions: 0.1 M $\text{LiClO}_4$ , ACN, $v=25\text{mV}\cdot\text{s}^{-1}$ . .....   | 107 |
| <b>Figure 49: Electropolymerization of monomer [6] by potentiodynamic voltammetry:</b> Cycles: one (black curve, interior), last (green curve, exterior). Conditions: 0.1 M $\text{LiClO}_4$ , ACN, $v=25\text{mV}\cdot\text{s}^{-1}$ . .....  | 108 |
| <b>Figure 50: Electrochemical profile of the electropolymerized films:</b> PEDOT (black curve) vs Poly- (6) (red curve). Conditions: 0.1 M $\text{LiClO}_4$ , ACN, $v=25\text{mV}\cdot\text{s}^{-1}$ . .....   | 110 |
| <b>Figure 51: SEM characterisation of thick electropolymerized homopolymer:</b> Lateral profile of electropolymerized film from (7). Thickness: 20 $\mu\text{m}$ . .....   | 111 |
| <b>Figure 52: Influence of EDOT-crown ether binding fraction on the electrochemical activity:</b> Charge-Discharge window of electropolymerized: P(7) with aniline binding (top) and P(10) with ether binding (bottom) in the first (black curves) or tenth (red curves) cycles of electropolymerization. Conditions: 0.1 M $\text{LiClO}_4$ , $[\text{M}]=5\text{mM}$ , ACN, $v=25\text{mV}\cdot\text{s}^{-1}$ . .....  | 112 |
| <b>Figure 53: Potentiodynamic voltammogram of different electrochemically formed copolymers between EDOT and (6):</b> Inset: Chemical structure of EDOT (black) and [6] monomers. Legend index: Molar ratio used of each monomer, EDOT (black index) vs [6] (red index), to the formation of each copolymer: 1:1 (black curve), 2:3 (green curve), 2:1 (red curve), 1:1 (blue curve). Conditions: 0.1M $\text{LiClO}_4$ , ACN, $v=25\text{mV}\cdot\text{s}^{-1}$ . ..... | 113 |
| <b>Figure 54: SEM images of electropolymerized films: a) PEDOT; b) P(6).</b> Scale: 10 $\mu\text{m}$ .....   | 114 |
| <b>Figure 55: Ionic Electrolyte effect on the electrochemical profile of 15-crown-5 based film:</b> Potentiodynamic voltammogram of a polymer film from [6] characterised in different electrolytes: Sodium (red) or Potassium (blue) in low (10 mM, dot) or high (100 mM, solid) concentrations. ....   | 116 |
| <b>Figure 56: Quantification of potentiodynamic voltammetry experiments:</b> Ratios $Q_c/Q_a$ vs Cation concentration ( $n=3$ ). Sodium cation (red dots), potassium (blue dots) and number of experiment (index number). <b>Red frame:</b> 15-crown-5 containing films from monomer [6]. <b>Grey frame:</b> PEDOT film (control). .....   | 117 |
| <b>Figure 57: Concentration effect on the electrochemical profile of P(6) , a 15-crown-5 based film:</b> Potentiodynamic voltammogram of a polymer film from [6] characterised in different concentration electrolytes: Solid curves: NaCl concentration from 0.1 mM (black) to 0.1 M (green). Dot curves: Voltammogram of the film on washing electrolyte (0.1M $\text{LiClO}_4$ , $\text{H}_2\text{O}$ , $\text{pH}=4$ ). .....  | 118 |
| <b>Figure 58: Comparison of the effect on the reversibility of the charge-discharge process in presence of alkaline cations:</b> Difference of potential, $\Delta E$ , between the oxidation and reduction peaks for the different electrolytes: 1, 10 or 100 mM of sodium (red) or potassium (blue) cations. ....   | 119 |

## Ch. V.- Appendices

- Figure 59: Influence of the scan rate on the charge-discharge process:** Variation of  $\log(i_p)$  vs  $\log(v)$  for the polymer film P(6). Inset: Variation of the current with the scan rate.  $i_{pa}$ : anodic peak current,  $i_{pc}$ : cathodic peak current. Scan rate ( $v$ ): 10 to 100; 150 and 200 mV/s (from black to green curves). Conditions: 0.1 M  $\text{LiClO}_4$  in ACN, AcOH (pH=4)..... 121
- Figure 60: Stability of film of P(7) after 100 cycles of charge-discharge process:** Potentiodynamic oxidative voltammogram before (black curves) and after (red curves) the 100 cycles. Conditions: 0.1M  $\text{LiClO}_4$ , ACN,  $v=25\text{mV}\cdot\text{s}^{-1}$ ; pH=7 (left), pH=4 (right). ..... 122
- Figure 61: Comparison of potentiometric titrations of:** PEDOT (left) and P(7) (right). ..... 124
- Figure 62: In-situ conductivity measurements:** Top: Electropolymerization of p(7) (aniline linking) (a) and p(10) (ether linking) (b) for five and three cycles, respectively. Bottom: Related conductance (G) recorded during the electropolymerization. .... 126
- Figure 63: Influence of the cation affinity of the ion-sensitive polymers on the conductance:** P(6) and P(7) films (left and right, respectively) exposed to 0.1M of KCl or NaCl aqueous electrolytes..... 127
- Figure 64: Scheme of the In-situ conductivity measurements set-up:** a) Comb type Pt interdigital microelectrode arrangement (IDME) with 34 separation strips; b) Schematic diagram of the two potentiostats for in-situ electrochemical-conductance method. The potentiostat (1) perform the potentiodynamic experiment, the potentiostat (2) maintains a constant potential ( $\Delta V$ ) during the conductivity experiment and the symmetry unity (3) which applies  $\Delta V$  between both combs of the IDME. .... 136
- Figure 65: Cytotoxicity study of the Ion Sensitive Inks:** Clonal  $\beta$  cells (INS832-13) were cultured for 24h on control coverslips (a and b) or coverslips covered with the studied ink (c and d) (Ink 4 in Table 3, Chapter II). Effect of thapsigargin (apoptosis) was evaluated: control (b) vs film-covered coverslips (d). Merge images are presented. Experimental conditions: **Green:** FYTC filter (live cells); **Red:** YFP filter (dead cells). ..... 154
- Figure 66: Quantification of apoptosis effect by inks and exposure to thapsigargin:** Cells cultured on coverslips (CS): a) Non-covered CS in medium culture (- control) in light grey; b) Non-covered CS under thapsigargin effect (+ control) in dark grey; c) Film-covered CS in culture medium in light blue; d) Film-covered CS under thapsigargin effect in marine blue. .... 156
- Figure 67: Physical characterization of a classical PEDOT:PSS vertical OECT[103]:** Transfer curve (black spheres) and transconductance curve (blue squares). .... 158
- Figure 68: Scheme of I/V conversion card on the cell activity simulation configuration:** Three filters (2 highpass, HP, and 1 lowpass, LP) are incorporated to the basic configuration presented in Annex 12... 158
- Figure 69: Illustration of the sinusoidal signals obtained from the electrical activity simulation:** Signal corresponding to a sinusoidal stimulation on gate at a frequency of 1000Hz. Yellow (top curve): Signal corresponding to  $V_2$  in Figure 68, obtained after passing raw signal by the first  $\text{HP}_1\text{-F}$ ; Green (middle curve): Signal corresponding to  $V_3$  in Figure 68, obtained after passing by the second  $\text{HP}_2\text{-F}$ ; Pink (bottom curve): Signal corresponding to  $V_{\text{OUT}}$  in Figure 68, obtained after passing by the last filter  $\text{LP-F}$ . .... 159
- Figure 70: Micrograph of micro-fabricated IS-OECT with Ink 3,** containing 18-crown-6 moieties (see Table 3 in Chapter II and Table 7). A film of PaC coats the entire surface with the exception of the channel area where the ink was deposited (rectangle of  $100\ \mu\text{m} \times 10\ \mu\text{m}$  between the gold electrodes, source and drain). ..... 161
- Figure 71: Electrical characterization of IS-OECT fabricated with Ink 3:** a) Output characterization; b) Transfer curve at  $V_{\text{DS}}=-0.4\text{V}$  (black curve) and corresponding transconductance (blue curve). The device dimensions are  $W=10\ \mu\text{m}$ ,  $L=100\ \mu\text{m}$  and film thickness  $t=100\text{nm}$ . .... 163

Figure 72: Scheme of the OEET- I/V card connections ..... 173

## 5 Bibliography

### General Introduction

1. Ashkan, K.; Rogers, P.; Bergman, H.; Ughratdar, I. Insights into the mechanisms of deep brain stimulation. *Nat. Rev. Neurol.* **2017**, *13*, 548–554.

### Chapter I

2. PEDOT: Principles and Applications of an Intrinsically Conductive Polymer Available online: <https://www.crcpress.com/PEDOT-Principles-and-Applications-of-an-Intrinsically-Conductive-Polymer/Elschner-Kirchmeyer-Lovenich-Merker-Reuter/p/book/9781420069112> (accessed on Aug 13, 2018).
3. Rasmussen, S.C. The Early History of Polyaniline: Discovery and Origins. *Subst. Vol 1 No 2 2017* **2017**.
4. McNeill, R.; Siudak, R.; Wardlaw, J.H.; Weiss, D.E. Electronic Conduction in Polymers. I. The Chemical Structure of Polypyrrole. *Aust. J. Chem.* **1963**, *16*, 1056–1075.
5. Contat-Rodrigo, L.; Pérez-Fuster, C.; Lidón-Roger, J.V.; Bonfiglio, A.; García-Breijo, E. Characterization of Screen-Printed Organic Electrochemical Transistors to Detect Cations of Different Sizes. *Sensors* **2016**, *16*, 1599.
6. Malliaras, G.; Friend, R. An Organic Electronics Primer. *Phys. Today* **2005**, *58*, 53–58.
7. Rivnay, J.; Owens, R.M.; Malliaras, G.G. The Rise of Organic Bioelectronics. *Chem. Mater.* **2014**, *26*, 679–685.
8. Bresadola, M. Medicine and science in the life of Luigi Galvani (1737–1798). *Brain Res. Bull.* **1998**, *46*, 367–380.
9. Bouton, C.E.; Shaikhouni, A.; Annetta, N.V.; Bockbrader, M.A.; Friedenber, D.A.; Nielson, D.M.; Sharma, G.; Sederberg, P.B.; Glenn, B.C.; Mysiw, W.J.; et al. Restoring cortical control of functional movement in a human with quadriplegia. *Nature* **2016**, *533*, 247–250.
10. Gribble, F.M.; Loussouarn, G.; Tucker, S.J.; Zhao, C.; Nichols, C.G.; Ashcroft, F.M. A Novel Method for Measurement of Submembrane ATP Concentration. *J. Biol. Chem.* **2000**, *275*, 30046–30049.
11. Rorsman, P.; Ashcroft, F.M. Pancreatic  $\beta$ -Cell Electrical Activity and Insulin Secretion: Of Mice and Men. *Physiol. Rev.* **2018**, *98*, 117–214.
12. Ashcroft, F.M.; Rorsman, P. KATP channels and islet hormone secretion: new insights and controversies. *Nat. Rev. Endocrinol.* **2013**, *9*, 660–669.
13. Henquin, J.C.; Ravier, M.A.; Nenquin, M.; Jonas, J.C.; Gilon, P. Hierarchy of the  $\beta$ -cell signals controlling insulin secretion. *Eur. J. Clin. Invest.* **2003**, *33*, 742–750.
14. Neshler, R.; Cerasi, E. Modeling Phasic Insulin Release: Immediate and Time-Dependent Effects of Glucose. *Diabetes* **2002**, *51*, S53–S59.
15. Molina, S.A.; Moriarty, H.K.; Infield, D.T.; Imhoff, B.R.; Vance, R.J.; Kim, A.H.; Hansen, J.M.; Hunt, W.R.; Koval, M.; McCarty, N.A. Insulin signaling via the PI3-kinase/Akt pathway regulates airway glucose uptake and barrier function in a CFTR-dependent manner. *Am. J. Physiol.-Lung Cell. Mol. Physiol.* **2017**, *312*, L688–L702.
16. Wan, M.; Leavens, K.F.; Hunter, R.W.; Koren, S.; von Wilamowitz-Moellendorff, A.; Lu, M.; Satapati, S.; Chu, Q.; Sakamoto, K.; Burgess, S.C.; et al. A Noncanonical, GSK3-Independent Pathway Controls Postprandial Hepatic Glycogen Deposition. *Cell Metab.* **2013**, *18*, 99–105.

## Ch. V.- Appendices

17. Li, X.; Monks, B.; Ge, Q.; Birnbaum, M.J. Akt/PKB regulates hepatic metabolism by directly inhibiting PGC-1 $\alpha$  transcription coactivator. *Nature* **2007**, *447*, 1012–1016.
18. Wilson, D.P.; Susnjar, M.; Kiss, E.; Sutherland, C.; Walsh, M.P. Thromboxane A<sub>2</sub>-induced contraction of rat caudal arterial smooth muscle involves activation of Ca<sup>2+</sup> entry and Ca<sup>2+</sup> sensitization: Rho-associated kinase-mediated phosphorylation of MYPT1 at Thr-855, but not Thr-697. *Biochem. J.* **2005**, *389*, 763–774.
19. Raoux, M.; Bornat, Y.; Quotb, A.; Catargi, B.; Renaud, S.; Lang, J. Non-invasive long-term and real-time analysis of endocrine cells on micro-electrode arrays: Long-term and real-time analysis of endocrine cells. *J. Physiol.* **2012**, *590*, 1085–1091.
20. Vantyghem, M.-C.; Defrance, F.; Quintin, D.; Leroy, C.; Raverdi, V.; Prévost, G.; Caiazzo, R.; Kerr-Conte, J.; Glowacki, F.; Hazzan, M.; et al. Treating diabetes with islet transplantation: Lessons from the past decade in Lille. *Diabetes Metab.* **2014**, *40*, 108–119.
21. Melton, D.A. Chapter Four - Applied Developmental Biology: Making Human Pancreatic Beta Cells for Diabetics. In *Current Topics in Developmental Biology*; Wassarman, P.M., Ed.; Essays on Developmental Biology, Part B; Academic Press, 2016; Vol. 117, pp. 65–73.
22. Grynkiewicz, G.; Poenie, M.; Tsien, R.Y. A New Generation of Ca<sup>2+</sup> Indicators with Greatly Improved Fluorescence Properties. **11**.
23. Rutter, G.A.; Varadi, A.; Tsuboi, T.; Parton, L.; Ravier, M. Insulin secretion in health and disease: genomics, proteomics and single vesicle dynamics. *Biochem. Soc. Trans.* **2006**, *34*, 4.
24. Lin, W.-J.; Salton, S.R. The Regulated Secretory Pathway and Human Disease: Insights from Gene Variants and Single Nucleotide Polymorphisms. *Front. Endocrinol.* **2013**, *4*.
25. Li, D.; Chen, S.; Bellomo, E.A.; Tarasov, A.I.; Kaut, C.; Rutter, G.A.; Li, W. Imaging dynamic insulin release using a fluorescent zinc indicator for monitoring induced exocytotic release (ZIMIR). *Proc. Natl. Acad. Sci. U. S. A.* **2011**, *108*, 21063–21068.
26. Jørgensen, M.C.; Ahnfelt-Rønne, J.; Hald, J.; Madsen, O.D.; Serup, P.; Hecksher-Sørensen, J. An Illustrated Review of Early Pancreas Development in the Mouse. *Endocr. Rev.* **2007**, *28*, 685–705.
27. Xie, R.; Carrano, A.C.; Sander, M. A systems view of epigenetic networks regulating pancreas development and  $\beta$ -cell function. *Wiley Interdiscip. Rev. Syst. Biol. Med.* **2015**, *7*, 1–11.
28. Wang, A.; Yue, F.; Li, Y.; Xie, R.; Harper, T.; Patel, N.A.; Muth, K.; Palmer, J.; Qiu, Y.; Wang, J.; et al. Epigenetic priming of enhancers predicts developmental competence of hESC-derived endodermal lineage intermediates. *Cell Stem Cell* **2015**, *16*, 386–399.
29. Dhawan, S.; Tschen, S.-I.; Zeng, C.; Guo, T.; Hebrok, M.; Matveyenko, A.; Bhushan, A. DNA methylation directs functional maturation of pancreatic  $\beta$  cells. *J. Clin. Invest.* **2015**, *125*, 2851–2860.
30. Rong, Z.; Wang, M.; Hu, Z.; Stradner, M.; Zhu, S.; Kong, H.; Yi, H.; Goldrath, A.; Yang, Y.-G.; Xu, Y.; et al. An effective approach to prevent immune rejection of human ESC-derived allografts. *Cell Stem Cell* **2014**, *14*, 121–130.
31. Russa, M.F.L.; Qi, L.S. The New State of the Art: Cas9 for Gene Activation and Repression. *Mol. Cell. Biol.* **2015**, *35*, 3800–3809.
32. Atwater, I.; Ribalet, B.; Rojas, E. Cyclic changes in potential and resistance of the beta-cell membrane induced by glucose in islets of Langerhans from mouse. *J. Physiol.* **1978**, *278*, 117–139.
33. Hamill, O.P.; Marty, A.; Neher, E.; Sakmann, B.; Sigworth, F.J. Improved patch-clamp techniques for high-resolution current recording from cells and cell-free membrane patches. *Pflüg. Arch. - Eur. J. Physiol.* **1981**, *391*, 85–100.
34. Lebreton, F.; Pirog, A.; Belouah, I.; Bosco, D.; Berney, T.; Meda, P.; Bornat, Y.; Catargi, B.; Renaud, S.; Raoux, M.; et al. Slow potentials encode intercellular coupling and insulin demand in pancreatic beta cells. *Diabetologia* **2015**, *58*, 1291–1299.

## Ch. V.- Appendices

35. Thomasjr, C.; Springer, P.; Loeb, G.; Berwaldnetter, Y.; Okun, L. A miniature microelectrode array to monitor the bioelectric activity of cultured cells. *Exp. Cell Res.* **1972**, *74*, 61–66.
36. Hofmann, F.; Bading, H. Long term recordings with microelectrode arrays: Studies of transcription-dependent neuronal plasticity and axonal regeneration. *J. Physiol.-Paris* **2006**, *99*, 125–132.
37. Koutsouras, D.A.; Perrier, R.; Villarroel Marquez, A.; Pirog, A.; Pedraza, E.; Cloutet, E.; Renaud, S.; Raoux, M.; Malliaras, G.G.; Lang, J. Simultaneous monitoring of single cell and of micro-organ activity by PEDOT:PSS covered multi-electrode arrays. *Mater. Sci. Eng. C* **2017**, *81*, 84–89.
38. White, H.S.; Kittlesen, G.P.; Wrighton, M.S. Chemical derivatization of an array of three gold microelectrodes with polypyrrole: fabrication of a molecule-based transistor. *J. Am. Chem. Soc.* **1984**, *106*, 5375–5377.
39. Giovannitti, A.; Nielsen, C.B.; Sbircea, D.-T.; Inal, S.; Donahue, M.; Niazi, M.R.; Hanifi, D.A.; Amassian, A.; Malliaras, G.G.; Rivnay, J.; et al. N-type organic electrochemical transistors with stability in water. *Nat. Commun.* **2016**, *7*, 13066.
40. Friedlein, J.T.; Donahue, M.J.; Shaheen, S.E.; Malliaras, G.G.; McLeod, R.R. Microsecond Response in Organic Electrochemical Transistors: Exceeding the Ionic Speed Limit. *Adv. Mater.* **2016**, *28*, 8398–8404.
41. Bernards, D.A.; Malliaras, G.G. Steady-State and Transient Behavior of Organic Electrochemical Transistors. *Adv. Funct. Mater.* **2007**, *17*, 3538–3544.
42. Yi, Z.; Natale, G.; Kumar, P.; Mauro, E.D.; Heuzey, M.-C.; Soavi, F.; Perepichka, I.I.; Varshney, S.K.; Santato, C.; Cicoira, F. Ionic liquid–water mixtures and ion gels as electrolytes for organic electrochemical transistors. *J. Mater. Chem. C* **2015**, *3*, 6549–6553.
43. Khodagholy, D.; Doublet, T.; Quilichini, P.; Gurfinkel, M.; Leleux, P.; Ghestem, A.; Ismailova, E.; Hervé, T.; Sanaur, S.; Bernard, C.; et al. In vivo recordings of brain activity using organic transistors. *Nat. Commun.* **2013**, *4*.
44. Rivnay, J.; Inal, S.; Salleo, A.; Owens, R.M.; Berggren, M.; Malliaras, G.G. Organic electrochemical transistors. *Nat. Rev. Mater.* **2018**, *3*, 17086.
45. Basiricò, L.; Cosseddu, P.; Scidà, A.; Fraboni, B.; Malliaras, G.G.; Bonfiglio, A. Electrical characteristics of ink-jet printed, all-polymer electrochemical transistors. *Org. Electron.* **2012**, *13*, 244–248.
46. Gu, X.; Yao, C.; Liu, Y.; Hsing, I.-M. 16-Channel Organic Electrochemical Transistor Array for In Vitro Conduction Mapping of Cardiac Action Potential. *Adv. Healthc. Mater.* **2016**, *5*, 2345–2351.
47. Lanzani, G. Organic electronics meets biology: Materials for bioelectronics. *Nat. Mater.* **2014**, *13*, 775–776.
48. Conte Camerino, D. Grand challenge for ion channels: an underexploited resource for therapeutics. *Front. Pharmacol.* **2010**.
49. Markets, R. and Ion Channel Modulators Market 2015-2022: Global Strategic Business Report 2018 - Industry & Product Overview, Recent Industry Activity & Focus on Key Players Available online: <http://globenewswire.com/news-release/2018/02/14/1347899/0/en/Ion-Channel-Modulators-Market-2015-2022-Global-Strategic-Business-Report-2018-Industry-Product-Overview-Recent-Industry-Activity-Focus-on-Key-Players.html> (accessed on Sep 27, 2018).
50. Lind, J.U.; Busbee, T.A.; Valentine, A.D.; Pasqualini, F.S.; Yuan, H.; Yadid, M.; Park, S.-J.; Kotikian, A.; Nesmith, A.P.; Campbell, P.H.; et al. Instrumented cardiac microphysiological devices via multimaterial three-dimensional printing. *Nat. Mater.* **2017**, *16*, 303–308.
51. Loskill, P.; Marcus, S.G.; Mathur, A.; Reese, W.M.; Healy, K.E.  $\mu$ Organo: A Lego®-Like Plug & Play System for Modular Multi-Organ-Chips. *PLOS ONE* **2015**, *10*, e0139587.
52. Esch, E.W.; Bahinski, A.; Huh, D. Organs-on-chips at the frontiers of drug discovery. *Nat. Rev. Drug Discov.* **2015**, *14*, 248–260.

## Ch. V.- Appendices

53. Organ-On-Chip Market Analysis & Trends - Organ (Heart-on-chip, Human-on-chip, Intestine-on-chip, Kidney-on-chip, Liver-on-chip, Lung-on-chip), Application - Forecast to 2025 Available online: <https://www.prnewswire.com/news-releases/organ-on-chip-market-analysis--trends---organ-heart-on-chip-human-on-chip-intestine-on-chip-kidney-on-chip-liver-on-chip-lung-on-chip-application---forecast-to-2025-300393217.html> (accessed on Sep 27, 2018).
54. Harding, J.; Mirochnitchenko, O. Preclinical Studies for Induced Pluripotent Stem Cell-based Therapeutics. *J. Biol. Chem.* **2014**, *289*, 4585–4593.
55. Rorsman, P.; Braun, M. Regulation of Insulin Secretion in Human Pancreatic Islets. *Annu. Rev. Physiol.* **2013**, *75*, 155–179.
56. Atkinson, M.A.; Eisenbarth, G.S.; Michels, A.W. Type 1 diabetes. *The Lancet* **2014**, *383*, 69–82.
57. La Torre, D.; Lernmark, Å. Immunology of  $\beta$ -Cell Destruction. In *The Islets of Langerhans*; Islam, Md.S., Ed.; Advances in Experimental Medicine and Biology; Springer Netherlands: Dordrecht, 2010; pp. 537–583 ISBN 978-90-481-3271-3.
58. Roze, S.; Saunders, R.; Brandt, A.-S.; de Portu, S.; Papo, N.L.; Jendle, J. Health-economic analysis of real-time continuous glucose monitoring in people with Type 1 diabetes. *Diabet. Med.* **2015**, *32*, 618–626.
59. Ashcroft, F.M.; Rorsman, P. Diabetes Mellitus and the  $\beta$  Cell: The Last Ten Years. *Cell* **2012**, *148*, 1160–1171.
60. Qian, W.-J.; Gee, K.R.; Kennedy, R.T. Imaging of  $Zn^{2+}$  Release from Pancreatic  $\beta$ -Cells at the Level of Single Exocytotic Events. *Anal. Chem.* **2003**, *75*, 3468–3475.
61. McQuade, D.T.; Pullen, A.E.; Swager, T.M. Conjugated Polymer-Based Chemical Sensors. *Chem. Rev.* **2000**, *100*, 2537–2574.
62. Lehn, J.M. CRYPTATES: INCLUSION COMPLEXES OF MACROPOLYCYCLIC RECEPTOR MOLECULES. 22.
63. Lehn, J.M.; Sauvage, J.P. Cation and cavity selectivities of alkali and alkaline-earth “cryptates.” *J Chem Soc D* **1971**, *0*, 440–441.
64. Simonet, J.; Rault-Berthelot, J. Electrochemistry: A technique to form, to modify and to characterize organic conducting polymers. *Prog. Solid State Chem.* **1991**, *21*, 1–48.
65. Sauvage, J.-P. From Chemical Topology to Molecular Machines (Nobel Lecture). *Angew. Chem. Int. Ed.* **2017**, *56*, 11080–11093.
66. Swager, T.M. *50th Anniversary Perspective* : Conducting/Semiconducting Conjugated Polymers. A Personal Perspective on the Past and the Future. *Macromolecules* **2017**, *50*, 4867–4886.
67. Benesi, H.A.; Hildebrand, J.H. A Spectrophotometric Investigation of the Interaction of Iodine with Aromatic Hydrocarbons. *J. Am. Chem. Soc.* **1949**, *71*, 2703–2707.
68. Scott, R.L. Some comments on the Benesi-Hildebrand equation. *Recl. Trav. Chim. Pays-Bas* **2010**, *75*, 787–789.
69. Hanes, C.S. CLXVII. STUDIES ON PLANT AMYLASES. 16.
70. Motulsky, H.; Christopoulos, A. Fitting Models to Biological Data using Linear and Nonlinear Regression. 351.
71. Motulsky, H.J.; Ransnas, L.A. Fitting curves to data using nonlinear regression: a practical and nonmathematical review. *FASEB J.* **1987**, *1*, 365–374.
72. Wen, Y.; Xu, J. Scientific Importance of Water-Processable PEDOT-PSS and Preparation, Challenge and New Application in Sensors of Its Film Electrode: A Review. *J. Polym. Sci. Part Polym. Chem.* **2017**, *55*, 1121–1150.
73. Wang, Y. Research progress on a novel conductive polymer–poly(3,4-ethylenedioxythiophene) (PEDOT). *J. Phys. Conf. Ser.* **2009**, *152*, 012023.
74. Groenendaal, L.; Zotti, G.; Aubert, P.-H.; Waybright, S.M.; Reynolds, J.R. Electrochemistry of Poly(3,4-alkylenedioxythiophene) Derivatives. *Adv. Mater.* **2003**, *15*, 855–879.

## Ch. V.- Appendices

75. Ponder, J.F.; Österholm, A.M.; Reynolds, J.R. Designing a Soluble PEDOT Analogue without Surfactants or Dispersants. *Macromolecules* **2016**, *49*, 2106–2111.
76. Wen, Y.; Xu, J. Scientific Importance of Water-Processable PEDOT–PSS and Preparation, Challenge and New Application in Sensors of Its Film Electrode: A Review. *J. Polym. Sci. Part Polym. Chem.* **2017**, *55*, 1121–1150.
77. Hofmann, A.I.; Cloutet, E.; Hadziioannou, G. Materials for Transparent Electrodes: From Metal Oxides to Organic Alternatives. *Adv. Electron. Mater.* **2018**, 1700412.
78. Svensson, P.-O.; Nilsson, D.; Forchheimer, R.; Berggren, M. A sensor circuit using reference-based conductance switching in organic electrochemical transistors. *Appl. Phys. Lett.* **2008**, *93*, 203301.
79. Groenendaal, L.; Jonas, F.; Freitag, D.; Pielartzik, H.; Reynolds, J.R. Poly(3,4-ethylenedioxythiophene) and Its Derivatives: Past, Present, and Future. *Adv. Mater.* **2000**, *12*, 481–494.
80. de Jong, M.P.; van IJzendoorn, L.J.; de Voigt, M.J.A. Stability of the interface between indium-tin-oxide and poly(3,4-ethylenedioxythiophene)/poly(styrenesulfonate) in polymer light-emitting diodes. *Appl. Phys. Lett.* **2000**, *77*, 2255–2257.
81. Hofmann, A.I.; Smaal, W.T.T.; Mumtaz, M.; Katsigiannopoulos, D.; Brochon, C.; Schütze, F.; Hild, O.R.; Cloutet, E.; Hadziioannou, G. An Alternative Anionic Polyelectrolyte for Aqueous PEDOT Dispersions: Toward Printable Transparent Electrodes. *Angew. Chem. Int. Ed.* **2015**, *54*, 8506–8510.
82. Grove, L.J.; Rennekamp, J.M.; Jude, H.; Connick, W.B. A New Class of Platinum(II) Vapochromic Salts. *J. Am. Chem. Soc.* **2004**, *126*, 1594–1595.
83. Zhou, Q.; Swager, T.M. Method for enhancing the sensitivity of fluorescent chemosensors: energy migration in conjugated polymers. *J. Am. Chem. Soc.* **1995**, *117*, 7017–7018.
84. McCullough, R.D.; Ewbank, P.C.; Loewe, R.S. Self-Assembly and Disassembly of Regioregular, Water Soluble Polythiophenes: Chemoselective Ionchromatic Sensing in Water. *J. Am. Chem. Soc.* **1997**, *119*, 633–634.
85. Pandey, P.C.; Prakash, R. Polyindole modified potassium ion-sensor using dibenzo-18-crown-6 mediated PVC matrix membrane. *Sens. Actuators B Chem.* **1998**, *46*, 61–65.
86. Lyons, M.E.G.; Breen, W.; Cassidy, J. Ascorbic acid oxidation at polypyrrole-coated electrodes. *J. Chem. Soc. Faraday Trans.* **1991**, *87*, 115.
87. Yu, H.; Xu, B.; Swager, T.M. A Proton-Doped Calix[4]arene-Based Conducting Polymer. *J. Am. Chem. Soc.* **2003**, *125*, 1142–1143.
88. Yu, H.; Pullen, A.E.; Büschel, M.G.; Swager, T.M. Charge-Specific Interactions in Segmented Conducting Polymers: An Approach to Selective Ionoresistive Responses. *Angew. Chem. Int. Ed.* **2004**, *43*, 3700–3703.
89. Hoa, D.T.; Kumar, T.N.Suresh.; Puneekar, N.S.; Srinivasa, R.S.; Lal, R.; Contractor, A.Q. A biosensor based on conducting polymers. *Anal. Chem.* **1992**, *64*, 2645–2646.
90. Hardy, J.G.; Mouser, D.J.; Arroyo-Currás, N.; Geissler, S.; Chow, J.K.; Nguy, L.; Kim, J.M.; Schmidt, C.E. Biodegradable electroactive polymers for electrochemically-triggered drug delivery. *J Mater Chem B* **2014**, *2*, 6809–6822.
91. Broda, C.R.; Lee, J.Y.; Sirivisoot, S.; Schmidt, C.E.; Harrison, B.S. A chemically polymerized electrically conducting composite of polypyrrole nanoparticles and polyurethane for tissue engineering. *J. Biomed. Mater. Res. A* **2011**, *98A*, 509–516.

## Chapter II

## Ch. V.- Appendices

92. Shi, H.; Wang, R.; Yang, J.; Ren, H.; Liu, S.; Guo, T. Novel imprinted nanocapsule with highly enhanced hydrolytic activity for organophosphorus pesticide degradation and elimination. *Eur. Polym. J.* **2015**, *72*, 190–201.
93. Llanes, P.; Sayalero, S.; Rodríguez-Eschrich, C.; Pericàs, M.A. Asymmetric cross- and self-aldol reactions of aldehydes in water with a polystyrene-supported triazolylproline organocatalyst. *Green Chem.* **2016**, *18*, 3507–3512.
94. Moad, G.; Rizzardo, E.; Thang, S.H. Living Radical Polymerization by the RAFT Process – A Second Update. *Aust. J. Chem.* **2009**, *62*, 1402.
95. Meziane, R.; Bonnet, J.-P.; Courty, M.; Djellab, K.; Armand, M. Single-ion polymer electrolytes based on a delocalized polyanion for lithium batteries. *Electrochimica Acta* **2011**, *57*, 14–19.
96. Proctor, C.M.; Rivnay, J.; Malliaras, G.G. Understanding volumetric capacitance in conducting polymers. *J. Polym. Sci. Part B Polym. Phys.* **2016**, *54*, 1433–1436.
97. Inal, S.; Malliaras, G.G.; Rivnay, J. Benchmarking organic mixed conductors for transistors. *Nat. Commun.* **2017**, *8*.
98. Koutsouras, D.A.; Gkoupidenis, P.; Stolz, C.; Subramanian, V.; Malliaras, G.G.; Martin, D.C. Impedance Spectroscopy of Spin-Cast and Electrochemically Deposited PEDOT:PSS Films on Microfabricated Electrodes with Various Areas. *ChemElectroChem* **2017**, *4*, 2321–2327.
99. Stavrinidou, E.; Leleux, P.; Rajaona, H.; Khodagholy, D.; Rivnay, J.; Lindau, M.; Sanaur, S.; Malliaras, G.G. Direct Measurement of Ion Mobility in a Conducting Polymer. *Adv. Mater.* **2013**, *25*, 4488–4493.

### Chapter III

100. Degirmenci, A.; Iskenderkaptanoglu, D.; Algi, F. A novel turn-off fluorescent Pb(II) probe based on 2,5-di(thien-2-yl)pyrrole with a pendant crown ether. *Tetrahedron Lett.* **2015**, *56*, 602–607.
101. Heinze, J.; Frontana-Uribe, B.A.; Ludwigs, S. Electrochemistry of Conducting Polymers—Persistent Models and New Concepts<sup>†</sup>. *Chem. Rev.* **2010**, *110*, 4724–4771.
102. Merz, A.; Kronberger, J.; Dunsch, L.; Neudeck, A.; Petr, A.; Parkanyi, L. Radical Dimerization of 5,5'-Diphenyl-3,3',4,4'-tetramethoxy-2,2'-bipyrrole:  $\pi$  Dimer in the Crystal,  $\sigma$  Dimer in Solution. *Angew. Chem. Int. Ed.* **1999**, *38*, 1442–1446.
103. Valencia, D.P.; González, F.J. Estimation of diffusion coefficients by using a linear correlation between the diffusion coefficient and molecular weight. *J. Electroanal. Chem.* **2012**, *681*, 121–126.
104. Ćirić-Marjanović, G. Recent advances in polyaniline research: Polymerization mechanisms, structural aspects, properties and applications. *Synth. Met.* **2013**, *177*, 1–47.
105. Shimidzu, T.; Ohtani, A.; Iyoda, T.; Honda, K. Charge-controllable polypyrrole/polyelectrolyte composite membranes: Part II. Effect of incorporated anion size on the electrochemical oxidation-reduction process. *J. Electroanal. Chem. Interfacial Electrochem.* **1987**, *224*, 123–135.
106. Aubert, P.-H.; Groenendaal, L.; Louwet, F.; Lutsen, L.; Vanderzande, D.; Zotti, G. In situ conductivity measurements on polyethylenedioxythiophene derivatives with different counter ions. *Synth. Met.* **2002**, *126*, 193–198.
107. Smie, A.; Synowczyk, A.; Heinze, J.; Alle, R.; Tschuncky, P. *i,i*-Disubstituted oligothiophenes, a new oligomeric approach towards the synthesis of conducting polymers. *J. Electroanal. Chem.* **1998**, *9*.
108. Salinas, G.; Del-Oso, J.-A.; Espinoza-Montero, P.-J.; Heinze, J.; Frontana-Uribe, B.A. Electrochemical polymerization, characterization and in-situ conductivity studies of poly-3,4-ortho-xyliendioxythiophene (PXDOT). *Synth. Met.* **2018**, *245*, 135–143.

## Ch. V.- Appendices

109. Voortman, T.P.; Bartesaghi, D.; Koster, L.J.A.; Chiechi, R.C. Cross-Conjugated n-Dopable Aromatic Polyketone. *Macromolecules* **2015**, *48*, 7007–7014.

### Chapter IV

110. Pedraza, E.; Karajić, A.; Raoux, M.; Perrier, R.; Pirog, A.; Lebreton, F.; Arbault, S.; Gaitan, J.; Renaud, S.; Kuhn, A.; et al. Guiding pancreatic beta cells to target electrodes in a whole-cell biosensor for diabetes. *Lab. Chip* **2015**, *15*, 3880–3890.
111. Perrier, R.; Pirog, A.; Jaffredo, M.; Gaitan, J.; Catargi, B.; Renaud, S.; Raoux, M.; Lang, J. Bioelectronic organ-based sensor for microfluidic real-time analysis of the demand in insulin. *Biosens. Bioelectron.* **2018**, *117*, 253–259.
112. Donahue, M.J.; Williamson, A.; Strakosas, X.; Friedlein, J.T.; McLeod, R.R.; Gleskova, H.; Malliaras, G.G. High-Performance Vertical Organic Electrochemical Transistors. *Adv. Mater.* **2018**, *30*, 1705031.
113. Rivnay, J.; Leleux, P.; Sessolo, M.; Khodagholy, D.; Hervé, T.; Fiocchi, M.; Malliaras, G.G. Organic Electrochemical Transistors with Maximum Transconductance at Zero Gate Bias. *Adv. Mater.* **2013**, *25*, 7010–7014.

